DSE - Premium Business Jet

Design a light business jet offering premium value through unparalleled in-class performance

W.F.J.P. Brugmans	1506765	K.C. Leung	4106849
J.H. Bussemaker	4144023	R.F. Mollee	4098595
M.B.P. Claeys	4101944	S.S. Ng	4178718
R.J. Groot	4097971	F.M. Sickler	4094085
E. Kireeva	4153324	Y. Tigchelaar	1507931

Final Report
Design Synthesis Excercise

TU Delft — Delft University of Technology

Aerospace Engineering

Preface

This report is the fourth and final progress report of Group 21 for the Design Synthesis Exercise. The Design Synthesis Exercise (DSE) is the concluding part of the Bachelor's study program (BSc). The objectives of the DSE are to enhance the skills of the students in: designing, applying knowledge, communication, working as a team and sustainable development. This project will be conduced in 11 weeks and the aim is to create the best result, which will not be flawless due to the time limitation. The assignment is to design a light business jet offering premium value though unparalleled in-class performance. Prior to this report a Project Plan, a Baseline Report and a Midterm Report were published.

This report is intended for educated readers with an interest in aviation. Readers who are particularly interested in the design of the different aircraft part sizing can find them in Part III Design Synthesis, where a Class II design is performed on the landing gear, aircraft systems, weight & balance, wing design, engine specification & nacelle design, aerodynamic analysis, aircraft structural characteristics, fuselage structural design and stability & control.

List of Symbols

Symbol	Definition	Unit
A	Aspect ratio	-
a_x/g	Braking decelleration	m/s^2
AC	Alternating current	V
AH	Flight hours per year	$-$
b	Width longeron	mm
b	Wing span	m
$\bar{c}$	Mean aerodynamic chord	m
C_D	Drag coefficient	-
C_{D_0}	Parasite drag	-
c_f	Skin friction coefficient	-
c_j	Specific fuel consumption	$lb/(lb \cdot h)$
C_l	2D Lift coefficient	-
C_{l_β}	Derivative of rolling moment with respect to sideslip angle	-
$C_{l_{\dot{\beta}}}$	Derivative of rolling moment with respect to rate of sideslip angle	-
C_{l_p}	Derivative of rolling moment with respect to roll rate	-
C_{l_r}	Derivative of rolling moment with respect to yaw rate	-
$C_{l_{da}}$	Derivative of rolling moment with respect to aileron deflection	-
$C_{l_{dr}}$	Derivative of rolling moment with respect to rudder deflection	-
C_L	Lift coefficient	-
$C_{L_{max}}$	Maximum lift coefficient	-
$C_{L_{max_{LDG}}}$	Maximum lift coefficient during landing	-
$C_{L_{max_{TO}}}$	Maximum lift coefficient during take-off	-
C_{L_α}	Lift slope	$1/rad$
C_{m_u}	Derivative of pitching moment with respect to speed	-
C_{m_α}	Derivative of pitching moment with respect to angle of attack	-
$C_{m_{\dot{\alpha}}}$	Derivative of pitching moment with respect to rate of angle of attack	-
C_{m_q}	Derivative of pitching moment with respect to pitch rate	-
$C_{m_{de}}$	Derivative of pitching moment with respect to elevator deflection	-
$C_{m_{TC}}$	Derivative of pitching moment with respect to thrust component	-
C_{n_β}	Derivative of yawing moment with respect to sideslip angle	-
$C_{n_{\dot{\beta}}}$	Derivative of yawing moment with respect to rate of sideslip angle	-
C_{n_p}	Derivative of yawing moment with respect to roll rate	-
C_{n_r}	Derivative of yawing moment with respect to yaw rate	-
$C_{n_{da}}$	Derivative of yawing moment with respect to aileron deflection	-
$C_{n_{dr}}$	Derivative of yawing moment with respect to rudder deflection	-
$C_{N_{max}}$	Maximum normal force coefficient	-
$C_{N_{min}}$	Minimal normal force coefficient	-
C_{X_0}	Derivative of X-force with zero angle of attack	-
C_{X_u}	Derivative of X-force with respect to speed	-

Symbol	Definition	Unit
C_{X_α}	Derivative of X-force with respect to angle of attack	-
C_{X_α}	Derivative of X-force with respect to rate of angle of attack	-
C_{X_q}	Derivative of X-force with respect to pitch rate	-
$C_{X_{de}}$	Derivative of X-force with respect to elevator deflection	-
C_{Y_β}	Derivative of Y-force with respect to sideslip angle	-
$C_{Y_{\dot{\beta}}}$	Derivative of Y-force with respect to rate of sideslip angle	-
C_{Y_p}	Derivative of Y-force with respect to roll rate	-
C_{Y_r}	Derivative of Y-force with respect to yaw rate	-
$C_{Y_{da}}$	Derivative of Y-force with respect to aileron deflection	-
$C_{Y_{dr}}$	Derivative of Y-force with respect to rudder deflection	-
C_{Z_0}	Derivative of Z-force with zero angle of attack	-
C_{Z_u}	Derivative of Z-force with respect to speed	-
C_{Z_α}	Derivative of Z-force with respect to angle of attack	-
$C_{Z_{\dot{\alpha}}}$	Derivative of Z-force with respect to rate of angle of attack	-
C_{Z_q}	Derivative of Z-force with respect to pitch rate	-
$C_{Z_{de}}$	Derivative of Z-force with respect to elevator deflection	-
C_{D_0}	Zero-lift drag	-
CGR	Climb gradient	%
C_{aed_m}	Airframe and design cost	$
C_{aed_r}	Airframe engineering and design cost	$
C_{apc_m}	Airline production cost	$
$C_{avionics_r}$	Cost of avionics equipment	$
C_{dst_r}	Development support and testing cost	$
C_{e_r}	Cost per jet engine	$
$\frac{CEF_{year}}{CEF_{1990}}$	Cost escalating factor	$-$
C_{fin_m}	Cost to finance manufacturing phase	$
C_{fin_r}	Cost of research and development phase	$
C_{fta_r}	Flight test airplanes cost	$
C_{fto_m}	Production flight test operation cost	$
C_{fto_r}	Flight test operations cost	$
C_{tsf_r}	Test and simulation facilities cost	$
D	Drag	N
D_b	Non-dimensional differential operator, asymmetric motions	-
D_c	Non-dimensional differential operator, symmetric motions	-
DC	Direct current	V
DOC_{depr}	Direct operating cost of depreciation	$
DOC_{fin}	Direct operating cost of financing	$
DOC_{flt}	Direct operating cost of flying	$
DOC_{lnr}	Direct operating cost of landing, navigation fees and registry taxes	$
DOC_{maint}	Direct operating cost of maintenance	$
ΔP	Cabin pressurization pressure different	kPa

Symbol	Definition	Unit
δ_a	Aileron deflection	$^\circ$
δ_e	Elevator deflection	$^\circ$
δ_r	Rudder deflection	$^\circ$
E	Endurance	hr
e	Oswald factor	-
$\bar{e}_{cp}$	Chordwise location of center of pressure	m
F_D	Depreciation factor	-
F_P	Fuel price	-
F_{cad}	Computer aided design factor	$-$
F_{diff}	Difficulty factor	$-$
F_{int}	Interior cost per pax	$\$$
F_{mat}	Correction factor material type	$\$$
F_{tsf}	Factor for extra facilities	$-$
g	Gravitation constant	m/s^2
h	Height longeron	mm
h_{cg}	Height center of gravity	m
h_{cruise}	Cruise altitude	ft
I_{xx}	Area moment of inertia	mm^4
I_{xy}	Area moment of inertia	mm^4
I_{xz}	Area moment of inertia	mm^4
I_{yy}	Area moment of inertia	mm^4
I_{yz}	Area moment of inertia	mm^4
I_{zz}	Area moment of inertia	mm^4
k	Cruise weight factor	-
K_g	Gust alleviation factor	-
K_γ	Bending stiffness axis	-
K_θ	Torsional stiffness axis	-
K_X	Non-dimensional radius of gyration about X-axis	-
K_{XZ}	Non-dimensional product of inertia	-
K_Y	Non-dimensional radius of gyration about Y-axis	-
l_m	Main gear distance	m
l_n	Nose gear distance	m
M_{cr}	Cruise mach number	-
n_{eng}	Number of engines	-
n_{pax}	Number of Passengers	$-$
n_{c1}	Number of Cabin Crew	$-$
n_{c2}	Number of Cockpit Crew	$-$
L	Lift	N
n_m	Number of aircraft manufactured	$-$
n_s	Number of struts	-
n_t	Number of tires	-
p	Roll rate	rad/s
P	Period	s
P_m	Main gear load	N
$P_{m_{tire}}$	Main gear tire load	N
$P_{n_{dyn_t}}$	Nose gear dynamic tire load	N
q	Dynamic pressure	$kg/(m^2 s)$
q	Pitch rate	rad/s
R	Range	km
Re	Reynolds number	$-$
R_{e_r}	Engineering labour cost	$\$/hr$
R_{m_r}	Manufacturing labour rate	$\$$
R_{m_t}	Tooling labour rate	$\$$
$R_{la,p}$	Maintenance labour rate	-
r	Yaw rate	rad/s

Symbol	Definition	Unit
s_{TOFL}	Take-off field length	m
S	Wing area	m^2
S_c	Canard area	m^2
S_h	Horizontal tail area	m^2
S_v	Vertical tail area	m^2
S_{wet}	Wetted area	m^2
SAL_1	Annual salary captain	$\$$
SAL_2	Annual salary co-pilot	$\$$
t	Thickness	mm
T	Thrust	N
T/W	Thrust loading	-
$T_{\frac{1}{2}}$	Time to half amplitude	s
T_{TO}	Take-off thrust	N
TOP	Take-off parameter	-
U_{de}	Gust line factor	-
$\hat{u}$	Non-dimensional component of V along X-axis	-
V	Speed	m/s
V_{div}	Divergence speed	m/s
V_s	Stall speed	m/s
V_{s_L}	Stall speed during landing	m/s
$V_{s_{TO}}$	Stall speed during take-off	m/s
W/S	Wing loading	N/m^2
W_{api}	Airco, anti-de-icing system weight	kg
W_{apu}	Auxiliary power unit weight	kg
W_{aux}	Auxiliary gear weight	kg
W_c	Canard weight	kg
W_E	Empty weight	kg
W_{els}	Electrical system weight	kg
W_{eng}	Engine weight	kg
W_f	Fuselage weight	kg
W_{fc}	Flight controls weight	kg
W_{FEQ}	Fixed equipement weight	kg
W_{fs}	Fuel system weight	kg
W_{fur}	Furnishing weight	kg
W_h	Horizontal tail weight	kg
W_{hps}	Hydraulics/pneumatics weight	kg
W_{iae}	Instruments/avionics weight	kg
W_{mg}	Main gear weight	kg
W_n	Nacelles weight	kg
W_{ng}	Nose gear weight	kg
W_{ox}	Oxygen system weight	kg
W_P	Powerplant weight	kg
$W_{passenger}$	Passenger weight	kg
W_{paint}	Paint weight	kg
W_{pl}	Payload weight	kg
W_{prop}	Propulsion system weight	kg
W_{struc}	Structure weight	kg
W_v	Vertical tail weight	kg
W_w	Wing weight	kg
$\bar{y}_{cp}$	Spanwise location of center of pressure	m

Symbol	Definition	Unit
α	Angle of attack	°
β	Angle of sideslip	°
ε	Twist angle	°
$d\varepsilon_h/d\alpha$	Downwash horizontal tail	—
$d\varepsilon_v/d\alpha$	Downwash canard	—
Γ	Circulation	°
Γ	Dihedral angle	°
ζ	Damping ratio	-
η	Span factor	-
θ	Angle of pitch	°
λ	Taper ratio	-
λ_b	Non-dimensional eigenvalue asymmetric motions	-
λ_c	Non-dimensional eigenvalue symmetric motions	-
μ_b	Relative density, asymmetric motions	-
μ_c	Relative density, symmetric motions	-
ρ	Density	kg/m^3
σ	Runway altitude factor	-
$\sigma_{fatigue}$	Fatigue strength	MPa
ω_0	Undamped natural frequency	rad/s
Λ	Sweep angle	°

Symbol	Definition
ABS	Anti-lock Braking System
ADF	Automatic Direction Finder
AEO	All engines operative
APU	Auxiliary Power Unit
C.G.	Center of Gravity
CBS	Cost Breakdown Structure
CVR	Cockpit Voice Recorder
FAR	Federal Aviation Regulations
FBS	Functional Breakdown Structure
FBW	Fly-by-wire
FCS	Flight Control System
FDR	Flight Data Recorder
FFD	Functional Flow Diagram
FMS	Flight Management System
FSW	Forward Swept Wing
FTA	Fault Tree Analysis
HLD	High Lift Device
IFCS	Intelligent Flight Control System
ISA	International Standard Atmosphere
MAC	Mean Aerodynamic Chord
MLW	Maximum Landing Weight
MTBF	Mean time between failures
MTOW	Maximum Take-off Weight
MTTR	Mean time to repair
OEI	One engine Inoperative
OEW	Operative Empty Weight
PD&D	Project Design & Development
RAMS	Reliability, Availability, Maintainability, Safety
RAT	Ram Air Turbine
RDTE	Research, Development, Test, Evaluation
SFC	Specific Fuel Consumption
VFR	Visual Flight Rules
VOR	VHF omnidirectional range

Table of Contents

Summary

In an era where 'time is money', an opportunity exists to offer a unique value proposition to customers by developing a Premium Light Business Jet. This jet, the Phoenix 5600, sets itself apart from the competition by combining flight speed in the transonic domain with short take-off and landing capability. Together, these aspects are expected to result in a significant decrease in travel time while maintaining point-to-point travelling. Simultaneously, sufficient capacity and comfort should be retained to be competitive in the light business jet market. Business jets are available for a wide range of performance and capability requirements. From a customer perspective, the use of business jets for air transport offers many advantages instead of using business- or first- class options offered by airlines. Flexibility, time saving and productivity ensure that the customer is not constrained by airline schedules and can travel at virtually any required time, have the capability of flying point-to-point and allow for meetings and conference calls.

The report is split into five parts, concept introduction, design approach, design synthesis, final concept and recommendations for future design. In concept introduction the design characteristics designed in the Project Plan, Baseline Report and Midterm Report are stated. In the design approach the method for designing the different parts of the aircraft is explained. In the design synthesis all the elements are actually sized and design mainly using the methods from Roskam and Torenbeek. In the final concept the design is put together and elaborated upon. Finally in recommendations for future design, the steps that can be taken after the DSE project are explained and recommendations for improvement of the currently used theory are stated.

Concept Introduction
Prior to the final report the top level requirements have been set for the Phoenix 5600 to be a light business jet which will offer premium value through unparalleled in-class performance. The top-level requirements are based on a market analysis from which the market gap is clearly visible. Between 2013 and 2023, 9250 new business jets will be produced which is equivalent to $260 Billion. This is a great market opportunity. From our market analysis Asia and America will be our main markets, they prefer a large range and a bigger cabin. With a range of 5600 km flying at a cruise speed of Mach 0.90 at a service ceiling of 41000 ft, the Phoenix 5600 should be able to carry 8 passengers for only a 16 - 20 M$ purchase price. In addition the runway lengths should be significantly shorter than those of the competition: only 1000 m take off and 800 m landing runway length. This would result that the Phoenix can reach 3% more airports worldwide. Finally the comfort level of the Phoenix 5600 should be significantly higher with only 60 dB cabin noise, comparable to an average meeting room, with high-tech technology for meetings and conference calls.

With a final runway length of only 819 m take-off distance and 746 m landing distance and a seat with of 60 cm, 6-8 cm more than most business jets. With the list price of only 15.9 M$ and operating cost of 2400$/h the Phoenix 5600 sets itself apart from the competition.

The design process is a intense and iterative process. Starting with 13 configurations a trade-off was made from which 4 configurations were selected, 3 subsonic and 1 supersonic aircraft. A Class I design is performed on these 4 configurations and a trade-off is done from which it can be concluded that 3 lifting surface, forward swept wing with T-tail and canard has the most favorable characteristics for our mission.

Design approach
The design approach used for the design of the Phoenix 5600 is Roskam and Torenbeek. As Roskam is written in the 1980's and new technology has been developed since we have to implement the new technology in the relatively old methodology. We have encountered for this by using reference aircraft, additional design options (airfoil selection), design information from lectures and guidance from professors of the aerospace engineering faculty.

Nowadays sustainable development plays a major role in all design processes. The Phoenix 5600 will be assessed at every aspect through its entire life cycle; the design of the product, the use of the product and the disposal of the product. The aircraft fulfills the FAR 25 regulations in addition to complying with ICAO Annex 16, vol. I, Chapter 4 for the noise requirements and ICAO Annex 16, vol. II for the emission re-

quirements.

Design synthesis
The Phoenix 5600 has a forward swept, low mounted wing with profile NACA 64212 Mod B, located under the aft of the passenger cabin. The canard is mounted low on the nose, under the cockpit. The T-tail is mounted on top and at the end of the tail cone. For longitudinal and directional stability and control, the aircraft features a T-tail with elevators and a rudder and a canard with a canardvator. For lateral control the wings feature ailerons. Stability & control shows that the symmetric eigenmodes; short period and phugoid are both stable as well as the asymmetric eigenmodes; aperiodic roll, spiral and Dutch roll. The wings feature Fowler flaps as high lift devices, because of their high efficiency combined with relatively low mechanical complexity.

The general structural arrangement of the fuselage will be semi-monocoque, where the skin (aluminum 7075-T6) carries part of the loads supported by fuselage frames and stiffeners, which allow for a light, stiff structure. The aircraft is internally pressurized at 1500 m (4921 ft) ISA equivalent while flying at 41000 ft, from the cockpit until the baggage compartment, which is located behind the passenger cabin. The aft bulkhead closes the baggage compartment at the back. In the front on the left (port) side, the cabin has a passenger access door. In the back on the right (starboard) side, the cabin has an overwing emergency exit (type IV). The baggage compartment is reachable from the outside port side.

Advantages of the forward swept wing are that there is extra space between the passenger door and the leading edge due to the aft located wings and increased wing efficiency because the root will stall first allowing the usage of ailerons during stall. Disadvantages include structural divergence and yaw instability. The aluminum 7150 wing is designed according to the safe-life approach with integral fuel tanks. This is because the wing is a very crucial part of the aircraft and some parts of the wing are difficult to access for inspection and maintenance. The wing is made from aluminum 7150 as this is the strongest available aluminum and not enough research has been done on composites to make a composite wing. The cabin itself is very spacious and features large windows, a large access door, a galley, a lavatory and state-of-the-art air conditioning, entertainment, electrical systems and more. The cockpit floor is raised slightly compared to the cabin floor for cockpit visibility and nose shape reasons. The cockpit windows allow excellent visibility for the pilots to ensure safe operations, also during high pitch flight.

The Pratt & Whitney PW545C engines are attached high on the aft of the fuselage at the position of the aft pressure bulkhead. This ensures that engines are as far away from the cabin as possible (reducing inside noise), that the engine inlets are not positioned in the wing wake and that the engine exhaust flow does not interfere with the aft empennage surfaces. The Phoenix 5600 will be equipped with a retractable tricycle gear with double tires on each aluminum 6061-T6 strut. The Oleo shock absorber will be implemented in the landing gear system to absorb the touchdown impact. The nose landing gear retracts to the front to ensure aerodynamic lock in case of hydraulic failure.

The research, development, test and evaluation cost, manufacturing cost, direct operating cost are determined and the list price of the Phoenix 5600 is only 15.9 M$. The sales reach break-even point at 200 units. When the 24.34% profit is included 580 aircraft need to be sold. A 24.34% profit is the average growth of the competitors and we have the opportunity to grow equally. The direct operating cost of the Phoenix 5600 is 2400 $/h. Each year 36 units will be produced.

Final concept
From the compliance matrix it can be seen that all the top-level requirements are met. The range, runway length, list price and direct operating cost even positively exceed the requirements. The aircraft can fly 1400 km further than the required range, the list price is 0.1 M$ lower than the required list price and the direct operating cost are 100 $/h lower than the required direct operating cost.

Table 1: Requirements Compliance Matrix

Category	Requirement	Required Value	Actual Value	Chapter
Performance	Range	4200 km	5600 km	Part IV Chapter 2
	Nominal cruise speed	Mach 0.90	Mach 0.90	Part IV Chapter 2
	Maximum speed	Mach 0.95	Mach 0.95	Part IV Chapter 2
	Payload	2 crew (max) 4 passengers (typical) 8 passengers (max) passenger baggage	2 crew 4 passengers 8 passengers 180 kg	Part III Chapter 5
	Service ceiling	41000 ft	41000 ft	Part IV Chapter 10
	RAMS	Similar as competitors	Achieved	Part IV Chapter 8
	Specific fuel consumption	0.5 lb/(lbf · h)	0.5 lb/(lbf · h)	Part III Chapter 13
	Take-off/Landing distance	1000 m / 800 m	819 m / 746 m	Part IV Chapter 10
Market	Pressurization	1500 m ISA equivalent	1500 m ISA	Part IV Chapter 12.1
	Noise levels (in-aircraft)	exceed competitors	60 dB	Part III Appendix K
	List price	16 - 20 M$	15.9 M$	Part IV Chapter 19
	Direct operating costs	2500 $/h	2398 $/h	Part IV Chapter 19
	Entry into service	2020	2020	Part IV Chapter A
Sustainability	Noise	Comply with ICAO Annex 16, vol. I, Chapter 4	Achieved	Part III Chapter 8
	Emissions	Comply with ICAO Annex 16, vol. II	Achieved	Part III Chapter 8

Recommendations for future design

The Phoenix 5600 can be designed into more detail in the future. The detailed design phase, testing phase, production preparation and certification will be the next steps to produce the premium light business jet with unparalleled in-class performance.

1 Introduction

In an era where 'time is money', an opportunity exists to offer a unique value proposition to customers by developing a Premium Light Business Jet, the 'Phoenix 5600'. This jet sets itself apart from the competition by combining flight speed in the transonic domain with short take-off and landing capability. Together, these aspects are expected to result in a significant decrease in travel time while maintaining point to point travelling. Simultaneously, sufficient capacity and comfort should be retained to be competitive in the light business jet market. The design process of the Phoenix 5600 is a long iterative process which requires a significant amount of time, dedication and commitment. The documentation of the design process can be divided into a Project plan, Baseline Report, MidTerm Report and Final Report. The Project Plan states the problem and globally contains the outlines and schedule of the design phases. In the Baseline Report, the first solutions of the problem are presented and traded off. In the Midterm Report, the solutions are narrowed down to one final solution which will be worked out in detail in the Final Report.

The purpose of the Final Report is to perform a Class II design on the chosen configuration, a forward-swept wing, three-lifting surface aircraft, which will be suitable for the stated mission. To be able to design in detail, many iterations are performed and the design is adapted accordingly. In addition, basic marketing and sales characteristics are estimated such as the list price, direct operating cost, and interior design. The aircraft is named the Phoenix 5600 after the legendary Phoenix bird, which rises from the ashes of its predecessor. The Phoenix 5600 is so luxurious and exceeds other aircraft in its class that it rises from the ashes of all the old designs and a new exquisite design is born. The range of the aircraft is 5600 km, therefore the name is Phoenix 5600.

The report is structured as follows. First, *Part I: Concept Introduction* focuses on what design steps have been performed until now. Also the functional flow diagram, the functional breakdown structure, the resource allocation and market analysis is executed. Secondly, *Part II: Design Approach* elaborates on design aspects including the operation and logistics, sustainable development strategy and RAMS. Following, in *Part III: Design Synthesis*, the design synthesis is done. This includes the sensitivity analysis, performance-, aerodynamic-, structural- characteristics, weigh & balance, stability & control and aircraft system characteristics are examined. Next, in *Part IV: Final Concept* it is elaborated on the configuration layout, technical risk assessment, future cost breakdown, return on investment and the compliance matrix are elaborated. Finally, in *Part V: Recommendations for Future Design*, the project design & development logic, project Gantt Chart, manufacturing, assembly & integration plan, conclusion and recommendation are stated.

Part I

Concept Introduction

2 Design Chronology

The documentation of the design process of the Phoenix 5600 is divided into a Project Plan, Baseline Report, Midterm Report and Final Report. In Section 2.1 an overview is given of the design progress until the Project Plan. In Section 2.2, the progress until the Baseline Report will be discussed. Finally, Section 2.3 gives the design and design characteristics which are determined for the Midterm Report. From here, further development of the design is discussed in this Final Report.

2.1 Project Plan

In the Project Plan the top level requirements for the project have been determined for the subsonic and supersonic design based on reference aircraft, which are shown in Table 2.1. In this report elaboration on each of the requirements can be found. In addition the Organizational Breakdown Structure has been determined and each group member received a managerial function and a technical function shown in Table 2.2.

Table 2.1: Top Level Requirements

Requirement	Subsonic Case	Supersonic Case	Unit
Range	5600		km
Nominal cruise speed	Mach 0.90	Mach 1.8	-
Maximum speed	Mach 0.95	Mach 2.0	-
MTOW	<16000	<35000	kg
Payload	4 passengers (typical) or 8 passengers (maximum) 2 crew (maximum) + baggage		-
Service ceiling	41000	51000	ft
RAMS	Similar to reference aircraft		-
Specific fuel consumption	0.5	0.73	$lb/(lbf \cdot h)$
Takeoff distance	1000	1800	m
Landing distance	800	1500	m
Cabin altitude	1500		m
Noise levels in aircraft	60		dB
List price	16 - 20	80	$M\$$
Direct operating costs	2500	TBD	$\$/h$
Entry into service	2020		-
Noise	Comply with ICAO Annex 16, Vol. I, Chapter 4		-
Emissions	Comply with ICAO Annex 16, Vol. II		-

Table 2.2: Team Member Functions

Team Member	Managerial Function	Technical Function
R.J. Groot	Chairman/Project Manager	Performance Engineer
F.M. Sickler	Secretary & PR Manager	System Engineer
W.F.J.P. Brugmans	System Manager	Propulsion Engineer
M.B.P. Claeys	Design Manager	Weight & Balance Engineer
E. Kireeva	Graphical Manager	Structural Engineer
J.H. Bussemaker	Graphical Managers	Aerodynamics Engineer
S.S. Ng	Risk & Control Manager	Economical Engineer
K.C. Leung	Quality Manager	Design Engineer
R.F. Mollee	Quality Manager	Operational Engineer
Y. Tigchelaar	Strategy & Policy Manager	Stability & Control Engineer

A Work Flow Diagram (WFD) of the DSE is made, showing schematically planned activities in a logical order which can be found in Appendix F of the Midterm Report [1]. In addition a Gantt Chart is made which assigns the planned activities of the Work Flow Diagram to members of the group and shows the

amount of time that is reserved for that activity and the deadlines. As some activities may take more or less time than planned, the Gantt Chart is updated constantly and can be found in Appendix D of the Midterm Report [1]. Finally the Project Plan elaborates on sustainable development and environmental awareness which are important factors to keep in mind during the design of a new product. For every developed part of the aircraft the environmental impact should be taken into account. The latest updates about sustainable development can be found in Chapter 7 of this report.

2.2 Baseline Report

In the Baseline Report the Functional Breakdown Structure (FBS) is made. The FBS determines all the functions that the aircraft system has to perform. As the design process continues the FBS is updated and the latest version can be found in Chapter 3. Also a Functional Flow Diagram (FFD) is constructed which shows the logical order of functions the product must perform. The latest FFD can be found in Chapter 3. Next a market analysis is performed to determine the necessary characteristics and aspects of the product in order to be competitive in the market. The potential consumers are identified and the opportunities in terms of price and range are determined. It has been concluded that there is a gap after the economic recession in which the demand for business jets is now growing in the emerging markets of Asia, Eastern Europe, Latin America, the Middle East and Africa. Even while the business jet demand in these regions is relatively small in proportion to the global demand, forecast predict this to increase rapidly and will most likely drive future expansion of the business jet market.

Furthermore, the requirements for the stakeholders and the subsystems are determined in the Baseline Report. The requirements of the subsystems are used in Chapter 15 to determine the system characteristics of the aircraft. Also the MTOW and list price are estimated. The MTOW is determined to be 8800 kg with a list price of 2153 $/kg for the subsonic aircraft and a MTOW of 34900 kg with a list price of 3616 $/kg for the supersonic aircraft. Following all possible configurations are considered and thirteen configurations are selected for the trade-off. The trade-off criteria are points such as cabin noise, originality, engines, fuel storage, accessibility etc. These trade-off criteria are given weight factors and each aircraft is given a grade for a certain criterion. Finally four configurations obtain the highest scores; three subsonic configurations and one supersonic configuration. Throughout the Midterm Report these four configurations will be examined and designed in more detail. The four chosen concepts are once more shown in Figure 2.1 and hereafter referred to as Design 1, 2, 3 and 4.

Figure 2.1: The Four Configurations

Next a technical risk assessment is done representing a general view on the major and minor risks that can be identified in the project. This is done with the help of a risk map, a risk mitigation approach and a fault tree analysis. Finally the contingency management describes how the contingencies will be handled during the remaining phase of the design project. The possible risks are analyzed and a method to solve the problems is presented.

2.3 Midterm Report

In the Midterm report, Designs 1, 2, 3 and 4 are further designed and finally a trade-off is made to end up with one design on which a Class II design can be performed. The Midterm Report is split-up into sections.

The Design Approach, in which the overall steps and criteria before starting the actual design process are evaluated. The Design Synthesis in which the Class I method from Roskam is performed on the four different design options and finally the Concept Selection in which the trade-off is made and the best design option is outlined.

Design Approach

First the N2 chart is created to evaluate the design steps which will be conducted for the Class I and Class II design. In the Midterm Report a Class I method is performed and in the Final Report the Class II method is performed. Secondly operations and logistics gives an overview of the different operational scenarios. Thirdly the preliminary weight estimation is derived from the fuel fractions and MTOW relations resulting in a MTOW of 8800 kg for the subsonic aircraft and 34900 kg for the supersonic aircraft. Next a sensitivity analysis is performed in order to determine which parameters are the driving characteristics of the design. From the obtained results it can be concluded that the speed and specific fuel consumption affect the weight in the most sensitive manner. Finally the sustainable development strategy was determined for the design phase, production phase and operational phase.

Design Synthesis

Using Class I Method from Roskam the fuselage interior, wings, high lift devices, propulsion system, weight & balance, landing gear, empennage, stability & control, drag polar and system characteristics are determined. First for the design of the fuselage several important aspects need to be considered; structural stress, weight, accessibility, minimal drag and countability. This resulted in a length of the subsonic fuselage of 17.69 m and for supersonic 41.52 m. Secondly the design of the wing resulted in:

- Design 1: NACA 64212 Mod B with ailerons and Fowler flaps as high lift devices.
- Design 2: Bell 540 OLS and NACA 23012 with no leading or trailing edge devices but with ailerons.
- Design 3: NACA 64212 Mod B with ailerons and Fowler flaps as high lift devices.
- Design 4: NASA SC20503 with a flaperon as trailing edge device.

Thirdly the propulsion system is sized; resulting in a Pratt & Whitney PW 545C engine for Design 1 and 3 which should deliver 37 kN take-off thrust. For Design 2 the Honeywell HTF7350 engine, which can deliver 50 kN take-off thrust and Design 4 will have a Pratt & Whitney JT8D-L-210 turbofan engine with 194.7 kN of take-off thrust. Also the nacelle is designed for each engine. A retractable landing gear with nose wheel configuration is chosen for all four designs with two wheels per strut. The empennage is designed using X-plot and a method based on tail volume coefficient. For subsonic design NACA 0012 is chosen as the airfoil profile for both vertical and horizontal surfaces. For supersonic design NACA 0003 is chosen in order to reduce drag as much as possible. An incidence angle of +3 ° for the canards and -3 ° is chosen for the horizontal tail. Design 4 will have a butterfly tail in a V-shape. Also the Class I stability and control characteristics are explored: the static longitudinal stability, static directional stability and minimum control speed with one engine inoperative. Finally the requirements for system characteristics are examined including the flight control system, fuel system, hydraulic system, electrical system, cockpit instrumentation, de-icing & anti-icing system, escape and water & waste system layout.

Concept Selection

In the concept selection the return of investment has been calculated using semi-empirical method. The preliminary cost estimation includes research and development cost (subsonic 521.5 M$, supersonic 1266.9 M$), manufacturing cost (subsonic 8747.6 M$, supersonic 14977.7 M$) and operating cost (subsonic $2639/h, supersonic $51492/h). The original task is to design a premium light business jet and the following parameters distinguish the Phoenix 5600 from the competitors; the minimum runway distance needed is shorter, the service ceiling is higher and the design will have unparalleled performance of a combination of range and cost. Finally a trade-off is made between the four designs where Design 1 scores highest with a total of 70.6 %. This winning design will be designed in more detail (Class II design) in this Final Report. Its unconventional lay-out makes it the design with the highest originality. Many challenges exist within the design; the goal is to use the advantages of the different design options to create a business jet with unique characteristics, distinguishing itself from the competition.

3 Functional Analysis

The functional diagrams, which are updated during the design process, are described in this chapter. Section 3.1 describes the updated functional flow diagram, which initially was created in the beginning of the design process. Section 3.2 discusses the updated functional breakdown structure.

3.1 Functional Flow Diagram

The Functional Flow Diagram (FFD) shows the logical order of functions the product must perform. The diagram is shown in Figure C.1 of Appendix C. The relationships between various functions offer a clear overview of the mission of the business jet. In the FFD some functions are performed in the same logical step, this is shown by an [and]. In some steps the flow could only perform one function, while multiple functions are possible; this case is shown by an [or]. A decision making function is required to decide when the functional flow splits up. In the FDD this happens by a computer and is shown by a [comp], the decision in this FDD is based on the decision speed.

3.2 Functional Breakdown Structure

For the determination of all functions that the aircraft system has to perform, creating a Functional Breakdown Structure (FBS) can be helpful. Unlike a Work Breakdown Structure, the FBS is a function-oriented tree instead of a work-oriented tree. In a FBS, the operations that have to be performed by the system are tree-wise structured, starting with the main functions of the system, and going further into detail on the lower levels of this tree chart. As can be seen in Figure D.1 of Appendix D. The main functions of the business jet system are part of the mission profile (i.e. Take-Off, Cruise, Maneuver and Landing). During these stages of flight, several subsystems interact to achieve the desired aircraft performance. The functions that the subsystems have to fulfill are listed in the sub-levels of the FBS.

Outside the main stages during flight, passengers and luggage have to be able to enter and exit the aircraft efficiently. When passengers are seated, their journey has to be fulfilled in the right level of comfort. Moreover, maintenance will be an important factor during the life cycle of an aircraft. The accessibility for aircraft maintenance is crucial, because the longer the aircraft is grounded, the higher the operating costs. Maintenance is categorized in different checks with service intervals that can be daily up until several years. The more frequent the check-up, the more general the inspection. The daily check is, for instance, very global. On the other hand, during the D check every part of the aircraft will be disassembled and gets a detailed check. The design has to allow for easy access and inspection for all different check-ups.

4 Resource Allocation

The resource allocation will be elaborated in this chapter. Especially technical resources tend to grow during the aircraft programme. For this reason a maximum value is established at the beginning if possible. This includes a reserve which is carefully managed during the entire project. The budget breakdown of the cost (Section 4.1), mass (Section 4.2) and zero-lift drag (Section 4.3) will be discussed.

4.1 Cost Breakdown

One of the aspects regarding the resource allocation is the cost. At the first stage of the aircraft programme a target value of the aircraft has been established which can be found in the Project Plan [2]. The target price of the future designed aircraft has been listed at a price of 16.0 M$ using data from other existing aircraft on the business jet market. The aim is to not exceed competitor price by 25%, which also has been taken as the contingency value [3]. The price of the aircraft has been listed to be between 16 - 20 M$.

At the second stage of the aircraft programme the budget has been estimated using semi-empirical data based on statistical data of existing aircraft. Only a few details of the design were known, the method of using parametric estimations provided a possibility to estimate the cost using limited details. The list price of the Phoenix 5600 has been estimated at 13.9 M$ per aircraft during the conceptual phase of the aircraft programme in the Baseline Report [4].

At the third stage of the aircraft programme a new list price has been estimated. This has been determined in the Midterm Report at 18.5 M$ which was 2.5 M$, or 16% higher than the estimated value in the previous phase [1]. This value has been estimated using 2.5 M$ has been used from the 4 M$ of available reserve.

After the concept has been chosen the aircraft components can be determined more specific. Current price such as avionics and man hour wages have been looked up to increase the accuracy of the total price of the aircraft. The large difference between the list price of stage two and three can explained by the fact that detailed knowledge of the aircraft component weights was not known during the Class I design in stage two. Roskam VIII Chapter 3 Equation 3.5 has given another method, which required only the $W_T O$, to estimate the aircraft component weights [5]. In stage four, when more details were known, Roskam VIII Chapter 3 Equation 3.4 has been used to calculate each aircraft component weight.

More details about the cost estimation of the Phoenix 5600 can be found in Chapter 19. The list price of the Phoenix 5600 is estimated to be 15.9 M$. The list price of the Phoenix 5600 during each stage is summarized in Table 4.1.The list price and the remaining reserve for each phase are depicted in Figure 4.1.

Table 4.1: List Price Estimation and Reserve

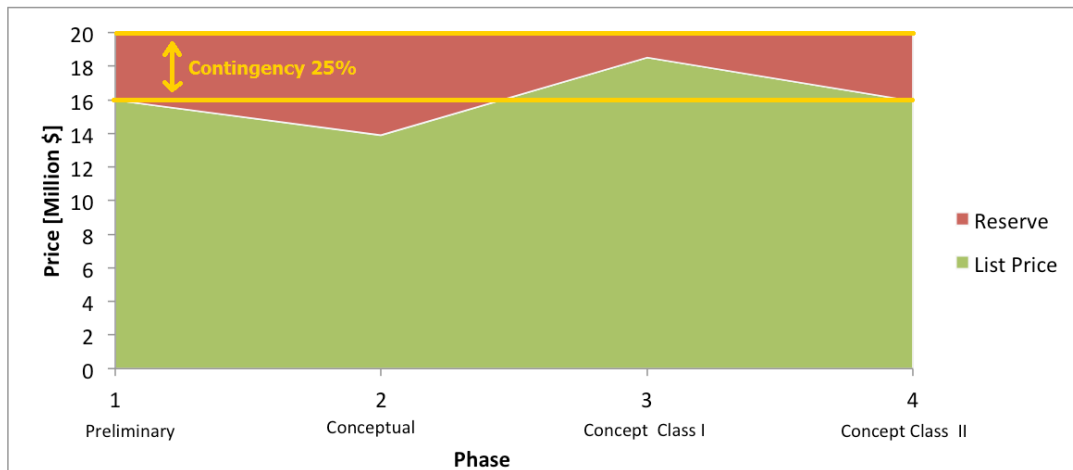| Phase	List Price [M\$]	Reserve Left [M\$]
Preliminary	16.0	4.0
Conceptual	13.9	6.1
Concept Design Class I	18.5	1.5
Concept Design Class II	15.9	4.1

Figure 4.1: List Price and the Reserve Development

From Figure 4.1 it can be concluded that the list price has been estimated accurate. The list price was estimated to be 16.0 M\$ at the first stage of the programme. At the end of the fourth stage 15.9 M\$ has been calculated to be the list price of the aircraft. This is 0.1 M\$ less than the initially estimated list price, which makes the aircraft even more competitive in business jet market.

4.2   Mass Breakdown

Another aspect is the MTOW of the Phoenix 5600. First the boundary of the MTOW of the aircraft was determined to be less than medium business jet [2]. It was determined that the MTOW should be less than 16000 kg.

During the second phase an estimation of the different weight components such as the OEW, payload and fuel have been made. Using reference data the mass of the different aircraft components can be estimated [4]. For the estimation of the aircraft component mass Aircraft design, Kundu has been used [6]. The choice of a contingency of 33% has been based on Table 3-4 in the Goddard Space Flight Center, Green book [7].

At the third stage of the aircraft programme the Class I weight estimation of Roskam has been used [8]. This resulted in a more accurate weight estimation of different components of the aircraft. During the final stage the Class II weight estimation of Roskam has been used [9]. Class I and Class II have many similarities, thus the weight estimations do not divert much from each other. A more detailed mass breakdown of the Phoenix 5600 can be found in Chapter 13.

The mass breakdown of the MTOW of Phoenix 5600 during each stage is summarized in Table 4.2.A more detailed mass breakdown and the remaining reserve for each phase are depicted in Figure 4.2.

Table 4.2: Mass Breakdown During the Design Phases

Phase	MTOW [kg]	Reserve Left [kg]
Preliminary	N/A	16000
Conceptual	11239	4761
Concept Design Class I	8835	7165
Concept Design Class II	9066	6934
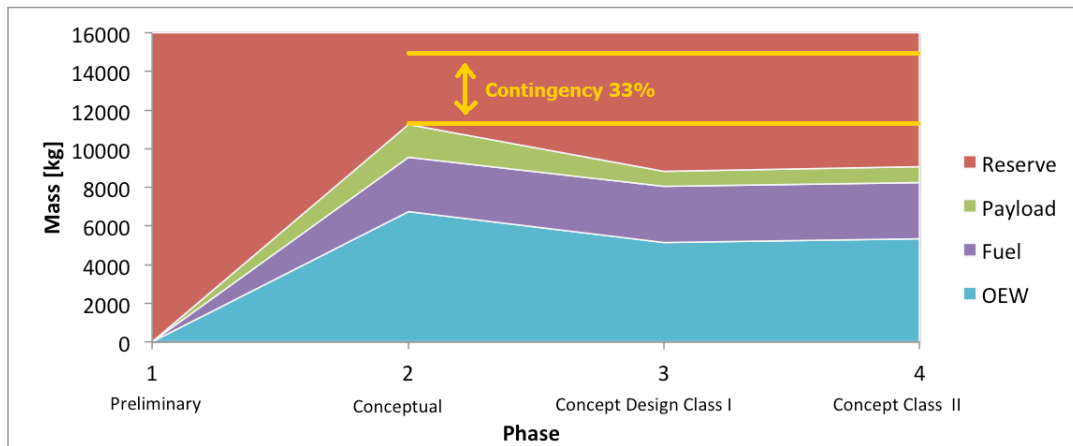
Figure 4.2: Mass Breakdown and Reserve Development

Figure 4.2 shows the development of the aircraft weight components. The mass breakdown of the third and fourth phases looks similar. The MTOWs calculated with Class I and Class II method have a difference of less than 3%. From the market analysis it has been concluded that priority on range and speed are the driving factors of the demand of new business jets models. This aims the design to be a light-weight, thus a low weight is favorable. The contingency has not been used in stage three and four, but it is important to have a contingency to allow the mass to grow in future design phases.

4.3 Drag Breakdown

The zero-lift drag C_{D_0} distribution has been introduced in Chapter 11. No requirement on the zero-lift drag has been set up at the start of the programme, it was not possible to establish a margin in which the zero-lift drag can grow. The zero-lift drag distribution over several aircraft components is shown in Figure 4.3.

Figure 4.3: Drag components breakdown

5 Market Analysis

Before the start of designing a technical product, it is essential to perform a market analysis. This analysis will investigate the opportunities for the product in the current and future market. The goal is to determine necessary characteristics and aspects of the product in order to be competitive in its market. Potential consumers will be identified and opportunities in terms of price and range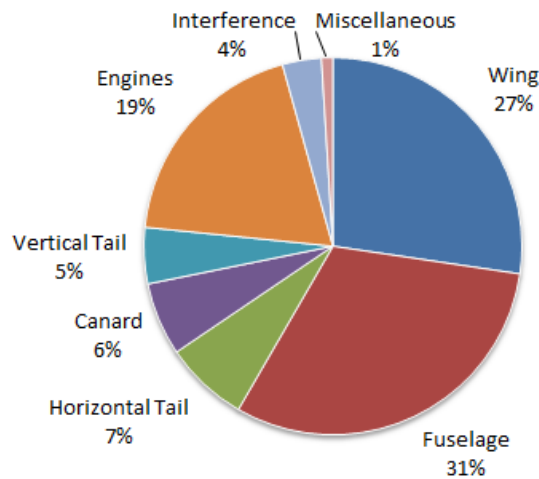 will be given. The market analysis is already performed in a previous stage during the design process. In this chapter the most important findings are presented. For more elaborate data on the market analysis one can consult the Baseline Report [4] and the Midterm Report [1]. In Section 5.1 a global market overview is presented with its opportunities. Section 5.2 discusses the main competitors in the market and Section 5.3 gives an overview how the designed business jet outshines the competition.

5.1 Global Overview

In this section, a summary of demands, period of business jet usage, growth, preference of specific types and purchase expectations will be presented for all geographical regions. All of the provided data below was retrieved from NBAA [10].

Figures 5.1 and 5.2 illustrate the business jet delivery forecast in units and in value respectively. As can be seen, the demand in both units and value dropped after crisis in 2008. Until 2011, there was an evident decline in demand, after which it began to slowly recover after 2012. Assuming absence of global catastrophes or economic crisis in the next 10 years, the predicted number of units that will be produced between 2013 and 2023 is about 9250 business jets. This value corresponds to approximately 260 B\$. The number of light-medium aircraft units delivered is estimated at 200-400 units per year 2020 till 2023. The Phoenix has an estimated delivery rate of 36 units a year, this results in a share of 9-18 % of the light-medium deliveries. Section 5.3 compares the Phoenix 5600 with its competitors, it will be made clear that the Phoenix has a much better performance while having a similar list price.
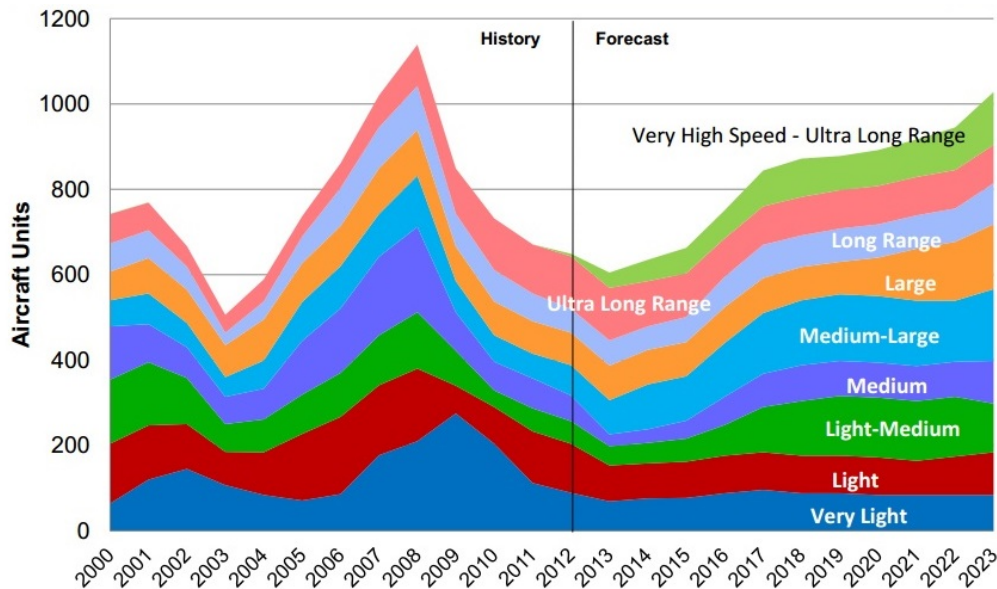
Figure 5.1: 2013 Business Jet Delivery Forecast in Units [10]
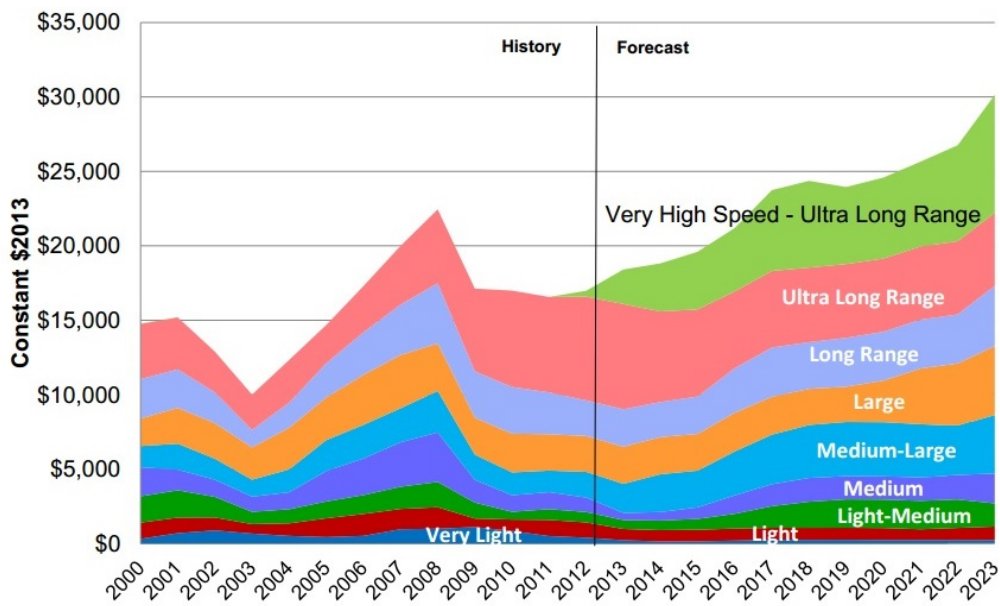
Figure 5.2: Business Jet Forecast Delivery in Value [10]

The business jet manufacturing market is divided into segments based on aircraft range, price and cabin size. There are currently no competitors in the group's ultra-large cabin market. Key competitive factors include aircraft safety, reliability and performance, comfort and in-flight productivity, service quality, technological and new-product innovation and price [11].
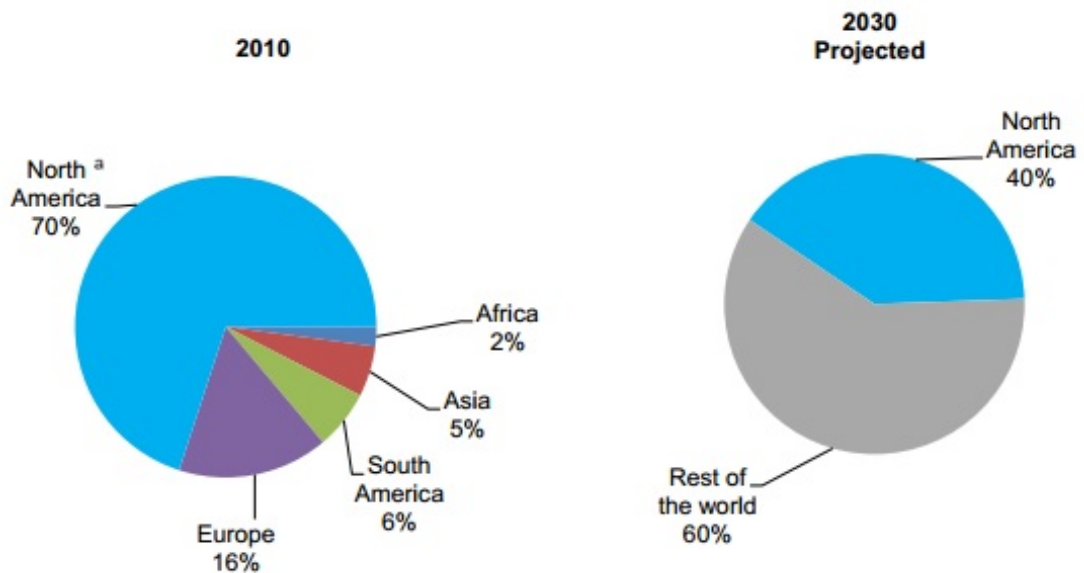
Figure 5.3: Business Jet Forecast in Delivery Value [12]

Finally, it is worth mentioning that the absolute dominance of U.S. in business jet market is expected to decrease from about 70% in 2010 to only 40% in 2030. This can be observed in Figure 5.3. This means that other regions in the world will become more and more of a threat and challenging competition will lead to optimization of every possible aspect in trade off, especially in the top-requirement list.

5.2 Competitors

Jet Aviation competes in its business-jet aircraft services primarily on price, service quality and timeliness. In its maintenance and repair activities, Jet Aviation competes worldwide with several other large companies, as well as smaller companies, particularly in the maintenance business [11] [12].

The global business jet industry currently consists of six major manufacturers. The U.S. based business jet industry has four main aviation firms: Cessna, Hawker Beechcraft Corporation, Learjet, and Gulfstream Aerospace Corporation, that have accounted for the majority of business jet production in both the United States and the world in recent years [12]. Canada holds another large aviation firm targeted for business jet producers, which is Bombardier. It closely links with U.S. domestic firms for manufacturing purposes. European countries, also represent a large market share. In this case, the top competitor among the companies is Dassault, a French aircraft manufacturer [11].

The stated companies compete globally in the business jet market on basis of the functionality, unique characteristics, and price of their aircraft [11]. There is a constant increase of new barriers for younger firms to enter the industry and market due to the bureaucratic establishment which significantly increases time expenditure on paper work and slows down the production phase for new aviation companies. This allows well-established and reliable companies to take advantage.

There are several top reasons which dictate the demand for new business jet model choices. As can be seen from Figure 5.4, priority on extended range dominates in all regions across the world. The second important reason is large cabin size. Those aspects will influence design choices of future premium business jet. Other reasons include performance, newer technology and brand, which vary in their importance depending on the region. Although not shown in the diagram, another vital parameter is price.
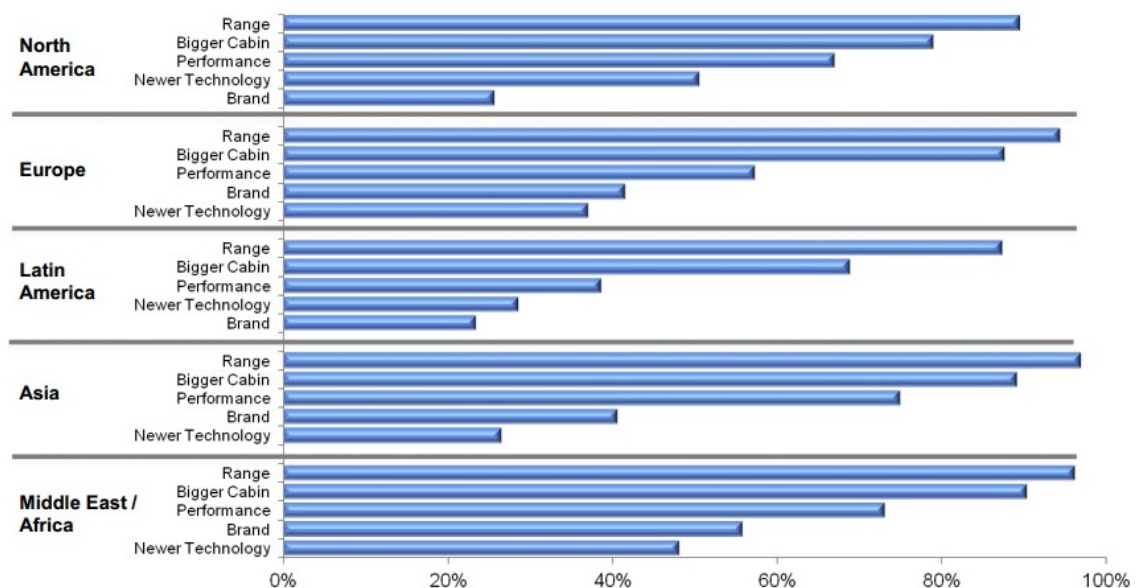
Figure 5.4: Top Reasons for New Business Jet Model Choice [10]

5.3 Differentiation

For a business jet to be successful, it needs to differentiate itself from the competition. In this section it is explained in which way the premium business jet is expected to be competitive.

5.3.1 Minimum Runway Distance

The minimum runway distance is an important parameter for business jets and one of the pillars of the design. When a business jet is able to land and take-off from a short airstrip, it will enable the business jet to reach more airports around the world. Especially for business jets, this is a favorable property, because the passengers might now land even closer to their destination, which will save time and in the business world, time is a valuable good. The required runway length of the subsonic business jet is 1000 m. The average runway length of the subsonic reference aircraft is 1277 m [4]. These minimum runway length is compared with a database of airport runway lengths around the world [13]. The results of the runway length analysis are once more summarized in Table 5.1. It can be concluded that the increase of landable airports for the subsonic design is 3 %.

Table 5.1: Results from the Runway Analysis

	Number of Landable Runways	Number of Not Landable Runways	[%]
Subsonic jet design	926	10	99
Average reference subsonic jets	898	38	96

5.3.2 Price

The target customer for whom the business jet is designed is expected to be wealthy, still it is very important to set a competitive price to increase the number of sales. So besides the landing distance, the selling price should be as low as possible without losing its profitability. The detailed cost estimation is performed in Chapter 19. The list price of the subsonic business jet is estimated to be $ 15.9 M. In Figure 5.5, the cost of the business jet and the reference jets are plotted with respect to the range.
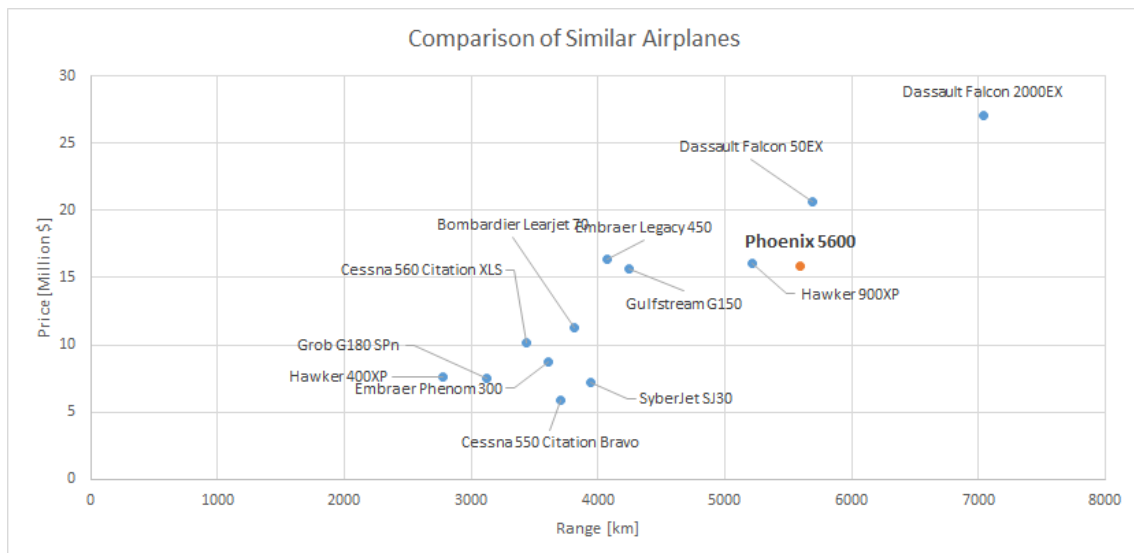
Figure 5.5: Competition With Respect to the Selling Price

It can be seen that the subsonic jet has an unmatched combination of range and cost. For the subsonic reference jets, the Dassault Falcon 50EX is the jet that comes closest to the design business jet. But this jet costs 3 M$ more. In Chapter 19, the average annual delivery per aircraft type of the reference data is
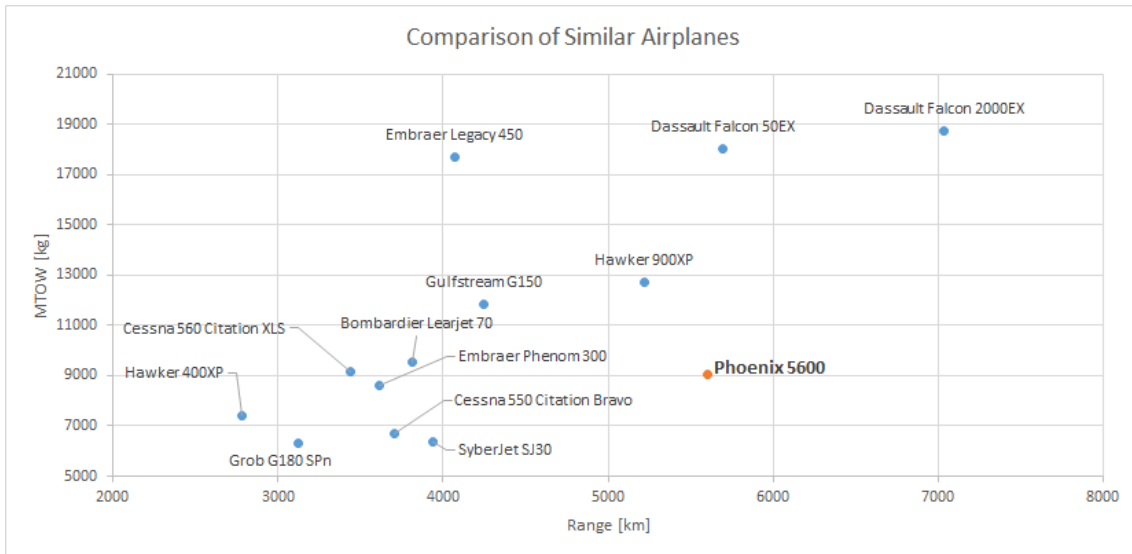
Figure 5.6: Competition With Respect to the Mass

estimated to be 36 units per year, which is, considering the unique qualities of the Phoenix 5600, at least the expected amount of units that will be sold per year.

5.3.3 Mass

The mass of the aircraft, as stated before, should remain under 16000 kg to be able to fit in the CS25 regulation range. The business jet Phoenix 5600 will weigh approximately 9000 kg. The comparison of the weights of the aircraft with respect to the range can be seen in Figure 5.6.

5.3.4 Speed

As stated in the introduction; 'time is money'. Hence, the speed of the aircraft is important in order to be competitive in the business jet market. The speed of the reference business jets and design business jets are plotted with respect to their range in Figure 5.8.
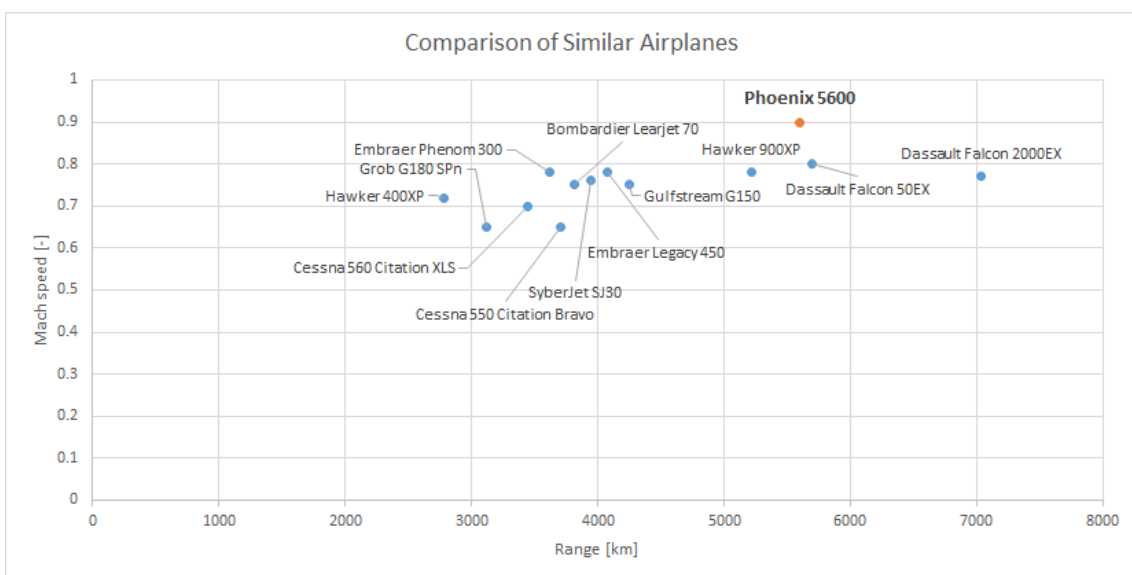
Figure 5.7: Competition With Respect to the Speed

As can be seen in the figure, the subsonic business jet design is faster than all its competitors, and can fly further than most. This is good promotion material and makes the design 'premium'.

5.3.5 Seat Comfort

The maximum duration of a flight for business jet will be around six hours, still it is required for the passengers to have some comfort during the flight. One way to express the comfort is the available seat width. The seat width of the subsonic business jet is designed to be 60 cm. Comparing width the seat width of the business class and first class of other aircraft, the subsonic seat can be labeled as very luxurious.
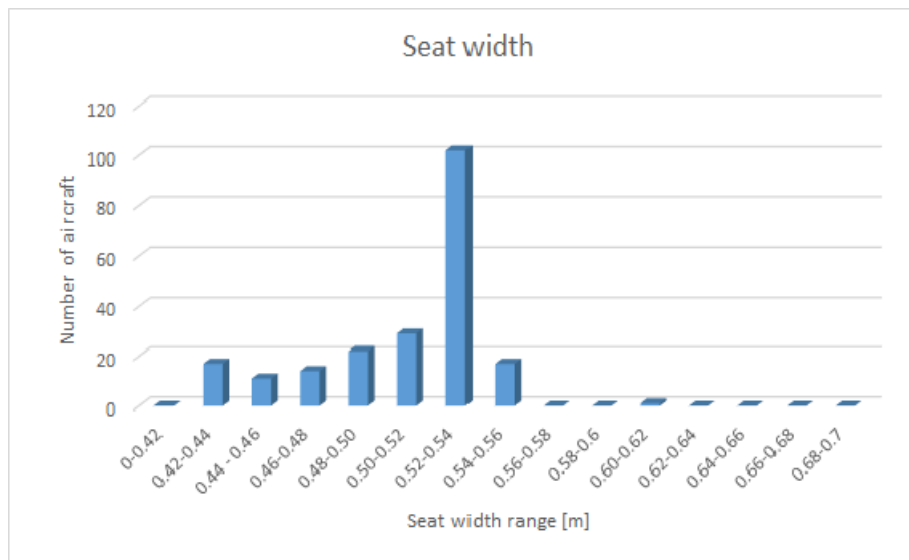
Figure 5.8: First and Business Class Seat Width (distance between armrests)

5.4 Conclusion

In conclusion, the business jet market analysis shows that a significant growth in the last two decades has occurred, driven by an increasing demand of corporations for business jets and the global recognition of the utility of business jet travel. In some cases, business aviation has become an alternative to commercial air transport, allowing users to travel to multiple locations in a single day, to continue working while in flight, and to reach destinations that are underserved by commercial airlines.

Despite positive trends, the recent economic recession has affected the demand for business jets drastically. The two largest markets for business jets, North America and Western Europe, experienced the greatest impact, which disproportionally affected the market for light and medium-sized jets. A bright spot in the overall demand picture is the growing interest for business jets in the emerging markets of Asia, Eastern Europe, Latin America, the Middle East, and Africa. Even while the business jet demand in these regions is relatively small in proportion to total global demand, forecasts predict this to increase rapidly, and will most likely drive future expansion of the business jet market.

The Phoenix 5600 provides different possibilities for different customers. The cabin can be customized to the customer's preference, the range provides enough distance for domestic and intercontinental flights. The Phoenix 5600 targets both corporations and private users.

From the analysis done in this chapter, it can be concluded that the business jet will be especially 'premium' with respect to the speed-range combination. It will be the fastest business jet available with a range which only one other business jet can match.

Part II

Design Approach

6 Operations & Logistics

A completed overview of the required operations & logistics of the Phoenix 5600 is presented in this chapter. The concept of operations and logistic processes are illustrated in the form of flow block diagrams in order to identify system characteristics that must be part of the design. The importance of this chapter is to identify what personnel and tooling are required for the operations of the aircraft. Section 6.1 describes the overall operations and logistics for the Phoenix 5600. Section 6.2 specifies on the maintenance process.

6.1 Operations & Logistics Concept Description

In order to describe the full cycle of airport operations, (functional) flow block diagrams are set up. These diagrams describe the different operational scenarios that the aircraft will go through from the hangar to take-off, from take-off to engine shutdown after the flight. The process can be divided in three parts: the first part of the process is the departure of the aircraft till the destination of the aircraft, the second is the loading and maintenance process and the third is the initiation of a new flight or the storage of the aircraft.

In the first part the aircraft is on the airport ready to start the taxi out and to arrive at the final destination. The aircraft will start taxiing to the designated runway on which the aircraft will take off. The aircraft will perform its mission. The first part of the operation activities is shown in Chapter C.

In the first part the aircraft is either already on the airport or in flight and will attempt to land at the final destination. The aircraft will begin the descent and is either able to land, or this is impossible due to complications at the airport and/or landing strip. Either the aircraft can try again at a later stage to land or has to go to an alternate airport. In both cases the aircraft will need fuel reserves. When the aircraft has finally safely landed it will taxi in and stage two can begin.

The second part consists of unloading and/or replacements; deboarding of the crew and passengers, baggage handling but also the cleaning of the aircraft, catering to restore food and drinks supply, fresh water replacement and sanitation making the aircraft ready for the next flight. The flow block diagram is shown in Figure 6.1.
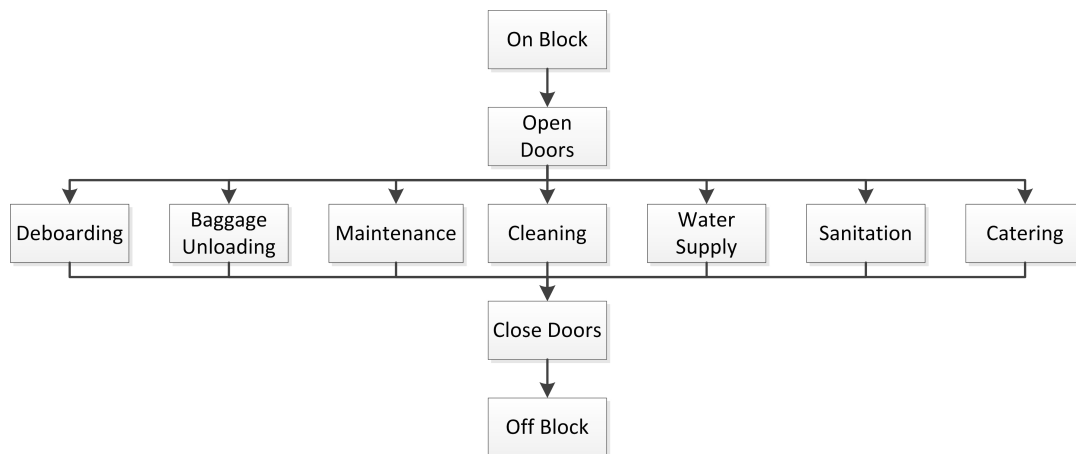
Figure 6.1: Flow Block Diagram of Ground Operations

The third part includes either making the aircraft ready for the next flight or the aircraft will be stored in the hangar. If a next flight is planned the aircraft is fuelled and the baggage is loaded. Simultaneously, the crew and passengers can board the aircraft. The doors will be closed after the aircraft is loaded. The aircraft will be de-iced if snow and ice have formed on the aircraft. Then the aircraft is able to taxi and take off again. The ground operations for take-off will consist of pre-flight checks, communication with ground control and the configuration of the aircraft for take-off. Following, the aircraft will line up at the runway, accelerate to rotation speed, rotate and climb out. In case of a one engine failure, the aircraft will

need to minimize altitude and speed. If so, using auto rotation, the aircraft will be able to return safely. If the aircraft is stored, the flight will be ended following by taxi to ramp and an engine shutdown. Normally, the aircraft is stored in the hangar to ensure space at gates for operational aircraft is available.
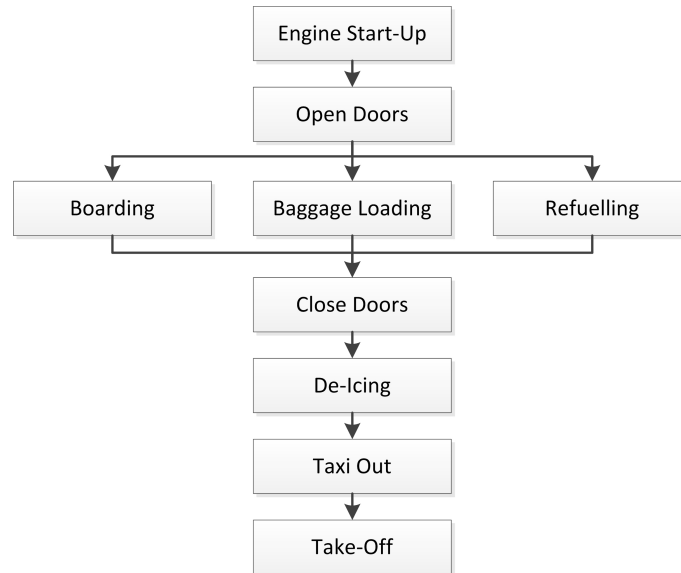
Figure 6.2: Flow Block Diagram of Aircraft Preparations

The maintenance process is rather complex as it consists of different stages and levels of detail. It is essential to form a general concept of the maintenance process in order to identify components that make a contribution to the operational activities of the designed system. In the next section, flow diagrams that illustrate the maintenance activities are given and elaborated upon.

6.2   Maintenance Concept Description

The conceptual maintenance process follows a predefined sequence of operating modes. Each operating mode is assessed on required performance, after which it is decided if the aircraft operates satisfactory or not. This is usually done by going through extensive checklists, which cannot be completely defined at this preliminary stage. In Figure 6.3, the decision is represented by either 'GO' or 'NO GO'. In case of satisfactory results, the maintenance sequence proceeds to the next operating mode. In case the aircraft does not meet the performance requirements, a maintenance iteration is initiated. This iteration consists of the identification of the fault up to unit level with the appropriate maintenance reaction. A faulty unit can be directly replaced, repaired on spot or removed and transported for repair and reintegration. This last option is defined as base maintenance.
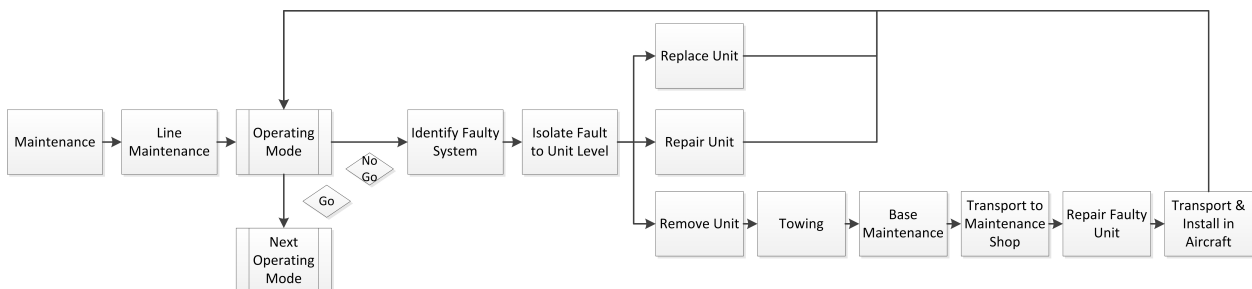
Figure 6.3: Flow Diagram of Maintenance Activities

The sequence of operating modes is illustrated in Figure 6.4. More information on the systems of the Phoenix 5600 is available, a refined sequence of the maintenance will be provided. The sequence is a combination of blocks in parallel and series. The electrical system and propulsion system are checked individually, as these checks would otherwise interfere with others. For example, checking the exterior of the aircraft for structural integrity and damage cannot be executed simultaneously with the propulsion system check.
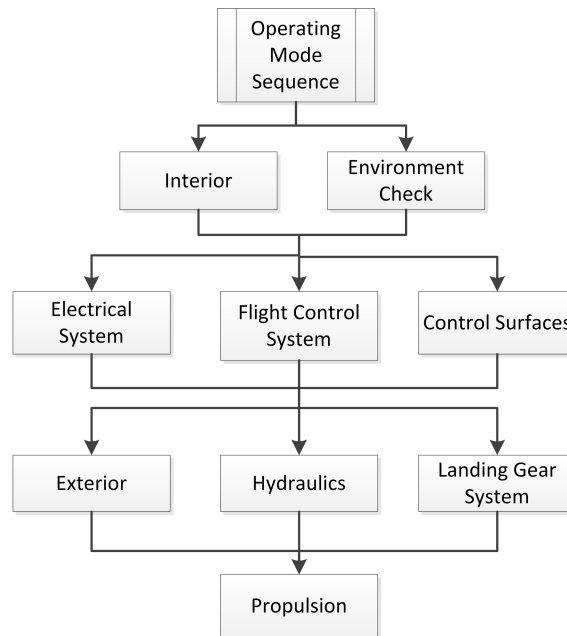
Figure 6.4: Flow Diagram of the Maintenance Operating Modes

7 Sustainable Development Strategy

The population of the world has grown and keeps on growing. More resources are used and consumed to satisfy people demands. According to Eurostat [14], each of the households living in the European Union generates a daily average of 1.4 kg of waste, or approximately 500 kg per year [15]. Yet, waste generated from other human activities such as manufacturing, waste supply, transportation and energy production have not been taken into account. All these human activities have a huge impact on the environment and also contribute to the increase of CO_2 level, which is the most important greenhouse gas emitted by human activities. The environmental awareness continues to grow and sustainable development is becoming more and more important. The important aspect is that people need to change their behavior towards the use and management of resources. In the Midterm Report [1] an approach with respect to sustainable development is stated. This chapter elaborates on this approach in more detail. The way sustainability is taken into account in the design process and the way the product contributes to sustainability will be addressed. Newly designed products are assessed at every aspect through its entire life cycle. The life cycle of an aircraft can be divided into three phases: the design of the product (Section 7.1), the use of the product (Section 7.2) and the disposal of the product (Section 7.3).

7.1 The Design of the Product

Materials: One of the aspects is to choose the material used wisely. The choice of the materials used influences the way how sustainability is achieved. First of all, several materials have been chosen based on their properties and the purpose of the product to be made. The production of the materials also needs to be taken into consideration with respect to sustainability. The materials aluminum alloys, titanium and carbon fiber reinforced polymer (CFRP) are used. However, recycling CFRP is difficult because of their complex structure of fibers, matrix and fillers [16]. Polymers of thermoset composites cannot be remolded [17]. The thermoset composites can be grinded into small pieces. The reinforced fibers can be separated and reused in new products. The resin and filler can be used as filler for other applications. Thermoplastic composite material can be reused by chopping the material into smaller pieces [18]. It can then be reheated, re-injected and reprocessed into a new product. These processes require a lot of energy. The main drawback of recycled CFRP is that the mechanical properties are less than its original material. Research on the scalability of CFRP is still going on. The aircraft will be mainly made of aluminum alloys[19]. Aluminum alloys can be recycled to a high grade using re-fusion technology [20]. More on material selection can be found in Section 12.1.2, Section 12.2.3 and Section 12.3.4.

**Paint:** In order to prevent the aircraft surface from corrosion, paint will be applied. In order to apply paint, the aircraft surface needs couple of preparations and treatments. Over decades chrome-based paint and treatments were used for corrosion prevention. A new paint SOCOMORE A1855 developed by SOCOMORE and Mankiewicz will be applied on the Phoenix 5600 which is more eco-friendly than general paint for aircraft surfaces, while its performance matches conventional types of paint [21] [22]. The paint and surface treatments of the paint do not contain chrome which has carcinogenic properties to human. The painters will not be exposed to the toxic substances while applying or removing paint.

Manufacturing: Lean manufacturing is a philosophy of minimizing waste. Waste is defined as anything that does not add value, neither to the product nor the stakeholders nor the environment. Minimizing waste leads to higher efficiency and sustainability. Transportation is the effort used to transport components [1]. The transportation process does not add necessarily value to the product, but does induce waste of energy and time. With respect to sustainability, transportation should be minimized as much as possible. The components used for the aircraft are mainly manufactured from the European domestic market. As a result, the environmental impact will be limited, the production costs will be significantly lower and the time wasted will be reduced. A detailed manufacturing and assembly plan can be found in Chapter 22.

7.2 The Use of the Product

Engine manufactures are constantly trying to reduce emissions, noise and specific fuel consumption (SFC). New materials are being developed to reduce engine weight. Research has been done on developing lighter

turbine blades, which give similar performance but will reduce weight. Due to lack of development time, it is not feasible to design a new custom built engine for the Phoenix 5600. An engine design cycle takes between 8-10 years, which will mean that the requirement of being in-flight in 2020 will not be met. Selecting an engine that is already in use will have the advantage that certification for noise and emission regulations is already done.

Noise: In order to protect the environment from aircraft noise pollution, aircraft need to qualify for certification. Noise originating from aerodynamics and the propulsion system need to be taken into account during the design of the aircraft. The regulations for aircraft noise certification levels are defined by the International Civil Aviation Organization (ICAO) which can be found in ICAO Volume I [23]. ICAO Volume I Chapter 3 describes the procedures of noise certification of all aircraft. ICAO Volume I Chapter 4 has adopted new noise level limitations on subsonic jet aircraft which are more strict than the limitations in ICAO Volume I Chapter 3. Noise certification tests are held on ground level near the runway. The measurement series are done at different measurement positions such as during approach, lateral and flyover. For the exact procedure and noise limits during the noise certification test, Midterm Report and ICAO Volume I can be consulted [1][23].

Emission: With growing demand for air transportation each year, global emission from the aircraft industry is becoming a bigger problem. Over the last years engines become more and more efficient which results in less emission. This trend is supported by ICAO, who sets new more strict regulations for aircraft emission every few years. The regulations for the aircraft emission are defined in ICAO Volume II [24], where ICAO Volume II Chapter 2 describes the emission for turbojet and turbofan engines at subsonic speeds. The following type of emissions shall be controlled for certification of aircraft engines:

- **Smoke**
- **Gaseous emissions**
    - Unburned hydrocarbons HC
    - Carbon monoxide CO
    - Oxides of nitrogen NO_x

For the exact procedure and emission limits during the emission certification test, Midterm Report and ICAO Volume II can be consulted [1][24]. The emission of the Phoenix 5600 must at least meet the emission criteria in order to qualify for the certification. The P&W 545C engine is the newest in its series. For this specific engine type precise data on emission is not available in public. However, a trend can be seen that for newer engines emission reduction is around 10% compared to their predecessor. Throughout the design process, the goal is to aim for minimum emission levels, as this minimizes the pollution caused by the aircraft during operation.

7.3   The Disposal of the Product

End of life: One of the aspects of sustainability in the design process is the end-of-life phase of the aircraft. After a service life of couple of decades the aircraft will eventually be withdrawn from service. Huge streams of waste will be generated. An aircraft is equipped with state of the art high technology products which contain a mix of different materials. However, some of those waste products will be wasted if it will not be reused. Actually, those products cannot be classified as waste, it may have intrinsic value. The end-of-life phase of the aircraft should not be overlooked, but should be strictly taken into considerations during the design of an aircraft. Designers need to be responsible for the use and management of the resources. Especially, the planning of end-of-life of the product is of utmost importance [25].

At first, avoid the use of resources if it is possible. If resources have to be used, try to reduce the use as much as possible. When a manufactured product reaches the end of its life cycle, several options can be chosen with respect to sustainability [25]. The choice on the option depends on the nature of the product, the grade of minimizing the environmental impact and the level of minimizing the incurred economic costs which is a trade-off itself. The options are depicted in Figure 7.1 and are stated below. The avoidance the use of material is most preferred; landfilling is least preferred.

- *Reuse* The product of the aircraft will be reused for the same or another purpose. This option is most favorable.
- *Remanufacture* The product will be repaired and refurbished in order to process the original product.
- *Recycle* The product will be reprocessed into a form that can be used for the same type of products.
- *Incinerate* The product will be incinerated to produce heat and energy.
- *Landfill* The product will be dumped into landfills. This option is highly unfavorable and causes much harm to the environment. Landfills cannot add value to the product. The other options may incur costs but can actually gain value e.g. in monetary form. It shall be chosen if the other options are not feasible.

Figure 7.1: Waste Hierarchy

When the options are known, the aircraft needs to be disassembled in different parts. The only options where no disassembly is required are incineration and landfill. The product will simply be incinerated or be dumped into a landfill. First of all, toxic and hazardous materials have to be removed. Special tooling and trained workers are required. This is a costly process which should be avoided beforehand during the design of the aircraft. Then all reusable items and parts of the retired aircraft that are airworthy will be removed, stored, transported and reused for a second life and purpose. Parts such as worn passenger seats can be removed from the aircraft to be further refurbished to other purposes like spare parts for other aircraft or just a seat in a living room. The entire aircraft does not have to be disassembled into the smallest level. Recyclable materials can be grouped together for further processing. This will save up on dis-assembly time and costs. Furthermore, groups of parts which need to be incinerated or landfills do not need to be disassembled. They can be processed altogether.

The market has discovered the opportunities to add value to waste material, business in sustainability. The company AELS (abbreviation of 'Aircraft End-of-Life Solutions'), based in the Netherlands, provides advice on end-of-life solutions and dis-assembly services for retired aircraft. The dis-assembly company may even pay the owner of the aircraft money in return, since highly recyclable material such as metals can be sold to other companies.

Airbus became the first aircraft manufacturer to provide end-of-life solutions for retired aircraft. This project was called the PAMELA, 'Process for Advanced Management of End-of-Life Aircraft', supported by the European Commission [26]. The purpose of the project was to set up a new eco-friendly and safe standards for the management of end-of-life aircraft [20]. It demonstrated that at least 85% of the aircraft materials can be recycled. The end-of-life approach of PAMELA has been divided into three phases: decommissioning, dis-assembly and selective dismantling. First the aircraft needs to be cleaned and decontaminated from toxic and hazardous materials and liquids. Then the water and fuel tanks will be emptied. The reusable parts will be removed during the dis-assembly phase. These will be tested and certified before they are used in other aircraft or purpose. In the final phase of the process the shell of the aircraft will be dismantled. Many materials will be removed from the shell such as foam, plastics, metals and textile. Normally aluminum alloys cannot be recycled for the same product. Since the waste was sent to a process called re-fusion, high grade aluminum can be reuse for aviation manufacturing [27] . PAMELA contributes to a responsible use of resources.

8   RAMS

The reliability, availability, maintainability and supportability (RAMS) characteristics are discussed in this chapter. At this point in the design process, most of these properties will be based on reference business jets. For most RAMS it is too early to give hard numbers and make conclusions about the business jet that is still in its Class II design stage. In Section 8.1, the reliability of the Phoenix 5600 will be discussed. This is followed by a description on availability in Section 8.2. Section 8.3 gives an elaborate overview on aircraft maintenance. Finally, in Section 8.4 supportability with respect to accessibility & engines will be discussed.

8.1   Reliability

The reliability gives an indication for the business jet to maintain its functionality when it is used as specified. This excludes accidents caused by pilot incapacitation, hijacking, sabotage or the air traffic controller. The reliability can be expressed as mean time between failures (MTBF). For the design business jet, no value can be given since it is not operational yet. More on reliability can be found in Section 17.3 discussing the fault tree analysis. In this fault tree analysis the causes, or combination of causes that lead to a top event are investigated in order to find the short critical base events.

8.2   Availability

The availability of the business jet gives insight in the relative amount of time of which the jet is functioning (not-broken). Once more, this value cannot be expressed for the designed business jet, but only for reference jets. The availability of aircraft is not made public by aircraft manufacturers. Therefore, no availability analysis can be done at this point.

8.3   Maintainability

The maintainability is related to the ability of the business jet to be restored when a specific maintenance task is performed as required. The maintainability can be expressed in the form of mean time to repair (MTTR). This specifies the total corrective maintenance time divided by the total number of corrective maintenance actions. Reference aircraft were analyzed to find information about the MTTR, but as for the availability, no information can be found on the MTTR of reference aircraft. In general aviation, the maintenance proceedings are divided into maintenance pre-flight, A,B,C and D checks [28]. The checks are ranked from least time-consuming to very time-consuming. Every higher level check includes the lower level checks. So, when the B level check is performed, both the A check and maintenance pre-flight have been executed. At the end of the section, an overview is given of all the checks and their characteristics

8.3.1   Maintenance Pre-Flight

The maintenance pre-flight is performed, as the name suggests, every time before the flight. It consists of a walk around the aircraft, checking for obvious damage. The general condition and security is checked and aircraft log is reviewed for discrepancies and corrective action. No special equipment or tools are required for this check and it takes little time to perform.

8.3.2   A Check

The A check is one step higher than the maintenance pre-flight. This check usually requires a maintenance station. Certain items will be checked and serviced by opening access panels. Examples of other checks that are performed during the A check are listed below. The A check is performed every 200 to 400 cycles.

- Check crew oxygen system pressure
- Operationally check emergency lights
- Grease actuator systems for landing gear

- Test the flap/slat electronics unit

8.3.3   B Check

The B check is a more detailed check than the A check. This is the highest check in which no components will be disassembled or removed. The B check will be performed every four to six months.

8.3.4   C Check

The C check is the first check which can be categorized as a heavy check. In this check, the individual systems and components are thoroughly checked for serviceability and function. This check is performed both visually and operationally. The C check is performed every 20 to 24 months and takes around 3 to 5 days. Examples of checks that are performed during the C check are listed below.

- Check the condition of entry door seals
- Check the flap asymmetry system
- Inspect engine inlet for cracks

8.3.5   D Check

The D check, also referred to as the structural check, is the most extensive check. During this check, the aircraft structure will be thoroughly checked by non-destructive tests. The tests reveal evidence of corrosion, structural deformation, cracking and other signs of deterioration. For these tests, the aircraft is extensively disassembled. This check occurs approximately every five years and takes about two months to complete. An example of a tool used for this D check is an X-Ray-tool to search for hidden cracks and other defects inside the material.

8.3.6   Maintenance Overview

A brief overview of all the maintenance checks is given in Table 8.1.

Table 8.1: Maintenance checks overview [29]

Check Type	Check needed every	Time required	Level of detail	Examples
Pre-flight	24-60 Hours	15-30 Minutes	very low	Check fluid levels, check visual damage
A	7-9 Days	0.5-1 Day	Low	Check servicing oil, filter replacement
B	4-6 Months	1-3 Days	Medium	Detailed systems check and operational checks
C	20-24 Months	1-2 Weeks	High	Minor structural inspection, test HLD system, APU check
D	5 Year	2 Months	Very High	Inspect stabilizer attach bolts, detailed inspection of wing box

8.4   Supportability

This section discusses the supportability of the Phoenix 5600. The accessibility and the engines will be discussed in more detail.

8.4.1   Accessibility

The supportability of the business jet is related to the ability to support the required resources for the execution of the specified maintenance task. Since the supportability for the Phoenix 5600 more or less coincides with conventional aircraft, no real problems are expected. The only difference is that the design has an additional canard, besides a horizontal tail. Both engines are mounted aft of the wing on the top side of the fuselage, which will make them harder to access to perform maintenance. But for business jet aircraft, this is a conventional configuration. The design has a low wing configuration, which makes it easier to access for refueling. A downside of the low wing is that ground personnel have to make detours around the wing.

8.4.2 Engine

The Phoenix 5600 uses the PW545C engine which is an existing engine. The Cessna Citation XLS+ is also equipped with the PW 545C. The Citation XLS+ has reached 575 units sold and is used internationally. The maintenance checks at airports and/or special maintenance services are currently already equipped with tooling to maintain and operate the PW 545C. The availability of spare parts is high, not only does the XLS+ use the same engine also many other aircraft(Citation Excel, Citation Bravo, Citation Encore+) use the PW 500 series. Many parts in the PW 500 series are similar and can be used for either one of the products from the PW 500 series. Pratt & Whitney owns more than 30 designated service facilities around the world, this improves the supportability as well.

Part III

Design Synthesis

9 Sensitivity Analysis

In this chapter, the sensitivity analysis of the business jet design is performed. This is done by determining the effect of input parameters on the MTOW. It is an important step in order to find out which parameters drive the design. It can also be useful in a later stage of the design process to predict the effect on the MTOW when some alternations have to be made to the input values. The method to find the sensitivity is obtained from Roskam I [8]. An explanation of this method can be found in the Midterm Report [1]. First a sensitivity of the MTOW is performed in Section 9.1, followed by an interpretation and discussion in Section 9.2. In Section 9.3 the sensitivity analysis is performed on the configuration. Conclusions and recommendations are stated in Section 9.4.

9.1 Resulting MTOW Sensitivities

The sensitivity of the MTOW with respect to the payload, empty weight, specific fuel consumption, L/D and speed can be calculated. The resulting sensitivities can be seen in Table 9.1.

Table 9.1: The result of the sensitivity analysis

Parameter	Value	Unit
Payload sensitivity	5.7	kg
Empty weight sensitivity	0.20	-
Range sensitivity	1.9	kg/km
Endurance sensitivity	2300	kg/hrs
L/D sensitivity	-1600	-
Specific fuel sensitivity	190,000	$1/kg/hr$
Speed sensitivity	-51	$kg/m/s$

9.2 Interpretation & Discussion

To obtain a better idea of the impact of certain sensitivity values, the values will be scaled to obtain a better insight of their impact on the MTOW.

9.2.1 Payload

To have a better insight in the influence of the payload on the MTOW, one could try to obtain the impact of increasing the number of passengers by one, while keeping the other mission specifications the same. In this case, the increase of MTOW can be obtained by using Equation 9.1. It can be seen that, if it is decided that an extra person is added, the estimated increase of the MTOW is 570 kg or 6.5%.

$$\Delta MTOW = \frac{\delta W_{pl}}{\delta MTOW} \cdot W_{passenger} = 570[kg] \quad \textbf{6.5\% increase} \tag{9.1}$$

9.2.2 Range Sensitivity

For the range sensitivity, an increase of 100 km above the mission range is assumed (i.e. from 5600 to 5700). The increase of the MTOW is estimated in Equation 9.2. It can be seen that the MTOW will increase by 190 kg or 2.2%.

$$\Delta MTOW = \frac{\delta R}{\delta MTOW} \cdot 100 = 190[kg] \quad \textbf{2.2\% increase} \tag{9.2}$$

9.2.3 Endurance Sensitivity

The business jet is not designed for long endurance but one does not want the aircraft to get into trouble when the loiter phase suddenly has to be doubled. The current loiter time is still rather generous and it can be checked what the effect will be if this value will be halved. (i.e. from 0.5 hr to 0.25 hr). The impact of the halved loiter time is calculated in Equation 9.3. It results in a decreased MTOW of 575 kg or 6.3%.

$$\Delta MTOW = \frac{\delta E}{\delta MTOW} \cdot -0.25 = -575[kg] \quad \textbf{6.3\% decrease} \tag{9.3}$$

9.2.4 L/D Sensitivity

The L/D value is mainly determined by the performance of the wing. It is favorable to obtain a high value to make the aircraft fly efficiently. Since the L/D value can only be estimated in the design phase, it would be desirable to be able to predict the changes of the MTOW when the L/D value turns out to be 5% lower than expected. For the subsonic case, this is calculated in Equation 9.4. The resulting weight change is -1600 kg or 11%. This weight change is quite significant. Though it could be expected since the L/D value works throughout the entire cruising phase which is relatively long for the Phoenix 5600.

$$\Delta MTOW = \frac{\delta \frac{L}{D}}{\delta MTOW} \cdot 12 \cdot 0.05 = -960[kg] \quad \textbf{11\% decrease} \tag{9.4}$$

9.2.5 Specific Fuel Consumption Sensitivity

The specific fuel consumption is mainly determined by the type of engine that will be mounted on the aircraft. A more efficient engine will result in a lower fuel consumption. In this case, it is checked what the effect is on the MTOW when the specific fuel consumption of 0.5 $kg/kg/hr$ is increased by 0.01 $kg/kg/hr$. The result for the subsonic business jet can be seen in Equation 9.5. An increase of 0.01 $kg/kg/hr$ in specific fuel consumption results in a relative increase of 21.0%. The disadvantage of choosing an engine with a low specific fuel consumption is the large size of the engine. A low specific fuel consumption is usually obtained by using a high by-pass-ratio. This will increase the drag caused by the engines and it will add up to the load the fuselage should hold.

$$\Delta MTOW = \frac{\delta c_j}{\delta MTOW} \cdot 0.01 = 1900[kg] \quad \textbf{21.0\% increase} \tag{9.5}$$

9.2.6 Speed Sensitivity

The nominal cruise speed set at Mach 0.9. It can be checked what happens when the aircraft flies 20 m/s faster. This is done in Equation 9.6. It can be seen that the weight of the aircraft will decrease by 1020 kg or 11.3%. But this value is only valid when the other parameters remain the same, while the speed also has a significant influence on the lift and drag, especially when it is approaching Mach 1. Also since the drag increases the required thrust will also have to increase when the speed increases.

$$\Delta MTOW = \frac{\delta V}{\delta MTOW} \cdot 20 = -1020[kg] \quad \textbf{11.3\% decrease} \tag{9.6}$$

9.3 Configuration Sensitivity

Besides the effect on the MTOW, it is also important for designers to obtain an insight in the effect of certain chosen design configurations. Two configuration choices which have been made for the Phoenix 5600 business jet are picked to discuss their effect on the overall design and controllability; the sweep angle and the canard configuration. This analysis will, in contrast with the MTOW analysis, be performed qualitatively since no exact numbers can be given.

9.3.1 Sweep Sensitivity

For the Phoenix 5600 business jet, a sweep angle of -35°(forward swept wing) has been chosen. Forward swept wings are very unconventional for aircraft in general. The choice of using forward swept wing has a big influence on the overall design of the aircraft.

Instead of a flow which moves to the tip of the wing, with forward swept wings, the flow tends to move in the direction of the fuselage. Therefore the wing tends to stall at the root instead of the tip. This an advantage with respect to controllability since the ailerons are located more towards the tip. This means that an aircraft with forward swept wing is better controllable during stall. Also at transonic speeds, the shockwaves appear first at the root, ensuring once more that the ailerons still function properly. Because of the inward flow, less vortices arise at the tip. This will decrease the induced drag of the aircraft. These effects result in less required thrust for the forward swept wing and better roll controllability.

Disadvantages include structural divergence, which is characterized as a torsional reaction to upward bending. Due to the bending load, the wing naturally twists in such a way that the local angle of attack increases at the tips, thereby increasing the tip loading and further increasing twist until the wing eventually fails. So this is a positive feedback system which will introduce high structural loads on the wing of the aircraft. [30] This phenomenon, defined as structural divergence, can be for example countered by aeroelastic tailoring, which is the use of carbon fiber laminates that have combined bending and torsional characteristics needed to counter spanwise twisting.

Another problem which arises when using a forward swept wing is the yawing instability. When the aircraft starts to turn using its rudder, the sweep angle of the inward wing decreases. The decrease of sweep angle results in an increase of drag which will push it further backward. This will cause the yawing maneuver and therefore the Dutch roll to be unstable.

The stall characteristic will also be more unstable when using forward sweep. The stall characteristic tends to be unstable for all swept wings because it will stall first aft of the wing causing an increased positive moment. But it will be more unstable for the forward swept wing since more lift is generated aft of the wing (at the root) and therefore the unstable moment will be larger.

As of 2011, there has been only one civilian jet operational that utilizes forward swept wings, the Hamburger Flugzeugbau HFB-320 Hansa Jet. Opposed to the design that is presented in this report, auxiliary fuel tanks are attached to the wing tips. Only 45 Hansa Jets have been built, ending production in 1973. The aircraft is entirely made of metal materials, which proves that aeroelastic tailoring is not the only solution to torsional divergence. [31]

Figure 9.1: The Hamburger Flugzeugbau HFB-320 Hansa Jet

9.3.2 Canard Sensitivity

A canard is usually used as a replacement for the horizontal tail. As for the horizontal tail, the canard controls the pitch of the aircraft. In contrast with the horizontal tail, the canard should produce positive lift to pitch upward. As the horizontal tail is required to produce negative lift for the aircraft to pitch upward, will cause the required lift to be produced by the main wing to increase.

Because the canard is located at the front of the aircraft, it will produce a downwash flow for the main wing. This will decrease the angle of attack of the main wing locally, which will affect the wing lift distribution. This might affect the controllability of the aircraft.

A big risk that arises when using a canard, is that when approaching stall, the main wing may stall first. If this happens the lift aft of the aircraft decreases which will depend the stall. To guarantee safe pitching stability, the canard will need to stall first, therefore less lift might be produced by the main wing which will increase the required size of the wing.

9.4 Conclusion & Recommendation

Adaptions in the design might be favorable either when the relative effect is very high or very low. As can be seen in the previous analysis, the effect of the L/D, the specific fuel consumption and the speed stand out as rather high values. The specific fuel consumption and L/D are respectively engine and aerodynamic properties which are hard to alter. Though during the further development of the aircraft, if a chance arises in which these values might be increased, this chance should be taken. The importance of these values for the design have now been proven. As for the speed of the aircraft, the effect is only valid when the other design parameters remain the same. However when approaching Mach 1, the drag will quadratically increase. Therefore it has been chosen to not increase the speed of the aircraft. Besides, the Phoenix 5600 is already the fastest compared to its competitors.

For the configuration sensitivity, there are quite some disadvantages to the forward swept wing and the canard. It is probably the reason why these configurations are so unconventional for business jet design. The factor which will have the biggest impact for the forward sweep will be the aeroelasticity effect. It will cause the wing to be very heavy since it will need to be very stiff. This effect will be coped with in Section 12.2 of Chapter 12. Still the design will not be altered due to the sensitivity analysis. One of the main driver currently for the design is originality and therefore it chosen to tackle these problems, instead of evading them.

10 Performance Characteristics

In this chapter, the performance characteristics of the Phoenix 5600 business jet are determined. In Section 10.1 the performance constraint analysis is performed in which a design point will be chosen. After that, loading diagrams will be constructed in Section 10.2 in order to calculate parameters such as dive speed, maneuver speed and maximum load which will be used in Chapter 12 to calculate stresses. A Payload-Range diagram is made for the Phoenix 5600 in Section 10.3. Next, engine specifications of the PW545C are stated in Section 10.4. Finally the performance analysis is conducted in Section 10.5.

10.1 Performance Constraint Analysis

The performance constraint analysis (PCA) is performed to provide initial sizing for the performance characteristics of the aircraft designs. A PCA produces a PCA diagram which implements performance constraint lines which limit the position of the final design point. The design point determines the amount of lifting surface required to provide the required lift and the amount of thrust required to overcome drag during various mission phases and scenarios. Using the output of the PCA, the aircraft engine can be selected and the wings can be sized.

The sizing of the wing area and thrust is done via the wing loading W/S and thrust loading T/W. The PCA diagram generated during the PCA shows the W/S (horizontal axis) versus the T/W (vertical axis). On the diagram the chosen design point, the constraint lines and design points of reference aircraft are shown. The constraint lines determine where the design point can be. During the selection of the design point, the knowledge that a lower thrust loading and a higher wing loading are better is used. A lower thrust loading is better because this requires smaller, lighter (and possible cheaper) engines. A higher wing loading is better because this requires less wing area, so a smaller, lighter wing can be designed. Due to the higher speed requirement, the thrust loading will be higher compared to reference aircraft.

The PCA also gives required C_L values for clean configuration, T/O configuration and landing configuration. A range of C_L will be used in order to create the plots. The position of the design point relative to these lines determines the final values of these C_L parameters.

The following performance constraint lines are implemented in the PCA:

- Stall speed
- Take-off field length
- Landing field length
- Climb gradient (OEI and AEO)
- Cruise speed
- Climb rate

In the performance chapter of the Midterm Report [1], the constraint lines and how they are determined are described. Section 10.1.1 describes the input of the PCA and Section 10.1.2 the output of the PCA. The PCA is performed using MATLAB.

10.1.1 Performance Constraint Analysis Input

Table 10.1 presents the input values used for the PCA. The stalling speed density comes from ISA condition at 5000 ft at a 35°C day. All other values come from the weight regression, mission requirements and Roskam I [8].

Table 10.1: PCA Input Values

Parameter	Value	Unit
Take-off weight, $MTOW$	9065.5	kg
Climb rate, R	22.43	m/s
Landing weight frac., $MLW/MTOW$	0.95	-
Stalling speed density, ρ_{stall}	0.9528	kg/m^3
Landing distance, s_L	800	m
Clean stall speed factor, $f_{clean,stall}$	1.3	-
Take-off field length, s_{TOFL}	1000	m
Take-off parameter, $TOP25$	37.5	ft^3/lbf
dC_{D_0} T/O flaps, $dC_{D_0,TO}$	0.015	-
dC_{D_0} landing flaps, $dC_{D_0,LDG}$	0.065	-
dC_{D_0} landing gear, $dC_{D_0,gear}$	0.015	-
dC_{D_0} Mach divergence, $dC_{D_0,Mach}$	0.004	-
Clean Oswald factor, e	0.85	-
Take-off Oswald factor, e_{TO}	0.80	-
Landing Oswald factor, e_{LDG}	0.75	-
Aspect ratio, A	8	-
Skin friction coefficient, c_f	0.003	-
Number of engines, n_{eng}	2	-
Cruise altitude, h_{cruise}	41000	ft
Cruise Mach number, M_{cruise}	0.9	-
Cruise weight factor, k	0.8	-

10.1.2 Performance Constraint Analysis Results

Using the input data presented in Table 10.1 the PCA diagrams are generated and through an iteration process a design point is chosen for the PCA. Iteration is required because some of the constraint line positions depend on S and T_{TO} which depend on the design point. Figure 10.1 presents the final results of the PCA
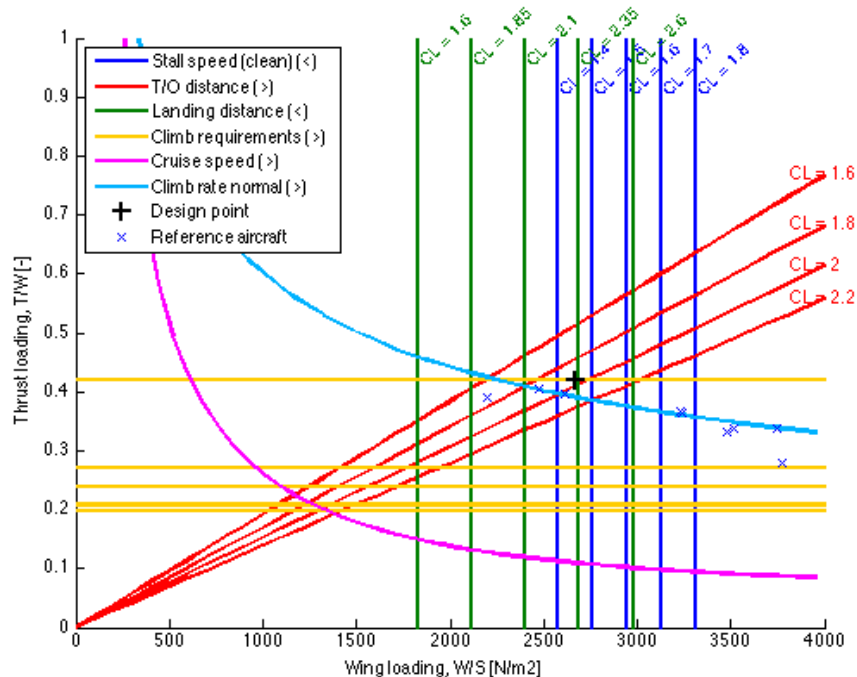
Figure 10.1: PCA Diagram for the Phoenix 5600

Table 10.2: Performance Constraint Analysis Output

Parameter	Value	Unit
T/O thrust loading, T/W	0.42	-
T/O wing loading, W/S	2670	N/m^2
Wing area, S	33.3	m^2
Total T/O thrust, T_{TO}	37	kN
Max lift coefficient clean config, $C_{L_{max,clean}}$	1.47	-
Max lift coefficient T/O config, $C_{L_{max,TO}}$	1.98	-
Max lift coefficient landing config, $C_{L_{max,LDG}}$	2.36	-

10.2 Loading Diagrams

In this section the loading diagrams, also known as V-n diagrams, are constructed for FAR 25 certified airplanes. The V-n diagrams are used to determine design limit and design ultimate load factors as well as the corresponding speeds to which airplane structures are designed. Both the V-n maneuver diagram and the V-n gust diagram are constructed.

In this section various speeds will be determined.

1. V_{S_1} +1-g stall speed of the minimum steady flight speed which can be obtained.
2. V_C design cruising speed
3. V_D design driving speed
4. V_A design maneuvering speed
5. V_B design speed for maximum gust intensity

10.2.1 V-n Maneuver Diagram

First the maximum normal force coefficient $C_{N_{max}}$ and the minimum normal force coefficient $C_{N_{min}}$ need to be determined as is done in Equations 10.1 and 10.2.

$$C_{N_{max}} = \sqrt{C_{L_{max}}^2 + C_{D_{atC_{L_{max}}}}^2} \qquad (10.1) \qquad\qquad C_{N_{min}} = 1.1 \cdot C_{L_{min}} \qquad (10.2)$$

Determination of +1g Stall Speed V_{S_1}
The stall speed is determined using Equation 10.3.

$$V_{S_1} = \left(\frac{2 \cdot \frac{GW}{S}}{\rho \cdot C_{N_{max}}} \right)^{0.5} \qquad (10.3)$$

Determination of Design Cruising Speed V_C
The mission specification calls for a cruise speed of M = 0.9 at 12800 m. This corresponds to 265 m/s at this cruise altitude. However, this is the true airspeed. The equivalent airspeed is different due to the dynamic pressure difference. Therefore a correction factor needs to take place to calculate the cruising speed which is shown in Equation 10.4.

$$V_C = M \cdot a \cdot \sqrt{\frac{\rho_c}{\rho_0}} \qquad (10.4)$$

Determination of Design Diving Speed V_D
The design diving speed is determined using Equation 10.5. The intersection of V_D and $n_{lim_{pos}}$ results in point D.

$$V_D = 1.25 \cdot V_C \qquad (10.5)$$

Determination of Design Maneuvering Speed V_A
The design maneuvering speed V_A can be determined by finding point A by intersecting the $C_{N_{max}}$ with the positive limit maneuvering load factor $n_{lim_{pos}}$. First $n_{lim_{pos}}$ needs to be determined, which is done in Equation 10.6. $n_{lim_{pos}}$ must be ≥ 2.5 at all times. V_A is not allowed to exceed V_C.

$$n_{lim_{pos}} \geq 2.1 + \frac{24000}{W + 10000} \tag{10.6}$$

Drawing the V-n Maneuver Diagram

The V-n maneuver diagram can now be drawn using points A, D, H, F and E. Points A and D are determined as described above, using the speeds. Now H can be determined by intersecting $C_{N_{min}}$ as given in Equation 10.2 and the minimum load factor -1.0. Next point F can be defined by intersection the minimum load factor -1.0 with the cruising speed. Finally point E can be determined by intersecting the diving speed with the zero-load line. The various values for drawing the V-n maneuver diagram can be found in Table 10.3. The V-n maneuver diagram can now be drawn using these values and can be found in Figure

Table 10.3: V-n Maneuver Diagram Values

Parameter	Value	Unit
$C_{L_{max}}$	1.47	-
$C_{D_{atC_{Lmax}}}$	0.0774	-
$C_{N_{max}}$	1.472	-
$C_{N_{min}}$	-1.1	-
V_{S_1}	61.7	m/s
V_C	128.6	m/s
V_D	160.8	m/s
$n_{lim_{pos}}$	2.90	-
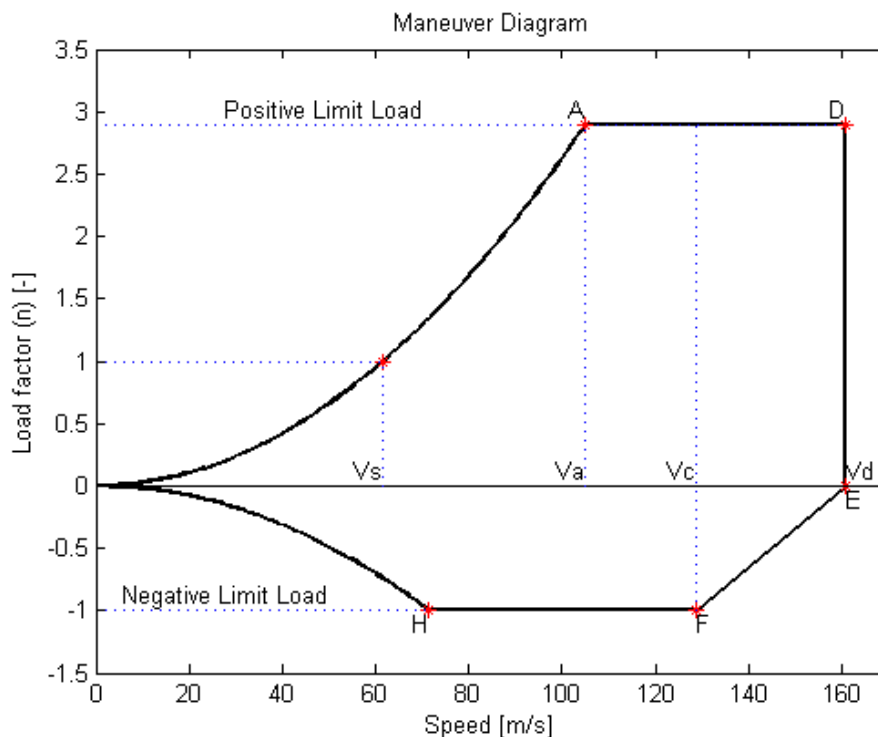
Figure 10.2: Maneuver Diagram

10.2.2 V-n Gust Diagram

In this section the V-n gust diagram will be constructed. For this diagram the gust load factor lines need to be designed, which is done using Equation 10.7. K_g is the gust alleviation factor given by Equation 10.8 where μ_g is given by Equation 10.9. All these equations are taken from Roskam V [9].

$$n_{lim} = 1 + \frac{K_g \cdot U_{de} \cdot V \cdot C_{L_\alpha}}{498 \cdot \frac{GW}{S}} \tag{10.7}$$

$$K_g = \frac{0.88 \cdot \mu_g}{5.3 + \mu_g} \tag{10.8}$$

$$\mu_g = \frac{2 \cdot \frac{GW}{S}}{\rho \cdot \bar{c} \cdot g \cdot C_{L_\alpha}} \tag{10.9}$$

The derived gust velocity is defined as follows:
For the gust line marked V_B: U_{de} = 84.67 - 0.003061h between 6096 and 15240 m.
For the gust line marked V_C: U_{de} = 66.67 - 0.002733h between 6096 and 15240 m.
For the gust line marked V_D: U_{de} = 33.34 - 0.001368h between 6096 and 15240 m.

Determination of Design Speed for Maximum Gust intensity V_B.
Point B" is determined from the intersection of the V_B gust line (the blue line in Figure 10.3) and the $C_{N_{max}}$ line. By intersecting Point B" with the speed axis, V_B can be determined. V_B is not allowed to be greater than V_C.

Drawing the Gust Diagram

All the gust parameters are known hence the gust diagram can be drawn resulting in Figure 10.3. First the gust lines are drawn. These are shown as the dotted linear lines. The intersection of V_C with the upper middle V_C gust line results in point C" and with the lower middle V_C gust line results in point F". An intersection of V_D with the upper inside V_D gust line results in point D" and with the lower inside V_D gust line results in point E". Finally point G" can be determined by intersection V_B with the lower outside V_B gust line.
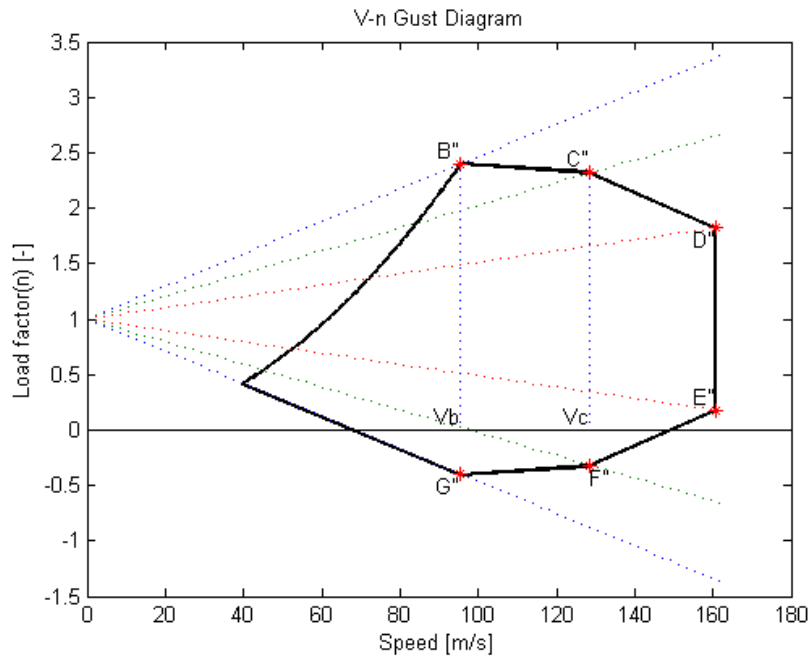
Figure 10.3: Gust Diagram

10.3   Payload-Range Diagram

A Payload range graph is been constructed for the Phoenix 5600 Business jet and is shown below in figure 10.4. A number of things can be distinguished; First of all, one should mentioned that the payload as has been used in this graph is defined excluding the crew and there baggage. Furthermore, the difference between the extra fuel and the fuel weight is has to be explained; The extra fuel is all the fuel required for the take-off procedure, the loiters, diverting to the alternate airport and landing procedure. This means that the "fuel weight" only includes the fuel that is actually used in the first cruise.

The most left marked point in the graph was the design point; this is the range that can be flown with a full capacity payload and is 5600 km. The next point (going from left to right) marks the nominal range at 6800 km. This range can be achieved only with the nominal payload of 4 persons. Finally, the last point marks the maximum range, also known as the ferry range at 8000 km.
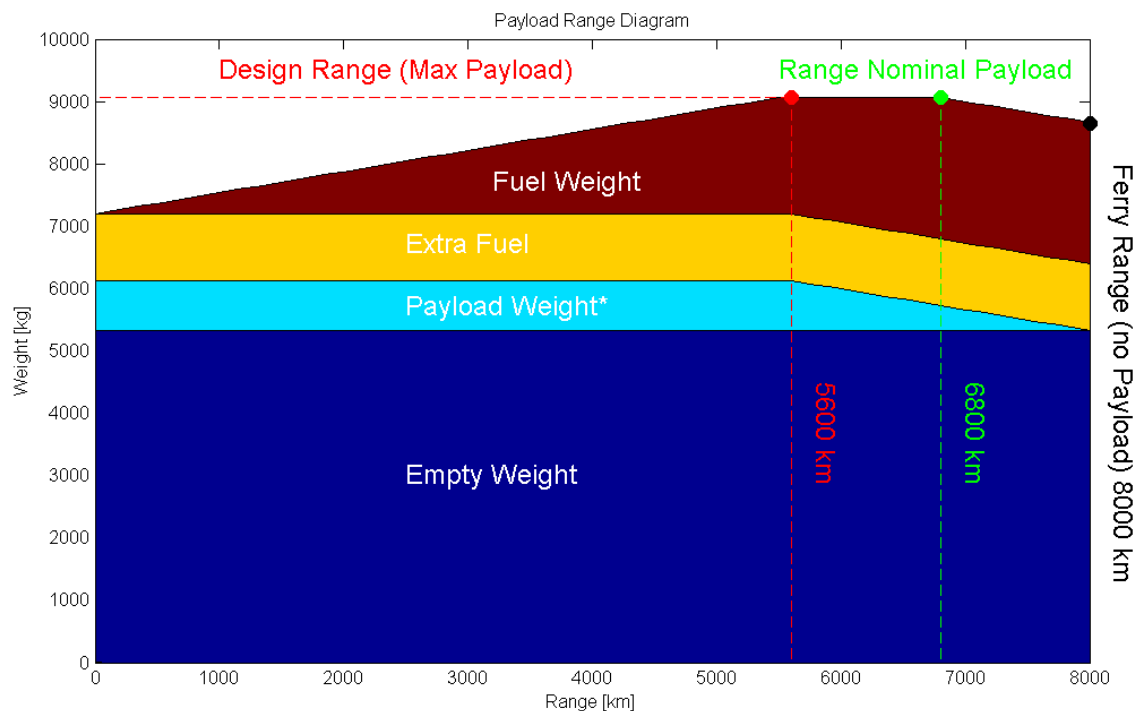
Figure 10.4: Payload Range Diagram

10.4   Engine Specifications

There are numerous types of propulsion systems to provide thrust for aircraft. From the requirements it is known that the Phoenix 5600 has a relatively high cruise speed in combination with a high cruise altitude. This limits the choice in engine type significantly. By choosing the PW545C turbofan engine, the aircraft will meet the required take-off thrust. Due to its high bypass ratio, the SFC will be low. This results in less fuel that has to be taken on board and less exhaust of emissions. The main specifications of the PW545C can be found in Table 10.4.

Table 10.4: Specifications of PW545C Engine

Parameter	Value	Unit
Engine Type	Two-shaft turbofan with full-length fan duct	-
Fan	Single stage	-
Bypass ratio	3.8	-
Weight	374	*kg*
Take-off Thrust	18.32	*kN*
SFC	12.35	*mg/Ns*
Length	1727	*mm*
Diameter	813	*mm*
Compressor	Two integrally bladed axial stages followed by one centrifugal impeller	-
Starting	Electric starter with dual high-energy igniters	-
Control System	Hydro-mechanical fuel control	-
Hot section inspection	2500	hrs
Overhaul	5000	hrs

A global nacelle design is performed in the Midterm Report [1]. The dimensions of the global lay out of the nacelle can be found in there. For more detailed design of the nacelle, engine manufacturer data is necessary which is not available in public. Therefore it is difficult at this stage to continue with the nacelle design. The mounting points of the engine are determined by the engine manufacturer. For fuselage mounted engines, like the PW545C, these points are fixed and do not have to be designed. For a structural analysis of the nacelle-fuselage connection, the location of the mounting points is needed. This means that to complete the design of the engine and nacelle, manufacturer data need to be provided.

10.5   Performance Analysis

In this section the aircraft performance will be analyzed. The performance aspects to be analyzed are: stall speed, landing & take-off distance, endurance and glide flight.

Flight Envelope   A flight envelope has been made containing the stall speed at various altitudes, the service ceiling and the maximum speed. The following subsections explain the methodology of the boundaries for the flight envelope. The flight envelope is presented in Figure 10.5.
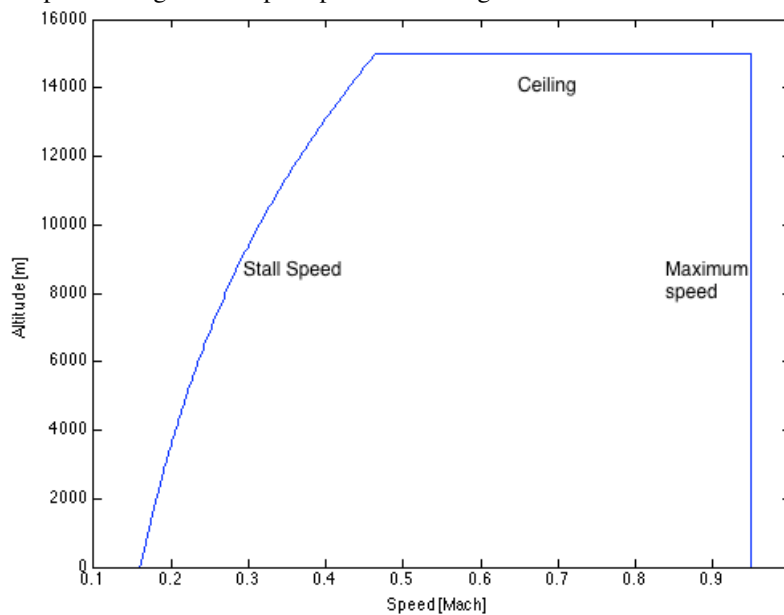
Figure 10.5: Flight Envelope

Stall Speed   The stall speed is calculated using Equation 10.10, using the results a flight envelope can be created. The stall speed is determined using a wing area of 33.3 m^2 and a MTOW which is equal to 9066 kg, this is the maximum weight and therefore would lead to the highest stall speed. The stall speed is related to the altitude by the air density, the air density varies with the altitude.

$$V_s = \sqrt{\frac{2 \cdot W}{\rho C_{L_{max}} S}} \tag{10.10}$$

Service Ceiling   The service ceiling is the maximum altitude the aircraft can operate. At the service ceiling the aircraft does not possess enough excess power to climb to a higher altitude. The rate of climb is defined by Equation 10.12 from [32]. The rate of climb for one inoperative engine cannot be calculated due to lack of data. Therefore it is unknown for this moment if this FAR 25 requirement will be met. The exact thrust at different altitude should be provided by the engine manufacturer. However the manufacturer data is lacking therefore an approximation is used, see Equation 10.11. [33] The throttle setting $delta_T$ is assumed to be constant and equal to one. The lift over drag ratio is assumed to be constant over the whole range of altitude. U_1 is the steady state speed which is assumed to be the cruise speed, during cruise the aircraft does not accelerate nor decelerate. The cruising altitude is also assumed to be constant therefore the cruise speed can be used as steady state speed.

$$T = T_0 \cdot \delta_T \cdot \frac{\rho}{\rho_0} \tag{10.11}$$

$$RC = 60 \cdot U_1 \cdot (\frac{T}{W} - \frac{D}{L}) \tag{10.12}$$

Maximum Speed   The maximum speed has been set by the requirements which is equal to 0.95 Mach. Verifying this result is extremely difficult, in the transonic region the drag behaves completely different. Accurate data for available thrust for different flight conditions is lacking and Roskam lacks a method to estimate the maximum speed. Therefore the maximum speed could not be determined. The maximum speed is the speed where the required thrust and the available thrust intersect, see Figure 10.6. In future time when all data is available it is suggested to create a graph like Figure 10.6 for the Phoenix 5600.
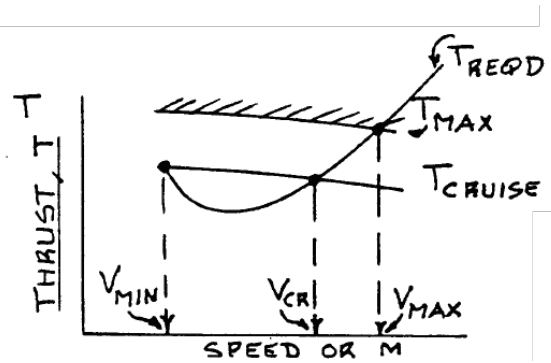
Figure 10.6: Thrust Diagram [32]

Take-off Distance   The take-off distance consists of two phases, the ground phase and airborne phase. To calculate the complete take-off distance s_{TO} which will comply with FAR 25 regulations, Equation 10.13 can be used.

$$s_{TO} = f_{TO} \cdot h_{TO} \left[\left(\frac{1}{\gamma_{LOF}} \right) + \frac{\left(\frac{V_3}{V_{s_{TO}}} \right)^2 \left(\frac{W}{S} \right)_{TO} \left[\left\{ \left(\frac{\bar{T}}{W} \right)_{TO} - \mu \right\}^{-1} + 1.414 \right]}{h_{TO} \cdot \rho \cdot g \cdot C_{L_{MAX_{TO}}} (1 + 1.414 \gamma_{LOF})} \right] \tag{10.13}$$

Landing Distance The landing distance consists of an airborne phase and a ground phase. The sum of the distances travelled during both phases adds up to the total landing distance. Figure 10.7 shows the airborne and ground phase.
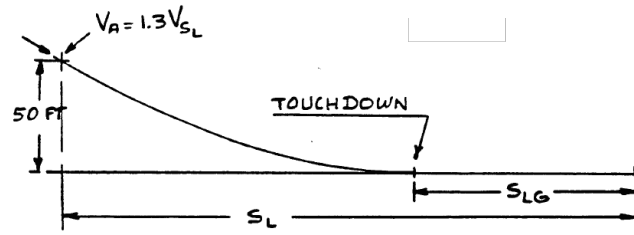
Figure 10.7: Definition of Landing Distrance [32]

The airborne phase distance can be calculated using Equation 10.14. The stall speed in landing configuration at sea level is 45 m/s. The approach speed is 1.3 times the stall speed and the screen height is 15.24 m.[32] The touchdown speed is assumed to be equal to the stall speed.

$$s_{air} = \frac{1}{\gamma} \frac{V_A^2 - V_{TD}^2}{2g + h_L} \tag{10.14}$$

The ground phase distance can be calculated by Equation 10.15. $\bar{a}/g$ can be taken as 0.6 for turbofan, ground spoilers, speed brakes and nose wheel braking.[32] A touchdown speed of 45 m/s has been used.

$$s_{ground} = \frac{V_{TD}^2}{2\bar{a}} \tag{10.15}$$

Endurance and Loiter The endurance of the aircraft has been analyzed using Equation 10.16. The aircraft has three loiter phases, the total endurance time for all three loiter phases is calculated. For the calculation a specific fuel consumption of 19.25 mg/Ns. This is a specific engine property of the PWC 545C. The lift over drag ratio has been calculated in the drag polar analysis and is 16. The initial and end weight can be determined using the weight fractions.

$$E = \frac{1}{c_j} \frac{L}{D} log(\frac{W_{initial}}{W_{end}}) \tag{10.16}$$

Glide and Descent In a descent the thrust is reduced and the flight path angle is shallow. To compute the rate of descent, the flight path angle γ has to be determined first. Using Equation 10.17 the rate of descent can be calculated. For a glide, thrust is reduced to zero. With a known altitude and γ, the maximum range of a glide can be computed with Equation 10.18 for constant lift-over-drag ratio. Using the rate of descent instead of γ, the glide time can be computed with Equation 10.19.

$$RD = (\frac{W}{S})(\frac{2}{\rho})(\frac{C_D^2}{C_L^3})(cos\gamma)^3 \tag{10.17}$$

$$R_{GL} = \frac{-h}{tan\gamma} \tag{10.18}$$

$$t_{GL} = \frac{h}{RD} \tag{10.19}$$

Range The cruise range is determined in order to verify the range requirement. The cruise range at constant altitude and constant speed is calculated using Equation 10.20 & 10.21 respectively Roskam VII [32]. The $C_{L_{cruise}}$ is 0.2 and $C_{D_{cruise}}$ is 0.012, these values have been determined in the drag polar analysis. The initial and end weight both have been calculating using the weight fractions. The f_{mj} variable has a value of 3.1 for ranges in km. [32]

$$R = \frac{f_{mj}}{c_j}\sqrt{(\rho S)}\frac{\sqrt{C_L}}{C_D}(W_{initial}^{0.5} - W_{end}^{0.5})$$ (10.20)

$$R = \frac{V}{c_j}\frac{L}{D}ln(\frac{W_{initial}}{W_{end}})$$ (10.21)

An overview performance characteristics that are discussed, can be found in Table 10.5 and 10.6.

Table 10.5: Performance Characteristics for Different Altitudes

Performance Characteristic	Altitude				Unit
	4000 m	8000 m	12800 m (cruise)	15000 m (ceiling)	
Stall Speed	66	83	115	137	m/s
Rate of Climb	1580.7	840.9	208.8	6.7	m/min
Climb Gradient	0.2	0.11	0.03	0	-
Rate of Descent	7.0	8.8	12.2	14.6	m/min

Table 10.6: Performance Characteristics

Performance Characteristic	Value	Unit
Take-off Distance	819	m
Range (constant altitude)	5686	km
Range (constant speed)	5044	km
Endurance	40.4	min
Glide Range	159	km
Glide Time	14.6	min
Landing Distance	746	m

10.5.1   Discussion of the Performance analysis

The performance analysis performed for this report is not very elaborate and still misses several performance aspects like the dive and maneuvering performance. The lacking manufacturing data leads making assumptions for the thrust at different flight conditions, this could lead to inaccurate results. It is strongly suggested to execute the performance analysis again when all data is complete. For now, the results give a good indication of the flight performance of the Phoenix 5600. From these results can be concluded that the main performance requirements are met at this point in the design process.

11 Aerodynamic Characteristics

In this chapter, the aerodynamic characteristics of the Phoenix 5600 are evaluated. In Section 11.1, the Class II drag polar analysis is performed. This is a more elaborate and detailed analysis to estimate the drag coefficient and illustrate corresponding aerodynamic plots. In Section 11.2, the wing lift distribution over the main wing of the aircraft will be calculated.

11.1 Drag Polar Analysis

In this section, the drag polar of the designed aircraft will be estimated using a Class II method.

11.1.1 Methodology

The main described methodology is based on Roskam VI [34]. The total drag polar consists of the components presented below. These components with corresponding symbol, are once more summarized in Equation 11.1.

- Wing drag coefficient.
- Fuselage drag coefficient.
- Empennage drag coefficient.
- Engines & nacelle drag coefficient.
- Flaps drag coefficient.
- Landing gear drag coefficient.
- Aircraft trim drag coefficient.
- Interference drag coefficient.
- Miscellaneous drag coefficient.

$$C_D = C_{D_{wing}} + C_{D_{fus}} + C_{D_{emp}} + C_{D_{en}} + C_{D_{flap}} + C_{D_{gear}} + C_{D_{trim}} + C_{D_{int}} + C_{D_{misc}} \tag{11.1}$$

The empennage drag coefficient includes the horizontal tail, vertical tail and canard as subcomponents. The interference drag coefficient is present due to the fact that the total drag of two or more components integrated together is always larger than the sum of the drag coefficients of those individual separate components. The miscellaneous drag coefficient is produced due to skin roughness, gaps, antennas, stores, struts and other external causes.

The drag polar consists of two main parts: the zero-lift drag and lift induced drag. The zero-lift drag is a sum of profile drag and wave drag as can be found in Equation 11.2.

$$C_{D_i} = (C_{D_o})_i + (C_{D_L})_i \tag{11.2}$$

The aircraft is expected to cruise at 0.9 Mach. This speed falls in the transonic regime. It implies that although the aircraft is flying below Mach 1, at certain parts of the aircraft the local airflow will reach Mach 1 or above. Due to this flow regime, the drag coefficient will result in a significant wave drag component of zero-lift drag. This is shown in Equation 11.3.

$$(C_{D_o})_i = (C_{D_p})_i + (C_{D_{wave}})_i \tag{11.3}$$

Note that each component has its own relations and design aspects that have been explored. The reader is advised to refer to Roskam VI, Chapter 4 [34] for further details. Below, the most important assumptions and aspects per component are listed:

Wing
The wing is one of the largest drag contributors because of the large wetted area. Due to the sweep angle of $-35°$, the wave drag is significantly reduced. Linear twist of the wing increases skin drag. However, it positively affects the structural aspect of the wing. The location of the maximum thickness, which is closer to the trailing edge, is also beneficial for skin drag.

Fuselage

The skin drag coefficient of the fuselage represents the largest proportion compared to the rest of the components. This is mainly due to a low fineness ratio which is a ratio between the fuselage length over the largest diameter. This has also a large influence on the wave drag during transonic speed regime. The base area of the fuselage equals 0.054 m^2 which corresponds to equivalent diameter of 260 mm. Such small dimensions allow the flow to reattach itself at trailing edge of the tail cone. This significantly reduces the wave drag.

Empennage

The zero-lift drag coefficients of the horizontal tail, vertical tail and canard are estimated using the same methodology as for the main wing. Since the wetted area of each sub-component is smaller than the main wing, the skin drag coefficient is also smaller.

Engines and Nacelle

The nacelles are treated as small fuselages and the zero-lift drag coefficient is estimated for each nacelle individually.

Trim

The trim accounts for the drag coefficient that is caused by the induced lift of horizontal and canard surfaces.

Interference

Although the interference effect has already been accounted for during the drag estimation of the wing, fuselage, empennage and nacelles, an additional interference drag is present due to the wing interaction with the fuselage. The interference drag is slightly higher for low mounted wings compared to mid-mounted wings. Also, since the exact dimensions of pylons are unknown, a reference value has been chosen as a fairing interference for nacelles to fuselage.

Miscellaneous

During the calculation of the skin roughness, it is assumed that for the standard metal sheet manufacturing process, a paint coating mass-production spraying method is used.

Flaps

The drag contribution of Fowler flaps is assumed to be significant in subsonic speed regime during take-off and landing. Since the flaps are uninterrupted, the drag increment is significantly smaller compared to an interrupted flap configuration.

Landing Gear

Similarly, the drag contribution of landing gear is assumed to be significant in subsonic speed regime during take-off and landing. The drag contribution is separately estimated for the nose and main gears.

11.1.2 Results

The drag polar is affected by many parameters such as Reynolds number, Mach number, angle of attack and altitude. In this example, the drag polar is estimated for cruise speed of Mach 0.9, at cruise altitude of 41000 ft and cruise angle of attack of $0.87°$, which corresponds to a $C_{L_{cr}}$ of 0.2. Those values have been determined in Midterm Report (see Table 11.2).

In Table 11.1, the drag coefficient is shown per aircraft component and divided into zero-lift drag coefficient and lift induced drag coefficient. From Table 11.1, it can be observed that the largest zero-lift drag is contributed by fuselage. The wing has the second largest contribution as expected. In addition, in Figure 11.1, the drag coefficient against lift coefficient have been plotted for clean, take-off and landing configurations.

Table 11.1: Drag Coefficient Breakdown per Aircraft Component

Aircraft component	C_{D_0}	C_{D_L}
Wing	0.00834	0.01794
Fuselage	0.00947	0.01520
Horizontal Tail	0.00219	0.00491
Canard	0.00191	0.00584
Vertical Tail	0.00146	0.00265
Engines	0.00582	0.00366
Trim	-	0.00538
Interference	0.00102	0.00133
Miscellaneous	0.00030	0.00067
Total	0.03048	
Take-off		
Flaps	0.012	-
Landing Gear	0.02	-
Landing		
Flaps	0.06	-
Landing Gear	0.025	-

Figure 11.1: Drag Polar Clean Configuration

In the drag polar plot it can be observed that the zero-lift drag coefficient is equal to 0.030. This is rather on the higher range of values compared to reference aircraft. This is mainly caused due to the presence of a canard as an extra empennage surface compared to conventional aircraft models. Also, since the fuselage is the largest profile drag contributor, the low fineness ratio has a significant increase in the C_{D_0} value.

11.1.3 Verification

Before proceeding to a next design step, it is important to make sure that the calculation method has been applied and executed accurately. It is also important to determine whether the designed parameters result in realistic values. A drag polar verification is performed for cruising conditions with a clean configuration. A linear plot of C_D-C_L^2 is created based on previously found values. This plot is presented in Figure 11.2. The gradient of the curve should be equal to $\frac{1}{\pi A e}$.
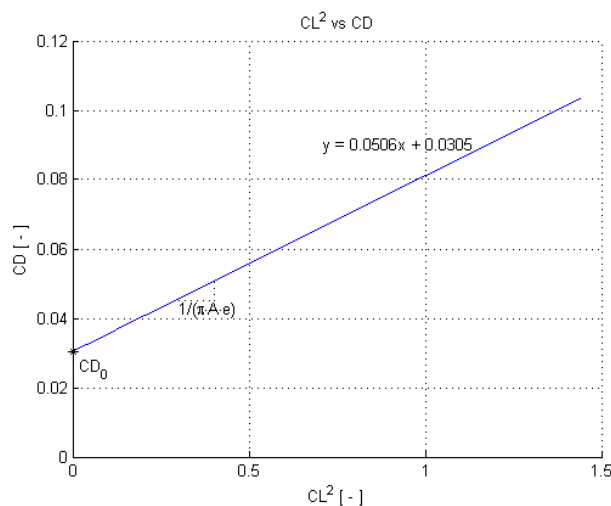
Figure 11.2: C_D-C_L^2 Plot

The estimated gradient of the slope is equal to 0.0506. After substituting the aspect ratio, the Oswald factor

results in 0.786. This value is within the range of Oswald factors of the reference aircraft that were examined in Baseline and Midterm Reports. C_{D_0} also corresponds to the calculated 0.030 value. The reference C_{D_0} values for a clean flight phase range between 0.019 to 0.032 depending on the aircraft configuration. Those values were found from drag polar plots in Roskam VI [34].

11.2   Wing Lift Distribution

Besides the drag polar analysis, the wing lift distribution should also be calculated. This is an important parameter to increase the accuracy of the structural analysis since the exact load distribution can be obtained. Furthermore, the wing lift distribution can be used to calculate aerodynamic stability parameters. In addition, the stall angle of attack can be determined from the wing lift distribution, as well as the location on the wing where this stall condition will occur.

11.2.1   Method

The method which is used to calculate the wing lift distribution is called the Vortex Lattice Method (VLM) [35]. The VLM is based on the Prandtl Lifting Line theory. The difference is that while the Prandtl Lifting Line theory uses only one horse shoe vortex per wing, VLM uses a lattice of horse shoe vortices. The concept used to calculate the lift is indicated in equation 11.4. It basically states that the lift generated by any section of the wing is a function of the local circulation, density and the speed. In which $\Gamma(y)$ represents the circulation over the wing at any location y.

$$L(y) = \rho \cdot V \cdot \Gamma(y) \tag{11.4}$$

The program which is used to perform the VLM for a wide range of aircraft geometries at any flight condition is Tornado [36]. The program code is implemented in Matlab. Tornado asks for a certain geometry and flight condition as an input. After this, a lattice is generated. When the lattice is produced, computational operations can be performed. For this section, only the 'static computation at a selected state' is used. After the results are saved under a certain 'identity tag', the computations can be plotted for the selected flight conditions. For this analysis, only the cruise phase flight conditions are used.
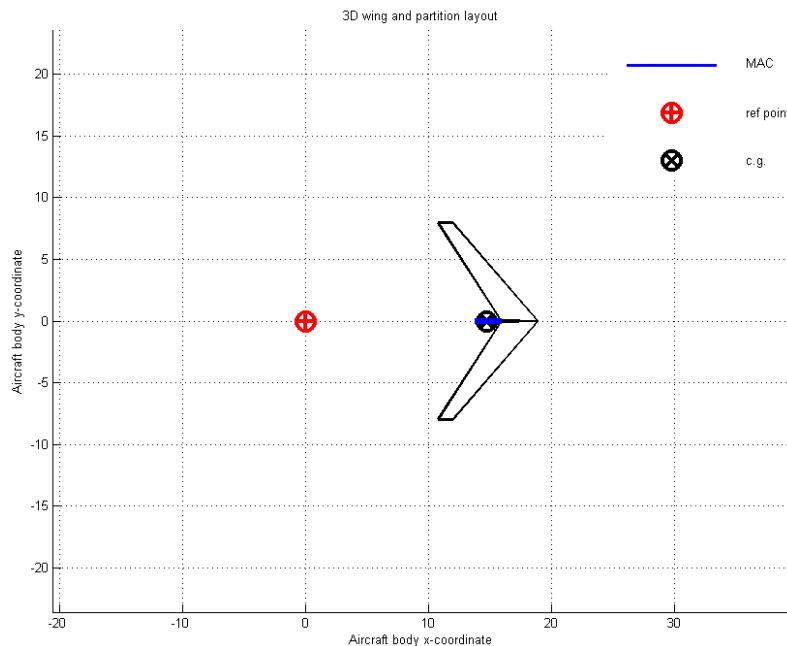
Figure 11.3: Shear Force Distribution Over the Wing

11.2.2 Results

The program is very elaborate, and can even give estimates of the stability derivatives. But for this first analysis, only the local C_L, shear force and bending moment are obtained. Figure 11.3 shows the input geometry of the wing. For simplification, only the main wing is analyzed without the other two lifting surfaces. This will decrease the accuracy of the results, especially at the root of the wing since the canard will cause a downwash in front of the wing. In real life the presence of the downwash of the canard would decrease lift generated by the wing. The results for the analysis of the local C_l value can be seen in Figure 11.4. The resulting shear force and moment due to the lifting force is shown in Figure 11.5 and 11.6.
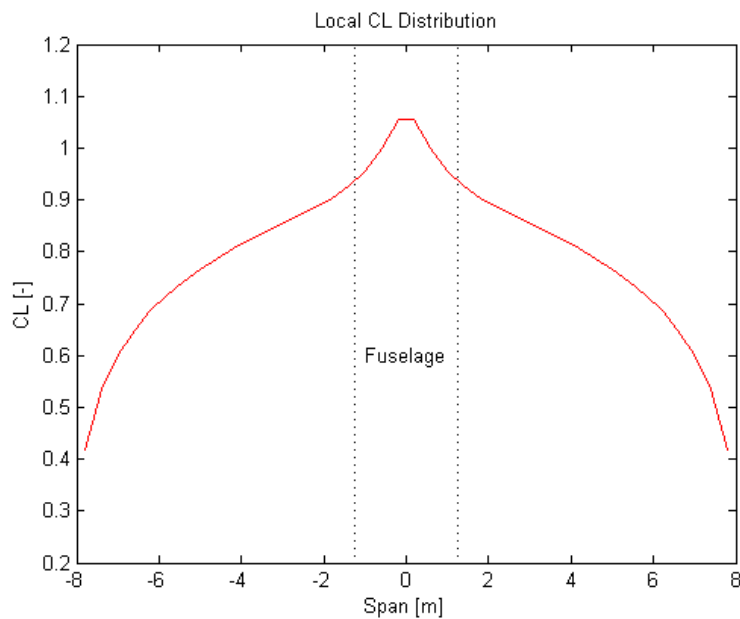
Figure 11.4: Local C_L Distribution over the Wing in Cruise
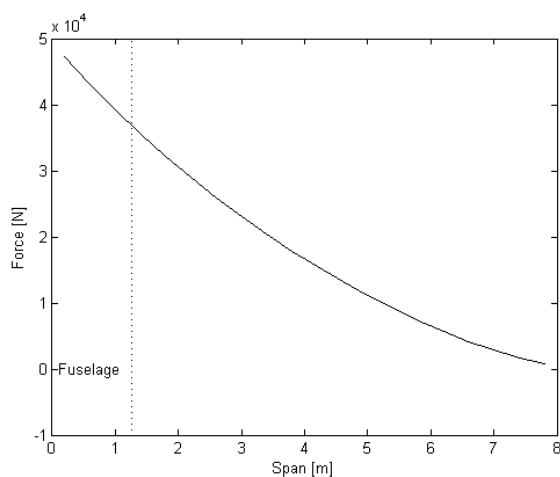
Figure 11.5: Shear Force Distribution
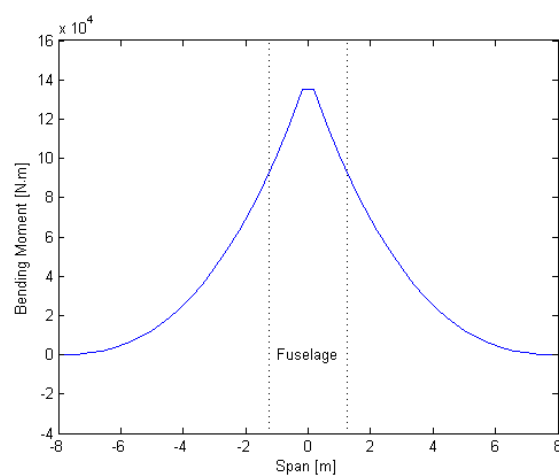
Figure 11.6: Bending Moment Distribution

Now by comparing the local C_l values for different angles of attack with the obtained 2D Cl_{max} values the stall angle of the entire wing can be determined. The Cl_{max} values depend on the Reynolds number which is influenced by the chord length of the wing. Figure 11.7 shows the 2D CL_{max} and the local C_L values of the wing. The stall angle and location on the wing can be found by looking at the tangent intersection of the two lines. As can be seen, the angle of attack at which the wing starts to stall is around 5.8°at 6.1 m

measured from the center of the fuselage. The obtained local C_l is in this case 1.12. The result for this angle of attack is very doubtful. From research on comparable business jet [37], the stall angle is set on $14°$.
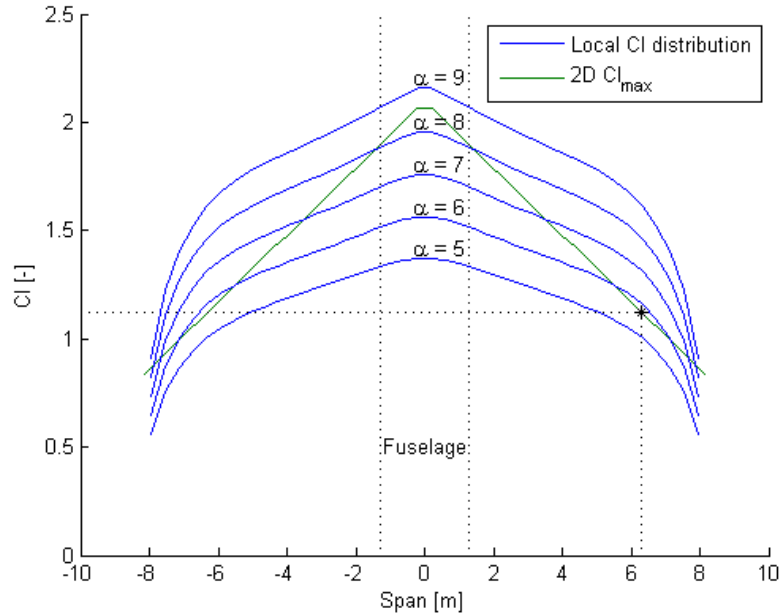
Figure 11.7: Stall Angle of the Wing Analysis

Now that the local Cl_{max} is determined for the 2D wing. The maximum C_L for the entire wing can be determined using equation 11.5.

$$CL_{max_w} = \frac{1}{S} \cdot \int_0^1 c(c_{lw_{stall}})d\eta = \frac{16.3218}{33.3} \cdot 1.9341 \cdot \int_0^1 c(c_{lw_{stall}})d\eta = 1.07[-] \qquad (11.5)$$

So the maximum lift coefficient produced by the wing is 1.07. The complete lift slope as a function of the angle of attack can be seen in Figure 11.8. Note that initially calculated value of the stall angle suggests to re-investigate the methodology preferably with a different calculating tool.
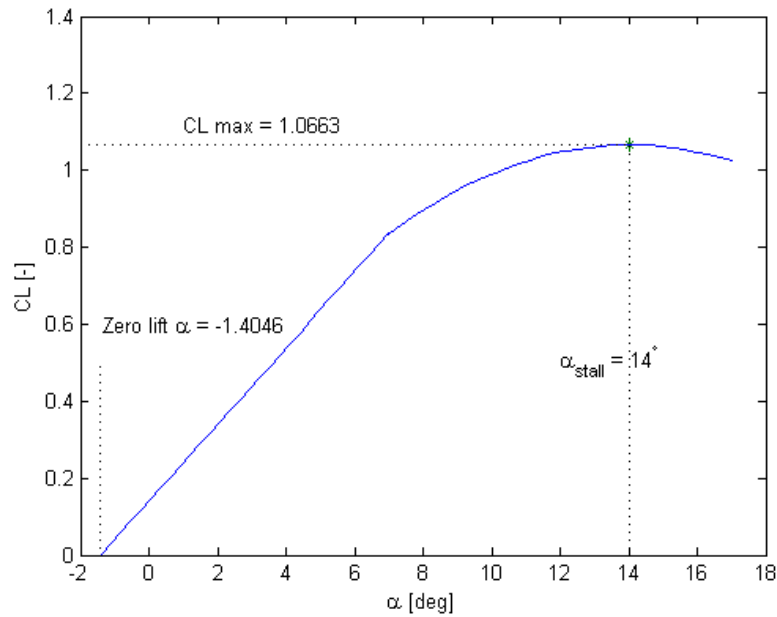
Figure 11.8: Wing Lift Curve of the Entire Wing

12 Structural Characteristics

In this chapter the structural characteristics of the Phoenix 5600 are determined. In Section 12.1 the structure of the fuselage is analyzed. After that, the wing is analyzed in Section 12.2 and finally the landing gear is designed in Section 12.3.

12.1 Fuselage Structural Design

This section describes the fuselage structural design process and presents the results of this process. Subsection 12.1.1 describes the general layout of the fuselage. Subsection 12.1.2 describes the analytical fuselage design. Subsection 12.1.3 describes the actual fuselage design as performed using CATIA. Subsection 12.1.4 describes the structural analysis performed on the fuselage structure.

12.1.1 General Layout

The fuselage is the central part of the aircraft where all main components are attached to and where the payload is carried. The fuselage structure carries all loads on the fuselage, while staying as light as possible. First the general features of the fuselage are described and after that the structural features of the fuselage are analyzed.

General Features

The outside shape of the fuselage has already been determined during Class I design, and is found to be still appropriate for Class II design. The fuselage consists of three parts: the nose, the cabin and the tail cone. The nose contains the cockpit and the nose landing gear bay. The nose landing gear and canard are attached to the nose. The nose skin contains cutouts for the landing gear doors and the cockpit windows. The cabin contains the passenger facilities. The wing is attached to the cabin part of the fuselage through the wing-fuselage integration structure. The cabin skin contains cutouts for the passenger access door, passenger windows, the emergency exit and the wing-fuselage integration structure. The tail cone contains the baggage compartment. The aircraft tail and the aircraft engine structure are attached to the tail cone. The tail cone skin contains a cutout for the baggage door.

Structural Features

The general structural arrangement of the fuselage will be semi-monocoque. This arrangement is based on the monocoque layout, where the outer skin carries all structural loads. In the semi-monocoque arrangement, the skin carries part of the loads, supported by fuselage frames and stiffeners (longerons). This structural arrangement allows for a light, stiff structure which gives a large internal volume to be used. The skin carries most of the cabin pressurization loads. The skin and the longerons together carry fuselage bending loads. The fuselage frames carry the loads from the cabin floor and other fixed equipment. The fuselage frames are also attachment structures for the wing box, engine integration, nose gear strut and empennage spars.

Next to the skin, frames and longerons, the fuselage structure will also include the following structural features (from the front to the back):

- **Front pressure bulkhead:** this bulkhead seals off the front of the pressure cabin. It is located in the nose, in front of the cockpit.
- **Landing gear bay frames:** these frames are located at the side of the cutout for the landing gear bay. They reinforce the skin area around the landing gear bay.
- **Cockpit window struts:** the cockpit window structure includes three struts.
- **Cabin floor frames:** the floor of the passenger cabin and cockpit is supported by extra frames.
- **Cabin door frame:** the door cutout is surrounded by a frame which carries loads and to which the door is attached.
- **Emergency exit frame:** the emergency exit cutout is surrounded by a frame which carries loads and to which the emergency exit is attached.

- **Wing box integration structure:** this structure carries and distributes all loads from the wing box to the main fuselage structure.
- **Baggage door frame:** the baggage door is surrounded by a frame which carries loads and to which the door is attached.
- **Aft pressure bulkhead:** the aft pressure bulkhead seals off the pressure cabin behind the baggage compartment. The aft pressure bulkhead has a spherical shape, this allows it to carry the pressurizations loads more efficient.

External Structural Features

This section describes the structural layout of the external features attached to the fuselage, except the wing. This includes the following features:

- Vertical tail
- Horizontal tail
- Canard
- Engine integration structure

Due to time constraints these features will be designed to a less detailed extend than the fuselage. More detailed design of these features will be performed during the detailed design process.

The vertical tail, horizontal tail and canard structures will be laid out in similar ways. This is because they all perform similar functions (generate lift in certain directions), they all have the same general form (tapered, swept) and all have one control surface (elevator, rudder, canardvator). The general structural layout of the empennage surfaces will consists of two spars running from the root to the tip, stiffeners running in the spanwise direction on the skin and ribs, running in the direction of the airflow. The ribs feature circular cutouts for weight savings. The control surface actuators are attached to the ribs or the aft spar.

The empennage front spar will be located between 15% and 25% of the chord, as can be found in Roskam III [38]. The empennage aft spar will be located between 65% and 70% of the chord. The aft spar location differs slightly from the values suggested by Roskam [38], this is because of control surface size constraints. The rib spacing will be around $24\,in$ as suggested by Roskam [38].

The front spars of the vertical and horizontal tail and the aft spars of the vertical and horizontal tail will coincide in order to carry all the horizontal tail loads efficiently through the vertical tail to the fuselage. Figure 12.1 shows the general structural layout of the empennage. The canard will be laid out in a similar way.
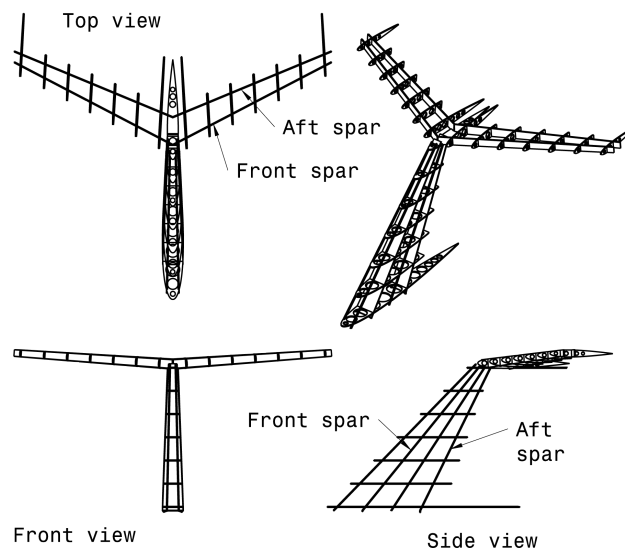
Figure 12.1: Empennage General Layout

The engine integration structure will carry the weights of the engine and nacelle and the thrust of the engine. The structure will transfer the loads from the three engine attachment points into the fuselage. The engine structure will be connected to the fuselage through a strut with an airfoil like shape to reduce drag.

12.1.2 Analytical Design

In order to reduce the amount of iterations required, analytical sizing for certain structural components is performed before the actual structural design starts. The analytical design will determine the skin thickness, longeron shape and dimensions and frame spacing. Furthermore, the general frame cross section and thickness will be based on reference data and the material for the fuselage structure will be selected.

The analytical design will be performed on the cylindrical part of the fuselage. This part is radially symmetrical, aiding in simplifying the analytical design. The analytical design is performed using MATLAB scripts. First the skin thickness calculation and material selection procedure is described. The analytical frame design is performed and finally the analytical longeron design is done.

Skin Thickness and Material Selection

First, the skin thickness will be determined and the material will be chosen. The skin thickness will be sized based on the pressure difference between the surrounding air and the internal cabin. The inside pressure will be that of the pressure in the ISA at the cabin altitude of $1500\,m$. The outside pressure will be the ISA pressure at the cruise altitude of $41000\,ft$. It is assumed the skin will be able to carry all these loads while staying below the fatigue strength (not yield strength) of the material.

As the required skin thickness depends on material, the material to be used for the skin, frames and longerons will also be chosen during this part. Staying below the fatigue strength of the material means that the material will never fail due to fatigue stresses. This is preferable because during one flight the cabin will be pressurized when the aircraft climbs and de-pressurized again when the aircraft descends. And as the aircraft flies many flights and replacing the skin often will be very costly, it is preferred that the skin will stay below fatigue strength during a flight. The skin thickness is calculated using Equation 12.1.

$$t = \frac{\Delta P \cdot (D_f/2)}{\sigma_{design}} \tag{12.1}$$

For each material the required skin thickness is calculated. From that, the weight per meter of fuselage length can be calculated. And knowing the price per weight unit, the price per meter of fuselage can also be calculated. Finally all output values for the different materials are compared and the most optimal material and corresponding skin thickness is chosen. A minimum thickness of $0.5\,mm$ is set, as a thickness lower than this value will introduce handling difficulties during manufacturing and assembly [39].

Five materials are analyzed. All materials are commonly used in the aerospace industry [39]. Table 12.1 presents the materials which are analyzed. Note that quasi-isotropic composite is not a specific material type, but it is included to show the effect of the properties of composites (high fatigue strength and low weight but high price). Also note that the prices are not precise as price differs greatly based on raw material costs, transportation costs (distance from the factory to the final assembly line) and batch.

Table 12.1: Material Properties

Material	$\sigma_{fatigue}$ [MPa]	ρ [kg/m^3]	Price per kg [€/kg]
Aluminum 7075-T6	159 [40]	2810 [40]	6.6 [39]
Aluminum 2024-T3	138 [41]	2780 [41]	6.6 [39]
Steel AM-350	530 [42]	7822 [42]	4.4 [39]
Titanium Ti-6Al-4V	240 [43]	4438 [43]	22 [39]
Quasi-isotropic composite	436 [39]	1609 [39]	176 [39]

The required thickness is calculated by sizing for hoop stress [44]. A safety factor of 1.5 is taken into account. Table 12.2 presents the output of the MATLAB script with which the calculations is performed.

Table 12.2: Thickness Calculation Results

Material	t [mm]	Price per m [€/m]	Weight per m [kg/m]
Aluminum 7075-T6	0.8	118	17.8
Aluminum 2024-T3	1.0	145	22.1
Steel AM-350	0.5	137	31.0
Titanium Ti-6Al-4V	0.6	465	21.1
Quasi-isotropic composite	0.5	1124	6.4

As can be seen, the quasi-isotropic composite does indeed yield to a very light structure, but is around 10 times as expensive as aluminum and steel. Titanium is also much more expensive than steel and aluminum. The prices of the two aluminum types and steel lie approximately together. Weight per meter is an exact result, so aluminum 7075-T6 is selected as the material for the fuselage structure as this gives the lightest structure. A skin thickness of $0.8\,mm$ is selected.

Frame Design

After the skin thickness has been determined and the material has been selected, the frames will be designed. The frame cross sectional area cannot be determined easily using an analytical method. So the frame is designed using reference values. A C-shape is chosen for the frame cross sections. Roskam III [38] gives a value for the frame depth of $1.5\,in$. Rounding this off, a value of $40\,mm$ is taken as the profile height. The flange lengths are selected at $20\,mm$. The frame thickness is selected at $0.5\,mm$.

The frame spacing can be determined analytically. This is done by calculating the frame spacing which allows the floor panels to have a maximum deflection at a certain load. The material properties of a typical honeycomb structure floor panel are taken [45]. As the highest loads on floor panels are induced by high-heeled shoes, the design load will be the 90 percentile female weight (extrapolated from [46] to $75\,kg$), applied as a point load. The maximum allowable floor deflection is set at $1.5\,mm$.

The floor deflection is calculated by modelling the floor panel as a beam clamped at two sides with the force applied exactly half way. The distance between the two sides is the frame spacing. The calculations give a frame spacing of $0.63\,m$, which lies within dimensions suggested by Roskam [38].

Longeron Design

The longerons are designed based on the maximum bending moment the aircraft will experience. This bending moment is calculated by taking the weight of the fuselage including components and payload and multiplying this with the maximum load factor as determined from the V-n diagram (see Section 10.2.2 of Chapter 12) and a safety factor. This weight is then applied to a clamped beam with length of the distance between the wing position and the nose of the aircraft. This is because the fuselage (also during structural analysis) will be clamped at the wing box, as the structure will be evaluated in a static condition, which means all forces are in equilibrium. It is assumed that the wing carries all weight loads, so clamping the fuselage structure in the wing box is a valid assumption.

The longerons will be sized based on the required area, A and moment of inertia, I to withstand buckling due to this moment. However, a check is also performed to make sure the longerons will have sufficient moment of inertia so they can prevent tension and compression yielding.

It is assumed that only a certain part of the fuselage circumference will carry the buckling loads and that the rest of the circumference will be radial symmetrically populated with the determined longer distribution in the load-carrying part of the circumference. This circumference is taken to be $60°$ of the whole circle. The critical buckling stress is calculated using Equation 12.2. The stress each longeron experiences is calculated

using Equation 12.3 which is derived from material and structural properties [39].

$$\sigma_{crit} = \frac{4 \cdot \pi \cdot E_{long} \cdot I_{long}}{A_{long} \cdot s_{frames}} \quad (12.2) \qquad \sigma_{long} = \frac{M_{max}}{n \cdot \left(A_{long} \cdot n + A_{skin} \cdot \frac{E_{skin}}{E_{long}} \right)} \quad (12.3)$$

$$\lambda_{overdesign} = min \left(\frac{\sigma_{fail}}{\sigma_{long}}, \frac{\sigma_{crit}}{\sigma_{long}} \right) \qquad (12.4)$$

The final longeron shape and distribution will be based on two factors: the weight per meter of fuselage length and the how much the selected longeron shape is over-designed, which is calculated using Equation 12.4. Both factors should be minimized, but the latter cannot be lower than one, as that would mean that the shape will not be able to carry the buckling loads. Three global longeron shapes are selected: an L-shape (1), a Z-shape (2) and an extended Z-shape (3). Figures 12.2, 12.3 and 12.4 present the three shapes, with appropriate dimensions.
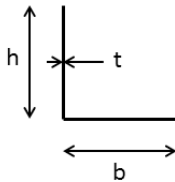
Figure 12.2: L-shape (Shape 1)   Figure 12.3: Z-shape (Shape 2)   Figure 12.4: Extended Z-shape (Shape 3)
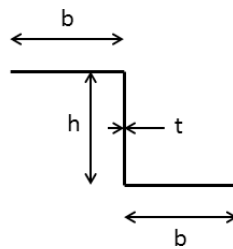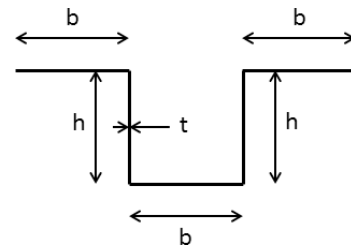
The h, b and t parameters and the number of stringers n is varied between certain ranges. For each combination, the weight of the stringers is calculated and how much they are over-designed. Then the longeron configuration with the best combination of these two factors is finally chosen as the final longeron configuration. Two extra limitations are taken into account: b and h can only differ from each other by 10 % to rule out unrealistic longeron designs. Also, b and h must both be at least ten times larger than t, to let it be a thin-walled construction. Table 12.3 presents the results of the analytical longeron design.

Table 12.3: Longeron Design Results

Parameter	Value	Unit
Shape	Z-shape	-
h	18	mm
b	17	mm
t	0.2	mm
n	2	-
n_{total}	12	-

12.1.3 Structural Design

Now the skin, stringers and frames have been sized in the analytical structural design process, the actual fuselage structure can be designed. The fuselage structure is designed in CATIA.

Frames Design

First, the lengthwise positions of the frames are determined while keeping the frame spacing determined during the analytical frame design in mind. This is done in a way to maximize structural synergy and subsequently to minimize weight. Once the lengthwise positions are determined, these positions are projected onto the fuselage skin to determine the final positions of the frames. Nearby irregular skin shapes such as the nose structure, frames can also have other orientations than straight up. Frames will feature cutouts to

let the longerons pass through as it is vital for their structural integrity that these run all the way from the front to the back of the aircraft, instead of being cut off at each frame.

Around major cutouts, like doors, cockpit windows and the nose gear bay, frames are also positioned to reinforce the structure as cutouts interrupt the load paths through the skin. In addition, extra beams will be inserted to support the floor.

Also, the front and aft pressure bulkheads are designed. The front pressure bulkhead is located in the nose in front of the cockpit. The front bulkhead does not have a very large diameter so it can maintain a planar shape. The aft pressure bulkhead, however, does have a large diameter equivalent to the entire fuselage diameter, so it is designed as a semi-spherical shape. It will also have extra frames and stringers mounted on it. Figure 12.5 shows the fuselage frames layout in side and top views.
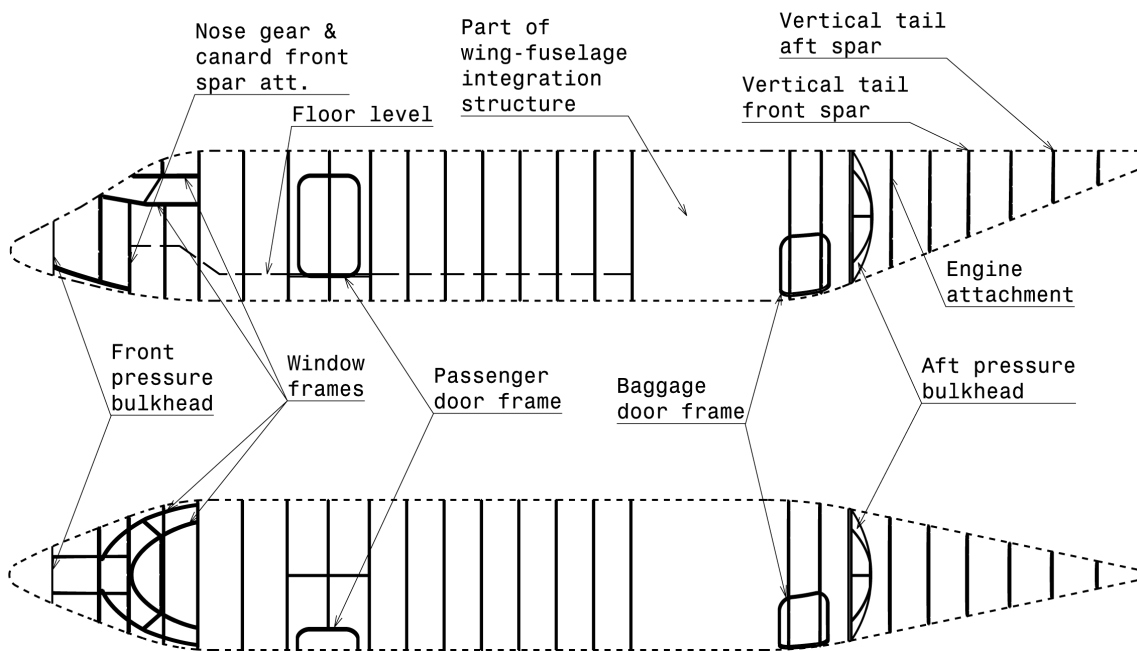
Figure 12.5: Fuselage Frames Layout

Longerons Design

The longerons run from the front to the back and on the cilindrical part of the fuselage (cabin) they are evenly distributed over the circumference of the skin. In the tail cone and the nose, when they converge to one point, some stringers stop early as it is not necessary to continue all of them to one point. The local stiffness of the structure would be unnecessary high in that case. Figure 12.6 shows the longerons layout.
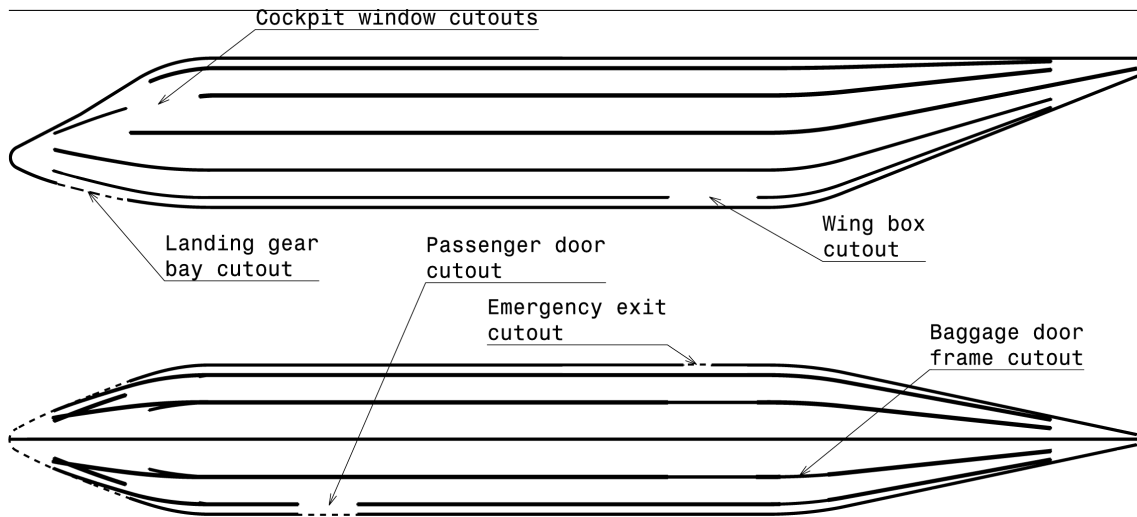
Figure 12.6: Longerons Layout

Wing Integration Design

The wing integration structure is an important part of the fuselage as this is the part where the highest loads during flight are carried through. The wing box runs through the fuselage. At the intersection of the wing spars (as they were determined during Class I wing design) and the fuselage skin, the wing box changes sweep angle. This means that in the fuselage, the wing box is oriented perpendicular to the length of the fuselage. In the wing integration section, a higher frame density is used than determined in analytical design. Also, some reinforcing elements are introduced to carry loads from the wing box to the skin and other frames. Figure 12.7 shows the wing integration structure.
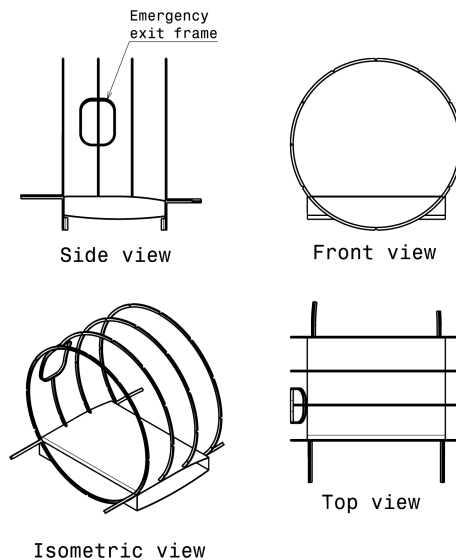
Figure 12.7: Wing Integration Structure

Results

Figure 12.8 shows the total fuselage structure.
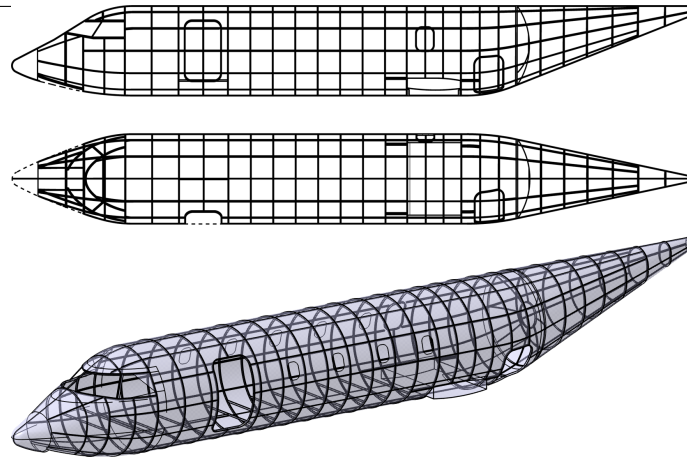
Figure 12.8: Fuselage Structure Layout

12.1.4 Structural Analysis

Structural analysis is performed on the fuselage design to validate the structural integrity and to make sure that the structure does not fail under several load scenarios. Structural analysis is performed using the structural analysis module in CATIA. This module is a finite element analysis tool.

Validation

To validate the CATIA stuctural analysis module, a mesh convergence study is performed. For a simple problem (clamped I-beam with a force applied at the end), the deflection is calculated using the CATIA structural analysis module with different mesh sizes. The error is then determined and a conclusion is drawn. Figure 12.9 shows the validation model in CATIA.

Figure 12.9: CATIA Structural Analysis Validation Model

First, the deflection of the beam is calculated analytically. The E-modulus and the moment of inertia are checked to be the same as the CATIA model. The deflection is calculated to be $23.0\,mm$. The beam has a length of $2\,m$. The mesh size is compared relatively to the beam length. For the fuselage, the mesh size is compared relatively to the longest dimension as well: the fuselage length. The CATIA structural analysis module itself also reports a global error rate. This is also included in the table to compare this to the analytically calculated error. Table 12.4 presents the results of the convergence study. Figure 12.10 gives a representation of how CATIA presents data graphically.
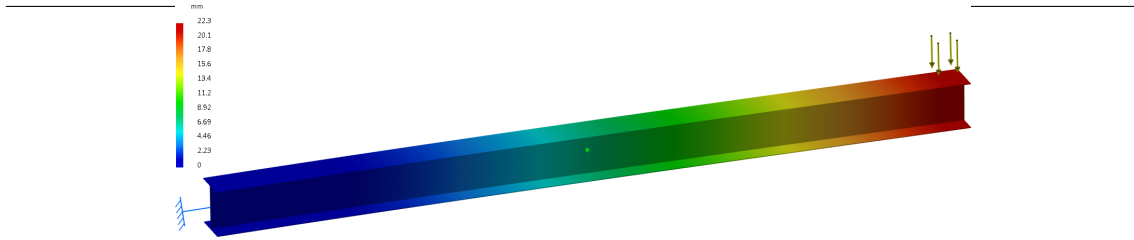
Figure 12.10: CATIA Structural Analysis Graphical Data Representation

Table 12.4: CATIA Structural Analysis Validation Results

Mesh size [mm]	Relative size [%]	Deflection [mm]	Error [%]	Error CATIA [%]
200	10.00	0.29	99	53
100	5.00	1.49	94	59
50	2.50	6.64	71	59
20	1.00	21.2	8	22
10	0.50	22.3	3	10
5	0.25	22.7	1	7
2	0.10	22.9	0	7

As can be seen, errors can be huge if the mesh size is chosen too large. From 0.50% of the longest dimensions and lower, the error is acceptably low. Also, the error reported by CATIA does not exactly coincide with the deflection error, but this can be because the error reported by CATIA is the global error rate, which also includes other components like stresses and energy. It can however be concluded that if CATIA reports an error rate of 10% or below, that the results can be reliable within an error margin of around 5%.

Load Cases

This subsection describes the load cases used for structural analysis of the fuselage. First, all loads which the fuselage structure experiences must be identified:

- **Component weights:** this includes the weight of the fuselage structure itself, fixed equipment, payload, crew, aft empennage, canard, engine and nose gear. The combined weight of the fuselage structure and the fixed equipment is distributed evenly over the whole structure. The weights of the external components (canard, nose gear, engine and aft empennage) are applied to the corresponding load carrying frames.
- **Cabin pressurization:** the pressure difference between the cruise altitude and the cabin altitude. The pressure is applied to the front and aft pressure bulkheads and the outer skin between the front and aft bulkheads.
- **Thrust:** the thrust generated by the engine. The thrust is applied to the corresponding engine load carrying frame.
- **Nose gear:** the force the nose gear exerts on the fuselage when it makes contact to the ground. The load is applied to the corresponding nose gear load carrying frame.
- **Control surface forces:** these are the forces generated by the control surfaces on the aft empennage: the elevator and the rudder. The load is applied to the corresponding aft empennage load carrying frame.
- **Aerodynamic drag:** the force generated by the air flowing around the fuselage. This force is distributed over the entire outer skin of the fuselage.

The canard also contains a control surface, but it is assumed that it does not exert extreme forces on the fuselage. Also, it is assumed that the control forces of the rudder and elevator are of a higher magnitude than the aerodynamic forces generated by the empennage surfaces due to high α or β angles. Six load cases are designed:

1. **Engine spool up:** in this load case, the aircraft is on the ground and ready for take-off. Brakes are applied to the main landing gear to make sure the aircraft does not start rolling yet while the engines spool up to full take-off thrust. All weights are applied at 1 g. Thrust is applied to the corresponding load carrying frames. No drag, control surface deflections and pressurization loads are present. The nose gear exerts a force of 8% of MTOW on the corresponding load carrying frame.

2. **Max wing loading:** in this load case, the aircraft is in flight at cruise altitude and experiences the maximum wing loading as determined in Section 10.2. All weights are applied at 2.9 g. The thrust is set to equal drag. The drag force is calculated from the Class II drag polar analysis in Section 11.1. The control surface loads and nose gear load are not present. The pressure difference is applied and set to the difference of the ISA pressures at cruise altitude and at cabin altitude.

3. **Max negative wing loading:** in this load case, the aircraft is in flight at cruise altitude and experiences the maximum negative wing loading as determined in Section 10.2. All loads applied are the same as for load case 2, except that the weights are applied at -1 g.

4. **Max control deflection:** in this load case, the aircraft is in flight at cruise altitude and experiences a maximum aft empennage control deflection. The loads applied are the same as for load case 2, except that all weights are applied at 1 g and control deflection forces are present. Both the control surfaces (elevators and rudder) are deflected positive 25°.

5. **Max negative control deflection:** in this load case, the aircraft is in flight at cruise altitude and experiences a maximum negative aft empennage control deflection. The loads applied are the same as for load case 4, except that the control surfaces are deflected negative 25°.

6. **Max load:** in this load case, the aircraft is in flight at cruise altitude and experiences the maximum wing loading and maximum aft empennage control deflection. The loads applied are a combination of load case 2 and 4.

Results

In order for CATIA to perform the structural analysis, a model mesh must be created. This is done automatically by CATIA. However, during the generation of the mesh, CATIA would fail every time, giving an error on which components would fail. Due to the amount of errors and the complexity of the model, more time is required (one 'meshing session' takes about 5 hours until the error occurs) than available to prepare the model for CATIA structural analysis. This means the structural analysis of the fuselage has not been performed as not enough time was available.

12.2   Wing Design

In this section, the forward swept wing (FSW) structure is designed and analyzed. First, the design process is presented and explained. Finally, results and findings are presented at the current stage of the design process.

12.2.1   Design Considerations

Since the wing box is the most essential and critical load carrying member of the wing and one of the most important components of the whole aircraft, the design philosophy was chosen using a Safe-Life Approach. This implies that the wing box will be slightly over designed to make sure that it operates within the given time span without a need of being heavily repaired. Since it is difficult to repair a severely damaged structure, it is wise to incorporate a high safety factor, on the other hand, any additional material will increase the weight of the aircraft and subsequently the cost. Therefore, with respect to a trade-off between safety and cost, a safety factor of 1.5 is chosen in calculations and design analysis.[47] Note that this safety factor is acceptable in the current wing box design since the chosen material is aluminum, which has a relatively predictable behavior. It is also important to follow inspections and maintenance procedures to reduce any

risks of separate component failure.

The chosen design configuration induces several complications in the structural analysis and design of the wing box (see Section 9.3 of Chapter 9). As the sweep angle is $-35°$, its effect on the design of the entire aircraft is significant. Due to a limited amount of time for the structural analysis, it was decided to first consider a conventional metal construction over a composite structure. This means that the divergence issue will be solved by adjusting the structural configuration rather than material configuration, which is the case for aeroelastic tailoring. By making the leading edge of the wing structure stiffer than the trailing edge, upward bending of the wing will affect the back part of the wing more than the front side, resulting in a twist that stabilizes the twist motion rather than diverging it. In fact, by doing this, the shear center shifts towards the leading edge, in front of the aerodynamic center, which is the condition for a non-divergent FSW. This solution allows the use of more conventional materials such as aluminum alloy, which eases the manufacturing process and decreases production costs.

The fuel is stored in the wing box according to the 'wet wing' concept, also called integral fuel tanks. This option is the most weight efficient and has therefore the least impact on the structural integrity of the wing. Still, a sealant has to be applied in order to protect the aluminum from being affected by the fuel. When designing and locating the fuel tanks, safety aspects have been take into account. Integration of the wing to the fuselage and location of the wing box location are designed in such a way that takes into account a failure of landing gear components, electric wiring and generators or engine ignition.

12.2.2 Design Process

The wing box will take several types of loads. It supports the landing gear structure, fuel tanks and high lift devices. The wing can be bended in both directions, upward due to lift and downward due to its own weight. As described earlier, bending induces a twist deflection.

A model of the wing box is built in CATIA as detailed as possible. Now, loads can be applied on the structure to simulate stresses and deflections. The lift distribution is assumed to be linear, weight of the wing box and landing gear assumed to act as a point force. The goal is to iterate the design in CATIA until the simulated stresses are below the maximum allowable stress value. The most extreme load cases will be assessed computationally using the V-n diagram (Section 10.2.2 of Chapter 10 and CATIA stress simulation. For verification, one load case is assessed analytically.

The torsional divergence of the wing can also be analyzed in CATIA, but in order to make an educated estimation of its impact, the divergence speed of the wing will be calculated analytically. This speed depends on the geometry, structural characteristics and material characteristics of the wing structure. The optimal shear center location is, in this context, the variable that needs to be determined.

12.2.3 Material Selection

The used material for the wing structure is aluminum alloy since it has a combination of qualities which out-performs in trade-off with respect to other material choice. It is the most conventional material choice available since its properties and structural behavior are well known and predictable. Although compared to composite structures, aluminum does weigh more and has lower yield stress, the strength-to-weight ratio is still significantly high. The manufacturing phase is more straightforward, it requires less time in assembly process also the maintenance checks are less time consuming. This results in high cost saving advantages.

The exact type of aluminum that is used for the wing structure is alloy 7150. Alloy 7150 is the highest strength aluminum currently available for commercial aircraft applications with yield strength of 570 MPa [48]. It is currently being used for upper wing skins on large commercial aircraft where high compressive yield strength is the major requirement. Also, it has a high fatigue resistance quality (172 MPa [49]) and has moderate corrosion resistance.

In the design process a number of different aluminum alloys were considered, namely 2024, 6063-T6 and

7075. However during the structural analysis it was found that the material has to be chosen based on the highest yield stress, alternatively, the wing box with given geometry would fail. Note that the material properties depend on the shape, thus all the examined materials were compared in a metal sheet shape of 1mm thickness [48].

12.2.4   Wing Components

The wing includes many components besides the structure itself. Fuel tanks and cables of the hydraulics system for high-lift devices and aileron have to be implemented and therefore continuously accounted for during the design. These additional components affect the detailed design of structural parts. We divide all the wing components in three categories: structural components, fuel system components and HLD & control surface components. Below, the main members that each component consists of are listed:

Table 12.5: Wing Components

Structure	Fuel System	HLD & Control Surface
Spars	Tanks	Flaps & Ailerons
Ribs	Pumps	Cabling
Stiffeners	Anti-sloshing Baffles	
Skin	Lines	
HLD & Control Surface Support	Sensors	
	Sealant	
	Vents, Drains, Inlet & Outlet	

Structural Components

Below, each main member of the structure is treated separately and explained with respect to the presented design.

Spars
The geometry of the wing box is dictated to a large extent by its spars. A front spar and a rear spar connect the top and bottom skin of the wing. They are located at 10% and 65% of the chord respectively to account for the required fuel space needed. In order to counteract the undesired torsional divergence, the structure requires high torsional rigidity, thus the spars are connected with a thin walled aluminum alloy sheet to create a wing box. The resultant torsional rigidity is many times higher than the sum of front and rear spars. At this stage in the design, this thickness is chosen to be constant along the span.

Ribs
The ribs are chordwise reinforcements between the front and rear spar. They play an important role in torsional stiffness of the structure. The ribs will vary in dimensions along the span of wing and have circular holes to minimize weight and leave space for fuel lining, pumps and cabling components. Some of the ribs will be located in fuel tanks and some ribs will serve as a boundary between fuel tanks, resulting in two different rib designs. Because sloshing of fuel should be avoided, the wing ribs that are located in the fuel tanks have an adjusted geometry at the bottom, allowing fuel to move freely below the rib without sloshing. The spacing between ribs is initially estimated using reference data, but as the design progresses, it follows that multiple spacings are required. Naturally, at the root more ribs are required for reinforcement since there is a highest stress concentration. See Figure 12.11 for sketches of both rib types used.
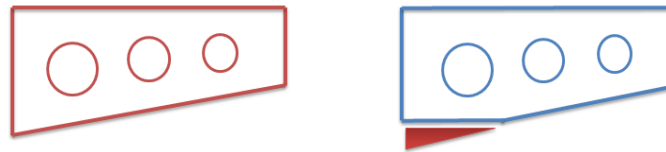
Figure 12.11: Rib Types

Stiffeners

The stiffeners are thin strips of aluminum that reinforce the plates and skins with respect to bending. Longitudinal stiffeners are located inside the wing box, attached to the top and bottom skin. This shape was chosen because at the top and bottom walls, the normal stress is maximum. Its open profile also improves the inspection procedure and reduces the amount of trapped fuel in the wing box. This is the left cross section illustrated in Figure 12.4. More longitudinal stiffeners are located towards the front of the wing, as this part needs most reinforcement. The upper surface of the wing box will be in compression which implies that the longitudinal stiffeners can buckle before even reaching the maximum load. This was taken into consideration while designing stiffener dimensions. Vertical stiffeners are attached to the outside of the spars and have a conventional L-shape profile as can be seen in Figure 12.2 on the right hand side. Their main purpose is to counteract the shear stress. Again, the configuration and spacing between stiffeners changes throughout the design progress. The spacing of vertical stiffeners on the front spar is constant and relatively small, while the spacing on the rear spar increases towards the tip. The dimensions of the stiffeners are chosen to be constant along the wing span.

Skins

An upper and bottom skin connect the spars and define the required airfoil geometry. The skins are, as all other main structural components, made of aluminum so that attachment of different parts is not an issue during assembly. The thickness of the wing skin should be in the range of $0.5 - 3$ mm as the wing weight can increase significantly due to a large skin thickness and the thin walled assumption cannot hold.

Fuel System Components

Below, each main member of the fuel system is treated separately and explained with respect to the presented design. Then, a general overview of all the main components and their location is given in a Figure 12.12.

Tanks

The fuel tanks should have a total volume sufficient to cover the design range of the aircraft including reserves. The required maximum fuel weight is 2938.5 kg, which (using a jet fuel density of 0.81 kg/L) corresponds to a volume of 3.63 m^3. The fuel tanks start as close to the root of the wing as possible, and continue until 85% of the wing span. In addition, the part of the wing box that is located inside the fuselage is also used as fuel storage. A surge tank is added at the tip after the last tank to provide extra space in case the fuel expands or the main tanks cannot hold all the fuel inserted. Using the CATIA model, the space in the main fuel tanks is determined to be 2.82 m^3, which is about 75-80% of the required total fuel space. The rest of the required volume can be stored in an extra fuel tank under the cabin floor, as business jets do not require significant baggage space. Naturally, more pumps, fuel lines and sealant are needed.

Pumps

The fuel pumps carry, along with the fuel lines, the fuel from the tanks to the propulsion units. Both are designed to supply 1.5 times the maximum required fuel flow by the engines. This quantity depends on the take-off thrust and specific fuel consumption and is determined by:

$$\text{Max. Fuel Flow} = 1.5 T_{TO}(c_j) \tag{12.5}$$

From this, a maximum fuel flow of 0.679 kg/s is found, during maximum take-off trust. The fuel pumps are implemented into the rib holes. Detailed design is not feasible at this stage in the design process.

Anti-sloshing Baffles
During special maneuvers such as climb, turn or roll, the fuel shifts around the fuel tank causing shift in center of gravity and change in moment of inertia. This has a negative effect on the lateral control. As stated earlier, the rib configuration prevents the fuel from sloshing.

Lines
The fuel lines carry the fuel towards the propulsion units. In the wing structure, lines are used when no fuel tank is present. These lines continue through the fuselage and end at the propulsion units. Just as for the fuel pumps, the rib holes are the attachment points. Again, detailed design is not feasible at this stage in the design process.

Sensors
The sensor system includes a fuel quantity indicating system. Multiple sensors need to be inserted into different locations of one fuel tank to be able to measure the fuel volume in each flight condition. Ultrasonic transducers will be used to measure exact fuel level. They will be located at the bottom of the tank, and the amount of remaining fuel is assessed based on time it takes for an emitted ultrasound to reach fuel surface and reflect back to the sensor. [50]

Sealant
In order to prevent from leakage and to ensure that structural members are not affected by the fuel, a fire resistant sealant is applied that encloses the fuel tank. External coating is also required to protect the fuel from lighting strike.

Vents, Drains, Inlet & Outlet
The venting system prevents excessive pressures from building up in the tanks and ensures that a positive pressure is provided in the tanks during flight. The fuel inlet is placed at the highest point possible, at the tip and bottom of the wing. The fuel outlet is located at the root and bottom of the wing.
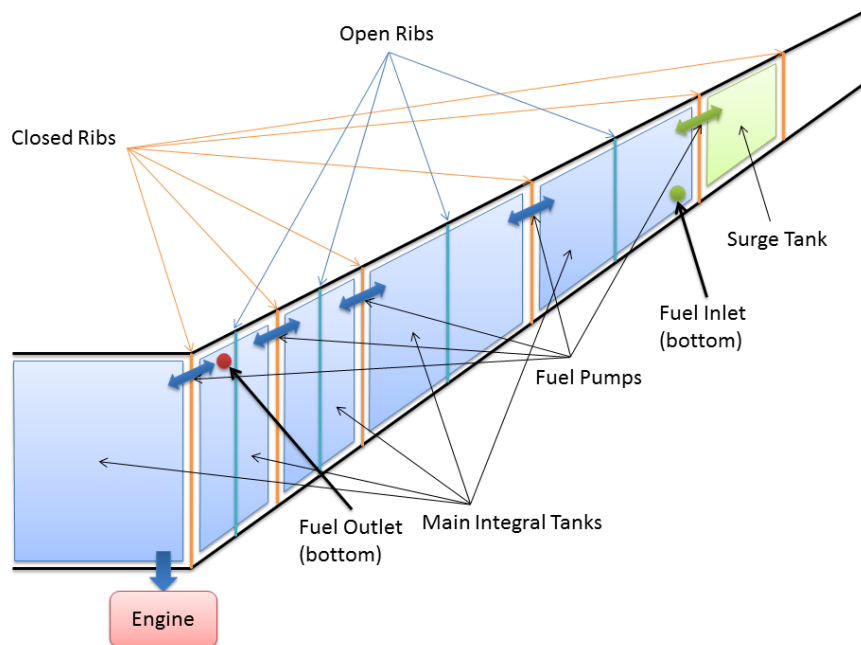
Figure 12.12: Overview of the Fuel System's Main Components

HLD & Control Surface Components

Below, each main member of the control surface and HLD configuration is treated separately and explained with respect to the presented design. Detailed design of these components is not feasible at this stage in the design process. The actuators are treated in Chapter 15.

Flaps & Ailerons

The flaps and ailerons are attached to the aft wing spar. For the ailerons, only a rotation point is needed, while for the Fowler type flaps a construction that extends the flap must be implemented.

Cabling

The cabling from flight control system to aileron and Fowler flap is placed in to the compartment behind the wing box aft spar. These cables should be designed to not interfere with moving structural parts of the ailerons and flaps.

12.2.5 Torsional Divergence & Shear Center Location

As stated before, it is essential for FSW configurations to have a wing structure that does not induce torsional divergence. In this section, a method is presented that analyzes the torsional divergence characteristics of the wing.

Approach

If a shear force is applied on a cross section, the location of the shear center with respect to the applied force determines if twisting is induced in the structure. In case of a FSW, the shear center should be shifted past the acting lift force, so that the wing does not twist in a direction that increases the local angle of attack. In reality, this comes down to reinforcing the leading edge of the wing structure, which is the actual approach to solving the torsional divergence issue.

The shear center location can be used to derive a relation to the dynamic pressure at which the wing will diverge. This dynamic pressure corresponds with a divergence speed. A cross section is made at the resultant lifting force, after which the shear center is determined. The shear center location is calculated using a simplified model of the wing box, depending only on the thickness of both spars and skins. As these thicknesses are constant along the span of the wing, this calculation fixes the values for the entire wing. In order to make the structure as light as possible, the desired shear center location is set to be only 1% of the wing box chord in front of the aerodynamic center. Then, for the cross section at the resultant lift force, a divergence speed is calculated. This speed should be higher the maximum speed during cruise, i.e. 0.95 Mach.

Shear Center & Aerodynamic Center

The aerodynamic center of the wing is located at approximately quarter chord. This corresponds to 27.3% of the wing box chord, starting from the front spar. For the automatic calculation of the shear center, depending on the thicknesses of spars and skins only, the cross section's dimensions are averaged to create a symmetric profile. The cross section is made perpendicular to the aerodynamic center axis, to allow further calculations on the divergence speed, which uses the exact same location of cross section. In the first iteration, the shear center was calculated to be at 39.9% of the wing box. By increasing the thickness of the front spar and decreasing the thicknesses of the skin and aft spar, the shear center was shifted to approximately 26.3%. The corresponding values are listed in Table 12.6.

Table 12.6: Potential Torsional Divergence Solution

	Thickness [mm]
Front Spar	40.80
Aft Spar	8.00
Top Skin	2.00
Bottom Skin	2.00

Applying these dimensions in CATIA, with the corresponding aluminum density, gives a total weight of the wing box of 809.66 kg, which is 79.25% of the Class II weight budget of 1021.60 kg of the entire wing. Although the wing box is the heaviest component in the wing, other components of the wing have yet to be sized. At the current design stage there is 211.94 kg available for the remaining components. Those components include airfoil skin, pumps, wires, hydraulic systems, HLD, main landing gears attachments, electronics, de-icing systems, external lighting, etc. However considering the value of the weight budget for the remaining components it is evident that the wing box is heavily overdesigned. Based on a rough estimation the weight for entire airfoil wing skin becomes approximately 140 kg. Skin thickness of 0.8 mm is used as well as 2700 kg/m^3 density of Aluminum alloy 6061 T4 [51]. This leaves 71.94 kg for other mentioned components. Therefore iterations are strongly required for the wing weight budget. More elaboration on this topic can be found in Section 12.2.7.

Final Wing Design

Technical drawings and CATIA renders of the wing box can be found below. Figure 12.13 represents a see through configuration of a half span wing whereas Figure 12.14 shows entire wing span. For more detailed dimensions of the geometry of a wing box the reader is directed to Appendix E.
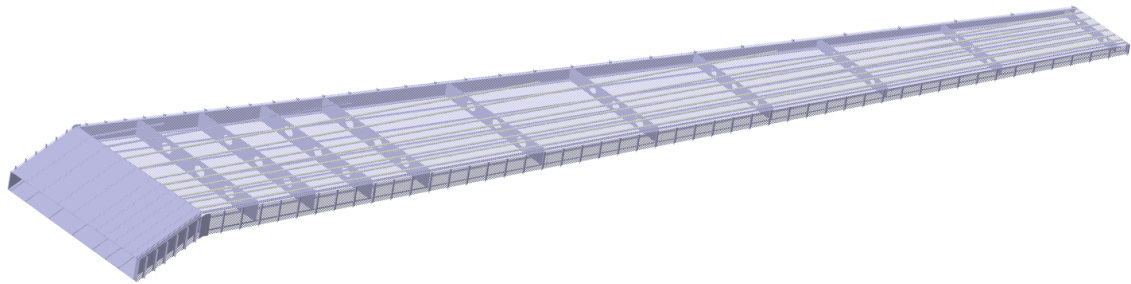
Figure 12.13: Half Span Wing Box
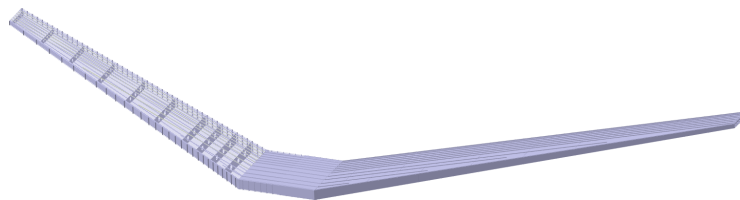
Figure 12.14: Full Span Wing Box

Divergence Speed

Using the definition of the shear center location with respect to the aerodynamic center, a divergence speed can be determined. The model used for this calculation can be found in Figure 12.15. The model shows a semi-rigid wing, which can bend around the bending stiffness axis K_γ and twist around the torsional stiffness axis K_θ. These axes rotate with a certain sweep angle, resulting in the reference frame $(\bar{x}, \bar{y})$. The resultant lift force acts at the center of pressure, which is defined as $(\bar{e}_{cp}, \bar{y}_{cp})$.
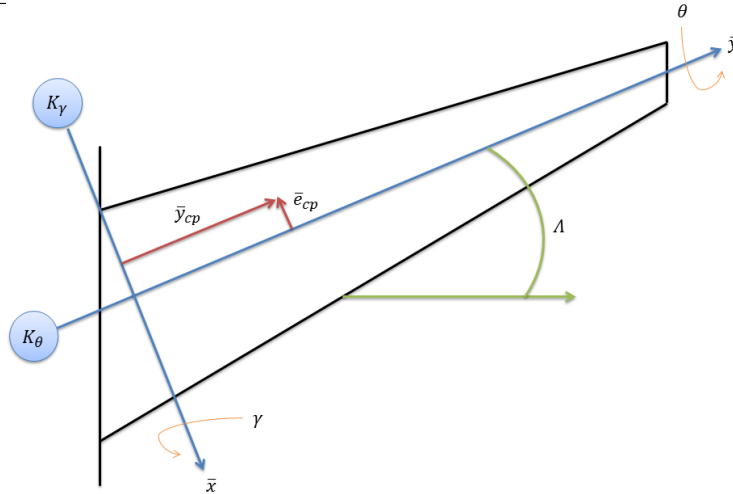
Figure 12.15: Top View of the Forward Swept Wing [52]

The resultant of the lift force is assumed to be located at $1/3$ of the span and at quarter chord of the wing. This lift force depends on the dynamic pressure, surface area, C_{L_α} and effective angle of attack:

$$L = qSC_{L_\alpha}\alpha_{eff} \tag{12.6}$$

Where the effective angle of attack is defined as:

$$\alpha_{eff} = \theta\cos\Lambda - \gamma\sin\Lambda \tag{12.7}$$

The static equations that relate the resultant lift force to an angular displacement are:

$$K_\theta\theta = L\bar{e}_{cp} \tag{12.8}$$

And:

$$K_\gamma\gamma = L\bar{y}_{cp} \tag{12.9}$$

These stiffness constants contain the geometrical properties that were determined in the shear center calculation in the form of a torsional constant J and moment of inertia I_{xx}. Combining all the information above in matrix format gives:

$$\begin{bmatrix} K_\theta & 0 \\ 0 & K_\gamma \end{bmatrix} \begin{Bmatrix} \theta \\ \gamma \end{Bmatrix} = qSC_{L_\alpha} \begin{bmatrix} \bar{e}_{cp}\cos\Lambda & -\bar{e}_{cp}\sin\Lambda \\ \bar{y}_{cp}\cos\Lambda & -\bar{y}_{cp}\sin\Lambda \end{bmatrix} \tag{12.10}$$

Rewritten:

$$\begin{bmatrix} K_\theta - qSC_{L_\alpha}\bar{e}_{cp}\cos\Lambda & qSC_{L_\alpha}\bar{e}_{cp}\sin\Lambda \\ -qSC_{L_\alpha}\bar{y}_{cp}\cos\Lambda & K_\gamma + qSC_{L_\alpha}\bar{y}_{cp}\sin\Lambda \end{bmatrix} \begin{Bmatrix} \theta \\ \gamma \end{Bmatrix} = 0 \tag{12.11}$$

A linear relation for the dynamic pressure can be found by taking the determinant of the matrix above:

$$q = \frac{-K_\theta K_\gamma}{SC_{L_\alpha}(K_\theta\bar{y}_{cp}\sin\Lambda - K_\gamma\bar{e}_{cp}\cos\Lambda)} \tag{12.12}$$

Its relation to divergence speed is given by:

$$q = \frac{1}{2}\rho V_{div}^2 \tag{12.13}$$

Applying the equations above to the relevant cross section at the resultant lift force gives a divergence speed of 1.44 Mach, which is significantly higher than the maximum cruise speed of 0.95 Mach. In conclusion: according to this calculation, the wing does not diverge and is therefore stable. This result was not expected, as the aircraft was initially not designed to fly at supersonic speed and the sweep angle of $-35°$ should affect the divergence speed significantly. In order to understand the relations between the various parameters and

the validity of the result, plots are created. First, Figure 12.16 shows the relation between the sweep angle and dynamic pressure for the designed wing box.
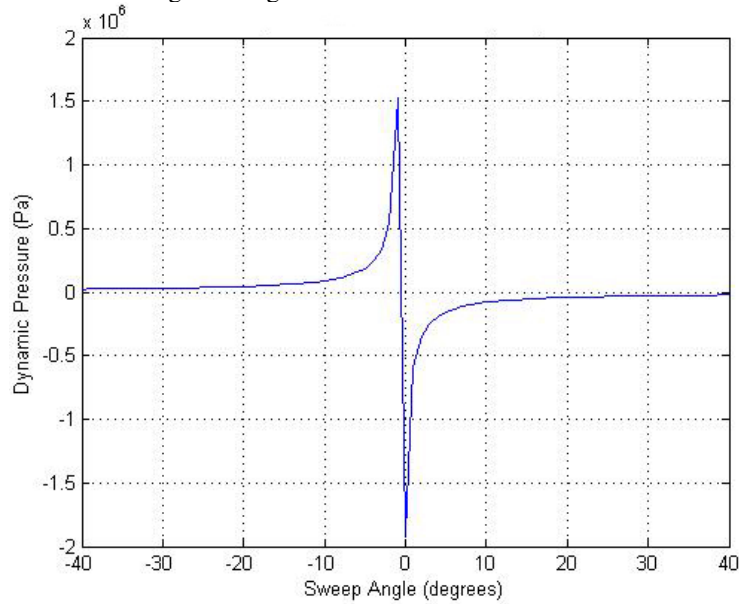
Figure 12.16: Plot of Dynamic Pressure vs. Sweep Angle

In Figure 12.16, an asymptote can be found at a sweep angle of zero degrees. This means that for an unswept wing, the divergence speed goes to infinity, while it decreases for a more forward swept wing. Only negative solutions for the dynamic pressure exist for positive values of the sweep angle, which means that a backward swept wing does not show any divergence. Figure 12.17 shows the relation between the distance aerodynamic center to shear center and the corresponding divergence Mach number. Here, the sweep angle is set at $-35°$:
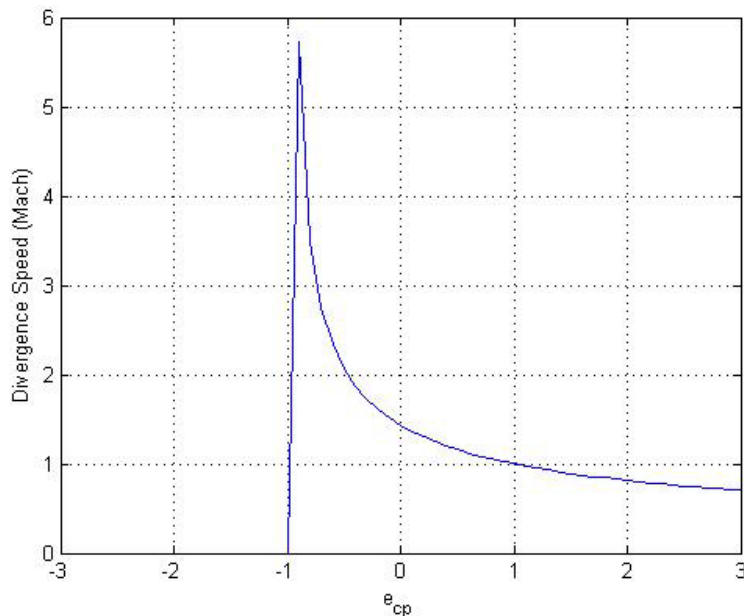
Figure 12.17: Plot of Distance from Aerodynamic Center to Shear Center vs. Mach Number

In Figure 12.17, an asymptote can be found at approximately $\bar{e}_{cp} = -1\,m$. This means that if the shear center is located one meter in front of the aerodynamic center, the aircraft is completely divergence free and

is able to fly at any given speed. As it is impossible to locate the shear center outside the closed wing box, this condition is not feasible for our design. On the other hand, the plot shows that the shear center could still be located behind the aerodynamic center for a given maximum cruise speed of 0.95 Mach, which is by definition an incorrect result. This is most likely due to the simplified approach, using discretization of the wing into one cross section to investigate the divergence behavior of the entire wing. In the next section, an elaboration on this issue can be found.

Complication Analysis

If considering a local cross section of a wing box, the wing does not seem to diverge, however by analyzing the entire wing configuration globally, the current wing design will not be able to escape the torsional divergence. Because at the root the wing attaches to the fuselage, the highest stress concentration is located at this point. The resultant lift of the entire wing is located at approximately at one third of the span and a quarter chord length of the aerodynamic center. Since the wing box and wing have a closed cross section, the shear center can only be within the closed area. This implies that the shear center cannot be shifted any further than the leading edge. By taking a moment from this location to the root it can be seen that the shear center at the root is still behind the aerodynamic center even if the shear center is located at the leading edge. This is demonstrated in Figure 12.18.
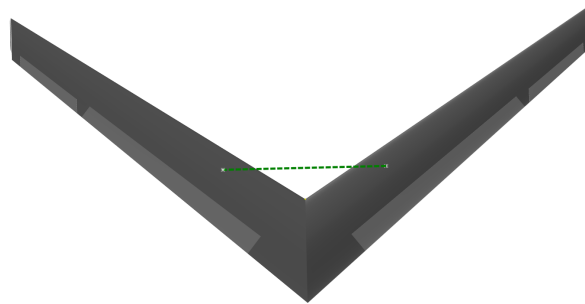
Figure 12.18: Location of Resultant Force

This implies that in the given geometrical configuration of the wing and wing box, the aircraft will not be able to fly without diverging. The sweep angle of the wing is too high. This also explains why the slightly forward swept Hansa Jet in Figure 9.1 could be solved using a structural solution.

From this point of view, the most optimum wing configuration would have a low aspect ratio to decrease moment arm and decrease stress distribution. Maximum sweep angle should be chosen such that location of aerodynamic center where result lift force passes, cannot be outside of the enclosed area of the wing cross section at the root. After analyzing Figure 12.16 more closely, it can be suggested to decrease the forward sweep angle to at least 10°or lower considering the divergence problem alone. It can be seen that lowering the value will result in an exponential growth of dynamic pressure. However changing the wing geometry would have a strong influence on the overall aircraft design. First of all, higher aspect ratio and high sweep angle decrease critical Mach number and therefore increase drag. Note that currently, the zero-lift drag is already rather high, increasing it anymore would require change of engines. Substituting new engines would most likely result in an increase of the overall MTOW. From there of, a snow ball effect takes place and the entire iteration would be required.

12.2.6 Structural Analysis

Before presenting the results that have been obtained with CATIA using similar approach as was explained in Section 12.1, it is important to state all assumptions that were considered during numerical analysis.

Assumptions:

- The closed-section beam which represents the wing box is assumed to be clamped at the root of the wing - This assumption basically results in no deflection or twist at the root and means the internal stresses will increase from the tip to the root of the wing
- The drag created by the wing is neglected
- The wing box bears all the loads
- The wing box is made of isotropic material, and will thus act as a perfect beam - The aluminum alloy will have perfect isotropic properties
- Both the gravitational force on the wing and the weight of the landing gear are assumed to act as a single point load
- There will be no deformation of the wing box under the given loads
- The cross section will be assumed to be a thin-walled
- Mesh size in the CATIA was chosen to be 10 mm

Load Cases

Next, it is important to identify all the forces that the wing box has to withstand as well as examine the different load cases. The following forces will have effect on the structural analysis:

- **Lift distribution:** the entire wing is assumed to have linear lift distribution with the resultant force acting at a quarter chord length from leading edge. The wing box is expected to hold maximum total lift force together with HLD induced lift.
- **Component weights:** this includes the weight of the wing box, fuel tanks, pumps, skins, HLD and other wing components.
- **Fuel weight:** the fuel weight is distributed throughout 85% of the wing span and acts through the lower skin of the wing box. The fuel weight counteracts the lift force and reduces stress concentration at the root.
- **Main gear:** the force the main gear exerts on the wing box during taxiing and on the ground. The load is applied to the corresponding location of the main gear. During flight phases landing gear is added to the component weight force.

Load Case 1. Cruise condition, maximum load factor, empty fuel tank: The first load case is considered to be the most critical one, because the wing box is subjected to the highest load factor of 2.9 as was determined in V-n Diagram, in Chapter 10. Under the conditions of cruise altitude and velocity, the aircraft will have empty fuel tank. This condition can occur at the end of a long flight when all the reserved fuel is used up. A safety factor is included in all load calculations.

Load Case 2 Cruise condition, full fuel tank: The second load case is similar to the previous one, however the fuel tank will be full which is expected to lower stress values in the wing. Also normal conditions will be considered with a load factor of 1.

Load Case 3 Stationary Position: The third load case examines the wing box on the ground with full fuel tanks. It is important that the wing does not deflect under its own weight when there is no lift induced. The main landing gear force will act upward and reduce stress caused by the weight component force and fuel weight.

Results

This section will present Figures with stress and deflection distribution for all three load cases as well as a Table with summarized maximum values.

Load Case 1
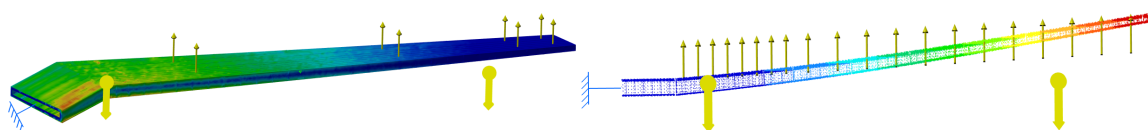
Figure 12.19: Stress Distribution for Load Case 1   Figure 12.20: Load Case 1 Wing Box Displacement

As can be seen from Figure 12.19, the red colored regions represent the highest Von Mises stresses at the root. This is expected since the wing box is clamped at the root. At the tip where the wing box is free to bend and rotate the absolute value of stress is minimal. Note that the four large yellow arrows represent the weight of the components. Figure 12.20 shows maximum deflection compared to all load cases which equals to 616.3 mm. This value is reasonably representative given the extreme loads that the wing box is undergoing.

Load Case 2

In Figure 12.21 it can be seen that the maximum stress is located near the root towards the leading edge. However the maximum stress of the entire wing box is 2.6 times smaller compared to the maximum stress of load case 1. The deflection in Figure 12.22 is also smaller compared to the first load case.
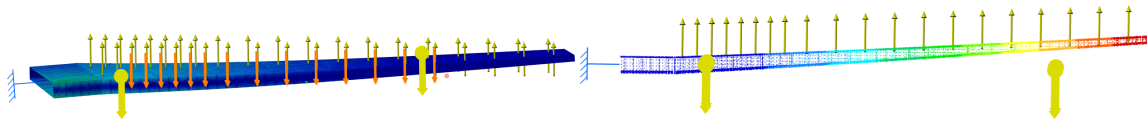
Figure 12.21: Stress Distribution for Load Case 2   Figure 12.22: Load Case 2 Wing Box Displacement

Load Case 3

In Figure 12.23, the orange arrows pointed downwards represent the fuel weight. The landing gear force is shown as yellow arrows located in the swept part of the wing near the root. In Figure 12.24, the tip of the wing box deflects downward.
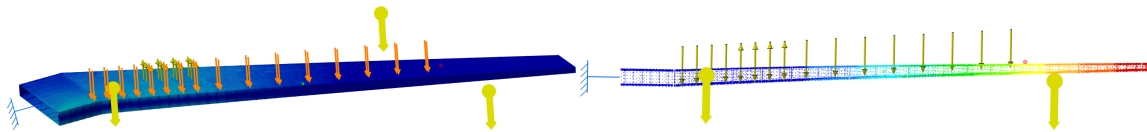
Figure 12.23: Stress Distribution for Load Case 3   Figure 12.24: Load Case 3 Wing Box Displacement

Table 12.7: CATIA Structural Analysis Results

	σ_{max} [MPa]	δ_{max} [mm]
Load Case 1	334.68	616.3
Load Case 2	129.75	121.5
Load Case 3	99.03	67.8

The Table 12.7 summarizes the maximum deflection and maximum Von Mises Stress in the wing. As expected, the maximum deflection at the tip occurs during load case 1. The maximum stress of 334.68 MPa is 1.61 times smaller compared to the maximum allowable stress of the Aluminum alloy 7150.

Verification of Stress Analysis

In order to verify the design and methods used, an analytical calculation is executed. Several parameters are determined analytically and compared to the numerical outcome that was calculated in CATIA. For appropriate comparison, the intermediate and final results of each approach are examined. Cruise condition will be examined with a full fuel tank and load factor of 1. The Moment of inertia is examined at the root location. Note that this calculation is performed for half of the wing span. In the analytical analysis, Equations 12.14 and 12.15 are used to determine normal and shear stresses, respectively:

$$\sigma = \frac{I_{xx}M_z - I_{xz}M_x}{I_{xx}I_{zz} - I_{xz}^2}x + \frac{I_{zz}M_x - I_{xz}M_z}{I_{zz}I_{xx} - I_{xz}^2}z \tag{12.14}$$

$$q_b = -\frac{I_{xx}S_x - I_{xz}S_z}{I_{xx}I_{zz} - I_{xz}^2} \int_0^s txds - \frac{I_{zz}S_z - I_{xz}S_x}{I_{zz}I_{xx} - I_{xz}^2} \int_0^s tzds \qquad (12.15)$$

The results of the analytical calculation can be found in Table 12.8. The moment of inertia, mass, maximum stress and deflection are listed together with the marginal error in percentage (with respect to the computational results).

Table 12.8: Analytical vs Numerical Results

	Moment of Inertia I_{xx} [m^4]	Mass [kg]	σ_{max} [MPa]	δ_{max} [mm]
Numerical	0.0070	404.83	129.75	91.5
Analytical	0.0068	400.21	125.79	88.8
Marginal Error [%]	2.79	1.14	3.05	2.96

From Table 12.8, it can be seen that using the analytical approach, all values are slightly smaller compared to analysis performed in CATIA. This can be explained by the fact during analytical approach, more assumptions had to be included in order to simplify the analysis. In general, the smaller the cross section, the bigger the influence of the thin walled assumption is on the accuracy of the results. Therefore, the most critical location is the tip. Since CATIA does not use simplifications and calculates exact dimensions, it has higher values of moment of inertia and weight of the wing box.

12.2.7 Conclusion & Recommendations

In conclusion, given the current geometry of the wing, the designed aircraft will not be able to fly safely at the current design stage. This means that further iteration is required to solve this problem. There are a number of solutions which can be considered in future research.

First of all, the sweep angle can be reduced in order to coincide the shear center at the root with aerodynamic center at the resultant lift force. However, this will increase the drag and reduce critical Mach number, which is highly undesirable. The aspect ratio and taper ratio can also be adjusted to shift the shear center to the desired location. These changes in configuration affect the control and stability characteristics as well as the weight and balance properties, which has to be taken into account.

Making the leading edge of the wing a load carrying member also improves the shear center location. This means that the wing box can be designed to consist of the leading edge skin and one aft spar. This can be done, because slats are not a part of the design. The fuel system is also affected by this modification and needs to be redesigned. In addition, one has to take into account that the structural analysis of such a curved profile is relatively complex and time consuming.

Another solution involves an unsymmetrical cross section of the wing box. For example, the stiffeners and ribs can be placed at different angles. This will have a larger effect on the coupled bending and torque terms in the divergence matrix in Equation 12.10. Increasing only the K_θ and K_γ terms will be insufficient because the aerodynamic center is too far in front as previously mentioned.

Finally, an alternative methodology using composite materials should be considered. Aeroelastic tailoring seems to be more advisable and appropriate solution for the given sweep angle and wing configuration. The layer configuration of the composite can be designed to induce coupling between bending and twisting so that the wing box naturally twists down when it bends upward. The coupling is represented by the variables in the divergence matrix next to the K_θ and K_γ terms, which are zero for no coupling characteristics. Note that the divergence matrix would still have to be kept symmetric to ensure appropriate and real dynamic pressure values. When designing a composite wing structure, one has to account for the different thermal expansion coefficient with respect to connected metal parts, such as the integration in the fuselage. General attachment methods between composite and metal components have to be analyzed in detail. Another advantage of using composite material is lower weight. Compared to Aluminum alloy 2024 T3, the density of composite material is 1.73 times lighter (see Table 12.1). This means that if the currently designed wing

box was build using Quasi-isotropic composite, it would be equivalent to 45.8% of the total wing weight budget. This however is not an equivalent comparison as the wing box would have to be designed using different methodologies and characteristics and thus the geometry would be different. Cost of the composite material would be the limiting factor.

Overall, the structure was examined using static loads. From structural point of view, the wing box is able to carry the maximum load in the flight envelope, but the dynamic characteristic of the flight will diverge the wing and make it unstable. In the future, it is essential to examine more dynamic loads and their consequence on the wing box. For example, the landing gear was considered to be more of a static load but it also has a dynamic impact during landing.

Although certain load cases already have been examined, the wing box design is still in a preliminary design stage. More load cases have to be considered with different input parameters such as different altitude, velocities, number of passengers, fuel weights and many more. Several criteria that will have a large impact on the future design are the HLD and control surface components, since the wing box will carry all the loads from Fowler flaps and ailerons. Note that the wing box is most probably overdesigned at this stage. This means that, in general, further analysis should be performed to optimize the structure in terms of weight and cost reduction.

Another recommendation for future continuation of the design is to eliminate as many of the assumptions as possible and analyze the wing box with more precision. This in turn will be more time consuming. In addition, a more detailed design process will have to be carried out, which will determine characteristics such as the rivet type and pitch, the external paint type and fuel system attachments.

12.3 Landing Gear Design & Integration

This section elaborates on the design of the landing gear system. This includes calculations of the aircraft tire selection, the strut dimensions, shock absorber dimensions and the retraction schemes. In the Midterm Report [1], the configuration for the landing gear is decided to be a retractable nose wheel configuration. The method to analyze the empennage design will differ from the other structural components. Roskam IV [53] will be used instead of CATIA. Therefore the approach of this section will be different.

12.3.1 Tire Selection Procedure

In order to select correct aircraft tires the following procedure has been used.

1. **Main gear tires:** The maximum static load on each main gear strut is determined using Figure 12.25. The aircraft is FAR 25 certified resulting in a multiplication of 1.07 of loads. To account for unexpected extra weight during the design process, the load is multiplied by another factor of 1.25. To calculate the maximum static load on each main gear tire the load on the main gear strut is divided over the number of tires, see Equation 12.16.
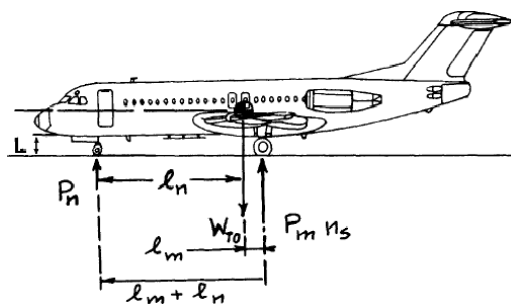
$$P_{m_t} = \frac{P_m}{n_t} \qquad (12.16)$$

Figure 12.25: Nose Strut and Main Gear Strut Load Definition [53]

2. **Nose gear tires:** The maximum static load on the nose gear tires is determined in the same way as the main gear tires. Using Figure 12.25 the nose gear strut load is determined. Multiply this load with 1.07 and 1.27 for FAR 25 regulations and allowance leaves room for aircraft weight growth. Dividing the strut load over the number of tires will result in the load per tire.

3. **Maximum dynamic load per nose gear tire:** The dynamic load for the nose gear tires is determined using Equation 12.17. Roskam suggests a value of 0.45 for a_x/g for dry concrete with anti-skid brakes. For type III tires the determined load from Equation 12.17 has to be divided by a factor of 1.45 to obtain design maximum dynamic load.

$$P_{n_{dyn_t}} = W_{TO} \frac{(l_m + a_x/g \cdot h_{cg})}{n_t (l_m + l_n)} \tag{12.17}$$

4. **Maximum tire operating speed:** The maximum tire speed will be the highest tire speed which occurs either during landing or take-off. The tire speed is calculated using Equations 12.18 & 12.19.

$$Landing : V_{tire/max} = 1.2V_{s_L} \tag{12.18} \qquad Take-off : V_{tire/max} = 1.1V_{s_{TO}} \tag{12.19}$$

5. **Tire selection:** Select the tires that meet the maximum load and the tire speed requirement.

The inputs & outputs from the procedure are shown in Tables 12.9 & 12.10 respectively.

Table 12.9: Input Variables Tire Selection

Parameter	Value	Unit
l_m	1.17	m
l_n	8.93	m
h_{cg}	1.45	m
W_{TO}	9066	kg
n_s	2	-
n_t	2	-
V_{s_L}	43.2	m/s
$V_{s_{TO}}$	25.6	m/s

Table 12.10: Output Variables Tire Selection

Parameter	Value	Unit
P_n	10.3	kN
P_m	39.3	kN
$P_{n_{design}}$	13.7	kN
$P_{m_{design}}$	52.6	kN
$P_{n_{dyn_t}}$	5.33	kN
P_{n_t}	6.86	kN
$P_{m_{dyn_t}}$	26.3	kN
$V_{tire/max}$	116.0	m/s

After the procedure, tires which meet all the requirements have been listed. Many tires have been left out based on their size, these tires did meet all requirements but were designed for larger aircraft and did not fit in the fuselage when stored. Tables 12.11 & 12.12 show the possible tires for the nose wheel and main gear respectively.

Table 12.11: Selection of Nose Wheel Tires [54]

$D_{0_{MAX}}$ [inch] (m)	$D_{0_{MIN}}$ [inch] (m)	W_{MAX} [inch] (m)	W_{MIN} [inch] (m)	Ply Rating	$Pressure_{inflation}$ [psi] (bar)	P_{max} [lbs] (kg)	Speed Index [mph] (km/h)
13.75(0.3492)	13.2(0.3353)	6.1(0.1549)	5.75(0.1461)	12	95 (6.55)	2450 (1111)	120 (193)
17.5(0.4445)	16.8(0.4267)	6.3(0.1600)	5.9(0.1499)	8	55 (3.79)	2350 (1066)	120 (193)
17.13(0.4351)	16.54(0.4201)	6.89(0.1750)	7.5(0.1905)	8	61 (4.21)	2490 (1129)	120 (193)

Table 12.12: Selection of Main Wheel Tires [54]

$D_{0_{MAX}}$ [inch] (m)	$D_{0_{MIN}}$ [inch] (m)	W_{MAX} [inch] (m)	W_{MIN} [inch] (m)	Ply Rating	$Pressure_{inflation}$ [psi] (bar)	P_{max} [lbs] (kg)	Speed Index [mph] (km/h)
20.85(0.5296)	20.1 (0.5105)	7.3 (0.1854)	6.85 (0.1740)	16	125 (8.62)	6650 (3016)	150 (241)
21.25(0.5398)	20.6 (0.5232)	7.3 (0.1854)	6.8 (0.1727)	12	166 (11.45)	6400 (2903)	225 (362)
21.76(0.5527)	21.14 (0.5370)	7.05 (0.1791)	6.73 (0.1709)	12	135 (9.31)	6700 (3039)	160 (258)
22.15(0.5626)	21.55 (0.5478)	5.7 (0.1448)	5.35 (0.1359)	12	250 (17.24)	7100 (3221)	160 (258)

For the tire selection a Load Classification Number (LCN) analysis has been performed. The LCN is a number expressing the relative effect of an aircraft on the runway pavement. The Torenbeek method [55] has been used for the analysis. The LCN analysis resulted in no possible tires for the Phoenix 5600. The LCN constraint of the Torenbeek method is 38 years old which is outdated, therefore the LCN analysis has not been included in the tire selection.

12.3.2 Shock Absorber Sizing

In order to size the shock absorber of the landing gear system the following procedure has been used.

1. **Kinetic energy main landing gear** It is assumed that all kinetic energy from the touchdown needs to be absorbed by the tires and shock absorbers of the main landing gear. This can be calculated by Equation 12.20.

$$E_t = n_s P_m n_g (\eta_t s_t + \eta_s s_s) \tag{12.20}$$

2. **Shock absorber length main landing gear** The length of the absorber of the main landing gear s_s can be calculated using Equation 12.21. It is suggested by Roskam to add 0.0254 m to s_s which gives the design strut length s_{design} as shown in Equation 12.22. The main gear tire deflection is calculated with Equation 12.23. The selected tires for the landing gear are highlighted by green.

$$s_s = \left(\frac{0.5(n_s P_m / g) w_t^2}{n_s P_m N_g} - \eta_t s_t \right) / \eta_s \qquad (12.21)$$

$$s_{s_{design}} = s_s + 0.0254 \qquad (12.22)$$

$$s_t = D_{0_{MAX}} - D_{0_{MIN}} \qquad (12.23)$$

3. **Diameter of the shock absorber/strut** The approximate diameter in [m] of the shock absorber/strut can be estimated from Equation 12.24.

$$d_s = 3.800 \cdot 10^{-3} + 5.119 \cdot 10^{-4} \sqrt{P_n} \qquad (12.24)$$

4. **Shock absorber nose gear** The required length of the shock absorber of the nose gear can be calculated using Equations 12.20 – 12.22 with some modifications:

   - $n_s P_m$ in Equation 12.21 needs to be changed to P_n
   - P_m needs to be changed to P_n
   - s_t is the nose gear tire deflection

The inputs & outputs from the procedure are shown in Tables 12.13 & 12.14 respectively.

Table 12.13: Input Variables shock absorber

Parameter	Value	Unit
n_s	2	-
n_t	2	-
P_n	10.3	kN
P_m	39.3	kN
n_g	2	-
η_t	0.47	-
η_s	0.80	-
w_t	3.66	m/s

Table 12.14: Output variables Shock Absorber

Parameter	Value [m]
$s_{s_{nose}}$	0.540
$s_{s_{design_{nose}}}$	0.565
$s_{t_{nose}}$	0.0140
$d_{s_{nose}}$	0.0548
$s_{s_{main}}$	0.415
$s_{s_{design_{main}}}$	0.440
$s_{t_{main}}$	0.0190
$d_{s_{main}}$	0.0954

12.3.3 Verification of Tire Selection & Shock Absorber

A verification of the calculations for the tire selection and the shock absorber has been performed. The numerical solutions from MATLAB will be checked by results from MAPLE. The error should be zero because both programs use the same equation to calculate the results. However during the calculations intermediate round off could lead to deviations in the results. As long as the marginal error stays small it can be concluded that the equations have been implemented correctly. The results of the verification process are shown in Table 12.15. The error fluctuates at a value about $5.63 \cdot 10^{-5}$ % due to the difference in significant digits of floating-point numbers. MATLAB uses 16 significant digits where MAPLE only uses 10 significant digits.

12.3.4 Strut Material

The material of the strut can be chosen. Aluminum and titanium alloys are commonly used in aerospace designs. The landing gear system needs to be corrosive resistant since the landing gear can be wetted by rain and surface water from the runway. Furthermore, the landing gear is a very complex system. It consists of multiple actuators and hinges.

The static and dynamic forces on the nose gear and main landing have been determined in Section 12.3.2. The struts need to withstand those compressive forces on ground and during landing. The required yield strength can be calculated using Equation 12.25. A safety factor of 1.25 is required [56]. The inputs & outputs from the procedure are shown in Tables 12.16 and 12.17 respectively.

$$\sigma = 1.25 \cdot \frac{P}{A} \qquad (12.25)$$

Table 12.15: Landing Gear Verification Results

Parameter	Numerical Solution	Maple Solution	Unit	Marginal error [%]
P_n	10.3	10.3	kN	$5.631 \cdot 10^{-5}$
P_m	39.3	39.3	kN	$5.630 \cdot 10^{-5}$
$P_{n_{design}}$	13.7	13.7	kN	$5.624 \cdot 10^{-5}$
$P_{m_{design}}$	52.6	52.6	kN	$5.629 \cdot 10^{-5}$
$P_{n_{dyn_t}}$	5.33	5.33	kN	$5.630 \cdot 10^{-5}$
P_{n_t}	6.86	6.86	kN	$5.628 \cdot 10^{-5}$
$P_{m_{dyn_t}}$	26.3	26.3	kN	$5.630 \cdot 10^{-5}$
$V_{tire/max}$	116.0	116.0	m/s	$5.630 \cdot 10^{-5}$
ss_{nose}	0.540	0.540	m	$5.629 \cdot 10^{-5}$
$ss_{design_{nose}}$	0.565	0.565	m	$5.637 \cdot 10^{-5}$
st_{nose}	0.0140	0.0140	m	$5.630 \cdot 10^{-5}$
ds_{nose}	0.0548	0.0548	m	$5.632 \cdot 10^{-5}$
ss_{main}	0.415	0.415	m	$5.630 \cdot 10^{-5}$
$ss_{design_{main}}$	0.440	0.440	m	$5.629 \cdot 10^{-5}$
st_{main}	0.0190	0.0190	m	$5.634 \cdot 10^{-5}$
ds_{main}	0.0954	0.0954	m	$5.631 \cdot 10^{-5}$

Table 12.16: Strut Material Selection Input

Parameter	Value	Unit
$P_{n_{design}}$	13.7	kN
$P_{m_{design}}$	52.6	kN
ds_{nose}	0.0548	m
ds_{main}	0.0954	m

Table 12.17: Strut Material Selection Output

Parameter	Value [MPa]
σ_{nose}	18.3
σ_{main}	23.1

The stress on the nose gear strut and main gear strut are 18.3 MPa and 23.1 MPa, respectively. Aluminum Alloy 6061-T6 can be used as the material of the struts. Its yield strength is the lowest of the list, Table 12.18, which still satisfy our stress. Aluminum Alloy 6061-T6 is also the least expensive [57].

Table 12.18: Material Properties [58] [59] [60]

Material	Yield strength [MPa]	Density [kg/m^3] x 10^3
Aluminum Alloy 6061-T6	276	2.70
Aluminum Alloy 7075	503	2.81
Aluminum Alloy 8090-T8151	370	2.54
Aluminum Alloy 8091-T8	538	2.55
Aluminum Alloy 8093	348	2.55

12.3.5   Actuator Sizing

For the actuator sizing, the retraction schemes of the nose and main landing gear have been used (see Figures 12.27 and 12.28). The distance between the hinge points for the actuator in fully retracted and extracted condition are measured using Equation 12.26. The angles and distances are described by Figure 12.26. The maximum length and minimum length determine the actuator extended and retracted length. The dimensions of the actuator length for the nose and main landing gear are shown in Table 12.19.

$$l_r = \sqrt{[(z_p + Rcos\phi)^2 + (x_p - Rsin\phi)^2]} \tag{12.26}$$
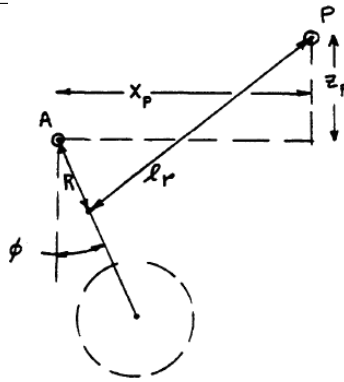
Figure 12.26: Angles and Length Definition for the Actuator Sizing

Table 12.19: Actuator Length

	Minimum length [mm]	Maximum length [mm]
Nose gear actuator	550	1100
Main gear actuator	370	740

12.3.6 Retraction System

The nose gear retracts forward into the space in the nose of the fuselage. By retracting forward, drag is used to assist in pushing the forward oriented retraction system into the deployed position. Due to the limited storage in the wing, the retraction system of the main landing gear will be retracted into the near bottom of the fuselage.

The retraction mechanisms for both nose gear and main gear have been designed using CATIA. Each system is shown in three different phases: retracted, half deployed and deployed. The nose landing gear is shown in Figure 12.27, in which a side view is presented. The main landing gear is shown in Figure 12.28, only one half of the airplane is shown since the main landing gear is symmetrical. Both retraction mechanisms use the same method and an actuator is used to rotate the plate which deploys or retracts the gear.

Figure 12.27: Nose Landing Gear Retraction Scheme
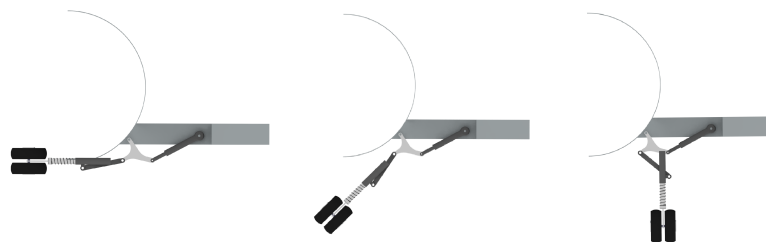
Figure 12.28: Main Landing Gear Retraction Scheme

13 Weight & Balance

In this chapter the entire weight and balance estimation and iterations are discussed. For this chapter, the chronological order of the design process is taken as guideline to describe the taken steps. First starting out with the Class II weight estimations in Section 13.1. After these are made and verified, the Class II balance is performed in Section 13.2. Iterations have to be performed to optimize the position of subsystems. During the weight and balance estimation, Roskam V [9] is continuously used as a guideline through the design process.

13.1 Class II Weight Estimation

In this section the class II weight estimation is discussed. First, the method is described, followed by the verification and finally the results are summarized.

13.1.1 Method

From Class I weight & balance(see Midterm report [1]), a rough estimate for the total weight and C.G. position were determined. The Class II weight estimation will give a more precise outcome. In Roskam aircraft are categorized in different groups. For the business jet design the equations described under the civil aviation method should be used. Note that Roskam uses equations from other design methods for the weight and balance estimation. For the weight determinations of the subsystems, the methods described in Roskam are selected and the average of the results is taken. For civil aviation specifically, the used equations are derived by General Dynamics (GD) and Torenbeek [55]. In order to minimize the chance to mis-interpreting the equations, verification using reference aircraft is necessary. The equations that are used, are not repeated in this report due to their amount and complexity. No alterations are made in most of these equations (those who were altered are mentioned in Section 13.1.2).

13.1.2 Verification of Weight Estimation

For the weight estimation the software tool MATLAB is used [61]. Because of error sensitivity, it is decided to verify each single equation with known reference data. This is useful not only for avoiding mistakes, but where necessary the equations are "calibrated" by changing the so called fudge-constants. This means changing the parameters of the equations so that the results are correct for (a group of) reference aircraft, for which the real weights are known. This is necessary because the equations are derived by using a rather wide range of aircraft. Making this range smaller and most important closer to the Phoenix 5600 design, will result in more accurate results. The required data to do this can be found in Appendix A from Roskam V [9]. In order to make this verification, a single reference aircraft is used. This reference aircraft is the Lockheed Jetstar [62]. The verification method points out that some fudge constants have to be changed. From Torenbeek, equations for the wing, empennage and fuselage have to be adapted. For GD's method, the equation for the fuselage weight estimation has to be adapted as well. By changing these constants, the computed value is much closer to the known weight of the reference aircraft. Which results in more accurate estimations for the business jet design. When all the weights of the subsystems are added up, the empty weight that has been estimated by the equations is around 1% of the real value of the reference aircraft. The results of the Class II weight estimation can be found in Table 13.1.

13.1.3 Class II Weight Estimation Results

Table 13.1: Weight Estimation Results

(sub) Part	Symbol	Class I Estimation [kg]	Class II Estimation [kg]
Wing	W_w	934.69	1021.60
Horizontal tail	W_h	94.29	68.22
Vertical tail	W_v	91.81	142.65
Canard	W_c	62.03	44.38
Fuselage	W_f	912.30	714.14
Nacelles	W_n	174.90	250.38
Nose gear	W_{ng}	48.13	48.72
Main gear	W_{mg}	272.76	248.28
Structure	W_{struc}	**2590.92**	**2538.37**
Engine	W_{eng}	-	748
Fuel system	W_{fs}	-	88.90
Propulsion system	W_{prop}	-	42.20
Powerplant	W_p	**827.88**	**879.10**
Flight controls	W_{fc}	-	236.21
Hydraulics/pneumatics	W_{hps}	-	79.09
Instruments/avionics	W_{iae}	-	225.69
Electrical system	W_{els}	-	310.15
Airco/anti-de-icing	W_{api}	-	247.71
Auxiliary power unit	W_{apu}	-	66.60
Oxygen system	W_{ox}	-	16.98
Furnishings	W_{fur}	-	462.42
Auxiliary gear	W_{aux}	-	47.27
Paint	W_{paint}	-	37.46
Fixed Equipment	W_{FEQ}	**1581.14**	**1729.58**
Empty Weight	W_E	**4999.9**	**5147.05**

13.2 Class II Balance

Once all weights are known, balancing the aircraft is the next step. First, the center of gravity of each part (same as in Table 13.1) is determined individually. For balancing the aircraft, [9] and [63] provide helpful data to find the center of gravity of all the structural parts. Second, by taking the moments around a fixed point, the origin is located 5m before the nose and 5m below the fuselage center line, the center of gravity of the empty jet can be determined.

The next step is to generate the so called "potato diagrams" (loading diagrams) to determine the C.G.-range and location. These diagrams take all the additional weights (fuel, payload, crew) into account. For each loading scenario a different loading diagram is created with accessory C.G.-range and location. The scenarios are the same as in the Midterm Report [1];

- Scenario 1: crew (and their bags) → passengers → baggage of the passengers → fuel (first wing, if still required then the tail)
- Scenario 2: fuel (first wing, if still required then the tail) → crew (and their bags) → passengers → baggage of the passengers
- Scenario 3: crew (and their bags) → baggage of the passengers → passengers → fuel (first wing, if still required then the tail)
- Scenario 4: fuel (first wing, if still required then the tail) → crew (and their bags) → baggage of the passengers → passengers

13.2.1 Iteration Process

At this point, the iteration process can be initiated. This is a rather complex process: initial values need to be chosen for the location of the structural parts. This results in the weights of all subsystems (some of

them are depending upon distances between them) and an initial C.G.-range and location. However, at this point not all the requirements are met. Therefore the locations of subsystems need to be altered slightly and/or other input values such as strut length and main gear width can be changed as well. This is the start of the first iterations, each time using the results of the previous run as input. Once one requirement is met, the parameters can be changed accordingly so that not only the initial requirement is met, but in addition the next requirement as well.

This can only be done by designing the first iterations for the requirement which has the biggest solution range. At this point the driving parameters such as wing location and main gear location can be used. For more concise requirements, only parameters who do not have a big influence in the overall design can be used (i.e. strut length and main gear width).

Besides, weight changes of particular subsystems as the wing, fuselage and empennage will also influence the iteration process. When the wing is designed completely to carry all loads, its weight can differ from the Class II weight estimation. The implementation of a new iteration loop is necessary to cope for these changes.

There are 6 requirements that should be met, they are stated below in the order they are solved;

- Location of the wing cannot be too much aft
- Location of the main gear should lie within the spars of the wing
- Tip over requirement
- Lateral clearance requirement
- Span clearance requirement
- Nose wheel loading requirement

The parameters that can be used are (in order of influence);

- Location of all the structural components
  - Location of the wing
  - Location of the engines
  - Location of the main gear
  - Location of the bulkhead
  - Location of the canard (rest of empennage is fixed)
  - Location of the nose gear
- Length of the struts
- Width of the main gear

After all the requirements are met, the MATLAB code is run one more time, without changing any locations. This way the correct weights can be calculated for the subsystems who are depended on the distances between one another. At this point the first stage of the iterating process is done. Now the correct empty weight has been obtained. However, this W_E proves to be 55 kg higher than the initial estimation and thus requires a new MTOW. For this new MTOW, the PCA analysis has to be done again (see Section 10.1 of Chapter 10. From the PCA, the wing loading is increased and this results in an increase of the wing surface of 1.3 m^2. An increased wing surface gives an additional 18 kg weight increase. Then the process is iterated until the wing loading is not effected anymore by the weight increment. The final iteration that needs to be taken into account is that the increase of the MTOW also means that the W_f need to increase, and this extra W_f again gives an increase in MTOW. Luckily this iteration converges as well and a new MTOW (9065.5 kg), W_f (2938.5 kg), W_E (5147 kg) and wing area (33.3 m^2) are obtained.

Over the iterations, all the intermediate values are saved; The change of location of the different parts, the C.G. range and location, the W_E, the MTOW and the wing area. Some of the most important values are presented in Figure 13.1.
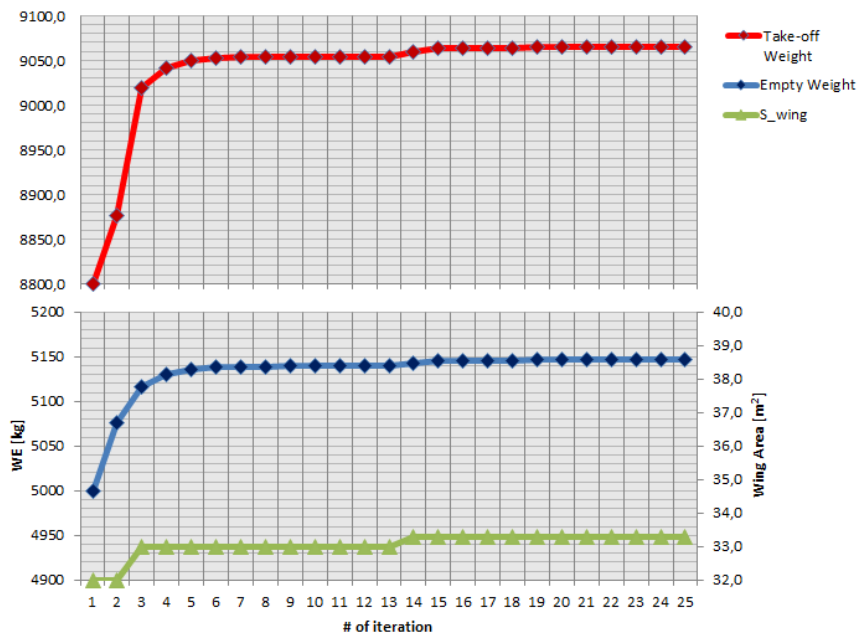
Figure 13.1: Iterated Weight Values

In Figure 13.1 the first iteration values are actually the results of the Class I estimation. The second iteration point in the graph is thus the first data point where the Class II estimation is used. It can be seen that the weights (MTOW and W_E) increase at this point. Due to the increase in MTOW a new value of the Wing Area needs to be determined. Note that the wing area is plotted using the right axis. An increase of 1 square meters is implemented. A Bigger wing naturally results into a higher weight, this is why another increase in weight will be going through the third iteration. The iteration process of the weight is now repeated for optimization, until the calculated value of the MTOW and W_E are equal to those that were used in the input. This is achieved at iteration 13. Now it needs to be checked if the wing area is still sufficient to carry the increase in the MTOW. Sadly this is not the case, and the wing area has to be increased an additional 0.3 square meters. This means again an increase in weight, which has to be iterated. At Iteration 25 the calculated values coincide again with the input values, and this time the wing area is still sufficient to carry the weight. Note that the MTOW changes more than the Empty weight. This is to be expected, since the variables in the MTOW are both the W_E and the W_f. The W_f also changes in throughout the iteration process, but is not plotted here. Since it is basically the MTOW (upper red line) minus the W_E (middle blue line) minus a constant (the payload).
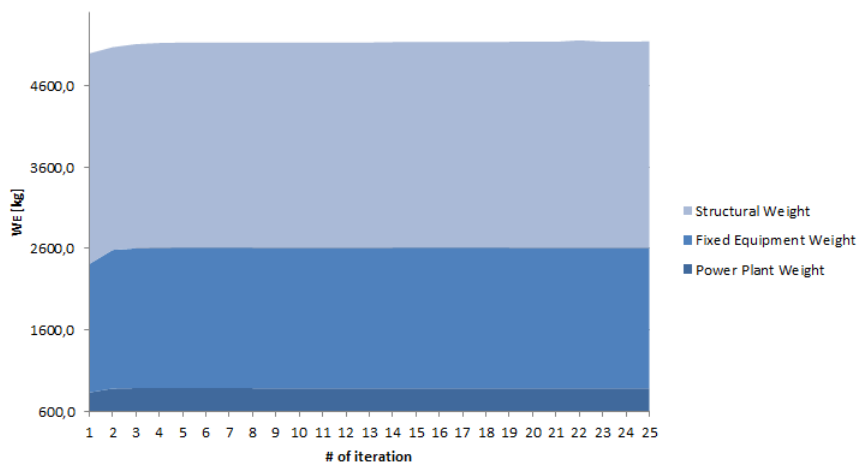
Figure 13.2: Iterated Empty Weight Values

In Figure 13.2 the W_E from Figure 13.1 is divided into the structural, fixed equipment and power plan weight. This image clearly indicates that the relation between these components remains the same trough the iteration process.

13.2.2   Class II Balance Results
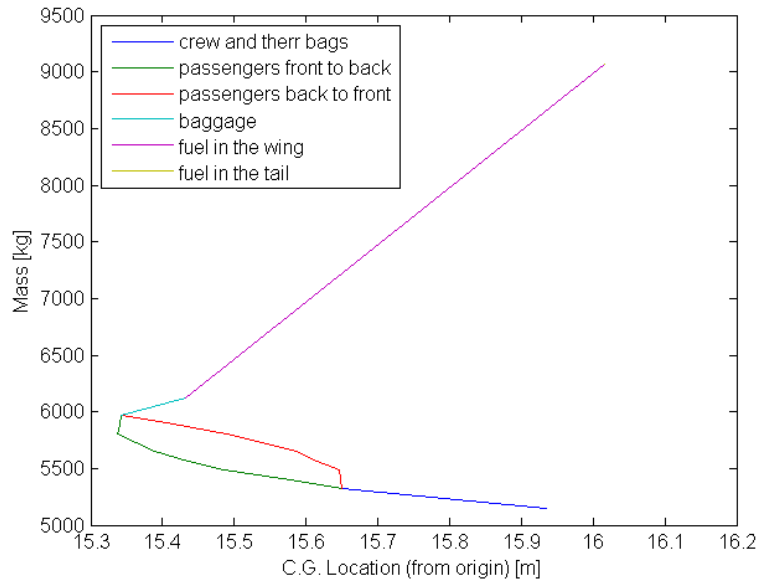
Figure 13.3: First Loading Scenario Diagram
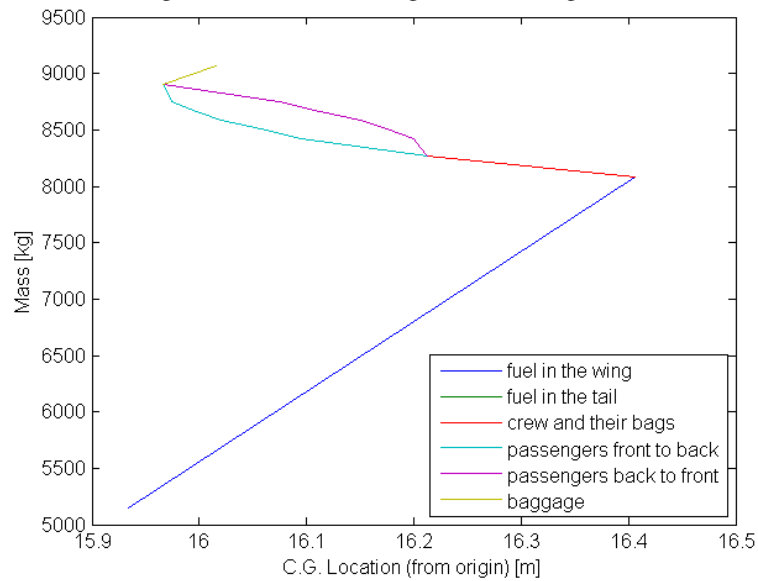
Figure 13.4: Second Loading Scenario Diagram
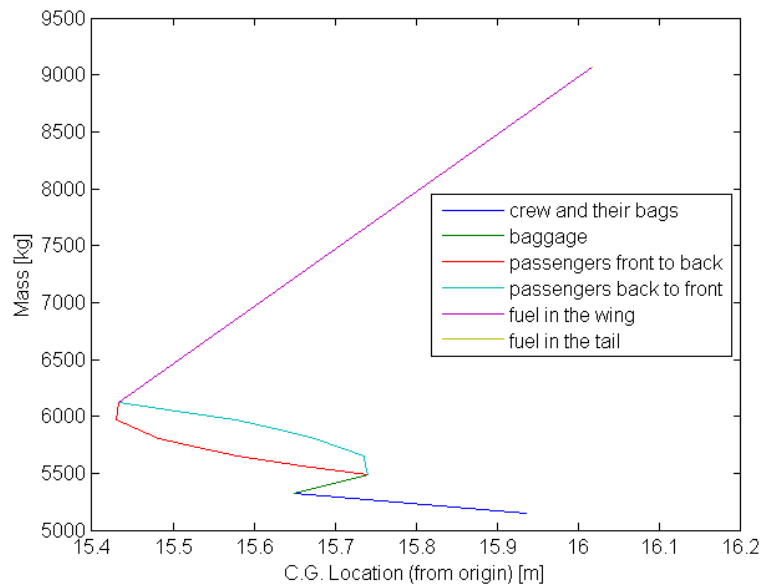
Figure 13.5: Third Loading Scenario Diagram
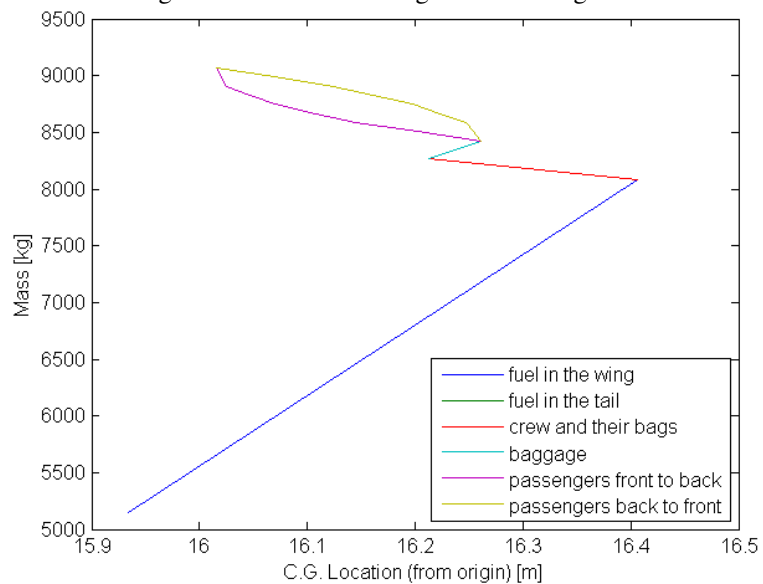
Figure 13.6: Fourth Loading Scenario Diagram

It was clear from calculations that the fuel will not fit entirely inside the wings, the remaining fuel will be put inside of the fuselage at the location of the wing to keep the C.G. travel as small as possible. No fuel will be present inside the tail, and is therefore not visible in the graph, but it is stated in the legend. Note that the C.G. locations are defined from the origin.

Table 13.2: C.G. Data

	Most fwd C.G location [m]	Most aft C.G. location [m]	C.G. travel [m]	C.G. travel [% MAC]
Class I	13.96	15.07	1.11	0.520
Class II	15.03	16.73	1.70	0.787

14 Stability & Control

This chapter presents the stability & control analysis of the Phoenix 5600. In Section 14.1 the stability derivatives are evaluated. Section 14.2 presents the static stability. Equations of motion for the dynamic stability analysis are set up in Sections 14.3 (symmetrical) and 14.4 (asymmetrical), and also the eigenvalues and eigenmodes are calculated in these sections. If the eigenmodes of the aircraft prove to be unstable, the design is altered and the process will be iterated. Adjustments to the configuration parameters are presented in Section 14.5.

14.1 Stability Derivatives

In this section the stability derivatives are evaluated. Each subsection presents the definition of each type of derivative, and the factors that can be used to influence the derivatives. The values of the stability derivatives are most accurately found using flight-data. Since the Phoenix 5600 is still in its design phase, no flight-data is available and the values have to be calculated using equations found in literature, based on reference aircraft and empirical data. The calculation itself is done using a MATLAB program. Appendix F presents the equations used for these calculations, as well as the initial values found and the final values found for the stability and control derivatives after the adjustments presented in 14.5.

14.1.1 Verification of Stability Derivatives

The used calculations of the stability and control derivatives were verified with a couple of methods. First, sanity checks were performed to check if the used equations make sense. The found derivatives were compared with derivatives of reference aircraft to check if the results were in the right range. Also, the equations were applied to reference aircraft to check if the same derivatives were found as stated. At last, as a final check Ir. H. Benedictus of the Control & Simulation Department was contacted to review our work.

Derivatives with respect to airspeed (C_{X_u}, C_{Z_u} and C_{m_u})
The airspeed derivatives change under the influence of Mach number, Reynolds number and dynamic pressure.

Derivatives with respect to angle of attack (C_{X_α}, C_{Z_α} and C_{m_α})
The angle of attack derivatives determines the behavior of the aircraft with respect to the angle of attack. An important angle of attack derivative is the moment derivative C_{m_α}. In order for the aircraft to be stable, C_{m_α} should be negative, i.e. the aircraft produces a correcting moment when the angle of attack is increased. The moment derivative is mainly determined by the location of the aerodynamic center of the aircraft, which has to lie behind the center of gravity for stable aircraft.

Derivatives with respect to rate of angle of attack ($C_{X_{\dot\alpha}}$, $C_{Z_{\dot\alpha}}$ and $C_{m_{\dot\alpha}}$)
With the exception of the moment derivative, these derivatives are of less importance.

Derivatives with respect to sideslip angle (C_{Y_β}, C_{l_β} and C_{n_β})
The derivative of the lateral force and yawing moment with respect to a side slipping motion are mostly determined by the fuselage and vertical tailplane. The fuselage usually has a destabilizing effect while the vertical tail plane has a stabilizing effect. The rolling moment derivative, also indicated as the 'effective dihedral', is mainly influenced by the dihedral angle and the sweep angle as well as the wing fuselage interaction. The wing fuselage interaction can cause a significant difference in angle of attack between the two wings, causing a rolling motion.

Derivatives with respect to rate of angle of sideslip ($C_{Y_{\dot\beta}}$, $C_{l_{\dot\beta}}$ and $C_{n_{\dot\beta}}$)
These derivatives are of less importance. Only the vertical tail has a significant contribution.

Derivatives with respect to pitch rate (C_{X_q}, C_{Z_q} and C_{m_q})
The pitch rate derivatives predicts the effect on the aerodynamic parameters when the pitch is changed. The effect on the drag coefficient can be neglected.

Derivatives with respect to roll rate (C_{Y_p}, C_{l_p} and C_{n_p})
The roll rate derivatives determine the response of the aircraft during roll. The wing and the vertical tail plane have a big influence on these derivatives. When the size of the vertical tail increases, the aircraft give more resistance to roll. The roll rate derivatives also have a big influence on the Dutch roll characteristics.

Derivatives with respect to yaw rate (C_{Y_r}, C_{l_r} and C_{n_r})
The yaw rate derivative determines to a large extend the Dutch roll eigenmotion. The yaw rate can be controlled using the rudder. It will cause an increase in lift for one wing due to the increased speed and will decrease the lift for the other wing causing the aircraft to roll. Furthermore a side force is introduced which is mainly caused by the vertical tail.

Derivatives with respect to the elevator angle ($C_{X_{\delta_e}}$, $C_{Z_{\delta_e}}$ and $C_{m_{\delta_e}}$)
Expresses the variation of aircraft drag, lift and moment with the elevator deflection angle. The moment derivative is of most importance.

Derivatives with respect to the aileron angle ($C_{Y_{\delta_a}}$, $C_{l_{\delta_a}}$ and $C_{r_{\delta_a}}$)
Expresses the side force Y, rolling moment l and yawing moment n, obtained by deflecting the ailerons. The rolling moment is of most importance.

Derivatives with respect to the rudder angle ($C_{Y_{\delta_r}}$, $C_{l_{\delta_r}}$ and $C_{r_{\delta_r}}$)
Expresses the side force Y, rolling moment l and yawing moment n, obtained by deflecting the rudder. The yawing moment is of most importance.

14.2 Static Stability

The static stability is the stability of the aircraft around the equilibrium position, to which the aircraft should return after a disturbance. An indicator of static stability is the static margin, which is the distance between the neutral point and the center of gravity. Static stability is achieved when the neutral point of the aircraft lies aft of the center of gravity. The location of the neutral point is calculated with Equation 14.1.

$$\bar{x}_{n.p.} = \frac{\left(x_{ac_{wf}}C_{L_{\alpha_{wf}}} + x_{ac_h}C_{L_{\alpha_h}}\eta_h\left(\frac{S_h}{S}\right)\left(1 - \frac{d\varepsilon}{d\alpha}\right) - x_{ac_c}C_{L_{\alpha_c}}\eta_c\left(\frac{S_c}{S}\right)\left(1 + \frac{d\varepsilon_c}{d\alpha}\right)\right)}{\left(C_{L_{\alpha_{wf}}} + C_{L_{\alpha_h}}\eta_h\left(\frac{S_h}{S}\right)\left(1 - \frac{d\varepsilon}{d\alpha}\right) + C_{L_{\alpha_c}}\eta_c\left(\frac{S_c}{S}\right)\left(1 + \frac{d\varepsilon_c}{d\alpha}\right)\right)} \tag{14.1}$$

The static margin is found to be $\bar{x}_{n.p.} - \bar{x}_{c.g.} = 0.1215$, so in terms of static stability the aircraft will be stable with a static margin of 12.15%.

14.3 Dynamic Stability: Symmetric Analysis

The dynamic stability of the aircraft comprises the maneuvers and recovery to equilibrium position, which for the symmetric (or longitudinal) motion is evaluated with the equations of motion, presented in Equation 14.2.

$$\begin{bmatrix} C_{X_u} - 2\mu_c D_c & C_{X_\alpha} & C_{Z_0} & 0 \\ C_{Z_u} & C_{Z_\alpha} + (C_{Z_{\dot{\alpha}}} - 2\mu_c)D_c & -C_{X_0} & C_{Z_q} + 2\mu_c \\ 0 & 0 & -D_c & 1 \\ C_{m_u} & C_{m_\alpha} + C_{m_{\dot{\alpha}}}D_c & 0 & C_{m_q} - 2\mu_c K_Y^2 D_c \end{bmatrix} \begin{bmatrix} \hat{u} \\ \alpha \\ \theta \\ \frac{q\bar{c}}{V} \end{bmatrix} = \begin{bmatrix} -C_{X_{\delta_e}} \\ -C_{Z_{\delta_e}} \\ 0 \\ -C_{m_{\delta_e}} \end{bmatrix} [\delta_e] \tag{14.2}$$

Using a MATLAB program, the equations of motion are rewritten to a state-space model. The eigenvalues belonging to the state-space model, with the initial values for the deriviatives, are stated in Equation 14.3. Since both sets of complex conjugate eigenvalues have a negative real part, the Phoenix 5600 will be stable in symmetric flight. The adjustments that were made to the configuration parameters, which are stated in Section 14.5, have little effect on the eigenvalues in the symmetric case, as can be seen in Equation 14.4.

$$\lambda_{c_{1,2}} = -0.0150 \pm j0.0119 \tag{14.3}$$
$$\lambda_{c_{3,4}} = -0.0001 \pm j0.0005$$

$$\lambda_{c_{1,2}} = -0.0158 \pm j0.1408 \tag{14.4}$$
$$\lambda_{c_{3,4}} = -0.0001 \pm j0.0005$$

The various characteristics of the symmetric motions are next calculated from the eigenvalues λ_c. Using an impulse input of 1 second on the elevator of $\delta_e = 2°$, two modes can be distinguished: phugoid mode and short period mode. The values presented are applicable only for the final response.

14.3.1 Short Period Mode

The short period corresponds to eigenvalues $\lambda_{c_{1,2}}$. The response of the aircraft in the short period eigenmotion can be seen in Figure 14.1.

- The period $P = 2.9045\,s$
- The time to half amplitude $T_{\frac{1}{2}} = 0.3566\,s$
- The undamped natural frequency $\omega_0 = 2.9079\,rad/s$
- The damping ratio $\zeta = 0.66829$

14.3.2 Phugoid Mode

The phugoid corresponds to eigenvalues $\lambda_{c_{3,4}}$. The response of the aircraft in the phugoid eigenmotion can be seen in Figure 14.2.

- The period $P = 96.3824\,s$
- The time to half amplitude $T_{\frac{1}{2}} = 75.6518\,s$
- The undamped natural frequency $\omega_0 = 0.065831\,rad/s$
- The damping ratio $\zeta = 0.13915$
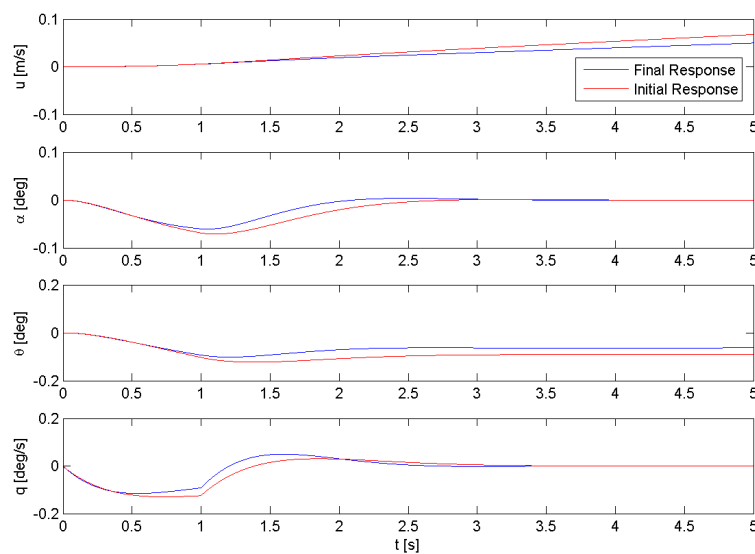
Figure 14.1: Phoenix 5600 Response, Short Period Mode
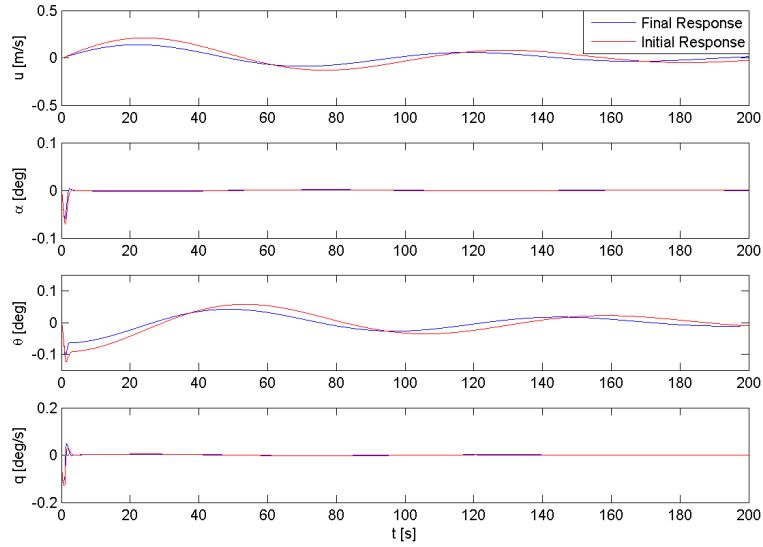
Figure 14.2: Phoenix 5600 Response, Phugoid Mode

14.4 Dynamic Stability: Asymmetric Analysis

The dynamic stability of the asymmetric (or lateral-directional) motion is evaluated with the equations of motion, presented in Equation 14.5.

$$
\begin{bmatrix}
C_{Y_\beta} + \left(C_{Y_{\dot\beta}} - 2\mu_b\right)D_c & C_L & C_{Y_p} & C_{Y_r} - 4\mu_b \\
0 & -\frac{1}{2}D_b & 1 & 0 \\
C_{l_\beta} & 0 & C_{l_p} - 4\mu_b K_X^2 D_b & C_{l_r} + 4\mu_b K_{XZ} D_b \\
C_{n_\beta} + C_{n_{\dot\beta}} D_b & 0 & C_{n_p} + 4\mu_b K_{XZ} D_b & C_{n_r} - 4\mu_b K_X^2 D_b
\end{bmatrix}
\begin{bmatrix}
\beta \\ \varphi \\ \frac{pb}{2V} \\ \frac{rb}{2V}
\end{bmatrix}
=
\begin{bmatrix}
-C_{Y_{\delta a}} & -C_{Y_{\delta r}} \\
0 & 0 \\
-C_{l_{\delta a}} & -C_{l_{\delta r}} \\
-C_{n_{\delta a}} & -C_{n_{\delta r}}
\end{bmatrix}
\begin{bmatrix}
\delta_a \\ \delta_r
\end{bmatrix}
$$

(14.5)

The same MATLAB program that was used for the symmetric analysis was used for the analysis of the asymmetric motion, and also the same procedure was used to find the stability derivatives from Appendix F. The eigenvalues belonging to the asymmetric state-space model, with the initial values for the stability derivatives, are stated in Equation 14.6. As can be seen, two of the eigenvalues have a positive real part, and therefore the eigenmode corresponding to these eigenvalues will be diverging (or unstable). Adjustments are suggested to the configuration parameters of the aircraft to obtain a fully stable aircraft in the asymmetric case. The final adjustments made are presented in Section 14.5. As can be seen from the final eigenvalues in Equation 14.7, the Phoenix 5600 will be dynamically stable in asymmetric flight, for all three eigenmodes.

$$\lambda_{b_{1,2}} = +0.0044 \pm j0.1122 \qquad (14.6) \qquad\qquad \lambda_{b_{1,2}} = -0.0306 \pm j0.1408 \qquad (14.7)$$

$$\lambda_{b_3} = +0.0010 \qquad\qquad\qquad\qquad\qquad \lambda_{b_3} = -0.0003$$

$$\lambda_{b_4} = -0.1541 \qquad\qquad\qquad\qquad\qquad \lambda_{b_4} = -0.1537$$

The various characteristics of the asymmetric motions are next calculated from the eigenvalues λ_b. Three modes can be distinguished: aperiodic roll, spiral and Dutch roll.

14.4.1 Aperiodic Roll Mode

The aperiodic roll corresponds to eigenvalue λ_{b_4}. To simulate the aperiodic roll, an initial roll angle $\varphi = 15°$ is given together with a step input on the aileron of $\delta_a = 45°$. The initial and final response of the aircraft during the aperiodic roll can be seen in Figure 14.3. The value shown below is the value for the final response only.

- The time to half amplitude $T_{\frac{1}{2}} = 0.27708\,s$

14.4.2 Spiral Mode

The spiral corresponds to eigenvalue λ_{b_3}. The initial and final response of the aircraft during the spiral can be seen in Figure 14.4, which is simulated with an initial roll angle of $\varphi = 15°$. The value shown below is the value for the final response only.

- The time to half amplitude $T_{\frac{1}{2}} = 157.8783\,s$

14.4.3 Dutch Roll

The Dutch roll corresponds to eigenvalues $\lambda_{b_{1,2}}$, and is simulated with a step input of 1 second on the rudder of $\delta_r = 2°$. The initial and final response of the aircraft during the Dutch roll can be seen in Figure 14.5. The values shown below are the values for the final response only.

- The period $P = 2.742\,s$
- The time to half amplitude $T_{\frac{1}{2}} = 1.3912\,s$
- The undamped natural frequency $\omega_0 = 2.345\,rad/s$
- The damping ratio $\zeta = 0.21242$
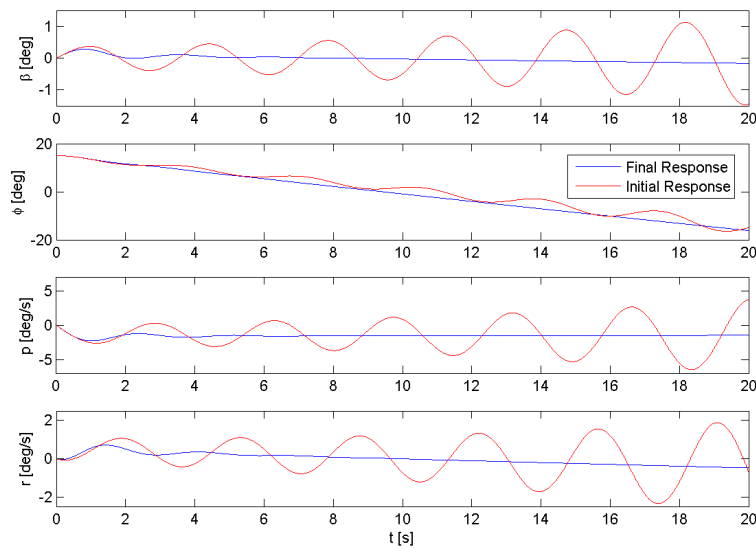
Figure 14.3: Phoenix 5600 Response, Aperiodic Roll Mode
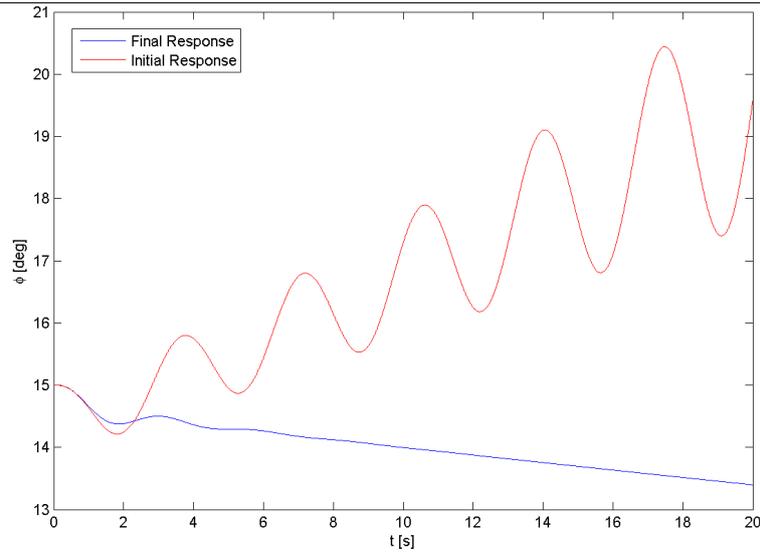
Figure 14.4: Phoenix 5600 Response, Spiral Mode
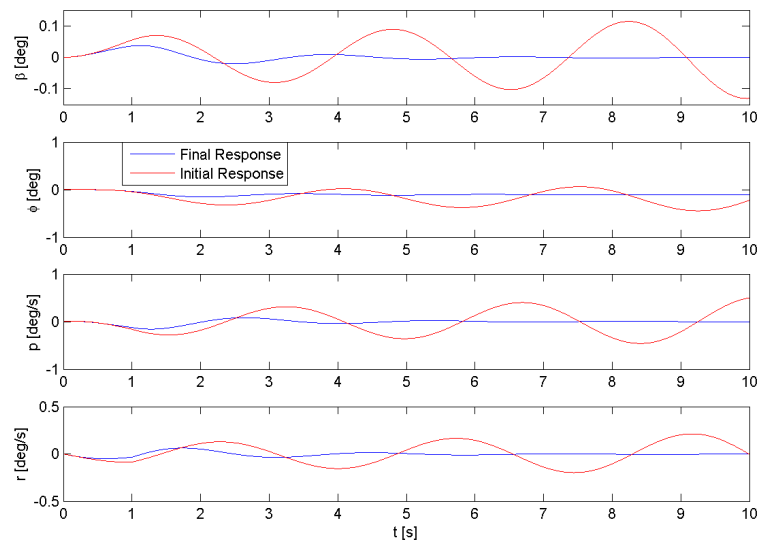
Figure 14.5: Phoenix 5600 Response, Dutch Roll Mode

14.5 Adjustments to Configuration Parameters

As presented in Sections 14.3 and 14.4, adjustments were made to the aircraft configuration parameters, to obtain stable eigenmodes. By making adjustment to the aircraft configuration parameters, the stability and control derivatives will change in value and with them the eigenvalues. All adjustments should remain in between a 10% range, as otherwise all iterations performed earlier (for instance weight & balance) should be done over again. Since only in the asymmetric analysis eigenvalues were found which include positive real parts, the adjustments will focus on the asymmetric plane. Adjusting the vertical tail area will have a favorable effect on the asymmetric derivatives. An adjustment to the horizontal tail or canard area, will result in adjusted symmetric derivatives, and is therefore not needed, although it might be necessary when other values change. The final adjustments made are:

- Increment of S_v with 10% to 8.58 m^2
- Increment of S_h with 10% to 8.80 m^2, to fit on vertical tail
- Installation of a yaw-damper: a sideslip angle β automatically generates a counteractive rudder deflection δ_r

15 Aircraft System Characteristics

In this chapter the aircraft system characteristics are determined in detail. In Appendix H of the Midterm Report [1] the requirements for the various subsystems are stated. In addition, in Chapter 20 of the Midterm Report all the design and safety requirements according to FAR 25 are stated. In the following sections all the systems will be sized as far as possible and the layout will be determined based on both the set requirements and the design and safety requirements. Starting with the landing gear system in Section 15.1, hydraulics, electronics, cockpit systems, environmental systems, emergency systems, propulsion systems, baggage systems, cabin systems and lightning systems (Section 15.13) are being discussed.

15.1 Landing Gear System

The landing gear system will be equipped with an anti-skid system (anti-lock braking system: ABS), which is designed to prevent the main landing gear wheels from locking up during landing, particularly on wet or icy runway surfaces. The applied pressure is reduced before the wheels lock up and then reapplied to continue the braking action, this repeats on an on/off cycle. A more elaborate design of the landing gear system can be found in Section 12.3.

15.2 Flight Control System

Nowadays almost all aircraft are equipped with an irreversible flight control system (FCS). Advantages of an irreversible FCS are mainly the flexibility in combining pilot control commands with automatic control commands, the ability to tailor handling qualities and finally the potential of lower weight. In irreversible flight control systems the flight controls are moved by means of actuators (servos). Actuators have two ends: a fixed end and a moving end. The fixed end is attached to the airplane structure. The moving end is attached to a control surface. Two types of actuators are used most frequently: hydraulic and electromechanical. In Table 15.1 the different types of actuators are compared. From this table it can clearly be seen that the electromechanical actuator has the most favorable characteristics. The electromechanical actuators consist of an electric motor which drives an output shaft via a ball-screw jack.

Table 15.1: Electrical Actuators vs. Hydraulic and Pneumatic Cylinders [64]

	Electrical Linear Actuators	**Hydraulic Cylinders**	**Pneumatic Cylinders**
Installation	Simple Wiring	Expensive plumbing, filtering	Expensive plumbing, filtering
Accuracy	Very repeatable ($\pm$ 0.013 mm)	Expensive position sensing, creep	Difficult to achieve
Control	Compatible with standard	Temperature changes control	Complicated
Speed	Variable speed 0 to 2 m/s	Difficult to control accuracy	Stick Slip and varying load
Reliability	Little maintenance	Contamination sensitive	Very contamination sensitive
Power	40 000 N	Unlimited force	Up to 25 000 N
Life expectancy	Millions of cycles	Usually Good	Usually Good
Environment	-30 - +70 °C	Temperature problem	Temperature problem
Load holding	Self-locking if power fails	Complex back-up systems	Complex back-up systems
Cost	Moderate initial, low operating cost	Installation, maintenance expensive	Installation, maintenance expensive

In the Midterm Report [1] various signaling methods were discussed; mechanical signaling, fly-by-wire (FBW) and fly-by-light. It is chosen to go for the fly-by-wire system because it is proven to work and gives many advantages over a mechanical signaling system. An extension to the FBW is the Intelligent Flight Control System (IFCS). This IFCS is able to compensate for aircraft damage and failure. It is therefore chosen to extend the FCS with the IFCS.

The FCS will have three redundant systems which will each work individually and have their own on-board computer for safety reasons. The electromechanical actuators also need at least two independent standby sources for electric power and redundant actuators. The actuators should be located at the aerodynamic surface controls such that maximum system stiffness is attained but should be easily accessible for inspection maintenance and removal. The layout of the flight control system is shown in Figure 15.1 and Figure 15.2.
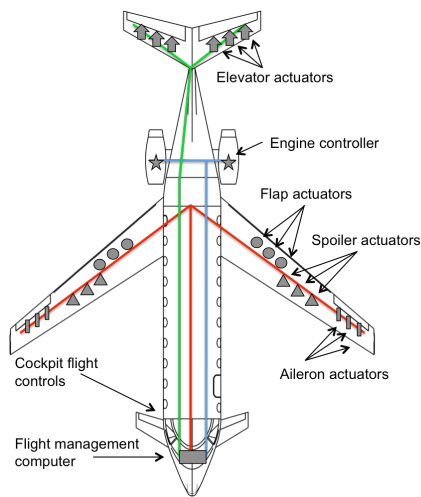
Figure 15.1: Flight Control System Top View
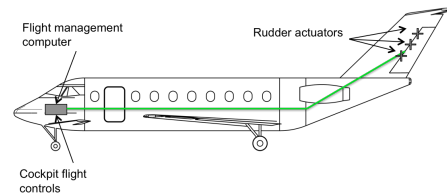
Figure 15.2: Flight Control System Side View

15.3 Hydraulic System

The primary task of the hydraulic system is to provide hydraulic power to actuators.

The maximum amount of hydraulic fluid required for operation of an airplane normally occurs in the landing phase. The hydraulic system consists of a hydraulic fluid reservoir, hydraulic pumps and accumulators. In Figure 15.3 the hydraulic system of the Phoenix 5600 is shown. In this figure it can be seen that this system has two engine driven pumps and an accumulator for emergency services.

In addition the characteristics of the Gates Learjet M25 which can be found in Table 15.2 are used as a reference for the Phoenix 5600. In Table 15.3 the various functions of the hydraulic system are shown. For normal operation A (2 engine driven) power from Table 15.2 is used. But the hydraulic pumps or their power source can fail, so also the alternate option is stated. For example the landing gear has a mechanical free-fall capability. Typical back-up systems for airplanes include: accumulators to provide short duration hydraulic pressure for lowering the landing gear or Auxiliary Power Unit (APU) and/or Ram Air Turbine (RAT) to provide long duration emergency stand-by power to operate the flight controls.

Table 15.2: Characteristics Hydraulic System

Pressure	1500 psi (10.34 MPa)	
Flow	4 gpm (0.25 L/s)	2 engine driven (A)
	0.3 gpm (0.019 L/s)	1 auxiliary driven (B)

Table 15.3: Hydraulic System Function Distribution

Powered units	Normal system	Alternate option
Main & nose landing gear	A	Manual release & free fall
Nose gear steering	A	Differential breaking
Brakes	A	B
Thrust reverser	A	Brakes
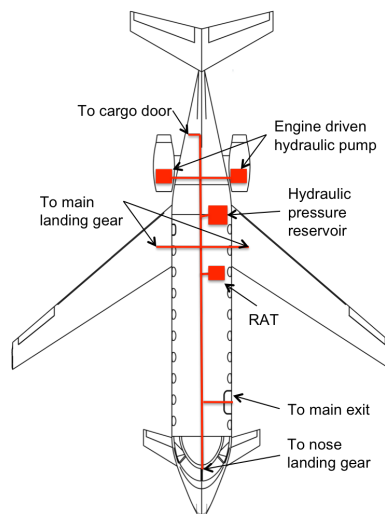
Figure 15.3: Hydraulic System Schematic

15.4 Electrical System

Auxiliary Power Unit (APU)
The APU is a small gas turbine engine, located in the tail cone of the aircraft. Bleed air is tapped from the compressor and connected into the air distribution system. The APU is used for starting the engines, but on the ground also for electrical power, hydraulic pressure and air-conditioning. The APU itself is started from the main aircraft battery [65].

Ram Air Turbine (RAT)
In the event of generator failure, continuous power can be provided by the Ram Air Turbine (RAT). The RAT is stowed in the fuselage and when deployed it generated energy from the airflow. The RAT can only be deployed between aircraft speeds of 120 - 430 knots. Typical RAT generators produce an AC output of 7.5 kVA. Heaters are installed in the RAT generator to prevent ice formation [65]. The APU is started from the main aircraft battery. Energy can only be stored when it is direct current, therefore the APU works on DC power. However all the systems work on AC power and converters are needed to transform the DC power to AC power. The higher the AC power the smaller the diameters of the cables need to be, which will reduce the weight of the aircraft. Therefore the AC power in the aircraft is set at 270VAC.
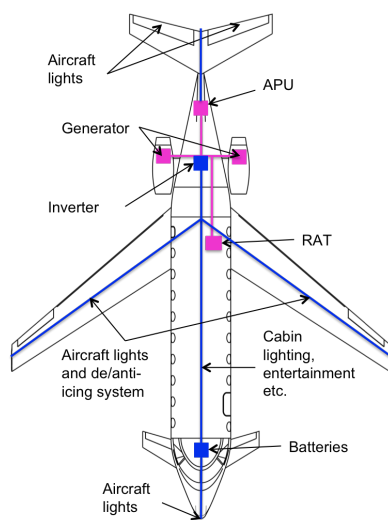
Figure 15.4: Electrical System Schematic
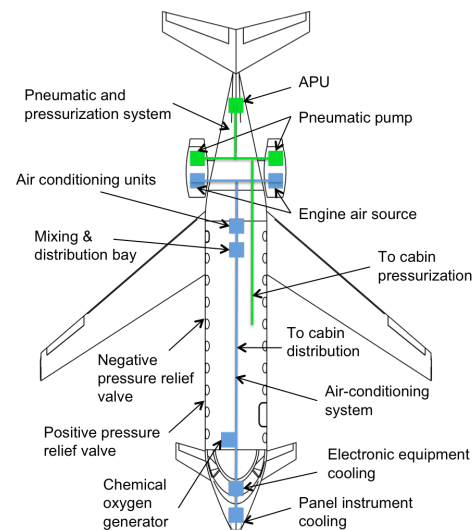
Figure 15.5: Environmental System Schematic

15.5 Environmental

Cabin Pressurization
The cabin altitude at cruise will be 1500 m ISA equivalent. There is a pressure differential of 67 kPa. There will be a positive pressure relief to protect the structure. In addition there is also a negative pressure relief which lets air into the cabin when the outside air pressure exceeds the inside air pressure. There will also be a possibility for depressurization. If the pressurization system fails at landing the cabin can still be depressurized and the doors can still be opened.

Pneumatic System
The pneumatic system is responsible for the air supply for the cabin pressure and air conditioning, ice protection and the cross engine start. The primary source of air is the engine compressor bleed air and the secondary source of air comes from the APU.

Air-conditioning System
The air-conditioning system ensures that the temperature and the humidity of the cabin air is pleasant between 15° and 25°. Per passenger 20 cubic feet per minute of cabin air is needed. The humidity of the air in the cabin is around 10% and 20%. Between 50% and 70% humidity is comfortable for humans. The humidity is kept lower because high humidity gives condensation which can corrode metals.

15.6 Cockpit System

Cockpit Instrumentation System
In the Midterm Report [1] the different items that have to be present on the cockpit avionics are presented. The cockpit avionics will be functional, uncluttered and visible for the crew. After doing research on various cockpit layouts for small business jets it is chosen to have a luxurious cockpit avionics system to match the premium standards. As the business jet is a light weight business jet a cockpit avionics system similar to the cockpit avionics system of the Cessna Citation M2 Light Business Jet, the Garmin G3000 as shown in Figure 15.6 is installed.

Flight Management System
The Flight Management System (FMS) is a specialized computer system for aircraft that automates a wide variety of in-flight tasks. The in-flight management of the flight plan is its primary task. Using sensors like GPS and INS the aircraft position can be determined by the FMS and the flight plan can be followed. The flight management system requires a number of subsystems: flight control computer, autopilot/auto throttle controls, thrust management computer, inertial reference system, flight data acquisition system and communication and advisory system. An example of a flight management system can be found in Figure 15.7.

Figure 15.6: Cockpit Avionics System
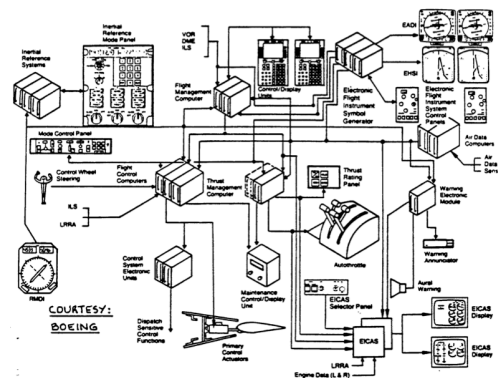
Figure 15.7: Flight Management System

Black Box

1. *Shall provide flight data storage of last 25 hours of flight.* The flight data recorder(FDR) operates on an endless-loop (new data record over the old data) principle and will record at least five parameters: pressure altitude, indicated airspeed, magnetic heading, normal acceleration, microphone keying. The microphone keying is recorded to correlate the FDR with the cockpit voice recorder (CVR)[66]
2. *Shall provide cockpit voice recording of last 2 hours of flight.* It will record the total audio environment in the cockpit area. This includes crew conversations, radio transmissions, aural alarms, control movements, switch activations, engine noise and airflow noise[66].
3. *Shall provide digital message storage of last 2 hours of flight.* The CVR shall also store the information that is received from communication with other aircraft or airports[66].
4. *Shall withstand 3400g.* An impact producing a 3400g deceleration for 6.5 milliseconds should be survivable for the black box. In addition a penetration force of 227 kg dropped from 3 meters should be survives as well as a crush force of 22.25 kN applied continuously for five minutes[66].
5. *Shall withstand severe fires.* In case of fire, the black box shall withstand a temperature of 1100 °C for 60 minutes[66].
6. *Shall have an underwater beacon which is detectable for 30 days at a depth of 6 km.* When the underwater location beacon is immersed in water it will begin to radiate an acoustic signal which can be received and transformed into an audible signal by a receiver. The nominal operating frequency is 37.5 kHz. The minimum operating life is 30 days but more is possible as long as the battery holds[66].
7. *Shall be highly visible.* As the maximum detection range of the underwater location beacon is 2 to 3 km it is important that the black box is highly visible, so it is easily recognized (normally the color is red)[66].

Antenna System

For communication between the ground and the airplane a large number of antenna systems are required. In the Midterm Report [1] the various antennas which are needed were elaborated on. In Figure 15.8 the locations of the different antennas can be found.
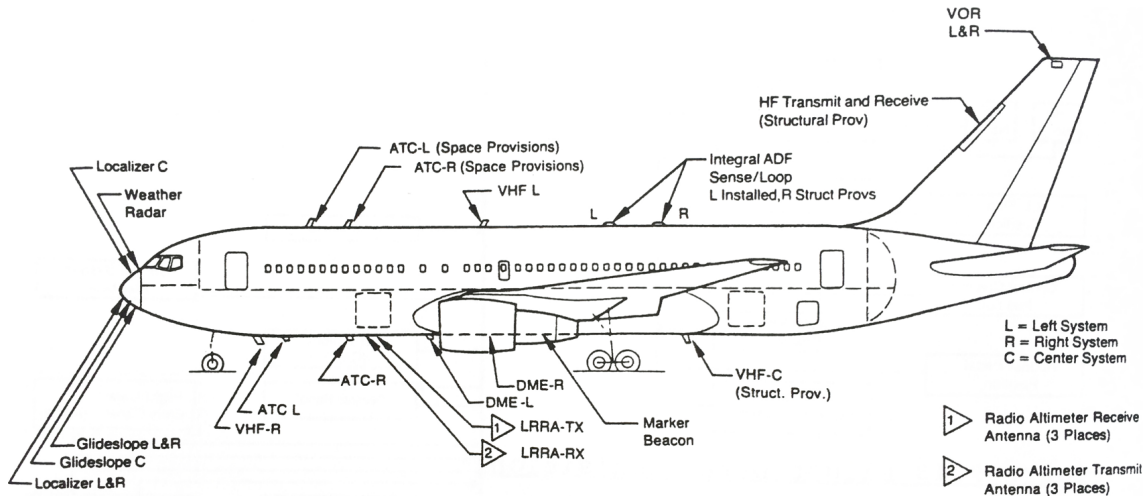
Figure 15.8: Locations of the Antennas

Communications and Advisory System

During the flight a large number of communications take place between the cockpit and the air traffic control station. Also the crew informs the passengers about the flight status.

Navigation System

The navigation system is required to provide information on the exact location at any moment of the flight of the aircraft. A variety of available instrumentation can be used: Automatic direction finder (ADF), inertial navigation, compasses, radar navigation, VHF omnidirectional range (VOR) and GNSS. Navigation will include planning, recording, and controlling the movement of the aircraft from one place to another. The techniques used for navigation in the air will depend on whether the aircraft is flying under visual flight rules (VFR) or instrument flight rules (IFR). In the latter case, the pilot will navigate exclusively using instruments and radio navigation aids such as beacons, or as directed under radar control by air traffic control. In the VFR case, a pilot will largely navigate using dead reckoning combined with visual observations. The VHF uses an airband between 108-137 MHz which has a range transmission at 35000 ft of 322 km with good weather.

15.7   De/Anti-icing System

De-icing system

The electro-impulse system portrayed in Figure 15.9 is chosen as the de-icing system. This system will deliver a mechanical impulse to the surface on which the ice has formed. The vibrations cause the ice to crack and break away. Advantages of the electro-impulse system are that the erosion surface can be metal, the surface life is the life of the aircraft, it can remove ice as thin as 0.12 cm and only uses 28V DC for 12 m span.

Anti-icing System

Electrically heated systems are used to prevent ice formation on pitot tubes, stall vanes, total air temperature probes, drain masts and engine inlet lips. In addition the aircraft is sprayed with freezing point depressant fluids, based normally on ethylene and propele hlycol over the area which is not allowed to freeze as can be seen in Figure 15.10.
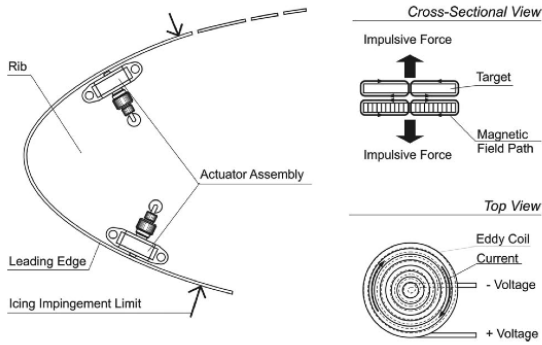
Figure 15.9: Electro Impulse De-icing System

Figure 15.10: Chemical Anti-icing System

Rain Removal

Rain removal is done by adding wind-shield wipers on the windows of the cockpit. In addition rain repellent is added into the wiper paths. The windscreen wiper system is based on 28V DC variable speed motors. Typical speeds are 160 cycles per minutes (low) and 250 cycles per minute (high).

Defog System

To prevent the windshield from fogging up on the inside and/or outside electrical wiring will be buried inside the windshield material. The wind screen heaters use 4 kW of power to keep the window temperature approximately 30°C.

15.8 Emergency System

Emergency Power System

In the event of generator failure, continuous power can be provided by the ram air turbine (RAT). The RAT is an air-driven device that is deployed in case that the aircraft loses normal power and derives energy from the airflow. The RAT can be deployed between aircraft speed of 120 to 430 knots. Typical RAT generators produces an AC output of 7.5 kVA. Heaters are installed in the RAT generator to prevent ice formation.

Fire Extinguishing System

The aircraft is divided into 3 sections when studying the fire extinguishing system. The engines/APU (class B), cargo bay (class A) and passenger cabin (class A). In Table 15.4 the various extinguishing strategies can be found for different types of fire.

Table 15.4: Fire Extinguishing Strategies

Class of fire	Fuel/heat source	Appropriate extinguishing strategies
Class A	Solid/organic	Water, vaporizing gas
Class B	Flammable liquids	Carbon dioxide, dry powder or vaporizing liquid
Class C	Flammable gasses	Dry powder, vaporizing liquids
Class D	Metals	Dry powder
Class E	Electrical equipment	Carbon dioxide, dry powder or vaporizing liquid
Class F	Cooking fat/oil	Carbon dioxide, dry powder or vaporizing liquid
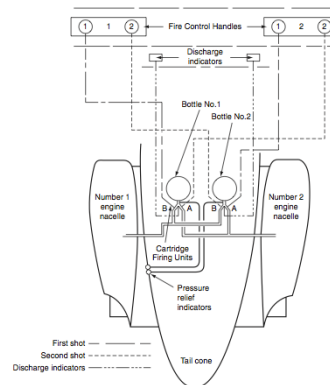
Figure 15.11: Fire Extinguishing for the Engines

In the cabin most fires are extinguished using hand-held fire extinguishers. The cargo bay and the engines/APU use a vaporizing liquid agent pressurized with dry nitrogen. When the fire switch is operated

a current is passed through the heater coil and a high pressure build up forces the agent to expel from the bottles as shown in Figure 15.11.

Lightning Strike Protection

An average of 1 lightning strike per 1500 flight hours occurs. To limit the damage of a lightning strike the entire structure has to be a good electrical conductor, with no gaps in the conductive path that may result in overheating and local melting.

Emergency Lighting

The exits must be labeled with Exit and this must be 5.5 in (14.0 cm) high on a white background and must have a 21 in^2 (135 cm^2) surface. The minimum brightness is set to be 400 microlamberts.

Emergency Doors

One Type IV overwing emergency exit will be used in addition to the main exit which will be easy to open. The main exit will be 1.7 m by 1 m and the emergency exit 26 in by 19 in (66 cm by 48 cm).

Emergency Oxygen

For flights at high altitudes oxygen is required after failure of the cabin pressurization system. Passenger oxygen is supplied from a chemical source. A mask is installed above each seat as shown in Figure 15.13 and per side two extra masks are installed in case of extra need (e.g. someone standing in the aisle). The mask will supply oxygen for 12 minutes which is enough time for the pilot to descent to an altitude where normal breathing is possible.

Emergency Life Support System

Our aircraft provides over water flights, so the aircraft must be equipped with life jackets. The life jackets must be within easy reach of each passenger. Therefore the life jackets are positioned underneath the seats.

Emergency Slides/Life raft

For overwater flights (in excess of 30 minutes) passenger transports must carry emergency rafts [53]. To have access to the water or ground, slides will automatically deploy with emergency exit door removal. At this moment the spoilers will retract automatically and the slides will be operational in all landing gear conditions. The inflation happens by stored gas. The emergency slides shown in Figure 15.12 also function as rafts and will have a capacity of 12 persons and include a survival kit, provision for radio transmitter, canopies and a sea anchor.
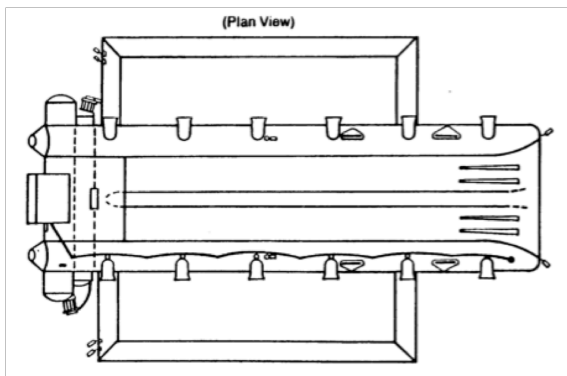
Figure 15.12: Emergency Slide/Raft   Figure 15.13: Cabin Oxygen System
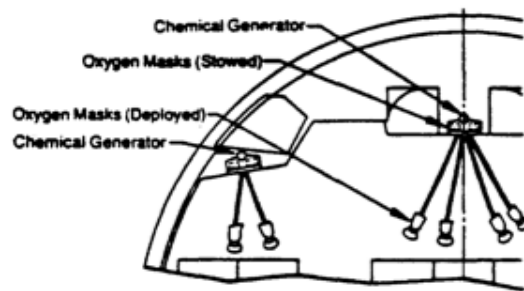
15.9 Water, Waste & Catering System

Water Management System

The water storage for passenger transports are typically sized for 1.14 L per passenger. For a light business jet with 8 passengers and 2 crew members a total storage of 11.4 L is needed. The water can be heated by running cold water through an electrically heated heat exchanger. The water system is pressurized by filtered bleed air from the integrated air system. An electric heater provides warm water to the washbasin.

Waste Management System

One lavatory will be installed which used very little water, about 1.9 L per flush. The lavatories use a vacuum (in flight pressure differential) system and do not use gravity to move the water, therefore smaller sewer pipes can be used. The waste will be collected in a collector tank. The flushing mixes the waste with the chemicals to suppress the smell. The collector tanks need to be emptied after each flight. The waste system will be designed to fit the standard airport equipment.

Catering System

Food and drinks can be heated using a convection oven (AL-GH3001-1 OVEN /HOT CUP) because of safety. Using this machine both food and drinks can be heated. If desired an additional coffee machine can be added to the galley.

15.10 Entertainment & Connectivity System

During the flight premium comfort is desired and conference calls need to take place. Therefore a Wi-Fi-network and GSM network will be set up. As we also provide over water flights a satellite network is chosen to provide this service. This will ensure connectivity at all times so conference calls can be executed. In addition a video system will be present on board which provides movies, documentaries, TV series, music, news and flight information. For this system VisiStream will be used as it only weighs 1.8 kg and used 20 W with a 2 TB memory. In the front of the aircraft a 46 in (117 cm) screen will be placed for presentations which uses 28 V DC power. In addition each chair has its own video screen which is touch screen and can be synchronized with the large screen so notes can be made during the presentation or conference call. For setting preferences each chair has its own touch screen VIP menu providing access to service, lights, reading, headset, shade, volume etc. There also will be charging possibilities for laptops, mobile phones or other electronic devices.

15.11 Propulsion System

For the pilot to control the propulsion a propulsion control system is needed. Parts of the control system are ignition control, starter system, fuel flow control and thrust reverser control. Ignition controls are part of the electrical system. The starter system consists of an electric starter motor which is geared to the engine. The pilot controls the power output of the engines using the throttles. A fuel system with its own controls supplies the fuel to the engines. The thrust reversers are used to help slow the airplane after touchdown. Thrust reversers are controlled with hydraulic controls.

15.12 Baggage System

The only baggage limit is that it has to fit on board. There is no large baggage system as our aircraft has a maximum of 8 passengers, the passengers can either bring their own luggage to the aircraft or have it taken by someone. An outside baggage door is present for the access to the storage of the baggage in the tail cone. Passengers can also bring items on board and store them in the overhead luggage compartments.

15.13 Lighting System

Cockpit Lighting

In the cockpit the lighting can be dimmed in case of a night flight, where the lights can be turned to red to ensure visibility. The warning lights are red and will not have a dimming function. The caution lights are amber and the indicating and advisory lights are green/blue en both these lights can be dimmed.

Cabin Lighting

For the cabin lighting, mood lighting is requested and therefore the Daylight Variable White Lightening System [67] is chosen as shown in Figure 15.14. This lighting system requires 28 V DC. Using this system white color temperatures, variable from warm to cool, intensity values, fade times and groups and zones can be determined. In addition several reading lights are installed for the comfort of the passengers.

Figure 15.14: Cabin Lighting [67]

Exterior Lighting

For the exterior lighting several lights have to be installed. These location and color of these lights can be found in Figure 15.15. The landing lights and the navigation lights both use 28 V DC.
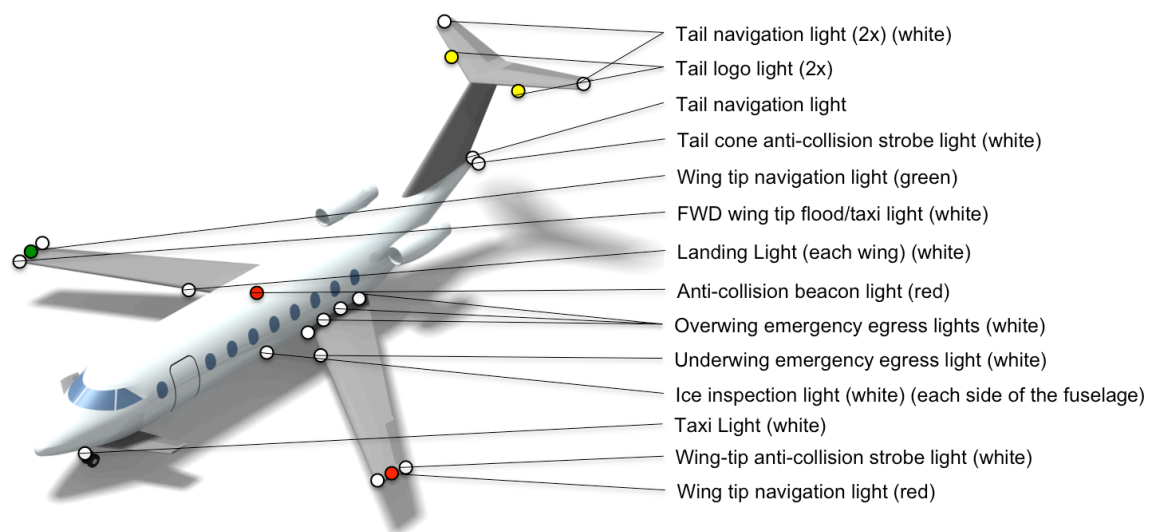
Figure 15.15: Exterior Lighting

Part IV

Final Concept

16 Configuration Layout

After discussing the structural, aerodynamic and performance characteristics, this chapter presents the overall outcome of the aircraft configuration of the Class II design phase. Section 16.1 describes the overall configuration and the most important features. Section 16.2 presents the configuration three view and renders of the aircraft.

16.1 Configuration Description

The Phoenix 5600 is a subsonic forward swept wing three surface design. The aircraft features a canard, forward swept, low mounted wing and a T-tail aft empennage configuration. The canard is mounted low on the nose, under the cockpit. The wing is mounted low on the fuselage, under and aft of the passenger cabin. The T-tail is mounted on top and at the end of the tail cone. The horizontal tail surface is attached to the top of the vertical tail surface and the horizontal tail root chord and vertical tail tip chord match lengths for optimal structural integration.

For longitudinal and directional stability and control, the aircraft features a T-tail with elevators and a rudder and a canard with a canardvator. For lateral control, the wings feature ailerons. The ailerons are smaller than on typical aft swept wings, because forward swept feature a more laminar airflow on the tips yielding higher aileron effectiveness. The wings feature Fowler flaps as high lift devices, because of their high efficiency combined with relatively low mechanical complexity.

The aircraft is internally pressurized from the cockpit until the baggage compartment, which is located behind the passenger cabin. The aft pressure bulkhead closes the baggage compartment at the back. In the front on the left (port) side, the cabin has a passenger access door. In the back on the right (starboard) side, the cabin has an over-wing emergency exit (type IV). The baggage compartment is reachable from the outside port side.

The cabin itself is very spacious and features large windows, a large access door, a galley, a lavatory and state-of-the-art air conditioning, entertainment, electrical systems and more. The cockpit floor is raised slightly compared to the cabin floor for cockpit visibility and nose shape restrictions. The cockpit windows allow excellent visibility for the pilots to ensure safe operations, also during high pitch flight. Detailed figures on the interior design of the Phoenix 5600 can be found in the Midterm Report [1].

The engines are attached high on the aft of the fuselage at the position of the aft pressure bulkhead. This ensures that the engines are as far away from the cabin as possible (reducing inside noise), that the engine inlets are not positioned in the wing wake and that the engine exhaust flow does not interfere with the aft empennage surfaces.

The nose landing gear is located under the cockpit and attached to the fuselage at the position of the front spar of the canard. The nose landing gear retracts to the front to ensure aerodynamic lock in case of hydraulic failure. The main landing gear is attached to the aft spar of the wing and retracts inwards toward the fuselage. The shape of the tail cone allows, in combination with the position of the landing gear, that sufficient space is available during take-off rotation to prevent tail strike.

16.2 Dimensioned Three View and Renders

6.8

Side view
Dimensions in m

21.6°

2.8

6.3

2.4

Baggage
door

Wing
root

1.3

19.1

⌀2.5

9.4

9.9

Pax
door

13.7

1

1.7

0.8

Canard

2

3.4

6

Top view
Dimensions in m

Elevator

0.9

Type IV overwing
emergency exit

1

1.9

Fowler
flaps

2.5

Aileron

Pax
door

35°

Canard w/
elevator

4.9

16.3

Front view
Dimensions in m

3.2

6.5

⌀2.5

3.5

3.4

1.1
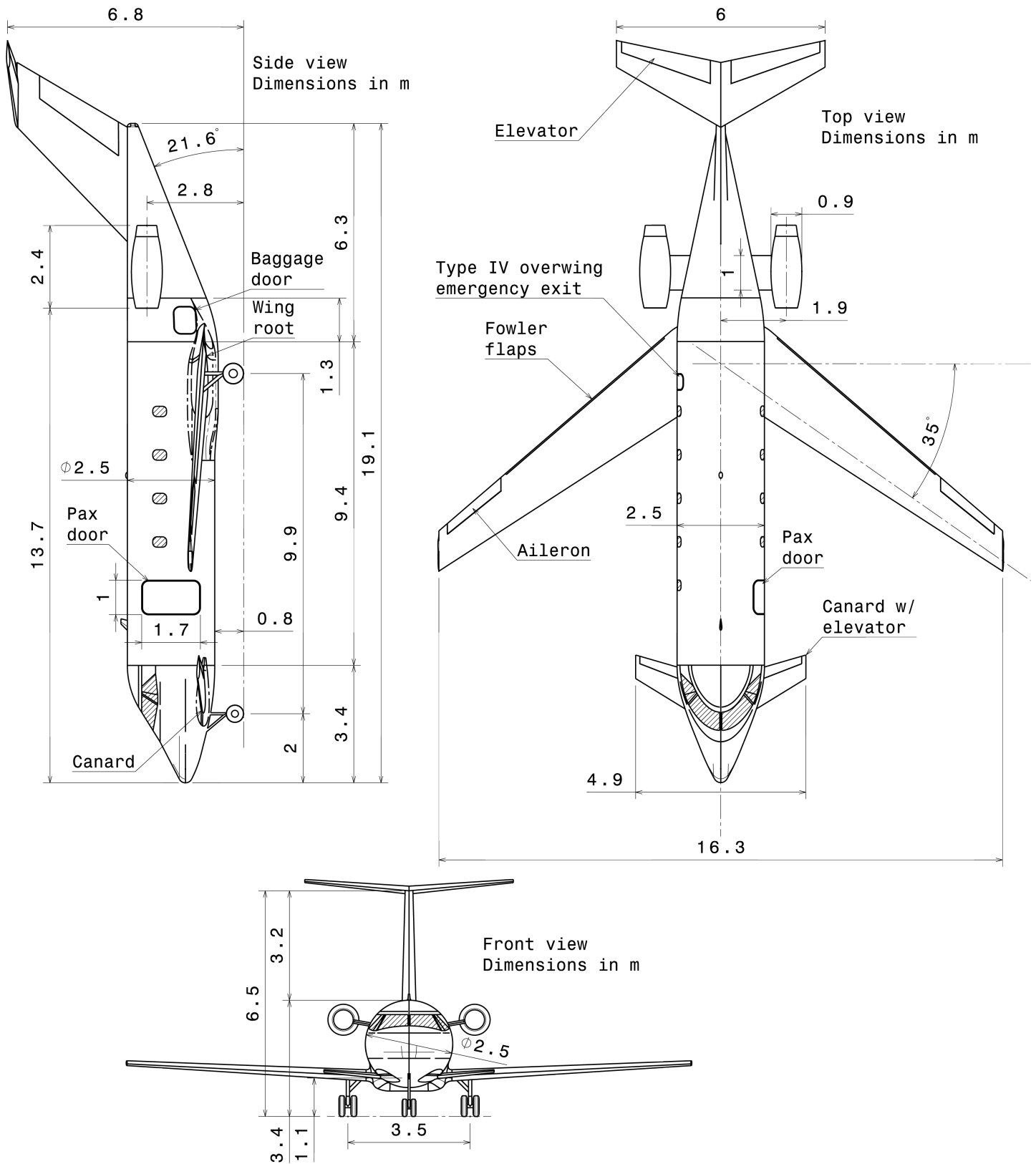
Figure 16.1: Phoenix 5600 Dimensioned Three View
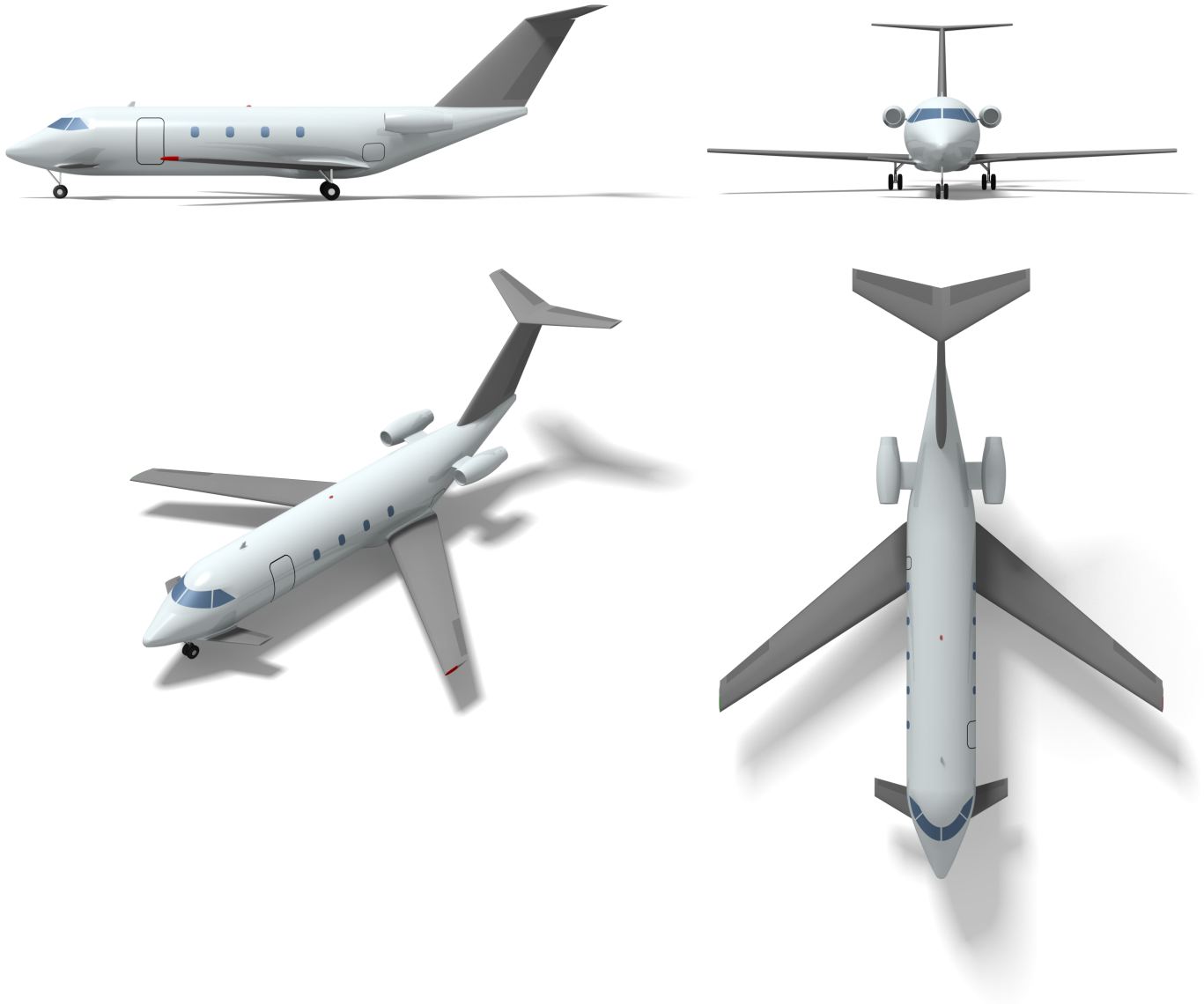
Figure 16.2: Phoenix 5600 Three View

17   Technical Risk Assessment / Risk Map

The Technical Risk Assessment for the product is performed in this chapter. This assessment consists of three parts. Initially, in Section 17.1, a Risk Map is created, representing a general view on the major and minor risks that can be identified at this point in the project. This means that small modifications in the design, with respect subsystems and the overall configuration of the aircraft, are treated in the Risk Map. Various design solutions can be considered for this configuration, based on existing and non-existing aircraft technologies. Thus, for a complete trade-off between design concepts, a first Technical Risk Assessment is needed to recognize significant risks of design solutions at this stage. Technical risks are assessed with respect to technical performance, time schedule and costs. Accompanying the Risk Map, an initial Risk Mitigation Approach is presented in Section 17.2. This explains the approaches that can lead to risk reduction. These approaches are specific for each design solution and differences in impact on risk reduction can be expected. Finally, a Fault Tree Analysis approach is given in Section 17.3, which will be the top-down prediction method that leads to RAMS definition. Minimum cut-sets will be defined in order to identify the combination of events that can lead to critical top events. As the Technical Risk Assessment is a continuous process that increases in complexity during the project, the Risk Map and Risk Mitigation are updated as a consequence of new developments in design solutions.

17.1   Risk Map

The Risk Map is used as a qualitative method. It shows the relation between the feasibility of a certain design option and the severity of its consequence. In order to create a complete Risk Map, three aspects need to be elaborated on. First, all elements/functions that can be considered as a design solution are identified. As stated before, these elements/functions will relate to the subsystems configuration of the aircraft only. After determining the list of all possible configurations, the probability of unsatisfying results for each item in the list is defined. Simultaneously, the consequence of each specific risk occurrence is determined. These two properties are assessed qualitatively, based on a combination of analysis/logic and lessons learned from previous designs. The results of the risk analysis are divided over three aspects: technical performance, time schedule and costs. The technical performance represents the stability and controllability characteristics and the amount of effort it takes to operate the aircraft efficiently. The schedule aspect deals with accessibility during production and operation, for example for maintenance procedures. The costs consist of production and operating costs.

For the main wing subsystem, the following elements are determined:

1. Three electrical mechanical actuators for ailerons
2. Three electrical mechanical actuators for flaps
3. Aluminum flaps
4. Aluminum high lift devices
5. Coating for fuel compartments
6. Fuel pumps through ribs

Table 17.1: Risk Map of the Phoenix 5600 Wing Subsystem

	Performance				Cost				Schedule			
Very low feasibility												
Low feasibility												
Medium feasibility			6	5	6	3, 4			6	1, 2		5
High feasibility	1, 2	3, 4			1, 2		5					
Very high feasibility									3, 4			
	Negligible	Marginal	Critical	Catastrophic	Negligible	Marginal	Critical	Catastrophic	Negligible	Marginal	Critical	Catastrophic

For propulsion system, these are the elements that are determined:

1. Engine ignition
2. Light weight turbine blades
3. Fuel system with fuel pumps
4. Provide electrical energy for electrical systems
5. Emission reduction
6. Noise reduction

Table 17.2: Risk Map of the Phoenix 5600 Propulsion Subsystem

	Performance				Cost				Schedule			
Very low feasibility								2				
Low feasibility				2	5, 6					4	3	
Medium feasibility	5, 6		3								1	
High feasibility					4	1						2
Very high feasibility		4		1			3		5, 6			
	Negligible	Marginal	Critical	Catastrophic	Negligible	Marginal	Critical	Catastrophic	Negligible	Marginal	Critical	Catastrophic

Finally, for the landing gear the elements below are determined.

1. Hydraulic landing gear arm
2. Landing gear wheels
3. Aluminum strut
4. Landing gear door actuators (three)

Table 17.3: Risk Map of the Phoenix 5600 Landing Gear Subsystem

	Performance				Cost				Schedule			
Very low feasibility												
Low feasibility							3					
Medium feasibility							1				1	
High feasibility	3		2				2					3
Very high feasibility	4			1	4				4	2		
	Negligible	Marginal	Critical	Catastrophic	Negligible	Marginal	Critical	Catastrophic	Negligible	Marginal	Critical	Catastrophic

For the main wing subsystem of the Phoenix 5600 business jet, it is decided to design a fully aluminum structure. Due to lack of time to perform a thorough investigation on the possibility to implement composite wing parts, aluminum is chosen for now. Aluminum is a 'safe' choice because it has already proven to be a good wing-box material. Furthermore, all the high lift devices and control surfaces will be equipped with three actuators. Each of the actuators is capable of providing the needed deflection by itself. The majority of the fuel is located in the wing-box in between the spars. The ribs provide sectioning of the fuel. This will safe space compared to internal fuel tanks, because the full wing-box can be used storing fuel. To prevent leakage of fuel, a sealant has to be applied on the inside of the wing box. Fuel pumps are installed to transfer fuel through the wing.

The configuration of the engine design is fixed at this stage in the design process. The critical elements of the propulsion are stated above. The engine ignition system is necessary to turn on the engine. Without this system, the engine is unable to start-up. The turbine blades on an engine are very costly. A lot of development time is needed to arrive at the most efficient and light weighted turbine blades. When they are damaged by a bird attack, this can be catastrophic for the total engine performance. The fuel system plays an important role providing fuel for combustion. It has to be designed with redundancy, otherwise problems can occur with fuel supply to the engine in case of fuel system failure. The engine not only provides thrust, but provides energy for all electrical systems on board. Loss of engine thrust will also result in loss of electrical power production. In this scenario, the auxiliary power unit (APU) takes over the electrical power supply.

The landing gear is designed in such a way that the landing gear strut will not fail under the designed loading. When the extraction mechanism will not function properly, the landing gear can still completely be extracted due to the way it is designed. The drag will cause the landing gear to fully extract. The landing gear doors are operated by three actuators each. All the actuators are capable of providing the needed operation by itself.

17.2   Risk Mitigation Approach

In the risk mitigation approach, the highest-ranking risks of the technical risk map are located and measures are identified to decrease the risk. High risk results from a combination of low feasibility and high impact. From the technical risk map for the wing group (Table 17.1), it can be seen that the following wing elements score exceptionally high:

- Coating for fuel compartments
- Fuel pumps through ribs

The coating for the fuel compartments is vital. Without this, painting corrosion of the aluminum structure will occur. This can lead to material failure and fuel leakage. Both can have catastrophic effects. Mitigation of this risk can be done by setting short maintenance intervals for the fuel compartments. This requires proper access possibilities to the fuel compartments. Otherwise, costly time will be lost due to maintenance. The fuel pumps that will pump the fuel from one section to the other are crucial as well. By pumping fuel from one wing to the other, or from one section to the other, the aircraft can be balanced during flight. Redundancy with pumps and valves will be key, to be certain that this system will fail safe during flight.

From the technical risk map from the propulsion system (Table 17.2), it can be seen that the following elements score exceptionally high on risk:

- Engine ignition
- Light weight turbine blades
- Fuel system with fuel pumps

In order to make the aircraft fly, the engine has to produce thrust. Before the engine can produce thrust, the engine has to be started with the engine ignition system. This system is crucial during the ground phase. It can be costly in time and money when engines will not start. The aircraft cannot take off and maintenance needs to be done. During flight, the ignition system will not play a big role. Ones the engines are powered up, the ignition system is not needed anymore. Redundant electronic ignition modules have to be installed. For the turbine blades, risk mitigation will be more complex. Scarce resources have to be put in for the turbine blade design, manufacturing and testing. Therefore, failure of these blades during flight is not an option. Extensive testing while simulating more harsh environmental conditions than in real life and elaborate maintenance can prevent failure during operation. The fuel system is already discussed above, redundancy is most important. Furthermore, the amount of fuel in each section has to be mapped. This is done by sensors which are connected to the on-board computers.

From the technical risk map of the landing gear system (Table 17.3), it can be seen that there are a couple of elements with high risk:

- Hydraulic landing gear arm
- Aluminum strut

For the hydraulic landing gear arm and the aluminum strut applies that both systems have to be designed safe life. Failure of these systems is not allowed and can have critical consequences. Elaborate testing and in life maintenance are necessary to prevent failure of these systems.

17.3   Fault Tree Analysis

In this Section the Fault Tree Analysis (FTA) is performed. A FTA is a technique by which conditions and factors that can contribute to a specified undesired event are identified and organized in a logical manner and represented pictorially [68]. For the analysis of the Phoenix 5600 business jet at this point, two undesired events are identified. The first being a crash due to an engine failure and the second event is a crash during landing due to failure of the landing gear. Both FTA's can be seen in Figures B.1 and B.2 of Appendix B.

18 Future Cost Breakdown Structure

This chapter shows the cost breakdown structure (CBS) of the post-DSE activities. The CBS contains all cost elements that contribute to the overall costs related to the product design. This includes costs from research development test evaluation (RDTE) phase and the production phase, which are both defined in Project Design & Development (PD&D) logic found in Chapter 21.

18.1 Approach to Cost Breakdown Structure

The CBS shows all cost elements from RDTE and production phases systematically. The top level equals the total cost of those phases. Lower level gives a more detailed breakdown. This is the basis of the cost estimation of the aircraft program. The Return on Investment found in Chapter 19 describes the total cost of the entire aircraft programme more detailed.
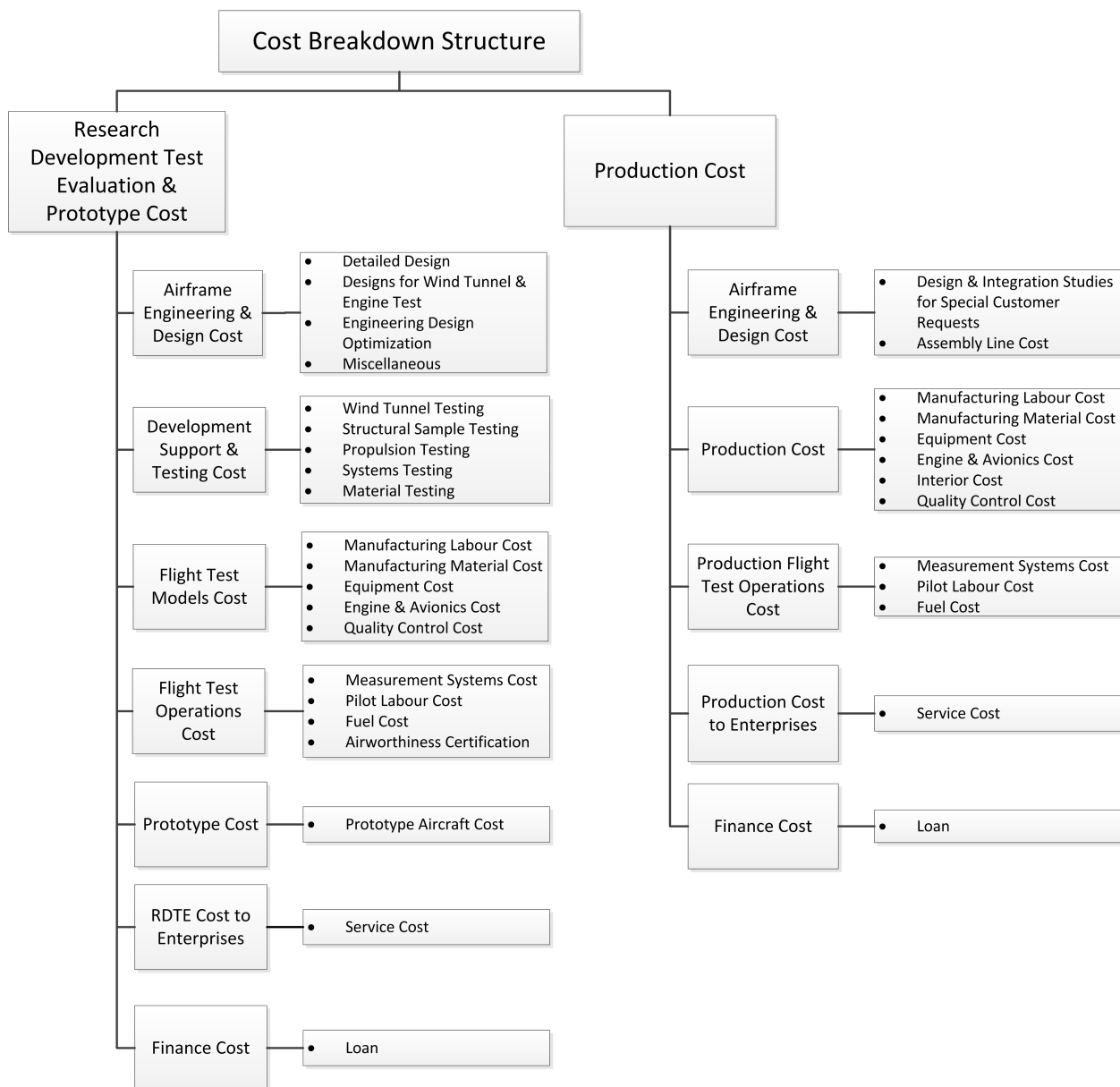
Figure 18.1: Cost Breakdown Structure Associated with post-DSE Activities

19   Return on Investment

In this chapter, the return on investment calculation is done. This analysis in mainly based on competitor data. The return on investment estimation has been estimated in Section 19.1. The methodology for the cost estimation is briefly documented in Section 19.2. The results of the cost estimation including the list price is presented in Section 19.3. Operating an aircraft will cost money. The operating cost analysis is done in Section 19.4. In Section 19.5 competitors' data is used to estimate the number of aircraft manufactured. The future market share has been estimated in Section 19.6. All the results obtained in this chapter are then once more summarized and discussed in Section 19.8.

19.1   Return on Investment Estimation

The return on investment is defined as the efficiency of an investment. For the return on investment for the Phoenix 5600, an analysis on the return on investment of the competitors has been performed. For the analysis it is assumed that the competitors stocks are traded at a fair value. The average year to year return of the last 5 years from six business jet manufacturers have been calculated, the results are shown in Table 19.1. The average annual growth of the competitors is 24.34%. For the project Phoenix 5600 the aim is to achieve return on investment of at least 24.34%. Although the Phoenix 5600 will be the first aircraft manufactured it clearly excels in performance compared to its competitors(see Section 5.3 of Chapter 5). Therefore the aim to achieve at least the same return in investment as the competitors is realistic.

Table 19.1: Average Annual Growth of Competitors

Company	Embraer	Boeing	Trextron (Cessna)	Dassault Aviation	Airbus	Bombardier	Average
Average Annual Growth [%]	18.73	27.32	34.17	27.45	32	6.34	24.34

19.2   Methodology

The cost estimations are based on Roskam VIII [5]. The research, development, test and evaluation cost is estimated using Chapter 3, the manufacturing cost is estimated using Chapter 4 and the direct operational cost is estimated using chapter 5. The list price is calculated by dividing the total costs over the number of aircraft manufactured. A profit equal to 24.34% of the total costs has been included in the costs, which represents the return on investment. A problem encountered during the total cost estimation is that the total costs are dependent on the number of aircraft to be manufactured. Therefore an estimation of the production size has been performed in order to find a value for the total costs and list price. The most important variable is the aeronautical manufacturers planning report weight, this is defined as the difference between the W_E and the components weight. The W_{ampr} is included in almost all the cost estimation equations. The method Roskam uses to estimate the cost is to start with estimating the man-hours required to complete a task, when the amount of man-hours is determined it is multiplied with the labor wage per hour.

19.2.1   Research, Development, Test and Evaluation Cost

The RDTE cost involves activities which take new airplanes from planning and conceptual design stage to certification. The RDTE cost is calculated using Roskam VIII Equation 3.1 [5], which can be distributed along six divisions:

Airframe Engineering and Design Cost C_{aed_r} Roskam VIII Equation 3.2 [5]. This part includes the cost of planning and design, such as: preliminary design, conceptual design, cost studies, design and construction of prototypes and test facilities needed.

Development Support and Testing Cost C_{dst_r} Roskam VIII Equation 3.7 [5]. This part of the RDTE cost includes wind tunnel testing, systems testing, structural testing, propulsion testing and the simulation for development support testing.

Flight Test Airplanes Cost C_{fta_r} Roskam VIII Equation 3.8 [5].In order to validate the conceptual design, one or more prototypes need to be tested in real life. Several aspects like the number of engines,

avionics and material type have large influence on the C_{ftar}. Roskam Equation 3.9 calculates the engine and avionics cost, Roskam Equation 3.11 estimates the man-hours to manufacture a prototype, Roskam Equation 3.12 focuses on the material cost and Roskam Equation 3.13 calculates the tooling man-hours.[5]

Flight Test Operations Cost C_{fto_r} Roskam VIII Equation 3.16 [5].This part consists of the cost related to all activities related to flight tests.

Test and Simulation Facilities Cost C_{tsf_r} Roskam VIII Equation 3.17 [5]. For testing of the aircraft new facilities may be required. New facilities will significantly increase the cost.

Cost to finance RDTE Phase C_{fin_r} Roskam VIII Equation 3.19 [5]. In many cases, the enterprise will borrow capital from financial institutions since it cannot finance all the cost from the company itself.

19.2.2 Manufacturing Cost

The manufacturing cost is dependent on the number of aircraft manufactured, as more aircraft are built the manufacture cost increase. However the manufacture cost does not increase linearly with the number of aircraft manufactured. The manufacturing cost can be broken down into the following cost categories:

Airframe Engineering and Design Cost C_{aed_m} Roskam VIII Equation 4.5 [5]. The C_{aed_m} cost is mainly generated by engineering and design of the airframe, but engineering design work necessitated by problems or changes in the design and analysis of reliability and maintainability also contribute to C_{aed_m}. Roskam Equation 4.6 estimates the amount of man-hours for the airframe engineering and design.

Airplane Production Cost C_{apc_m} Roskam VIII Equation 4.7 [5]. The category includes all the cost related to manufacturing an aircraft. The engine and avionics cost is estimated using Roskam VIII Equation 4.8, the interior cost by Roskam VIII Equation 4.9, the man-hours required for manufacturing by Roskam VIII Equation 4.11, the material cost by Roskam VIII Equation 4.12 and finally tooling by Roskam VIII Equation 4.15.[5]

Production Flight Test Operation Cost C_{fto_m} Roskam VIII Equation 4.17 [5]. The manufactured airplanes need to be ensured to meet the performance criteria before delivery. Every jet transport airplane will perform ten hours of flight test hour. The operating cost per hour in Section 19.4 will be used for the estimation.

Cost to Finance the Manufacturing Phase C_{fin_m} Roskam VIII Equation 4.18 [5]. Interest lost due to spending money or interest paid for borrowing money will contribute to the costs to finance the manufacturing phase.

19.2.3 Direct Operating Cost

Low Operating cost is favorable because airplanes have long service lifetime. Over the whole lifetime of the airplane the total operating cost exceed the list price, therefore it is important to have a low operating cost.

Direct Operating Cost of Flying DOC_{flt} Roskam VIII Equation 5.20 [5]. The cost related to flight crew (captain + co-pilot), fuel and insurance contribute to DOC_{flt}. Roskam VIII Equation 5.21 estimates the crew cost, Equation 5.525 calculates the fuel cost and Equation 5.31 the insurance cost.[5]

[Direct Operating Cost of Maintenance DOC_{maint} Roskam VIII Equation 5.33 [5]. For proper operation of the aircraft maintenance has to be performed. The maintenance cost can be split up in maintenance cost related to the airframe(Equation 5.35) and maintenance cost related to the engines(Equation 5.36).[5] The maintenance hours per flight hours are calculated, by using the maintenance labour wage per hour the contribution of the maintenance to the direct operating cost is calculated.

Direct Operating Cost of Depreciation DOC_{depr} Roskam VIII Equation 5.40 [5]. As the aircraft becomes older its value decreases. Depreciation is included in the direct operating because the lost in value is caused by operation. The most valuable parts are: airframe, engines and avionics. A depreciation factor of 0.85 has been used for most parts while the depreciation period varies from 5 till 10 years.

Direct Operating Cost of Landing Fees, Navigation fees and registry taxes DOC_{lnr} Roskam VIII Equation 5.47 [5]. For takeoff and landing the customer has to pay fees to use the runway, the cost is dependent on the MTOW describes by Roskam VIII Equation 5.51 [5]. Owning an aircraft results in registry fees.

Direct Operating Cost of Financing DOC_{fin} Roskam VIII Equation 5.55 [5]. Money used for the operating can be borrowed or own money can be used. In both cases it will lead to extra cost.

19.3 RDTE & Manufacturing Cost Estimations

For the cost estimation a large list of input variables have been used, these input variables have been presented in Table 19.2. For every input variable the source has been added, some variables do not have a source because it is a result from a calculation. For the labor wages the May 3013 report from the United States Department of Labor has been used and for the cost escalating factor the Federal Reserve Bank results have been used. Table 19.3 gives the cost estimation results for various categories that contribute to the total cost. Figure 19.1 shows the estimated list price versus the number of aircraft sold. It can be clearly seen that selling and manufacturing more aircraft will lower the production cost of a single aircraft. Figure 19.2 gives the profit/loss curve for the list price of 15.9 M\$. The red line indicates the line for the scenario where no ROI is included and the green line is the break even line for the scenario where 24.34 % ROI is included. the sales reach break-even point at 200 units, this happens at 2026. For break even when 24.34% profit is included 580 aircraft need to be sold, this happens in 2036. The reasoning for this selected number will be given in Section 19.5.

Table 19.2: Input Variables for the Cost Estimation

Symbol	Description	Value	Unit	Source
V_{max}	Maximum design speed	280	m/s	
R_{e_r}	Engineering labor cost	51.19	\$/hr	[69]
N_{rdte}	RDTE airplanes	4	-	[5]
F_{diff}	Difficulty factor	2	-	[5]
F_{cad}	Computer aided design factor	0.8	-	[5]
C_{e_r}	Cost per jet engine	$1.66 \cdot 10^6$	\$	[5]
N_e	Number of jet engines	2	-	
$C_{avionics_r}$	Cost of avionics equipment	$2.47 \cdot 10^6$	\$	[5]
R_{m_r}	Manufacturing labour rate	48.38	\$	[69]
R_{m_t}	Tooling labor rate	37.10	\$	[69]
F_{mat}	Correction factor material type	2.5	-	[5]
F_{tsf}	Factor for extra facilities	0	-	[5]
F_{int}	Interior cost per pax	4500	\$	[5]
N_{pax}	Number of passengers	8	-	
N_m	Number of aircraft manufactured	580	-	[70]
$CEF_{2014/1990}$	Cost escalating factor	1.8	-	[71]
N_{r_m}	production rate per month	2	-	
t_{pft}	Number of flight test hour	10	-	[5]

Table 19.3: Cost Estimation

Category	Value [$M\$$]
C_{aed_r}	69.3
C_{dst_r}	42.1
C_{fta_r}	244.2
C_{fto_r}	7.5
C_{tsf_r}	0
C_{fin_r}	36.3
C_{aed_m}	73.3
C_{apc_m}	7260.3
C_{fto_m}	62.3
C_{fin_m}	650.2
C_{profit}	1582.6
Total Cost	9222.4

Figure 19.1: List Price - # of Aircraft Manufactured   Figure 19.2: Profit versus Number of Aircraft Sold

19.4   Direct Operating Cost Inputs & Results

The direct operating cost used a set of input parameters including labor wages for pilots and maintenance labor wage. For those variables reports from Safety Standdown and United States Department of Labor have been used. The calculated direct operating cost for the Phoenix 5600 is 2398 $/h.

Table 19.4: Direct Operating Cost Results

Symbol	Description	Value	Unit	Source
SAL_1	Annual salary captain	90000	m/s	[72]
SAL_2	Annual salary co-pilot	67000	$/hr	[72]
AH	Flight hours per year	800	-	[5]
$R_{l_a p}$	Maintenance labour rate	26.55	$	[73]
F_D	Depreciation factor	0.85	-	[5]
F_P	Fuel price	4.70	$	[74]

19.5   Production Size Estimation

For the estimation of the amount of Phoenix 5600 to be manufactured the reference aircraft are used. GAMA 2013 [70] contains the statistical data over the number of business jet deliveries by aircraft type. By making use of the similar reference aircraft and their number of deliveries it is possible to estimate the Phoenix 5600 annual delivery and the total amount of units to be manufactured. Table 19.5 contains the annual deliveries for a number of similar reference aircraft. In the table some cells have been left blank because the aircraft was still in development or production has stopped.

Table 19.5: Annual Deliveries of Reference Aircraft [70]

	1999	2000	2001	2002	2003	2004	2005	2006	2007	2008	2009	2010	2011	2012	2013
Bombardier Learjet 40/45	43	71	63	27	17	39	49	56	57	48	33	16	24	23	1
Bombardier Learjet 70															18
Cessna 560 Citation XLS	39	79	85	81	48	55	64	73	82	80	44	22	27	31	31
Cessna 550 Citation Bravo	36	54	48	41	31	25	21	18							
Embraer Phenom 300											1	26	42	48	60
Gulfstream G150	9	11													
Hawker 400XP	45	51	25	19	24	28	54	54	41	35	11	12	1		
Hawker 900XP									32	50	35	28	22	17	
Emivest SJ30									1	1		2			
Falcon 50EX	11	18	13	10	8	5	5	5	2	1					

The average annual delivery per aircraft type of the reference data is 36 units per year. The reference aircraft includes products from business jet manufacture giants like Cessna and Bombardier. These giants

have several decades of experience in the market and a very broad client basis. Being a new company on this market, reaching the same sales numbers will be hard, but the Phoenix 5600 has better performance in for instance speed than the reference aircraft (see Section 5.3 in Chapter 5). Therefore, reaching the annual delivery estimate should not be a problem.

For the estimation of the total number of aircraft to be delivered reference aircraft are used. Only the reference aircraft which have been at least five years in full production are included. Table 19.6 shows the number of aircraft built for the reference aircraft. The average number of aircraft built is 580 units, this will be the total number of Phoenix 5600 to be produced. With a production rate of 36 units a year it will take 16 years to produce 580 units.

Table 19.6: Number of Aircraft Built for Reference Aircraft

Aicraft	Bombardier Learjet 40/45	Cessna 560 Citation XLS	Cessna 550 Citation Bravo	Embraer Phenom 300	Hawker 400XP	Hawker 900XP	Average
Number built	430	575	940	177	700	650	580

19.6 Market Volume & Share

According to GAMA 2013 the global business jet fleet will have 15,350 aircraft in 2020. [70] In this year the Phoenix will entry service with 36 deliveries, resulting in a market share of 0.23% in 2020. In 2020 the Phoenix 5600 only has entered the market for one year, therefore the market share of 2036 will also be estimated. In 2036 the Phoenix is at the end of production with a total of 580 units produced. GAMA predicts the number of total business jets in 2036 to be 27,297 units, according to this forecast the market share of the Phoenix 5600 will be 2.12% in 2036. The competitive positioning is shown in a radar plot in Figure 19.3. From the figure several things can be seen, the competitors who score high on the range and payload usually score low on the mass and MTOW. The Phoenix 5600 manages to score maximum points on the cruise speed & range and a high score on payload while still scoring average on MTOW and mass.

Figure 19.3: Competitive positioning

19.7 Discussion of Results

For the cost analysis several categories including the airframe, avionics, engines and interior cannot be determined exact. Reference data for the prices of these components are unavailable. Manufacturers tend to not list their product price because product prices are usually determined in negotiations. At a later stage of the design process when the component manufacturers are contacted the exact price can be obtained for more exact cost estimations. At this moment the estimation method of Roskam VIII [5] will be used for the

cost analysis. The importance of meeting the estimation of aircraft sales is really important. From Figure 19.2 it can be seen that the break-even point is reached at 200 units. According to the production rate of 36 units per year this point is reached in 2025. All extra aircraft sold after number 200 will be generating profit. To meet the estimations of the return on investment 580 units have to be sold. At the chosen production rate this number will be reached in 2036. To take in account possible deviations of the estimations a sensitivity analysis is performed. The most important variable is the number of aircraft sold, the derivative of the list price to a change of the number of aircraft sold is calculated. $\frac{\delta ListPrice}{\delta N_m} = -5913\$$ will represent the sensitivity of the list price to the number of sold aircraft.

19.8   Value Analysis

A project can have a positive return on investment but still not be valuable. Capital owned at present time is more valuable than capital owned in future time. Future capital can be discounted by the risk free rate to find the net present value, see Equation 19.1. In reality risk free interest rate does not exist therefore the US treasury bond yield rate is used because it is the world's largest economy. The yield rate on the US Treasury Bond of 10 years is 2.58% per year. [75] The RDTE costs are equally distributed over the period of 2014 - 2018. The manufacturing costs are distributed over 16 years starting at 2018 when full production starts. Payments are assumed to occur once a month. The cash flows and payment are displayed in Figure 19.8. The present value of the income is larger than the costs. Hence, the investment is profitable.

$$PV = \Sigma_{i=1}^{n} \frac{C}{(1+r)^n} \tag{19.1}$$
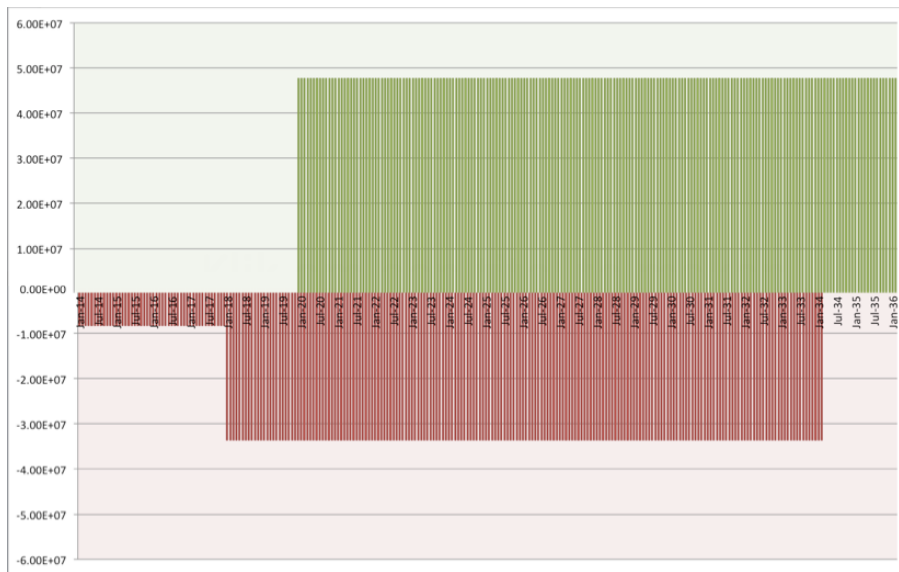
Figure 19.4: Cash Flow Diagram

Table 19.7: Present Value of the Cost and Income

	Cost [B$]	**Income** [B$]
Phoenix 5600 Present Value	5.16	6.46 B$

20 Compliance Matrix & Feasibility Analysis

The requirements compliance matrix is a table containing all requirements and indicates if the requirements are met. It specifies the actual value for a specific requirement at this point of the design. This actual value is compared with the required value. If an actual value does not meet the criteria it has to be explained which modifications would be required in order to meet the requirement (feasibility analysis). The requirements are imposed by the customer and presented in the project-guide [3].

Table 20.1: Requirements Compliance Matrix

Category	Requirement	Required Value	Actual Value	Chapter
Performance	Range	4200 km	5600 km	Part IV Chapter 2
	Nominal cruise speed	Mach 0.90	Mach 0.90	Part IV Chapter 2
	Maximum speed	Mach 0.95	Mach 0.95	Part IV Chapter 2
	Payload	2 crew (max) 4 passengers (typical) 8 passengers (max) passenger baggage	2 crew 4 passengers 8 passengers 180 kg	Part III Chapter 5
	Service ceiling	41000 ft	41000 ft	Part IV Chapter 10
	RAMS	Similar as competitors	Achieved	Part IV Chapter 8
	Specific fuel consumption	0.5 lb/(lbf · h)	0.5 lb/(lbf · h)	Part III Chapter 13
	Take-off/Landing distance	1000 m / 800 m	819 m / 746 m	Part IV Chapter 10
Market	Pressurization	1500 m ISA equivalent	1500 m ISA	Part IV Chapter 12.1
	Noise levels (in-aircraft)	exceed competitors	60 dB	Part III Appendix K
	List price	16 - 20 M$	15.9 M$	Part IV Chapter 19
	Direct operating costs	2500 $/h	2398 $/h	Part IV Chapter 19
	Entry into service	2020	2020	Part IV Chapter A
Sustainability	Noise	Comply with ICAO Annex 16, vol. I, Chapter 4	Achieved	Part III Chapter 8
	Emissions	Comply with ICAO Annex 16, vol. II	Achieved	Part III Chapter 8

The compliance matrix is shown in Table 20.1. The requirements that are marked dark green exceed the requirements set by the customer and make the Phoenix 5600 business jet outstanding compared to the competition. The range, list price and direct operating cost are marked dark green, indicating that the Phoenix 5600 can fly further than the competition with a relatively cheap operating cost while having a list price of 0.1M$ cheaper compared to the initial required value . The light green color indicates that the requirement is met. In Table 20.1 it can be seen that all the customer requirements are met. Thus a premium light business jet offering premium value through unparalleled in-class performance is designed. In the last column, Chapter in Table 20.1 the part and chapter can be found where the information is presented. Part I represents the Project Plan [2], Part II is the Baseline Report [4], Part III is the Midterm Report [1] and Part IV is the Final Report.

Part V

Recommendations for Future Design

21 Project Design & Development Logic

This chapter on project design & development logic (PD&D), shows the logical order of activities to be executed in the post-DSE phases of the project. In Figure 21.1 the various steps of the design process are shown as taught in the course Systems Engineering and Aerospace Design [76]. All the steps shown in Figure 21.1 are split up in phases that are conducted during the DSE (Section 21.1) and phases that still have to be done after the DSE (Section 21.2).
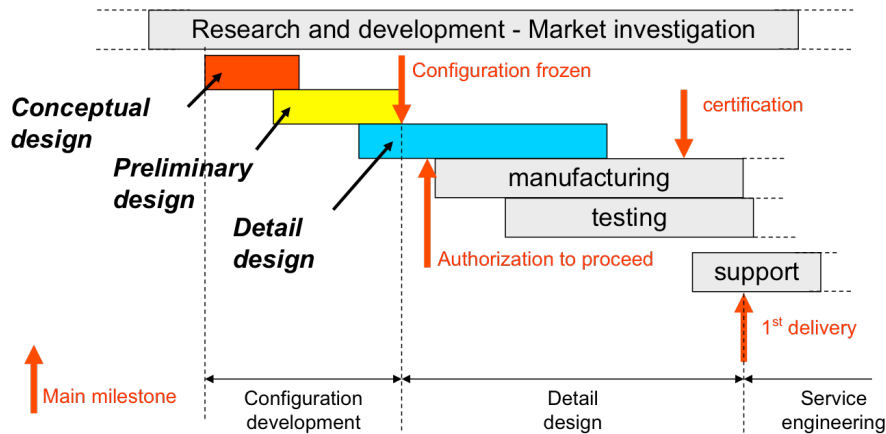
Figure 21.1: Design Process [76]

21.1 Phases Performed During the DSE

Market Investigation:
The start of the design process is marked by a market analysis, which determines the market needs. From this analysis many of the requirements of the aircraft to be designed follow. The initial phase of the requirements is its mission. The market investigation does not stop with the beginning of the design phase. Market trends can change and the desing must adapt to the changes in order to be successful.

Class I Design:
The Class I design is conducted during the DSE at the beginning of the conceptual design as shown in Figure 21.1. The approach for Class I is the fuel fractions method and the Brequet equations, from this the MTOW, OEW and fuel weight (including reserves) is determined.

Class II Design:
The Class II design is also conducted during the DSE at the beginning of the preliminary design as shown in Figure 21.1. The approach for Class II is the component weight estimation equations, from this the weights of the aircraft main components and systems is determined as well as the OEW.

21.2 Post-DSE Phases of the Project

The post-DSE phase of the project consists of the detailed design phase, testing phase, production preparation, certification and production. Figure 21.2 shows a block diagram of the post-DSE phase. Figure 21.3 presents the general Gantt chart of the post-DSE phase.
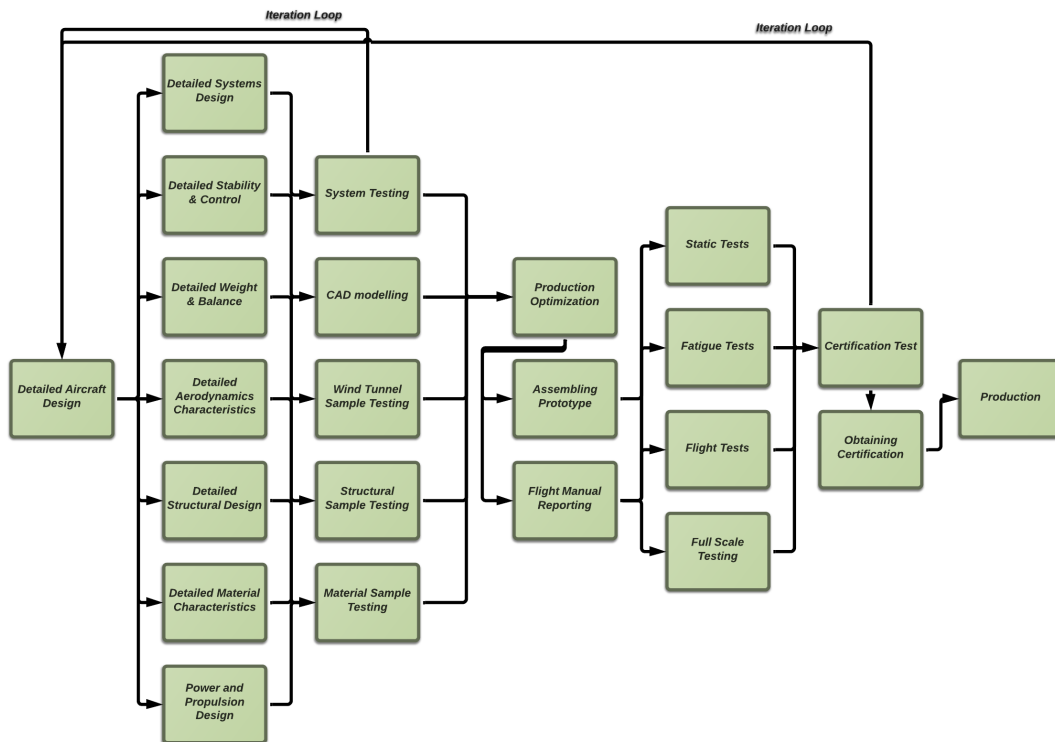
Figure 21.2: Future Design Process

ID		Task Mode	Task Name	Duration	Start	Finish		2014		2015		2016		2017		2018		2019		2020	
							H2	H1	H2	H1	H2	H1	H2	H1	H2	H1	H2	H1	H2	H1	H2
1																					
2			Detailed Design Phase	301 days	Mon 16-6-14	Mon 10-8-15															
49			Testing Phase	390 days	Mon 10-8-15	Fri 3-2-17															
67			Production Preperation	118 days	Thu 1-9-16	Mon 13-2-17															
74			Certification	256 days	Thu 2-2-17	Thu 25-1-18															
80			Production	505 days	Thu 25-1-18	Wed 1-1-20															

Figure 21.3: Overview Total Gantt Chart

Detailed Design Phase: 12 months
In the detailed design phase the design is further designed in detail including the weight estimation of all the individual components. The detailed design phase consists of the detailed aircraft sizing, detailed structural design, material characteristics, aerodynamics, stability & control, weight & balance, propulsion & power, and the system design. The CAD modeling is very important in this stage, to ensure that all the parts will fit together. In Figures 21.4 and 21.5 the various steps of the detailed aircraft design phases can be found. At the end of the design phase all the items including the rivet spacing will be determined so that the aircraft can be produced.

ID		Task Mode	Task Name	Duration	Start	Finish
1						
2			**Detailed Design Phase**	**301 days**	**Mon 16-6-14**	**Mon 10-8-15**
3			**Detailed aircraft sizing**	**250 days**	**Mon 16-6-14**	**Fri 29-5-15**
4			Wing sizing	93 days	Mon 16-6-14	Wed 22-10-14
5			Empennage Sizing	93 days	Mon 16-6-14	Wed 22-10-14
6			Fuselage Sizing	93 days	Mon 16-6-14	Wed 22-10-14
7			Subsystem Distribution	150 days	Mon 1-9-14	Fri 27-3-15
8			Landing Gear	93 days	Mon 16-6-14	Wed 22-10-14
9			Extra Time	46 days	Fri 27-3-15	Fri 29-5-15
10			**Detailed Structural Des**	**57 days**	**Wed 22-10-14**	**Thu 8-1-15**
11			Fuselage Structure	20 days	Wed 22-10-14	Tue 18-11-14
12			Wing Structure	20 days	Wed 22-10-14	Tue 18-11-14
13			Empennage Structure	20 days	Wed 22-10-14	Tue 18-11-14
14			Engine Integration Str	20 days	Fri 12-12-14	Thu 8-1-15
15			Landing Gear Structu	20 days	Wed 22-10-14	Tue 18-11-14
16			Skin Cut-out	23 days	Wed 12-11-14	Fri 12-12-14
17			**Material Characteristics**	**38 days**	**Thu 8-1-15**	**Mon 2-3-15**
18			Composite Analysis	38 days	Thu 8-1-15	Mon 2-3-15
19			New Material Analysi	38 days	Thu 8-1-15	Mon 2-3-15
20			**Aerodynamics**	**38 days**	**Mon 18-5-15**	**Wed 8-7-15**
21			Wing-Canard Interact	38 days	Mon 18-5-15	Wed 8-7-15
22			Control Surfaces and	38 days	Mon 18-5-15	Wed 8-7-15
23			**Stability & Control**	**38 days**	**Thu 26-3-15**	**Mon 18-5-15**
24			Stability Derivatives	20 days	Thu 26-3-15	Wed 22-4-15
25			Control Derivatives	20 days	Tue 21-4-15	Mon 18-5-15
26			Eigenmotions	38 days	Thu 26-3-15	Mon 18-5-15

Figure 21.4: Detailed Design Phase Gantt Chart

ID		Task Mode	Task Name	Duration	Start	Finish
27			**Weight & Balance**	**38 days**	**Tue 3-2-15**	**Thu 26-3-15**
28			Weight Estimation	38 days	Tue 3-2-15	Thu 26-3-15
29			Balance	38 days	Tue 3-2-15	Thu 26-3-15
30			**Propulsion & Power**	**38 days**	**Wed 22-10-14**	**Fri 12-12-14**
31			Detailed Power Budg	38 days	Wed 22-10-14	Fri 12-12-14
32			**System Design**	**150 days**	**Mon 1-9-14**	**Fri 27-3-15**
33			Instrumentation Sele	40 days	Fri 10-10-14	Thu 4-12-14
34			Fly-By-Wire Design	40 days	Thu 20-11-14	Wed 14-1-15
35			Wiring	50 days	Wed 31-12-14	Tue 10-3-15
36			CAD Modeling	50 days	Wed 31-12-14	Tue 10-3-15
37			Electrical System Des	40 days	Thu 20-11-14	Wed 14-1-15
38			Hydraulic System Des	40 days	Thu 20-11-14	Wed 14-1-15
39			Environmental Syster	40 days	Mon 1-9-14	Fri 24-10-14
40			Cockpit System Desig	40 days	Fri 10-10-14	Thu 4-12-14
41			Emergency System D	40 days	Fri 10-10-14	Thu 4-12-14
42			Entertainment and Co	40 days	Mon 1-9-14	Fri 24-10-14
43			Flight Control	40 days	Thu 20-11-14	Wed 14-1-15
44			Water Waste and Cat	40 days	Mon 1-9-14	Fri 24-10-14
45			Propulsion System	40 days	Fri 10-10-14	Thu 4-12-14
46			Baggage System	40 days	Mon 1-9-14	Fri 24-10-14
47			Lighting System	40 days	Fri 10-10-14	Thu 4-12-14
48			Extra Time	24 days	Wed 8-7-15	Mon 10-8-15
49			**Testing Phase**	**390 days**	**Mon 10-8-15**	**Fri 3-2-17**
67			**Production Preperation**	**118 days**	**Thu 1-9-16**	**Mon 13-2-17**
74			**Certification**	**256 days**	**Thu 2-2-17**	**Thu 25-1-18**
80			**Production**	**505 days**	**Thu 25-1-18**	**Wed 1-1-20**

Figure 21.5: Detailed Design Phase Gantt Chart

Testing Phase: 14 months

During the testing phase, the first tests will take place. As the aircraft is not produced yet, so all the individual components will be tested separately to see if their requirements are met. The system will be tested using a system test, to see if all the parts fit together CAD modeling is used. To test the aerodynamic structure a wind-tunnel test is conducted and to test the structural and material characteristics a fatigue test is performed. If an individual component does not meet the requirements, the part will need to be redesigned, therefore an iteration loop is shown in Figure 21.2. As soon as all the individual components are sized correctly the entire system can be optimized for production. When the system is ready the first prototype can be built and simultaneously the flight manual can be made. During this stage the airplane handling

characteristics are determined and simulator tests can be done with the pilots to ensure the aircraft is able to fly under all possible conditions. With the prototype full scale testing of the aircraft can be performed in addition to static tests, fatigue tests and flight tests. Figure 21.6 shows the Gantt chart for the testing phase.

ID		Task Mode	Task Name	Duration	Start	Finish	Half 2, 2015 J A S O N D	Half 1, 2016 J F M A M J	Half 2, 2016 J J A S O N D	Half 1, 201 J F M
1										
2			Detailed Design Phase	301 days	Mon 16-6-14	Mon 10-8-15				
49			Testing Phase	390 days	Mon 10-8-15	Fri 3-2-17				
50			System Testing	45 days	Mon 10-8-15	Fri 9-10-15				
51			CAD Modeling	90 days	Mon 10-8-15	Fri 11-12-15				
52			Windtunnel Sample Tes	45 days	Mon 10-8-15	Fri 9-10-15				
53			Structural Sample Testir	45 days	Mon 10-8-15	Fri 9-10-15				
54			Material Sample Testing	45 days	Mon 10-8-15	Fri 9-10-15				
55			Static Tests	80 days	Fri 9-10-15	Thu 28-1-16				
56			Fatigue Tests	80 days	Thu 28-1-16	Wed 18-5-16				
57			Flight Tests	80 days	Wed 18-5-16	Tue 6-9-16				
58			Full Scale Tests	91 days	Thu 29-9-16	Thu 2-2-17				
59			Cruise and Climb Perf	12 days	Thu 29-9-16	Fri 14-10-16				
60			Flutter Test	12 days	Fri 14-10-16	Mon 31-10-16				
61			VMU Test	12 days	Mon 31-10-16	Tue 15-11-16				
62			Cold Soak Test	20 days	Tue 15-11-16	Mon 12-12-16				
63			Hot and High Test	20 days	Mon 12-12-16	Fri 6-1-17				
64			Autoland Test	7 days	Fri 6-1-17	Mon 16-1-17				
65			Water Ingestion Test	10 days	Mon 16-1-17	Fri 27-1-17				
66			Acoustic Test	5 days	Fri 27-1-17	Thu 2-2-17				
67			Production Preperation	118 days	Thu 1-9-16	Mon 13-2-17				
74			Certification	256 days	Thu 2-2-17	Thu 25-1-18				
80			Production	505 days	Thu 25-1-18	Wed 1-1-20				

Figure 21.6: Testing Phase Gantt Chart

Production Preparation: 6 months
Preparation of the production should already start during the design phase. After the design of each part, the parts should be optimized for production to reduce the production cost. In addition the manufacturing, assembly and integration plan should be finished. All necessary means for the production should be ready and determined (e.g. suppliers, tools, supply chain, logistics). Before production the sales and marketing should have started. Normally aircraft are bought before they are produced. As 36 aircraft need to be produced every year, to be profitable the sales and marketing should start in an early stage of the process. Figure 21.7 shows the Gantt chart of the production preparation phase.

ID		Task Mode	Task Name	Duration	Start	Finish	)16	A	S	O	N	D	Half 1, 2017 J	F	M
1															
2			Detailed Design Phase	301 days	Mon 16-6-14	Mon 10-8-15									
49			Testing Phase	390 days	Mon 10-8-15	Fri 3-2-17									
67			Production Preperation	118 days	Thu 1-9-16	Mon 13-2-17									
68			Design Optimization for	60 days	Thu 1-9-16	Wed 23-11-16									
69			Tooling Equipment	30 days	Wed 23-11-16	Tue 3-1-17									
70			Contracting Suppliers	30 days	Tue 3-1-17	Mon 13-2-17									
71			Supplier Parts	30 days	Wed 23-11-16	Tue 3-1-17									
72			Supplier Logistics	30 days	Tue 3-1-17	Mon 13-2-17									
73			Location of Production	40 days	Tue 22-11-16	Mon 16-1-17									
74			Certification	256 days	Thu 2-2-17	Thu 25-1-18									
80			Production	505 days	Thu 25-1-18	Wed 1-1-20									

Figure 21.7: Production Preparation Phase Gantt Chart

Certification: 10 months
When the aircraft has successfully passed all the tests, certification is needed. To check if the aircraft complies with the rules for emission and noise various test will be performed. If the aircraft also passes these tests successfully the certification is obtained and the production process can be started. The certification process is very important because it shows that the aircraft performs according to the FAR25 regulations that it is designed for. Figure 21.8 shows the Gantt chart for the certification phase.

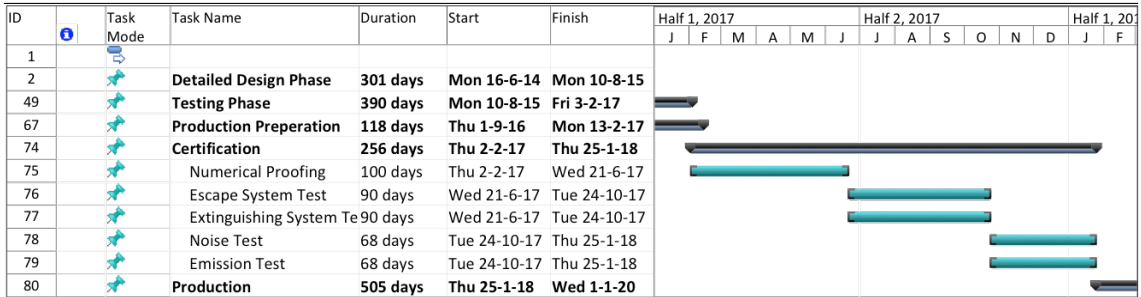| ID		Task Mode	Task Name	Duration	Start	Finish
1						
2			**Detailed Design Phase**	301 days	Mon 16-6-14	Mon 10-8-15
49			**Testing Phase**	390 days	Mon 10-8-15	Fri 3-2-17
67			**Production Preperation**	118 days	Thu 1-9-16	Mon 13-2-17
74			**Certification**	256 days	Thu 2-2-17	Thu 25-1-18
75			Numerical Proofing	100 days	Thu 2-2-17	Wed 21-6-17
76			Escape System Test	90 days	Wed 21-6-17	Tue 24-10-17
77			Extinguishing System Te	90 days	Wed 21-6-17	Tue 24-10-17
78			Noise Test	68 days	Tue 24-10-17	Thu 25-1-18
79			Emission Test	68 days	Tue 24-10-17	Thu 25-1-18
80			**Production**	505 days	Thu 25-1-18	Wed 1-1-20

Figure 21.8: Certification Phase Gantt Chart

Production: 24 months

After all the components off the aircraft comply with the FAR 25 requirements, the mission requirements and all the tests, the aircraft can be produced. The production of the entire aircraft will take up to 24 months. Figure 21.9 shows the Gantt chart for the production phase of the first aircraft. The whole production phase will take 16 years in total for a production rate of 36 units per year. Due to uncertainties of the sales it could be possible that the production stops after the first aircraft is manufactured. Therefore the minimum length of the production phase is 24 months.

ID		Task Mode	Task Name	Duration	Start	Finish
1						
2			**Detailed Design Phase**	301 days	Mon 16-6-14	Mon 10-8-15
49			**Testing Phase**	390 days	Mon 10-8-15	Fri 3-2-17
67			**Production Preperation**	118 days	Thu 1-9-16	Mon 13-2-17
74			**Certification**	256 days	Thu 2-2-17	Thu 25-1-18
80			**Production**	505 days	Thu 25-1-18	Wed 1-1-20
81			Production	505 days	Thu 25-1-18	Wed 1-1-20

Figure 21.9: Production Phase Gantt Chart

22 Manufacturing, Assembly & Integration Plan

A Manufacturing, Assembly and Integration Plan for the Phoenix 5600 business jet will be presented in this chapter. It elaborates on the activities required to construct the final product. Section 22.1 discusses the required assembly facilities and their locations. Section 22.2 presents the assembly line, where a schematic representation is shown and explained. Section 22.3 gives a conceptual floor plan of the assembly facility. In Figure 22.1 the overall, global assembly of the Phoenix 5600 is shown.
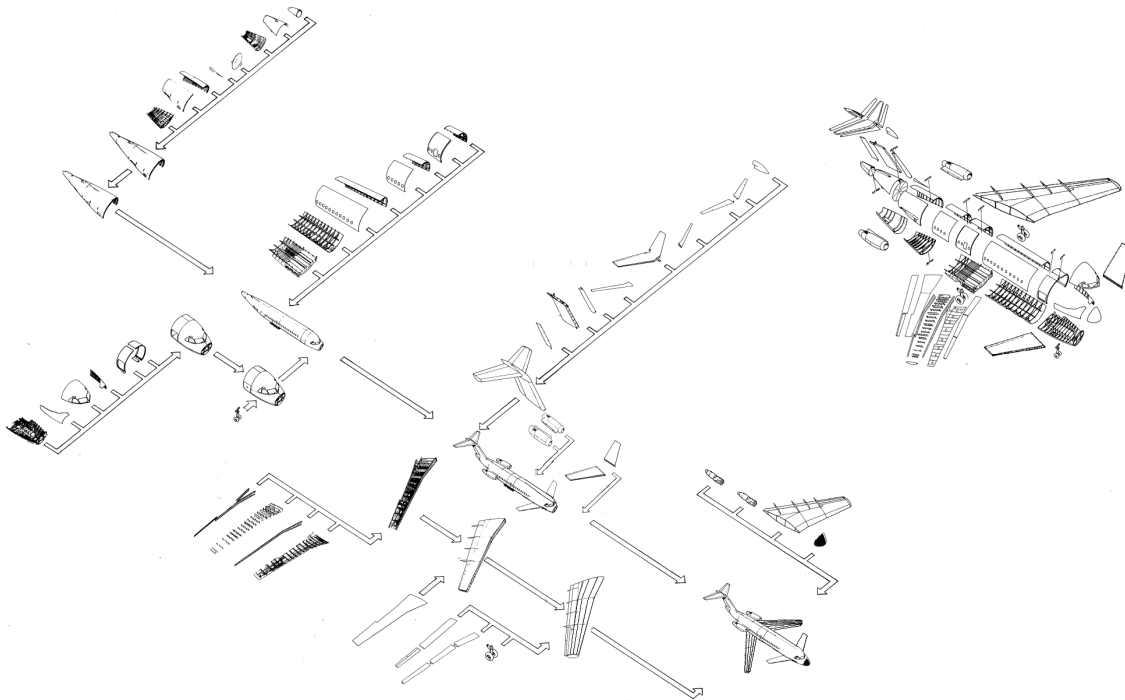

Figure 22.1: Manufacturing Sequence of the Phoenix 5600

22.1 Facilities

Many facilities will be required for the manufacturing process of an aircraft. A new assembly facility will be constructed for the final assembly of the aircraft. The location for the assembly facility will be in Rotterdam for several reasons. Firstly the Research & Development department is located in Delft which is close to Rotterdam. Having the manufacturing and R&D close to each other result in better communication between design and manufacturing. Problems encountered during manufacturing can be solved more efficient when engineers and craftsmen are located close. Secondly Rotterdam is easily accessible by water or by making use of Rotterdam airport which has a 2.2 km runway length. Thirdly many component or material manufacturers have facilities in Europe as can be seen in Figure 22.2 and Table 23. Figure 22.2 shows a map with the main components manufacturers.

All of the aluminum required for the structures will be imported from ALcao which has a facility in Hannover, Germany. Having the part manufacturing workshops located in Hannover will reduce the amount of scrap material transported to Rotterdam. The scrap material from part manufacturing can be directly transported back to the distributor of the raw material for re-use. The part manufacturing workshops will be in Germany thus also the extrusions, rolling, bending and forming facilities will be located in Germany.
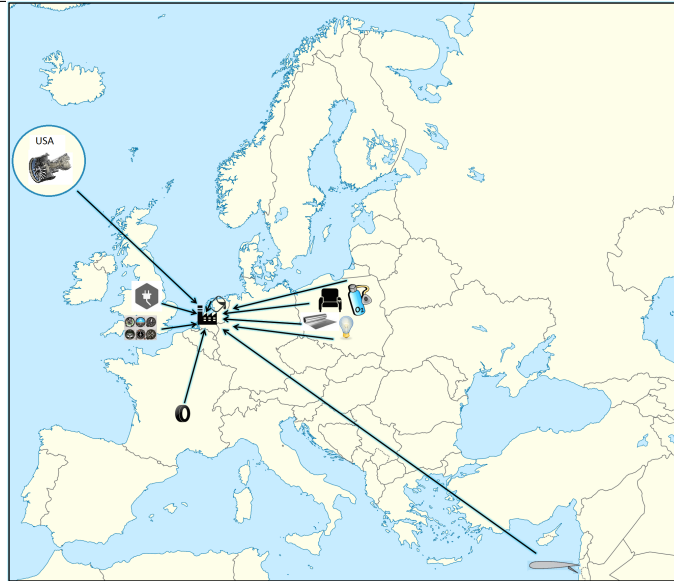
Figure 22.2: Map of Components Manufacturers

Table 22.1: Components Manufacturers Location

Component	Company	Location in Europe	Headquarter Location
Engines	Pratt & Whitney	None	East Hartford, USA
Structures	Alcao	Hannover, Germany	Pittsburgh
Tires	Michekub	Clermont Ferrand, France	Clermont Ferrand, France
Avionics	Garmin	Southampton, UK	Kansas, USA
Electronics	Ultra Electronics	Greenford, UK	Greenford, UK
HLD	Ashot Ashkelon Industries	None	Ashkelon, Israel
Interior/Oxygen/Lighting	B/E Aerospace	Lubeck, Germany	Miami, USA
Painting	Socomore	Lelystad, The Netherlands	Blagnac, France

22.2   Assembly

The aircraft will be manufactured in subassemblies which will be attached into a final assembly. This section elaborates on the subassembly description. Every subassembly will clearly be explained, also the manufacturing methods required for the process will be discussed. The assembly of the fuselage structure, wing and empennage are parallel processes. Having these subassemblies assembled parallel minimizes the time spent waiting for unfinished subassemblies and therefore maximizes the efficiency.

22.2.1   Fuselage Structure

The fuselage will be manufactured in three parts; the nose component, the main component and the tail component. Stringers, spars, ribs skin and other parts will be manufactured in workshops located near the Alcao factory. The finished parts will be transported to Rotterdam for subassembly. In Rotterdam the parts will be assembled into the three parts (nose, cabin and tail cone), the assembly processes of these parts will be parallel in time. When the three subassemblies have been finished the complete fuselage structure will be assembled. Figure 22.3 gives a schematic representation of the assembly of the fuselage structure.
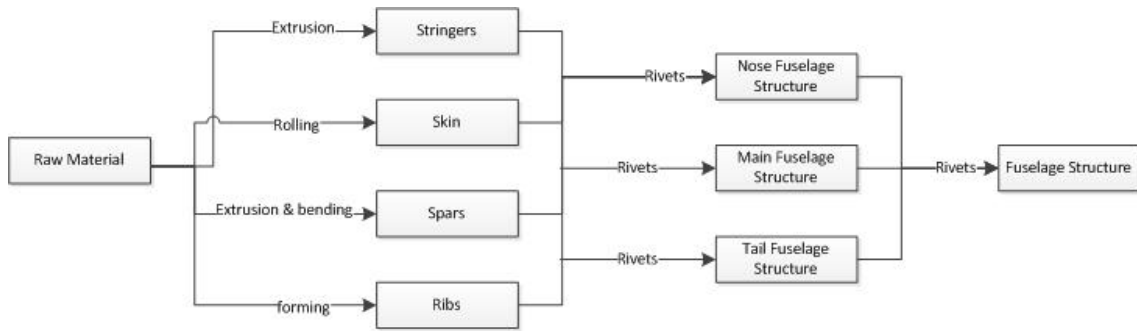
Figure 22.3: Schematic Representation of Fuselage Structure Assembly

22.2.2   Wing

The assembly of the wing is schematically visualised by Figure 22.4. The wing structure will be assembled from the parts manufactured in workshops. The wiring harness and other electrical systems will be installed on the wing structure. The fuel system will also be installed parallel to the electrical system installation. At last the control surfaces are installed.
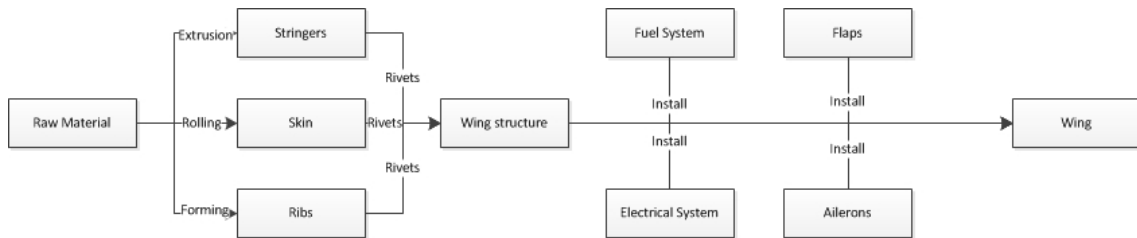

Figure 22.4: Schematic Representation of the Wing Assembly

22.2.3   Empennage

The empennage consist of the horizontal stabilizer, vertical stabilizer and canard, the assembly of these subassemblies is shown in Figure 22.5. The parts required will be manufactured from raw material in workshops. From the parts the structure for the empennage will be assembled. The wiring, electrical system and actuators for the control surfaces are installed on the structure. At last the control surfaces are installed.
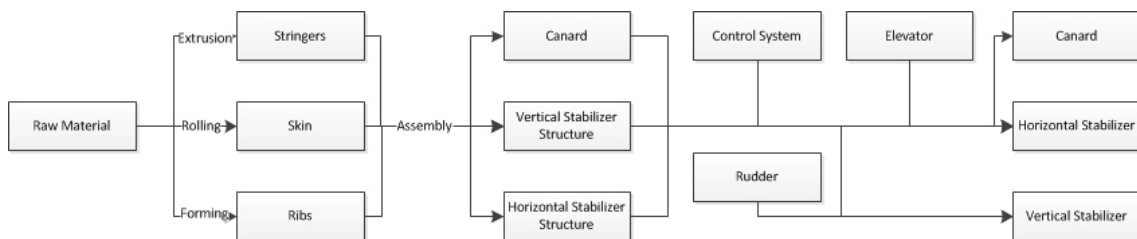

Figure 22.5: Schematic Representation of Empennage Assembly

22.2.4 Final Assembly

The final assembly line is where the subassemblies are connected to manufacture a complete aircraft. The final assembly starts with installing the electronics. When the wiring harness is installed, the interior can be done. The wing subassembly will be attached to the fuselage to create a wing body subassembly. The empennage subassemblies finished in the empennage assembly will be installed on the wing body subassembly. After the empennage has been installed, the pylon, nacelle and landing gear will be installed. When all main structural parts are installed the cabin is customized toward the customer's preference. The whole aircraft will be moved to the paint shop where the aircraft is painted. After paint has been applied the avionics and engines are installed.
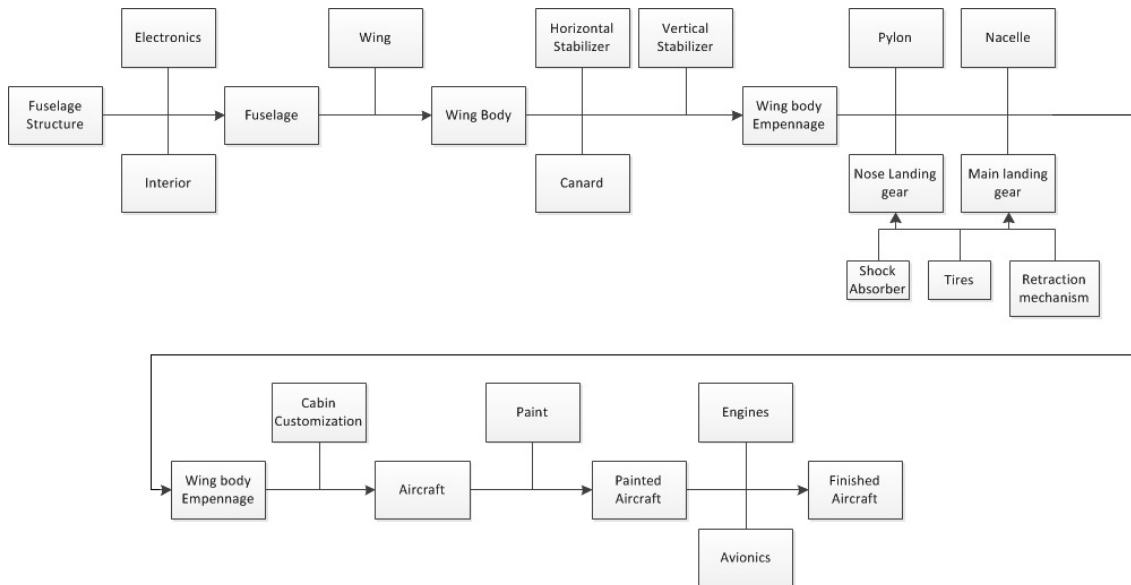

Figure 22.6: Schematic Representation of Final Assembly

22.3 Facility Lay Out

For the assembly facility a floor plan has been made, the floor plan is shown in Figure 22.7. The floor plan has been optimized for line production. The two entrances at the top side of the floor plan are meant for unloading of materials and parts for the assembly. The material can be stored in the space on the top side of the facility. The assembly facility has workstations for every subassembly. Moving further from the top side to the bottom side of the facility shows more detailed and finished subassemblies. The bottom side is the final assembly line, here the subassemblies are connected and installed to manufacture a final aircraft. The exit at right is the exit for the final assembly. The aircraft exiting the assembly facility will move to the paint shop. After applying paint the engines and avionics are installed, the installation of these two parts will be done as late as possible in the assembly process. The engines and avionics are very costly, having them installed as late as possible avoids high interest costs. The final assembly facility is planned to be finished in 2018 so full production can start. In order to enter the market with the Phoenix 5600 full production must start in 2018.
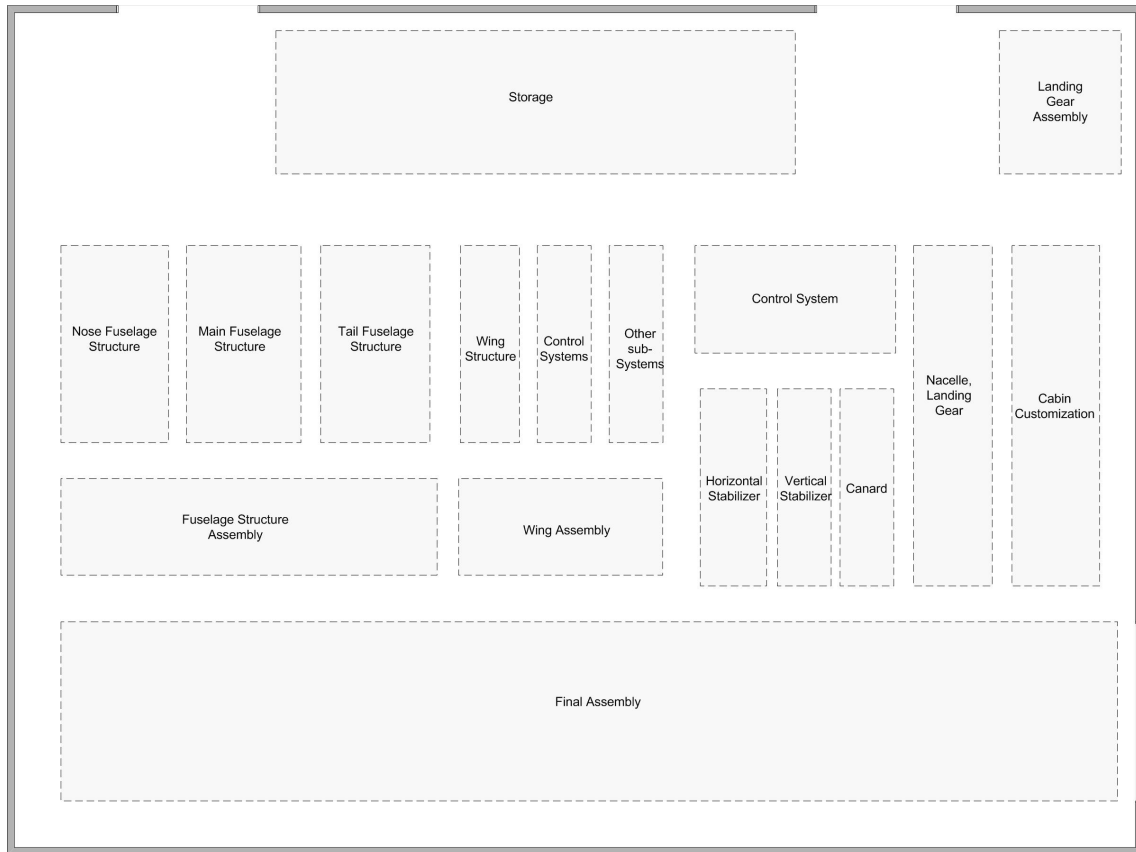
Figure 22.7: Assembly Facility Floor Plan

23 Conclusion

Design Approach Conclusions

Mainly aluminum alloys are used in the aircraft because of their good recyclability. SOCOMORE's eco-friendly paint will be used on the aircraft. Manufacturing will be influenced by the lean manufacturing philosophy. Noise and emissions will adhere to the appropriate ICAO guidelines. The order from most-preferred to least-preferred methods of end-of-life processing is: avoid, reduce, reuse, re-manufacture, recycle, incinerate and landfill.

No availability analysis is performed due to lack of data. Maintenance exists of the pre-flight check and the A through D checks (each is more time consuming and more in-depth). No problems are expected for supportability.

Design Synthesis Conclusions

Table 23.1: Performance Characteristics

Parameter	Value	Unit
Performance Constraint Analysis		
T/W	0.42	-
W/S	2670	N/m^2
S	33.3	m^2
T_{TO}	37	kN
$C_{L_{max,clean}}$	1.47	-
$C_{L_{max,TO}}$	1.98	-
$C_{L_{max,LDG}}$	2.36	-
Loading Diagrams		
$C_{D_{atC_{L_{max}}}}$	0.0774	-
V_{S_1}	62.0	m/s
V_B	95.5	m/s
V_C	125.6	m/s
V_D	157.0	m/s
$n_{lim_{pos}}$	2.92	-
Payload-Range Diagram		
$R_{fullpax}$	5600	km
R_{nompax}	6800	km
R_{ferry}	8000	km
Engine Specifications		
Bypass ratio	3.8	-
Engine weight	374	kg
Take-off thrust	18.32	kN
SFC	12.35	mg/Ns
Length	1727	mm
Diameter	813	mm
Hot section inspection	2500	hrs
Engine overhaul	5000	hrs
Performance Analysis		
Take-off distance	819	m
Range (constant altitude)	5686	km
Range (constant speed)	5044	km
Endurance	40.4	min
Glide range	159	km
Glide time	14.6	min
Landing distance	746	m

Table 23.2: Performance Characteristics for Different Altitudes

Performance Characteristic	Altitude				Unit
	4000 m	8000 m	12800 m (cruise)	15000 m (ceiling)	
Stall speed	66	83	115	137	m/s
Rate of climb	5186	2759	685	22	ft/min
Climb gradient	0.2	0.11	0.03	0	-
Rate of descent	23	29	40	48	ft/min

The aircraft will use Pratt & Whitney PW545C engines. The engine is a two-shaft turbofan with full-length duct, a single stage fan, a two stage compressor, an electric starter and hydro-mechanical fuel control.

Table 23.3: Drag Polar Analysis Results

Aircraft component	C_{D_0}	C_{D_L}
Wing	0.00834	0.01794
Fuselage	0.00947	0.01520
Horizontal Tail	0.00219	000491
Canard	0.00191	0.00584
Vertical Tail	0.00146	0.00265
Engines	0.00582	0.00366
Trim	-	0.00538
Interference	0.00102	0.00133
Miscellaneous	0.00030	0.00067
Total	0.03048	
Take-off		
Flaps	0.012	-
Landing Gear	0.02	-
Landing		
Flaps	0.06	-
Landing Gear	0.025	-

Table 23.4: Wing Lift Curve Parameters

Parameter	Value	Unit
$C_{L_{max}}$	1.07	-
α_{CL_0}	-1.4	°
α_{stall}	14.0	°

The general fuselage structure configuration is semi-monocoque. Fuselage structure features include the skin, frames, longerons, pressure bulkheads and floor frames. Skin cutouts are made for the passenger door, the baggage door, the emergency exit, the wing box and the windows (cockpit and cabin). Frames are positioned to maximize structural synergy. The empennage structure will contain spars, ribs and stringers. The fuselage structural design is performed in CATIA. No fuselage structural analysis is performed. The fuselage will be constructed from aluminum 7075-T6.

The primary load carrying structure in the wing is the wing box. Fuel is stored in the wing in integral fuel tanks. The wing box runs through the fuselage, under the floor. The wing box is designed using CATIA and its structural analysis workbench. The wing box will use Aluminum 7150. The wing box will contains spars, ribs and stiffeners. The skin will also carry part of the loads. Further iterations are required as the wing will suffer from unstable aeroelasticity characteristics in its current design. The landing gear struts material will be Aluminum 6061-T6.

Table 23.5: Structural Design Results

Parameter	Value	Unit
Fuselage		
Emp. front spar	0.15 - 0.25	$fr.c$
Emp. aft spar	0.65 - 0.70	$fr.c$
Emp. rib spacing	24	in
Skin thickness	0.8	mm
Frame shape	C	-
Frame depth	20	mm
Frame thickness	0.5	mm
Frame spacing	0.63	m
Longeron shape	Z	-
Longeron h dim.	18	mm
Longeron b dim.	17	mm
Longeron t	0.2	mm
Total nr. of long.	12	-
Wing		
Front spar t	40.8	mm
Aft spar t	8.0	mm
Top skin t	2.0	mm
Bottom skin t	2.0	mm
Wing box W	810	kg
Landing Gear		
l_m	1.17	m
l_n	8.93	m
n_s	2	-
n_t	2	-
V_{S_L}	43.2	m/s
$V_{S_{TO}}$	25.6	m/s
P_n	10.3	kN
P_m	39.3	kN
$P_{n_{dyn_t}}$	5.33	kN
P_{n_t}	6.86	kN
$P_{m_{dyn_t}}$	26.3	kN
$V_{tire/max}$	116.0	m/s
D_n	13.75	in
b_n	6.1	in
D_m	20.85	in
b_m	7.3	in
$s_{s_{nose}}$	0.540	m
$s_{s_{design_{nose}}}$	0.565	m
$s_{t_{nose}}$	1.40	cm
$d_{s_{nose}}$	5.48	cm
$s_{s_{main}}$	0.415	m
$s_{s_{design_{main}}}$	0.440	m
$s_{t_{main}}$	1.90	cm
$d_{s_{main}}$	9.54	cm

Table 23.6: Weight Estimation Results

(sub) Part	Symbol	Class II est. $[kg]$
Wing	W_w	1021.60
Horizontal tail	W_h	68.22
Vertical tail	W_v	142.65
Canard	W_c	44.38
Fuselage	W_f	714.14
Nacelles	W_n	250.38
Nose gear	W_{ng}	48.72
Main gear	W_{mg}	248.28
Structure	W_{struc}	**2538.37**
Engine	W_{eng}	748
Fuel system	W_{fs}	88.90
Propulsion system	W_{prop}	42.20
Powerplant	W_p	**879.10**
Flight controls	W_{fc}	236.21
Hydr./pneu.	W_{hps}	79.09
Instr./avi.	W_{iae}	225.69
Electrical system	W_{els}	310.15
Airco/anti-/de-icing	W_{api}	247.71
APU	W_{apu}	66.60
Oxygen system	W_{ox}	16.98
Furnishings	W_{fur}	462.42
Auxiliary gear	W_{aux}	47.27
Paint	W_{paint}	37.46
Fixed equipment	W_{FEQ}	**1729.58**
Empty weight	W_E	**5147.05**

Table 23.7: Balance Analysis and Stability & Control Analysis Output

Variable	Value	Unit
Wing area	33.3	m^2
Forward C.G.	15.03	m
Aft C.G.	16.73	m
C.G. travel	1.70	m
C.G. travel	0.79	$fr.\bar{c}$
Vert. tail area	8.6	m^2
Hor. tail area	8.8	m^2

Table 23.8: Eigenmotions

Eigenmotion	Period P [s]	Half time $T_{1/2}$ [s]	Undamped nat. freq. ω_o [rad/s]	Damping ratio ζ [-]
Short period	2.90	0.36	2.91	0.67
Phugoid	96.4	75.7	0.066	0.14
Aperiodic roll		0.28		
Spiral		160		
Dutch roll	2.74	1.39	2.35	0.21

All eigenmotions are stable. A yaw damper is needed and installed.

The landing gear system will feature an anti-lock braking system (ABS). The flight control system (FCS) will be irreversible, fly-by-wire with electromechanical actuators. The FCS will be installed three times for redundancy. The hydraulical system will be powered by the two engines, back-up will be provided by a hydraulic pressure reservoir, the auxiliary power unit (APU) and/or the ram air turbine (RAT). The APU and RAT will also provide back-up for the electrical system. The APU will also be used for starting the engines and for providing air pressure for the pneumatic system. Batteries are installed for operations when the APU is not running.

The cabin pressurization system will feature positive and negative pressure relief valves and a depressurization system. The primary source for the pneumatic system is engine compressor bleed air. The air-conditioning system will keep the temperature in the cabin between 15 ° and 25°, the humidity of the cabin will be kept between 10% and 20%. The air-conditioning system will refresh 20 cubic feet of air per minute. The cockpit will feature a Garmin G3000 avionics system. An electro impulse de-icing system will be used for de-icing the wings. Critical devices like pitot tubes, stall vanes, TAT probes, drain masts and the engine inlets will have electrically heated anti-icing systems installed. The cockpit will feature wind-shield wipers with rain repellent. The wind screen will be kept at 30°C to prevent fogging.

Fire extinguishing systems are installed in the engines, APU, baggage area and passenger cabin. The minimum brightness of the emergency lights will be 400 microlamberts. The aircraft has one Type IV overwing emergency exit. Passenger emergency oxygen is supplied from a chemical source, coming from masks above the seats. The aircraft will be equipped with life jackets and emergency slides. The emergency slides can also be used as lift rafts.

The water management system will be able to store 11.4 L of water. Water can be heated using bleed air and a heat exchanger. The waste management system will use the in-flight pressure differential to flush the lavatory, waste will be collected in a collector tank with chemicals. Food and drinks can be heated using a convection oven. Onboard Wi-Fi and GSM networks will be set up. The VisiStream entertainment system will be installed with a 46 in screen in the front of the cabin. Each chair will have its own touch screen. Power outlets will be available.

The engines will be started using electrical starting motors. Thrust reversers are installed. The baggage compartment is accessible via an outside baggage door. Cockpit lights can be dimmed, except emergency (red) and warning (amber) lights. The cabin lightning system will be the Daylight Variable White Lightening System.

Table 23.9: Sensitivity Analysis Results

Parameter	Value	Unit
Payload sensitivity	5.7	kg
Empty weight sensitivity	0.20	-
Range sensitivity	1.9	kg/km
Endurance sensitivity	2300	kg/hrs
L/D sensitivity	-1600	-
Specific fuel sensitivity	190,000	$1/kg/hr$
Speed sensitivity	-51	$kg/m/s$

The L/D, specific fuel consumption and cruise speed sensitivities are the most critical. The forward swept wing and canard are two items which make the design unconventional, they introduce some difficulties in the design. The most critical are the aeroelastic effects caused by the forward sweep of the wing.

Final Concept Conclusions
The final configuration of the Phoenix 5600 is a forward swept wing three surface with aft fuselage mounted engines and a T-tail. The aircraft has elevators, a rudder, ailerons and Fowler flaps. The main landing gear is attached to the aft spar of the wing. The nose gear strut and canard front spar is attached to one fuselage frame. The engines are attached to the aft pressure bulkhead.

The elements introducing the biggest risks are the coating for fuel compartments, the fuel pumps through ribs, the engine ignition system, the light weight turbine blades, the fuel system with fuel pumps, the hydraulic landing gear arm and the aluminum strut.

Table 23.10: Return on Investment Results

Parameter	Value	Unit
Return on investment aim	24.34%	-
Aircraft list price	15.9	M$
Break even point (units sold)	200	-
Return on investment reached (units sold)	580	-
Return on investment reached	16	years
Yearly production rate	36	1/year
Direct operating cost	2400	$/hr
Market share after return on investment reached	2.12%	-
Total program cost	5.16	B$
Total program income	6.46	B$

All top level requirements are reached. The range and the direct operating costs exceed the corresponding top level requirements.

Recommendations for Future Design Conclusions
During the DSE design phase the market investigation, Class I design phase and Class II design phase are performed. The post-DSE phase consists of the detailed design phase, testing phase, production preparation, certification and production. The aircraft will be assembled in Rotterdam, The Netherlands. Production will start in 2018.

Table 23.11: Components Manufacturers Location

Component	Company	Location in Europe	Headquarter Location
Engines	Pratt & Whitney	None	East Hartford, USA
Structures	Alcao	Hannover, Germany	Pittsburgh
Tires	Michekub	Clermont Ferrand, France	Clermont Ferrand, France
Avionics	Garmin	Southampton, UK	Kansas, USA
Electronics	Ultra Electronics	Greenford, UK	Greenford, UK
HLD	Ashot Ashkelon Industries	None	Ashkelon, Israel
Interior/Oxygen/Lighting	B/E Aerospace	Lubeck, Germany	Miami, USA
Painting	Socomore	Lelystad, The Netherlands	Blagnac, France

24 Recommendations

During the design process, several times design steps could not be performed in an optimal way. Sometimes data had to be 'guestimated' because of lack of data, other times lack of resources or time caused inaccuracies. In this chapter recommendations are provided to improve the design of the premium business jet, the Phoenix 5600. The following measures are recommended:

1. Performance Analysis
For the performance analysis, it is recommended to get more data on the engine performance. Especially data on the engine performance for different speeds and at different altitudes will be helpful. It will be difficult to get to this data, because engine manufactures will not give this sensitive data away. With this data the missing performance characteristics can be calculated and other calculations become more precise. Furthermore, the nacelle can be designed in more detail with this data available. Another element where the design progress is stuck due to lack of data is the nacelle-fuselage connection. The manufacturer determines the mounting points of the engine. But it is not clear where these points are exactly located. Therefore it is hard to calculate the required strength of this system to support the engine during operation. Just like the engine performance characteristics, it will be unlikely the engine manufacturer will supply this information.

2. Wing Lift Distribution
For the wing lift distribution, it is recommended to spend more time on making the wing lift distribution more accurate since at the moment the outcome is still very unlikely. Maybe the use a different program than Tornado might help in verifying the results.

3. Fuselage Structure
For the fuselage structural design, it is recommended that the frame cross sectional shapes are designed in more detail, including detailed stress analysis. The attachments of the fuselage to all external structure components (except the wing box) should also be designed in more detail. It is also recommended that a more in depth mesh convergence study is performed and that an even finer mesh (in the order of max. several times the skin thickness) is used for structural analysis.

4. Main Wing Design
For the main wing design, it is recommended to increase the complexity of the structural analysis. Further research can be done into torsional divergence by applying the described method to all positions on the wing instead of at the resultant lift force. For a metal wing box, using different thicknesses along the span or adjusting the rib, spar and stiffener configurations can still optimize the geometry. Other solutions include making the leading edge of the wing load carrying or shifting the wing box structure forward. Also the unsymmetrical properties of the cross section of the wing box can be examined in more detail, since this strongly affected the divergence velocity. Other detailed components such as control surface support and fuel system should be sized in detail so their effect on the structural behavior of the wing box can be analyzed. The use of composite materials is still an potential solution as its properties are unique and very suitable for countering torsional divergence. Therefore, it is strongly recommended to explore the composite coupling effect on the divergence matrix. Since only the static load cases for the wing box have been explored, it is essential to continue the analysis and investigate dynamic load cases such as dynamic impact of landing gear during landing as well as the effects of turbulent flows on wing structure. Finally, the manufacturing aspects should be analyzed in more detail. The attachment points and methods would be further elaborated. In particular, given the current geometry and material choice, rivets would be chosen. In case the composite material is chosen, a more extensive attachment method would be examined.

5. Landing Gear
For the landing gear it is recommended that a more detailed design is performed. The design of the shock absorber and actuator is currently only limited to the dimensional sizing. The exact system used for the shock absorber and actuator is planned to be designed in later stages of the design process. The weight of tires and other subsystems should be obtained by contacting the manufacturers in order to accurately estimate the landing gear weight. The braking system is not included in the Class II design, it is recommended to size the braking system as soon as possible as it is one of the important components of the landing gear.

6. Weight & Balance

For the weight and balance, it is recommended that equations are derived to estimate the weight of the canard to obtain a more accurate result. In addition more reference data can be consulted the equations can be calibrated more precisely.

7. System Characteristics

For the system design, it is recommended that the electrical system is designed into more detail. When extensive research is done on all the items that use electrical power and all these items, including the flight control system are designed in detail an electrical load profile can be designed. When this electrical load profile is known, the electrical summary can be determined. In addition the detailed designs can be drawn for the flight control system, hydraulic system, environmental system, cockpit system, de/anti-icing system, emergency system, water, waste & catering system, entertainment & connectivity system and finally the propulsion system. The wiring can be determined and drawn into CATIA.

8. Return on Investment

For the return on investment, it is recommended to perform a more detailed and elaborate market analysis in order to very accurately estimate the number of aircraft to be sold. Misjudging the number of aircraft to be sold could lead to the end of the Phoenix 5600 Company. In addition currently the Roskam method has been used for the cost estimation due to lacking data of the exact prices. Most manufacturers do not make their product prices public making it difficult to estimate the cost of components like the engines and avionics. The airframe can be estimated using the detailed CATIA drawings at later stages, right now the details of the CATIA drawings is too low for accurate estimations.

Bibliography

[1] W. Brugmans and J. e. a. Bussemaker, *Mid Term Review Design Synthesis Exercise: Premium Light Business Jet*. Delft University of Technology, 2014.

[2] W. Brugmans and J. e. a. Bussemaker, *Project Plan Design Synthesis Exercise: Premium Light Business Jet*. Delft University of Technology, 2014.

[3] W. Verhagen, *Project Guide Design Synthesis Exercise*. Delft University of Technology, 2014.

[4] W. Brugmans and J. e. a. Bussemaker, *DSE - Premium Business Jet Baseline Review*. Delft University of Technology, 2014.

[5] J. Dr. Roskam, *Airplane Design - Part VIII: Airplane Cost Estimation: Design, Development, Manufacturing and Operating*. DARcorporaion, 2006.

[6] A. K. Kundu, *Aircraft Design*. Cambridge, 2010.

[7] D. M. G. Ryschkewitsch, *Goddard Space Flight Center, Green book*. NASA, 1991.

[8] J. Dr. Roskam, *Airplane Design - Part I: Preliminary Sizing of Airplanes*. DARcorporaion, 2005.

[9] J. Dr. Roskam, *Airplane Design - Part V: Component Weight Estimation*. DARcorporaion, 2003.

[10] Honeywell, "Nbaa 2013 market update." `http://phx.corporate-ir.net/External.File?item=UGFyZW50SUQ9NTIzMjIwfENoaWxkSUQ9MjA4NTk0fFR5cGU9MQ==\&t=1`. [Published; October 2013].

[11] W. Dong, *A Chain-Type Price Index for New Business Jet Aircraft*. Business Economics 41, no. 1, 7th ed., 2006.

[12] U. S. I. T. Commission, "Business jet aircraft industry: Structure and factors affecting competitiveness." `http://www.usitc.gov/publications/332/pub4314.pdf`. [Published; April 2012].

[13] Aerolux, "Al-gh3001-1 oven / hot cup." `http://booksite.elsevier.com/9780340741528/appendices/default.htm`. [Online; 20/05/2014].

[14] T. Allen, "Eu28 population 505.7 million at 1 january 2013." `http://epp.eurostat.ec.europa.eu/cache/ITY_PUBLIC/3-20112013-AP/EN/3-20112013-AP-EN.PDF`. [Online; 12/06/2014].

[15] E. Commission, "Being wise with waste: the eus approach to waste management." `http://ec.europa.eu/environment/waste/pdf/WASTE\%20BROCHURE.pdf`. [Online; 12/06/2014].

[16] P. S. Pimenta, S., *Recycling carbon bre reinforced polymers for structural applications: Technology review and market outlook*. Elsevier, 2012.

[17] T. U. of Nottingham, "Routes to recycling or disposal of thermoset composites." `http://www.swcompositesgateway.co.uk/presentation/LCA\%20Worksho-Dr_Pickering_Sept_2013.pdf`. [Online; 30/06/2014].

[18] E. N. e. a. Roux, M., "High performance thermoplastic composite processing and recycling: From cradle to cradle." `http://www.selfrag.com/pdf/publications/Article-SEICO13-High-PerformanceThermoplastic-composite.pdf`. [Online; 30/06/2014].

[19] T. U. of Texas Arlington, "What is sustainability." `www.uta.edu/ce/ese/Modules/ME\%201105/ME\%20Sustainability.pptx`. [Online; 30/06/2014].

[20] Airbus, "Being wise with waste: the eus approach to waste management." `http://www.airbus.com/innovation/eco-efficiency/aircraft-end-of-life/pamela/`. [Online; 13/06/2014].

[21] SOCOMORE, "Toxic chromates now replaced in new aircraft exterior systems." `http://www.socomore.com/toxic-chromates-now-replaced-in-new-aircraft-exterior-systems/a54.html`. [Online; 19/06/2014].

[22] SOCOMORE, "Socosurf a1855." `http://www.socomore.com/socosurf-a1855/pr282.html`. [Online; 19/06/2014].

[23] ICAO, *Environmental Protection Volume I:Procedures for the Noise Certification of Aircraft*. International Civil Aviation Organization, 2008.

[24] ICAO, *Environmental Protection Volume I:Aircraft Engine Emissions*. International Civil Aviation Organization, 2008.

[25] L. S. Lee, S.G. and M. Khoo, *A Multi-Objective Methodology for Evaluating Product End-of-Life Options and Disassembly*. The International Journal of Advanced Manufacturing Technology, 2001.

[26] E. Commission, "Pamela - process for advanced management of end of life of aircraft." `http://ec.europa.eu/environment/life/project/Projects/index.cfm?fuseaction=search.dspPage\&n_proj_id=2859\&docType=pdf`. [Online; 13/06/2014].

[27] E. Commission, "End-of-life aircraft recycling offers high grade materials." `http://ec.europa.eu/environment/ecoap/about-eco-innovation/good-practices/eu/719_en.htm`. [Online; 13/06/2014].

[28] J. Hessburg, "Aviationpros." `http://www.aviationpros.com/article/10388655/whats-this-a-check-c-check-stuff`. [Online; 21/05/2014].

[29] J. Hessburg, "What's this 'a' check, 'c' check stuff?." `http://www.aviationpros.com/article/10388655/whats-this-a-check-c-check-stuff`. [Online; 16/06/2014].

[30] E. Torenbeek, *Advanced Aircraft Design*. John Wiley & Sons, Ltd, 2013.

[31] R. Sigel, "The lost hansa - germany's forgotten answer to the learjet." `http://www.jetgala.com/story_201002_02-Wings-The-Lost-Hansa.html`. [Online; 12/06/2014].

[32] J. Dr. Roskam, *Airplane Design - Part VII: Determination of Stability, Control and Performance Characteristics: FAR and Military Requirements*. DARcorporaion, 2006.

[33] A. Virginia Tech and O. engineering, "Performance." `http://www.dept.aoe.vt.edu/~lutze/AOE3104/thrustmodels.pdf`. [Online; 24/06/2014].

[34] J. Dr. Roskam, *Airplane Design - Part VI: Preliminary Calculation of Aerodynamic, Thrust and Power Characteristics*. DARcorporaion, 2008.

[35] W. H. Mason, ". aerodynamics of 3d lifting surfaces through vortex lattice methods." `http://www.dept.aoe.vt.edu/~mason/Mason_f/CAtxtChap6.pdf`. [Online; 24/06/2014].

[36] T. Melin, "Users guide and reference manual for tornado.." `http://www.redhammer.se/tornado/manual.pdf`. [Online; 24/06/2014].

[37] M. Fujino, "Development of the hondajet." `http://www.icas.org/ICAS_ARCHIVE/ICAS2004/PAPERS/582.PDF`. [Online; 20/06/2014].

[38] J. Dr. Roskam, *Airplane Design - Part III: Layout Design of Cockpit, Fuselage, Wing and Empennage: Cutaways and Inbouard Profiles*. DARcorporaion, 2011.

[39] M. dr. Christos Kassapoglou, "Ae2211-11 structural analysis and design." TU Delft Blackboard, 2013.

[40] I. ASM Aerospace Specification Metals, "Aluminum 7075-t6." `http://asm.matweb.com/search/SpecificMaterial.asp?bassnum=MA7075T6`. [Online; 06/06/2014].

[41] I. ASM Aerospace Specification Metals, "Aluminum 2024-t3." `http://asm.matweb.com/search/SpecificMaterial.asp?bassnum=MA2024T3`. [Online; 06/06/2014].

[42] A. T. Inc., "Am 350." `https://www.atimetals.com/Documents/am_350_tds_en_v2.pdf`. [Online; 06/06/2014].

[43] I. ASM Aerospace Specification Metals, "Titanium ti-6al-4v (grade 5), annealed." `http://asm.matweb.com/search/SpecificMaterial.asp?bassnum=MTP641`. [Online; 06/06/2014].

[44] dr. C.D. Rans, "Ae1202 mechanics of materials & structures." TU Delft Blackboard, 2012.

[45] H. Corporation, "Fibrelam product data." `http://www.hexcel.com/Resources/DataSheets/Panel-Data-Sheets/Fibrelam_global.pdf`. [Online; 11/06/2014].

[46] D. of Education and E. C. Development, "Girls weight-for-age percentiles." `http://www.education.vic.gov.au/Documents/childhood/parents/mch/mchgrowthbmigirl18yrs.pdf`. [Online; 9/06/2014].

[47] A. Burr and J. Cheatham, *Mechanical Analysis and Design*. Prentice Hall, 1995.

[48] A. Inc, "7150-t7751 aluminum plate and 7150-t77511 extrusions." `http://www.alcoa.com/global/en/products/product.asp?prod_id=610`. [Online; 26/06/2013].

[49] ThyssenKrupp, "Summary of alloys typical chemical composition and mechanical properties." `http://www.thyssenkruppaerospace.com/nc/materials/aluminium/aluminium-technical-data.html?print=1`. [Online; 05/06/2013].

[50] M. H. Roy Langton, Chuck Clark and L. Richards, *Aircraft Fuel Systems*. John Wiley & Sons, Ltd, 2009.

[51] L. MatWeb, "Asm aerospace specification metals inc.." `http://asm.matweb.com/search/SpecificMaterial.asp?bassnum=MA6061t6`. [Online; 30/06/2013].

[52] R. de Breuker, *Aeroelasticity. Simplified Aeroelastic Problems*.

[53] J. Dr. Roskam, *Airplane Design - Part IV: Layout of Landing Gear and Systems*. DARcorporaion, 2010.

[54] Michelin, "Aircraft tire engineering data." `http://www.airmichelin.com/uploadedFiles/MichelinAirDev/databook.pdf`. [Online; 2/06/2014].

[55] E. Torenbeek, *Synthesis of Subsonic Airplane Design*. Delft University Press, Kluwer Academic Publishers, 1982.

[56] A. Burr and J. Cheatham, *Mechanical Design and Analysis*. Prentice-Hall, 2nd ed.

[57] A. Spruce, "General aluminum information." `http://www.aircraftspruce.com/catalog/mepages/aluminfo.php`. [Online; 18/06/2014].

[58] A. International, *Aluminum and aluminum alloys*. Materials Park, 2nd ed.

[59] A. Kostrivas and J. Lippold, "Weldability of li-bearing aluminium alloys." `http://www.dunand.northwestern.edu/refs/files/p217.pdf`. [Online; 11/06/2014].

[60] U. S. P. A. Publication, "Aluminum-based alloy publication classification." `patentimages.storage.googleapis.com/pdfs/US20090068056.pdf`. [Online; 11/06/2014].

[61] Mathworks, *MATLAB*. Mathworks, r2013b ed., 2013.

[62] M. Olmstead, "The lockheed jetstar." `http://www.airliners.net/aircraft-data/stats.main?id=269`. [Online; 24/06/2014].

[63] S. T. Chai and W. H. Mason, *Landing Gear Integration in Aircraft Conceptual Design*. Virginia Polytechnic Institute and State University, 1996.

[64] I. M. C. Limited, "Electro-mechanical vs. hydraulic & pneumatic actuators." `http://www.inmoco.co.uk/electro-mechanical_vs_pneumatic_actuators`. [Online; 10/06/2014].

[65] M. Tooley and D. Wyatt., *Aircraft Electrical and Electronic Systems*. Elsevier, 2009.

[66] A. Government, "Black box flight recorders." `http://www.atsb.gov.au/media/4793913/Black\%20Box\%20Flight\%20Recorders\%20Fact\%20Sheet.pdf`. [Online; 21/05/2014].

[67] Daylight, "Variable white lighting system." `http://www.emteq.com/DAYLIGHT_white_lighting.php`. [Online; 5/06/2014].

[68] F. E. R. Commission, "Fault tree analysis, what is it?." `http://www.ferc.gov/industries/hydropower/safety/initiatives/november-workshop/fault-tree-analysis.pdf`. [Online; 3/06/2014].

[69] B. of Labor Statistics, "Occupational employment and wages, may 2013." `http://www.bls.gov/oes/current/oes172011.htm`. [Online; 17/06/2014].

[70] V. V. ABCO Data Systems, "Salary study 2012." `http://www.safetystanddown.com/wp-content/uploads/2012/06/Salary-study-6-12-lyt_June.pdf`. [Online; 16/06/2014].

[71] T. F. R. B. of Minneapolis, "Consumer price index, 1913-." `http://www.minneapolisfed.org/community_education/teacher/calc/hist1913.cfm`. [Online; 16/06/2014].

[72] G. A. M. Association, "2013 general aviation statistical databook & 2014 industry outlook." `http://www.gama.aero/files/GAMA\%202013\%20Databook-Updated-LowRes.pdf`. [Online; 16/06/2014].

[73] B. of Labor Statistics, "Aircraft and avionics equipment mechanics and technicians." `http://www.bls.gov/ooh/installation-maintenance-and-repair/aircraft-and-avionics-equipment-mechanics-and-technicians.htm`. [Online; 17/06/2014].

[74] C. Aviation, "Cutter aviation fbo network fuel prices." `http://www.cutteraviation.com/fbo-services/current-fuel-prices/`. [Online; 16/06/2014].

[75] Bloomberg, "Us generic govt 10 year yield." `http://www.bloomberg.com/quote/USGG10YR:IND`. [Online; 16/06/2014].

[76] D. ir. R. Vos and I. B. Zandbergen, *Introduction and Organization*. Delft University of Technology, 2012.

[77] J. Dr. Roskam, *Airplane Flight Dynamics and Automatic Flight Controls Pt. 1*. DARcorporaion, 2003.

[78] J. M. et al., *Flight Dynamics Lecture Notes*. Delft University of Technology, 2014.
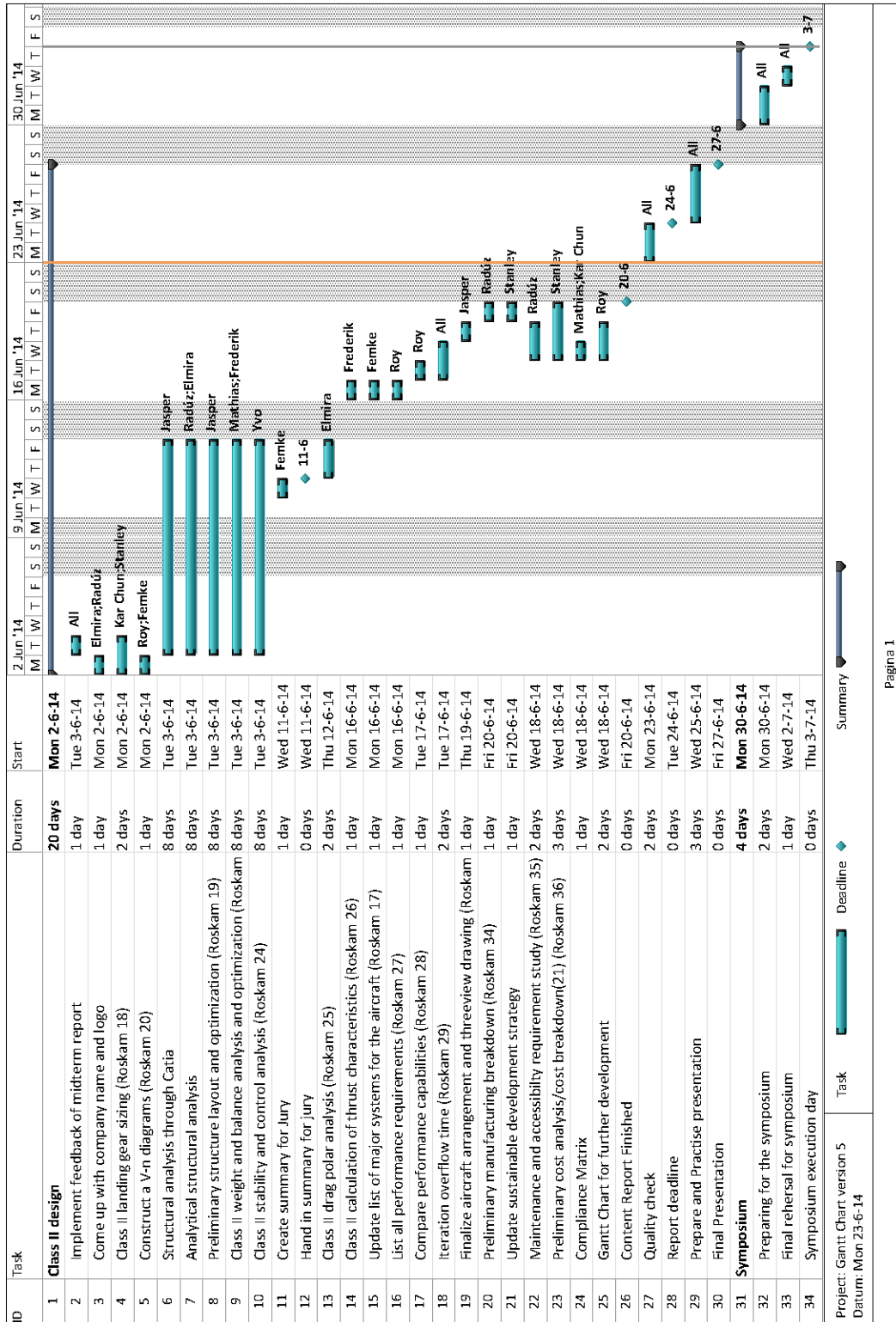
A   Gantt Chart

Figure A.1: The Gantt chart for the final report.
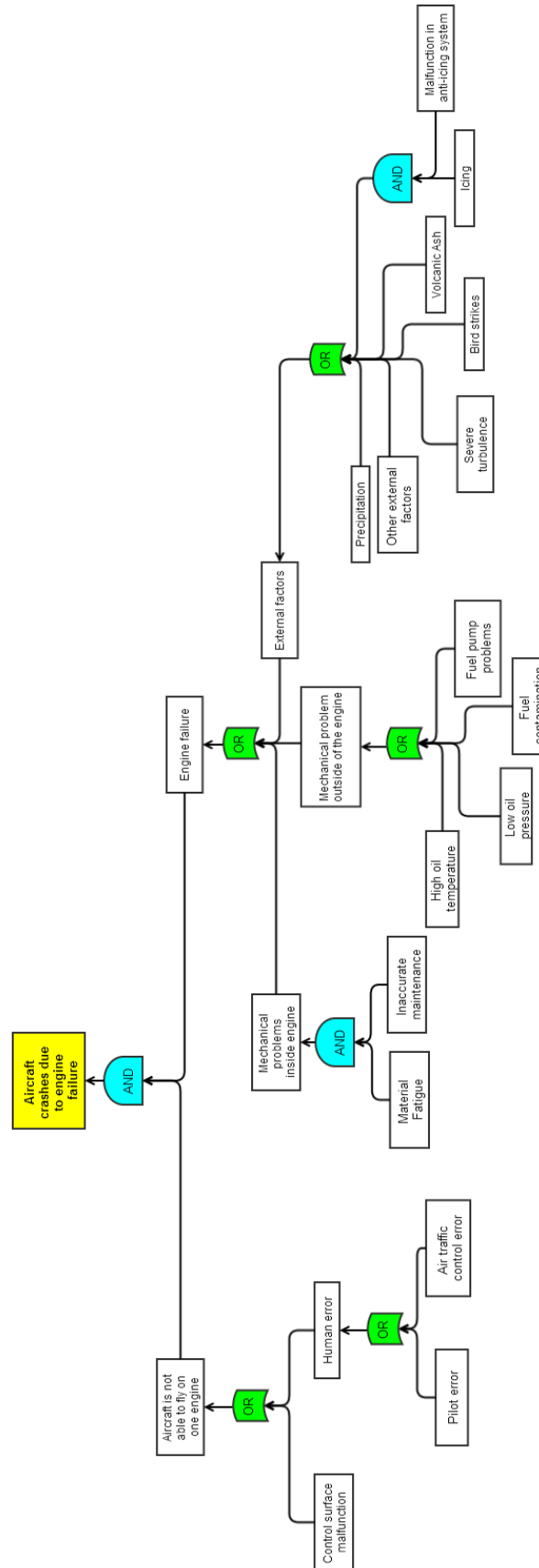
Figure B.1: The fault tree analysis for the engine failure event

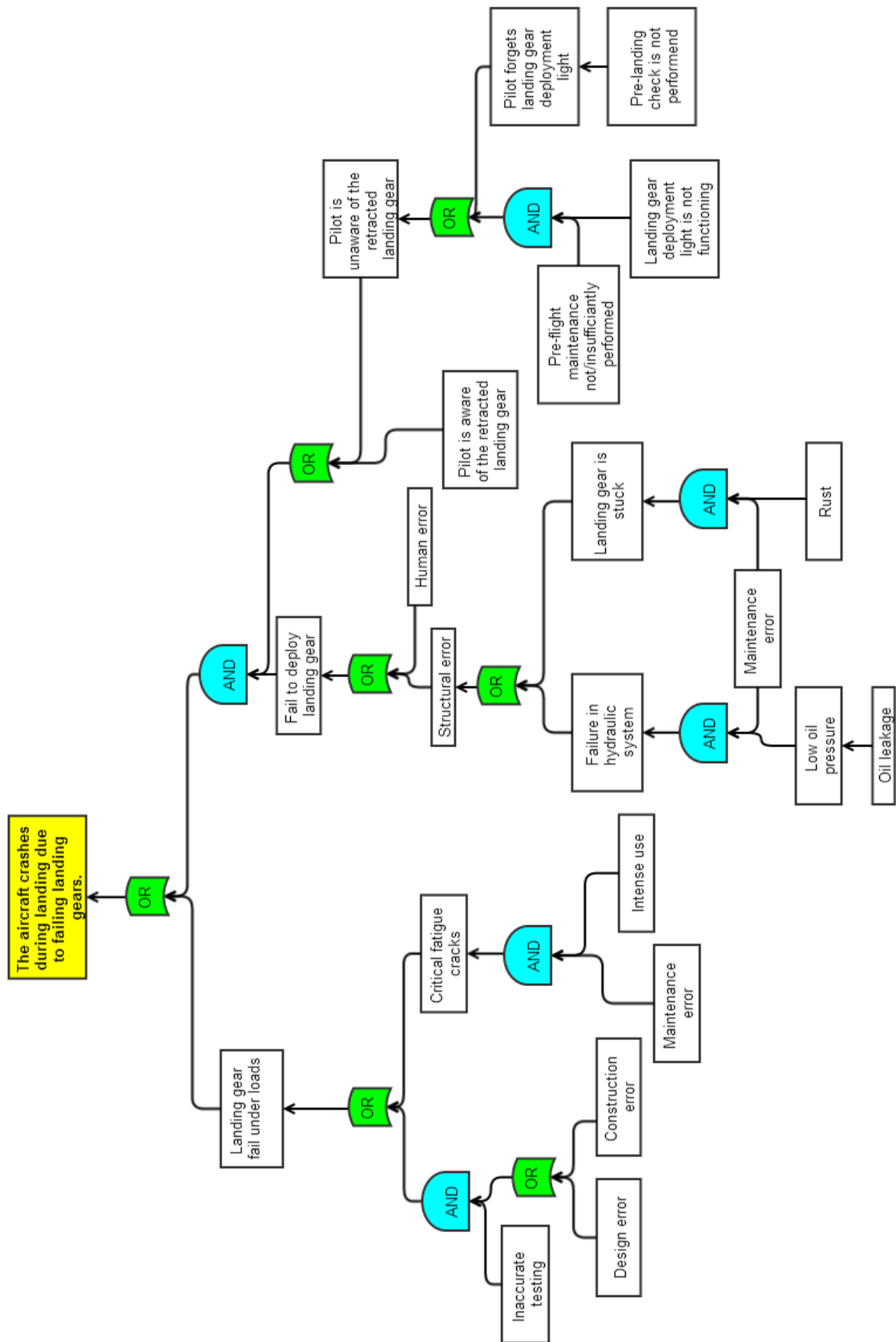Figure B.2: The fault tree analysis for the landing gear failure event

Figure C.1: Functional Flow Block Diagram (FFBD) of Business Jet System
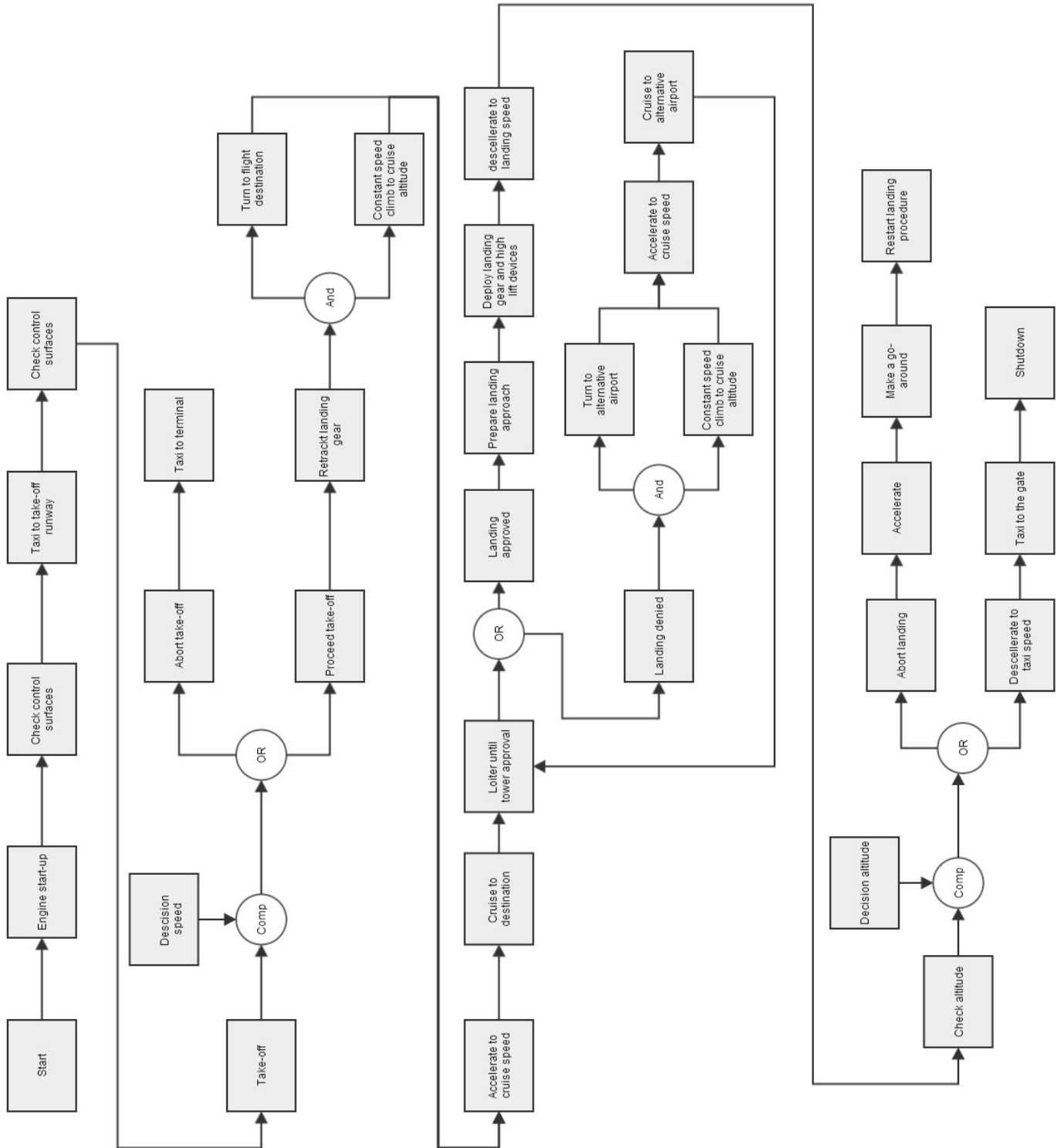
D Functional Breakdown Structure of a Business Jet System

Figure D.1: Functional Breakdown Structure (FBS) of Business Jet System

E   Wing Box Dimensions

Figure E.1: Detailed Geometry of the Wing Box

F Stability & Control Derivatives

Equations from Roskam 6 [34], Airplane Flight Dynamics and Automatic Flight Controls Pt. 1 [77] and Flight Dynamics Reader [78].

Table F.1: Stability & Control Derivatives

Derivative	Sign	Equation	Initial Value	Final Value
C_{X_0}		$\frac{W\sin\theta_0}{\frac{1}{2}\rho V^2 S}$	0	0
C_{X_u}		$-C_{D_u} - 2C_D$	-0.1385	-0.1385
C_{X_α}	>0	$C_L\left(1 - \frac{2C_{L\alpha}}{\pi A e}\right)$	+0.0753	+0.0729
$C_{X_{\dot\alpha}}$		neglected	0	0
C_{X_q}		neglected	0	0
$C_{X_{\delta_e}}$		neglected	0	0
C_{Z_0}		$-\frac{W\cos\theta_0}{\frac{1}{2}\rho V^2 S}$	-0.2633	-0.2633
C_{Z_u}		$-\frac{M_{cr}^2 C_L}{1-M_{cr}^2}$	-1.1234	-1.1234
C_{Z_α}	<0	$-C_{L_{\alpha_{wf}}} - C_{L_{\alpha_h}}\eta_h\frac{S_h}{S}\left(1-\frac{d\varepsilon}{d\alpha}\right) - C_{L_{\alpha_c}}\eta_c\frac{S_c}{S}\left(1+\frac{d\varepsilon_c}{d\alpha}\right)$	-7.6300	-7.7266
$C_{Z_{\dot\alpha}}$		$-2C_{L_{\alpha_h}}\eta_h\bar V_h\frac{d\varepsilon}{d\alpha}$	-2.7071	-2.9877
C_{Z_q}	<0	$-2C_{L_{\alpha_h}}\eta_h\frac{l_h}{\bar c}\frac{S_h}{S}$	-11.9327	-13.1921
$C_{Z_{\delta_e}}$	<0	$-\alpha_{\delta_e}C_{L_{i_h}} - \alpha_{\delta_{e_c}}C_{L_{i_c}}$	-0.5218	-0.5604
C_{m_u}		neglected	0	0
C_{m_α}	<0	$C_{L_{\alpha_{wf}}}\left(\bar x_{ref}-\bar x_{ac_{wf}}\right) - \eta_h\frac{S_h}{S}C_{L_{\alpha_h}}\left(\bar x_{ac_h}-\bar x_{ref}\right)\left(1-\frac{d\varepsilon}{d\alpha}\right)$ $+\eta_c\frac{S_c}{S}C_{L_{\alpha_c}}\left(\bar x_{ref}+\bar x_{ac_c}\right)\left(1+\frac{d\varepsilon_c}{d\alpha}\right)$	-0.5135	-0.9386
$C_{m_{\dot\alpha}}$	<0	$-2C_{L_{\alpha_h}}\eta_h\bar V_h\left(\bar x_{ac_h}-\bar x_{cg}\right)\frac{d\varepsilon}{d\alpha}$	-12.1283	-13.4565
C_{m_q}	<0	$-C_{L_{\alpha_h}}\frac{S_h}{S}\eta_h\left(\bar x_{ref}-\bar x_{ac_h}\right)^2 - C_{L_{\alpha_c}}\frac{S_c}{S}\eta_c\left(\bar x_{ref}-\bar x_{ac_c}\right)^2$	-35.4372	-37.864
$C_{m_{\delta_e}}$	<0	$\alpha_{\delta_e}C_{m_{i_h}} + \alpha_{\delta_{e_c}}C_{m_{i_c}}$	-2.0536	-2.2367
$C_{m_{TC}}$		neglected	0	0
C_{Y_β}	<0	$C_{Y_{\beta_w}} + C_{Y_{\beta_f}} + C_{Y_{\beta_v}}$	-1.0448	-1.1663
$C_{Y_{\dot\beta}}$		$2C_{L_{\alpha_v}}\frac{d\sigma}{d\beta}\frac{S_v}{S}\frac{l_p\cos\alpha+z_p\sin\alpha}{b}$	+0.0061	+0.0067
C_{Y_p}	<0	neglected	0	0
C_{Y_r}	>0	$-2C_{Y_{\beta_v}}\frac{l_v\cos\alpha+z_v\sin\alpha}{b}$	+0.6941	+0.7955
$C_{Y_{\delta_a}}$		neglected	0	0
$C_{Y_{\delta_r}}$		$\frac{C_{L_{\alpha_v}}}{C_{l_{\alpha_v}}}k'K_b\frac{\alpha_{\delta_{C_L}}}{\alpha_{\delta_{C_l}}}\frac{cl_d}{cl_{d_{theory}}}cl_{d_{theory}}\frac{S_v}{S}\eta_v$	+0.2537	+0.2790
C_{l_β}	<0	$C_{l_{\beta_{wf}}} + C_{l_{\beta_h}} + C_{l_{\beta_v}}$	-0.0833	-0.1022
$C_{l_{\dot\beta}}$		$C_{Y_{\dot\beta}}\frac{z_p\cos\alpha-l_p\sin\alpha}{b}$	+0.0010	+0.0012
C_{l_p}	<0	$C_{l_{p_w}} + C_{l_{p_h}} + C_{l_{p_v}} + C_{l_{p_c}}$	-0.4949	-0.4906
C_{l_r}	>0	$C_{l_{r_w}} + C_{l_{r_v}}$	+0.5782	+0.5931
$C_{l_{\delta_a}}$	>0	$\alpha_{\delta_a}C'_{l_\delta}$	+0.0330	+0.0330
$C_{l_{\delta_r}}$	>0	$C_{Y_{\delta_r}}\frac{z_v\cos\alpha-l_v\sin\alpha}{b}$	+0.0334	+0.0373
C_{n_β}	>0	$C_{n_{\beta_w}} + C_{n_{\beta_f}} + C_{n_{\beta_v}}$	+0.0734	+0.1241
$C_{n_{\dot\beta}}$		$C_{Y_{\dot\beta}}\frac{l_p\cos\alpha+z_p\sin\alpha}{b}$	+0.0028	+0.0031
C_{n_p}	<0	$C_{n_{p_w}} + C_{n_{p_v}}$	-0.0372	-0.0388
C_{n_r}	<0	$C_{n_{r_w}} + C_{n_{r_v}}$	-0.2672	-0.3092
$C_{n_{\delta_a}}$	>0	$K_a C_L C_{l_{\delta_a}}$	-0.0003	-0.0003
$C_{n_{\delta_r}}$		$-C_{Y_{\delta_r}}\frac{l_v\cos\alpha+z_v\sin\alpha}{b}$	-0.0963	-0.1071